

Single-Chain Nanoparticle Formation Induced by Metal Complexation

Zur Erlangung des akademischen Grades eines
DOKTORS DER NATURWISSENSCHAFTEN
(Dr. rer. nat.)

von der Fakultät für Chemie und Biowissenschaften
des Karlsruher Instituts für Technologie (KIT)

genehmigte
DISSERTATION

von

M.Sc. Hannah Rothfuß

aus Tübingen

1. Referend:	Prof. Dr. Christopher Barner-Kowollik
2. Gutachter:	Prof. Dr. Peter W. Roesky
Tag der mündlichen Prüfung:	09. Mai 2019

Die vorliegende Arbeit wurde im Zeitraum von Januar 2016 bis März 2019 unter Anleitung von Prof. Christopher Barner-Kowollik am Karlsruher Institut für Technologie (KIT) angefertigt.

Abstract

The sophisticated class of natural enzymes is outstanding for its designed substrate-targeted molecular recognition sites, allowing unprecedented catalytic efficacy. Scientists from various research areas aim for a replication of similar efficient synthetic systems. A promising pathway employs polymer chains to act as natural macromolecular mimics, where intramolecular linkages hold the single chains together, forming particles of a diameter typically between 3–30 nm. This area of polymer chemistry, termed single-chain nanoparticles (SCNPs), has become popular in recent years, as shown by the increasing amount of publications with numerous potential applications presented therein. Among the various chemical reaction pathways available to intramolecularly crosslink the polymer chains, the present thesis focuses on a metal-induced chain collapse. The precise interaction of polymeric framework with metal cores gives rise to functional soft matter materials.

Unlocking the potential of metal complexed SCNPs, the current thesis investigated catalytic systems, novel ligand moieties and sophisticated dinuclear crosslinking units. Inspired by catalytically active palladium(II)-SCNPs, a homogeneous, yet recyclable platinum(II) catalyst was generated in a first project. Here, the essential stable metal incorporation into the polymeric scaffold was provided by the utilization of triarylphosphine moieties, forming stable 2:1 phosphine-to-platinum(II) linkages. Another class of ligands, based on nitrogen-containing units, *i.e.* phenanthroline, was explored in the subsequent work. The emphasis was on the development of a versatile phenanthroline-containing ligand, applicable in controlled radical polymerization techniques to allow for the prediction and determination of the degree of functionalization in the corresponding (co)polymer. The obtained narrowly distributed, functionalized linear polymer chains, readily able to incorporate metal ions, yielded transition metal-SCNPs and luminescent lanthanide metallopolymers. Furthermore, the formation of intrachain crosslinks *via* intricate dinuclear metal centers was introduced. Access to nanoparticles was obtained when inserting carboxylic acids into linear polymer chains, which acted as bidentate bridging ligands, assembling around a dimetal core in so-called paddlewheel structures. On the basis of copper(II) and molybdenum(II) complexes, the emulation of such sophisticated structural arrangements in polymeric architectures was presented.

Finally, heterometallic SCNPs were synthesized, in which two types of metal ions were orthogonally incorporated into the polymer framework, marking the first step towards compartmentalized SCNPs. In two concepts, the generation of polymer chains containing two divergent ligand moieties, ready to direct the subsequently performed metal coordination, was demonstrated. By employing copper(II) and gold(I) in the first method, SCNPs with the potential for becoming a multi-step catalytic system were developed. In the second approach, the encapsulation of platinum(II) and europium(III) formed heterometallic SCNPs, combining catalytic activity with luminescent properties.

The thesis concludes with an outlook on the future of catalytically active SCNPs, pointing out challenges and further possible developments of those intriguing structures.

Zusammenfassung

Natürlich vorkommende Enzyme sind weithin bekannt für ihre bemerkenswerte katalytische Effizienz, die sie vor allem durch die perfekte Anpassung ihrer molekularen Erkennungseinheiten an die jeweiligen Ausgangssubstrate erhalten. Viele Wissenschaftler verschiedenster Forschungsbereiche haben es sich daher als höchstes Ziel gesetzt, auf synthetischer Ebene ähnliche Strukturen zu entwickeln, die die gleiche Effizienz wie die genannten Vorbilder aus der Natur aufweisen.

Ein vielversprechender Ansatz untersucht eine mögliche Nachbildung solch komplexer Aufbauten anhand von polymeren Nanopartikeln (Durchmesser 3–30 nm) welche aus Einzelketten bestehen, die durch intramolekulare Bindungen gefaltet wurden. Diese Strukturen aus dem Bereich der Polymerchemie, genannt Einzelketten-Nanopartikel (engl. single-chain nanoparticles, SCNPs) wurden in den letzten Jahren vielfach untersucht und weiter entwickelt, sodass bereits heute zahlreiche Publikationen bestehen, die über vielseitige mögliche Anwendungen von SCNPs berichten. Neben den mannigfaltigen Reaktionswegen, die dazu führen eine Kette intramolekular zu verknüpfen, liegt der Schwerpunkt der vorliegenden Arbeit auf einer Faltung der Kette, welche durch Metallionen ausgelöst wird. Während des Faltungsprozesses koordinieren dabei die Metalle an bestimmte funktionelle Einheiten in den Ketten und werden somit in die Polymere eingebaut. Dieses präzise Zusammenspiel zwischen polymeren Gerüststrukturen und Metallionen führt demnach zu funktionalen, anpassungsfähigen Materialien.

Um das Potential dieser metallkomplexierten SCNPs weiter auszuschöpfen, wurde in der vorliegenden Arbeit zum einen die Verwendung von SCNPs als katalytisch aktive Systeme untersucht, neue Liganden zur Metallkomplexierung in polymeren Einheiten entwickelt und eine Möglichkeit aufgezeigt, zwei Metallionen pro Vernetzungspunkt einzubauen. Inspiriert von katalytisch aktiven Palladium(II) SCNPs, wurde in einem ersten Projekt ein homogener, gleichzeitig wiederverwendbarer Platin(II) Katalysator entwickelt. Dabei wurden beständige Bindungen zwischen Metallionen und Polymerkette durch die Verwendung von Triarylphosphan-Liganden sichergestellt, welche stabile Phosphan–Platin(II) Verbindungen aufbauten. Nachfolgend wurde eine Gruppe von Liganden, welche über Stickstoffatome an Metalle koordinieren, am Beispiel des Moleküls Phenanthrolin untersucht. Der Fokus dieses

Projekts lag dabei auf der Entwicklung eines Phenanthrolin-Liganden, welcher in kontrollierten Polymerizationstechniken eingesetzt werden konnte. Dadurch wurde eine Vorsage und gleichzeitig die Bestimmung des Funktionalisierungsgrades im späteren Polymer ermöglicht. Die daraus erhaltenen engverteilten, funktionalen, linearen Polymerketten erlaubten anschließend den Einbau von Metallionen in das polymere Gerüst. In Abhängigkeit der verwendeten Metallen entstanden einerseits Übergangsmetall-komplexierte Nanopartikel und andererseits lumineszente Metallopolymere, bei Verwendung von Lanthanoiden. Des Weiteren wurde die Bildung von Vernetzungspunkten innerhalb der polymeren Einheit, bestehend aus zwei Metallzentren, gezeigt. Dafür wurden Carbonsäuren in eine lineare Polymerkette eingeführt. Nach Metallzugabe agierten die Carbonsäure-Gruppen als zweizählige, verbrückende Carboxylat-Liganden und bildeten eine sogenannte 'Paddlewheel' Struktur um eine zweikernige Metalleinheit. Durch die Verwendung von Kupfer und Molybdän Ausgangsverbindungen konnten diese anspruchsvollen Aufbauten innerhalb polymerer Nanopartikel nachgebildet werden.

Zuletzt wurden heterometallische SCNPs synthetisiert, bei denen zwei Arten von Metallionen selektiv an zwei unterschiedliche, funktionelle Gruppen innerhalb derselben Polymerkette koordinierten. Solch eine gerichtete, kontrollierte Komplexierung von Metallen ist der erste Schritt in Richtung Nanopartikel, welche innerhalb derselben Struktur verschiedene Areale unterschiedlicher Funktionen aufweisen. Anhand zweier Systeme konnte bisher gezeigt werden, dass durch die sorgfältige Wahl zweier unterschiedlicher Liganden in derselben Kette die nachfolgende Koordination zu Metallionen gesteuert werden kann. In der ersten Methode wurden Phosphaneinheiten und Carbonsäure-Gruppen eingesetzt, welche die Metalle Kupfer(II) und Gold(I) komplexierten. Die daraus entstandenen SCNPs haben das Potential als mehrstufige, katalytische Systeme verwendet werden zu können. Im zweiten Ansatz wurden Platin(II) und Europium(III) Ionen mittels Phosphan und Phosphanoxid-Liganden in die Polymerkette eingebaut, um in den resultierenden SCNPs katalytische Aktivität mit lumineszenten Eigenschaften zu kombinieren.

Die Dissertation schließt mit einem Ausblick auf die Zukunft katalytisch aktiver SCNPs, in welchem die Herausforderungen und möglichen weiteren Entwicklungen dieser faszinierenden Makromoleküle aufgezeigt werden.

Contents

1	Introduction	1
2	Theoretical Background	5
2.1	Polymerization Techniques	5
2.1.1	Reversible Deactivation Radical Polymerization (RDRP)	9
2.1.2	Nitroxide Mediated Polymerization (NMP)	11
2.1.3	Reversible Addition Fragmentation Chain Transfer Polymerization (RAFT)	15
2.1.4	Copolymerization	20
2.2	Supramolecular Metallopolymers	22
2.3	Single-Chain Nanoparticles (SCNPs)	25
2.3.1	General Remarks on SCNPs	25
2.3.2	Metal-Complexed SCNPs	30
2.4	Characterization of SCNPs	39
2.4.1	Size Exclusion Chromatography (SEC)	42
2.4.2	Diffusion Ordered Spectroscopy (DOSY)	45
2.4.3	Dynamic Light Scattering (DLS)	47
2.5	Coordination Complexes	50
2.5.1	General Remarks on the Formation of Transition Metal Complexes	50
2.5.2	Phosphine Ligands – Triphenylphosphine	55
2.5.3	Nitrogen Ligands – Phenanthroline and Derivatives	58
2.5.4	Oxygen Ligands – Carboxylates	61
2.5.5	General Remarks on Lanthanide Complexes	63
3	Platinum(II)-SCNPs as Homogeneous, Recyclable Catalysts	65
3.1	Motivation	65
3.2	Synthesis of a Phosphine-Containing Polymer	67
3.3	Synthesis of Pt(II)-SCNPs	70
3.4	Application of Pt(II)-SCNPs as Homogeneous, Recyclable Catalysts	77
3.5	Summary	85
4	Phenanthroline as a Versatile Ligand for Polymeric Material	87
4.1	Motivation	88

4.2	First Steps for a Polar Phen-Containing Polymer System	91
4.2.1	Evaluation of Suitable Polymerization Conditions for DMAA	92
4.2.2	Postfunctionalization	94
4.3	Polar System – Monomer Synthesis	96
4.4	Polar System – Polymerization Techniques	102
4.4.1	Copolymerization of Phen-Monomers <i>via</i> RAFT	102
4.4.2	Copolymerization of Phen-Monomers <i>via</i> NMP	105
4.4.3	Copolymerization Yielding P_{polar}	108
4.5	P_{polar} as a Polymer Scaffold for Transition Metal SCNP Formation	112
4.6	Polar System – Summary	119
4.7	Non-Polar System – Monomer Synthesis	120
4.8	Non-Polar System – Polymerization Techniques	122
4.9	P_{np} as a Polymer Framework for Lanthanide Metallopolymers	124
4.10	Non-Polar System – Photoexcitation in Solution	129
4.11	Non-Polar System – Summary	133
5	Carboxylate Paddlewheel Structures as Folding Motifs in SCNPs	135
5.1	Motivation	135
5.2	Synthesis of a Benzoic Acid Functionalized Copolymer and SCNP Formation	138
5.3	Model Complexes of $Cu_2(II)$ and $Mo_2(II)$ Structures	144
5.4	Spectroscopic Studies of the SCNPs and Model Complexes	147
5.5	Summary	151
6	Orthogonal Coordinated Heterometallic SCNPs	153
6.1	Motivation	153
6.2	A Gold and Copper Based System	156
6.2.1	Synthesis of a Terpolymer – Phosphines and Carboxylic Acids	157
6.2.2	Au(I) Functionalization	160
6.2.3	Au(I)/ $Cu_2(II)$ -SCNP Formation	164
6.3	Summary	170
6.4	A Europium and Platinum Based System	171
6.4.1	Synthesis of a Terpolymer – Phosphines and Phosphine Oxides	172
6.4.2	Eu(III)/Pt(II)-SCNP Formation	175
6.5	Summary	182
7	Conclusion	183
8	The Future of Catalytically Active SCNPs	187
9	Experimental Section	189
9.1	Materials	189
9.2	Instrumentals	191

9.3	Synthesis of Molecular Structures	196
9.4	Polymerizations – NMP Technique	213
9.5	Polymerizations – RAFT Technique	222
9.6	Synthesis of Metallopolymers	230
9.7	Formation of Single-Chain Nanoparticles	234
	Appendix	257
	Abbreviations	267
	Publications	271
	Conference Contributions	273
	Erklärung	275
	Acknowledgements	277

Introduction

Single-chain nanoparticles (SCNPs) are a class of polymeric materials, constituting the first steps exploiting precision macromolecular chemistry towards artificial mimics of biomacromolecules such as proteins. Here, functional single polymer chains are collapsed into nanoparticles *via* intrachain linkages, resulting in three-dimensional structures of a diameter sub-30 nm. In first approaches, the chain collapse was performed *via* hydrogen bond formation, imitating the folding mechanism of natural enzymes. Soon after, a library of possible crosslinking reactions was developed and is still expanding. Nowadays, intrachain bond formation can be thermally or photochemically induced and takes place between pendant groups of the polymer or with externally added linker molecules. Thereby, the linkages exhibit covalent, non-covalent or dynamic character.^[1-4] As versatile as the synthesis procedures are the possible applications. Today, SCNPs can already be found in areas such as sensing,^[5] drug delivery,^[6] as healable materials^[7] or in catalysis.^[8] Among the numerous possibilities of SCNPs formation, of specific interest is the chain collapse induced by coordination of functional units in the polymer chain to externally added metal ions. Thereby, the readily adjustable features of a polymer framework are combined with metal ions, which can exhibit luminescent, magnetic or catalytic properties.

When synthesizing SCNPs, of high importance is the application of controlled polymerization methods that tolerate a wide array of functional groups, to enable the synthesis of narrowly distributed, functionalized polymer chains ready for metal encapsulation. Subsequently, the exclusive linkage formation within the same chain is targeted, while preventing interchain linkages, thus network formation. In the specific case of metal-SCNPs, further demands address the ligand-to-metal ratio, suitable precursor metal complexes, stable metal incorporation into the chain and the placement of functional units along the chain to allow for their coordination to the metal centers without steric hindrance by the rigid backbone. So far, only a limited amount of transition metals has been explored in their ability to induce a single-chain collapse and even less SCNP systems were investigated for applications.

Thus, the current thesis sets out to expand the library of metal-SCNPs by exploring novel precursor metal complexes and ligand moieties, creating functional soft matter materials. Thereby, highly

appealing are experiments to investigate the catalytic or luminescent properties of the generated polymeric material.

In a previous work, the application of Pd(II)-SCNPs as a catalyst in a cross-coupling reaction was demonstrated.^[9] However, in the described procedure the metal–ligand bonds did not withstand the conditions of the reaction and the metal ions were released from the polymer framework. Thus, the first aim targeted in Chapter 3 is the synthesis of a metal-SCNP system, which retains its shape and function during catalysis to allow its further reuse (Figure 1.1, A). As a scaffold, a styrene-based polymer framework containing phosphine moieties is employed. Appropriately, platinum(II) is known to form stable 2:1 ligand-to-metal ratios with triarylphosphines, hence promising for Pt(II)-SCNP formation. Similar as palladium(II), also platinum(II) exhibits catalytic properties, for instance in the amination of ally alcohol.^[10] In addition, the combination of NMR active Pt(II) ions and phosphines enables insight into the folding unit and facilitates further proof for continuous metal incorporation into the polymer framework.

In the second project, the implementation of nitrogen-based ligands, *i.e.* phenanthroline units, within narrowly distributed polymer chains is investigated. In molecular complexes, phenanthroline is known as a versatile ligand, forming stable complexes to several metal ions in different coordination ratios. While there is little report in the literature about the use of phenanthroline in polymeric material, its modification into a monomer, allowing for its application in controlled polymerization reactions is explored. After monomer and polymer synthesis, the subsequent functionalization of the polymers either into SCNPs or linear metallopolymers is demonstrated in Chapter 4 (Figure 1.1, B).

The group of oxygen-based carboxylate ligands is introduced in Chapter 5 as an alternative type of ligand moieties, suitable for metal-SCNP formation. This group of ligands exhibits a wide array of possible coordination modes to metal ions, however, of specific interest is their arrangement as bidentate bridging ligands. Therefore, a dinuclear metal species is implemented between four carboxylate ligands, together forming a geometry called paddlewheel structure. By incorporating benzoic acid moieties into a polymer chain and selecting suitable precursor complexes, the assembly of such sophisticated architectures inside a polymer framework is presented (Figure 1.1, C).

Having established three ligand moieties suitable for metal incorporation, Chapter 6 sets out to expand the realm of SCNPs from mono-metallic to directed heterometallic SCNPs (Figure 1.1, D). The conditions under which heterometallic SCNPs can be obtained is investigated. Therefore, high focus is placed on an Au(I)/Cu₂(II)- and an Eu(III)/Pt(II)-SCNP system. By employing a combination of phosphines with carboxylic acids and phosphines with phosphine oxides, the systems are explored towards good accessibility for an orthogonal embedding of two metal species without

undesired interactions. Such heterometallic SCNP systems open doors for future compartmentalized three-dimensional polymeric structures, interesting as catalysts for multi-step or cascade reactions.

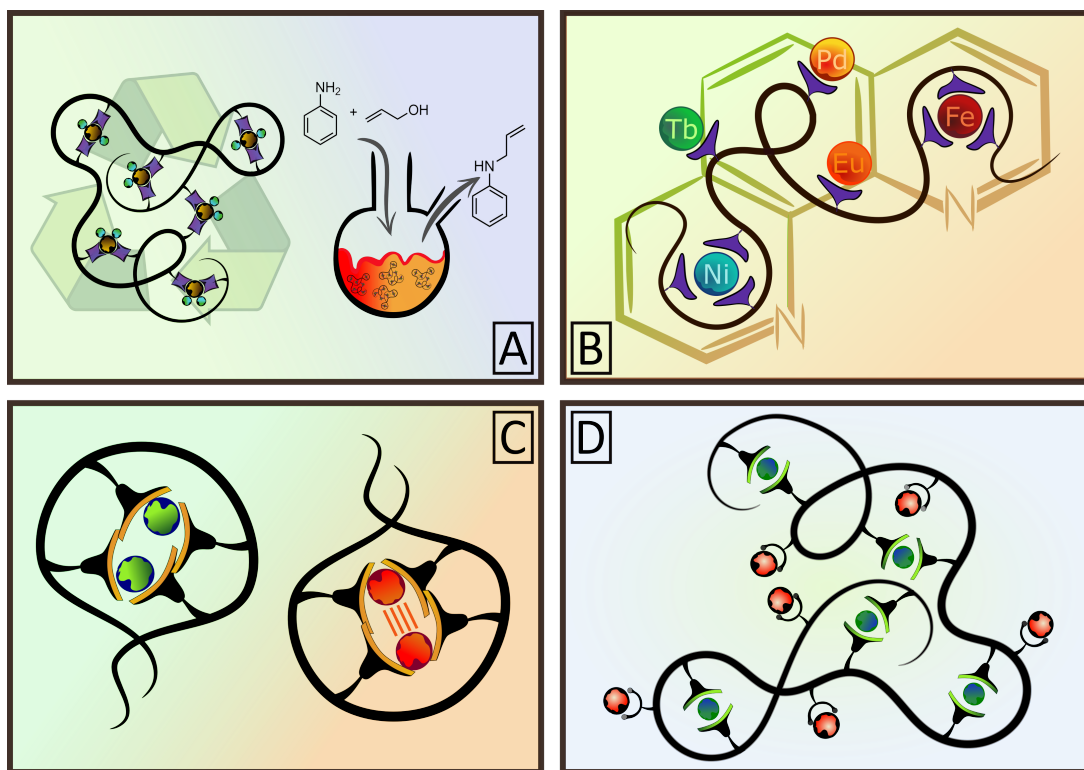


Figure 1.1: The current thesis sets out to expand the realm of SCNP chemistry for novel linker moieties in the polymer chain and their subsequent coordination to metal ions. In (A), the synthesis of a catalytically active, reusable SCNP system on the basis of platinum(II) is explored. The project in (B) addresses the synthesis of polar and non-polar polymer chains containing the versatile ligand phenanthroline to allow for a coordination to several transition and lanthanide metals. Furthermore, (C) investigates the creation of a paddlewheel structure as a crosslinking unit in SCNPs, in which two metal cores are incorporated into the same crosslinking unit in close proximity. Finally, the knowledge gained from the previous projects is combined in (D) to generate heterometallic, selectively coordinated SCNP systems.

In the frame work of the present thesis, a library of four ligand moieties and their interaction with various transition metals and lanthanides is investigated. Suitable reaction conditions for the implementation of ligand moieties into narrowly distributed chains are demonstrated, followed by appropriate reaction procedures for a successful metal incorporation into the polymer framework. Several analytical techniques, including NMR (^1H , $^{31}\text{P}\{^1\text{H}\}$, ^{195}Pt , ^{19}F and DOSY), IR and Raman spectroscopy, as well as SEC and fluorescence measurements are performed to elucidate the structure of the synthesized compounds and determine the respective metal–ligand folding units within the macromolecular architectures.

The following projects are part of a cooperative program in the SFB 1176, executed with Nicolai Knöfel from the group of Prof. Dr. Peter Roesky in the inorganic chemistry department (KIT).

Theoretical Background

The present chapter covers the theoretical background relevant to the current thesis. Since the topic of the dissertation is situated at the interface between polymer chemistry and inorganic chemistry, essential information about both aspects is collated. The polymer chains, employed in the presented projects, were realized by reversible deactivation radical polymerization methods, whose mechanistic differences will be highlighted in the first sections. After an introduction into the field of metallopolymers, a general overview over single-chain nanoparticles (SCNPs) is presented, followed by detailed information and latest investigations in the field of metal-complexed SCNPs. For a better understanding of metal incorporation into the polymeric framework, the subsequent section gives an outline of metal complex formation and several classes of ligand moieties, employed in the present thesis. The last section deals with the analysis of single-chain nanoparticle, pointing out particular challenges when characterizing such hybrid material.

2.1 Polymerization Techniques

Polymerization describes the process of consecutive reactions between single molecular units assembling into a macromolecule.^[11] The building blocks, so-called monomers, are connected to each other *via* covalent or non-covalent interactions, forming in its simplest structure a linear chain. Typically, synthetic polymers are categorized according to their mechanism of chain formation, i.e. **Step-Growth** or **Chain-Growth** polymerization.

Essential for **Step-Growth** polymerization are monomers with at least two functional units.^[12, 13] In a step-wise reaction, at first the monomers form dimers, than trimers and tetramers, oligomers and finally polymers. In doing so, the degree of polymerization increases at a slow rate, and high conversion is necessary to yield macromolecules of sufficiently high molecular weight.^[14] The relation between the degree of polymerization and the conversion is given by the **Carother's Equation**,

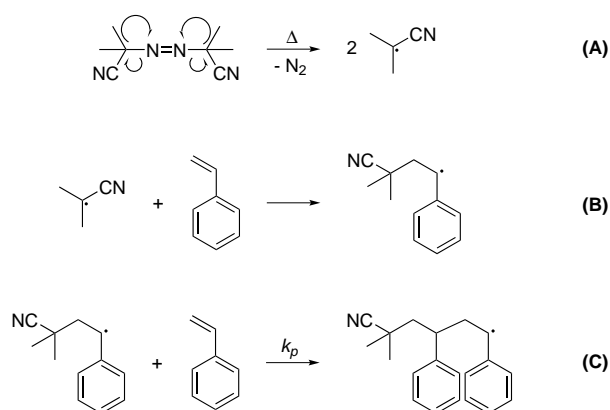
allowing the calculation of the molecular mass of the final polymer.^[15] Step-growth polymerization technique was not employed in the current thesis and will not be discussed further. Additional information can be found in standard textbooks.^[11]

In the synthesis of macromolecules *via* **Chain-Growth** polymerization, monomers add to a reactive site of a propagating polymer, usually the chain end, thereby extending its chain length. In each monomer addition, the reactive site is regenerated, enabling new monomer attachment. The entire process of chain propagation comprises three elementary steps:

Initiation by an active species (initiator), propagation of the chain *via* addition of monomers and chain termination.^[16] However, for most of the chain polymerizations exist also a fourth reaction step, the chain transfer event. Thereby, the reactive center of a propagating polymer is transferred to another polymer chain, a solvent molecule or free monomer. While this process terminates the growth of one polymer chain, simultaneously a new reactive site is created. Thus, chain transfer reactions lead to shorter chain lengths and lower the average molecular weight.^[17, 18]

As a result from undesired termination or transfer reactions, the polymer chains have a high discrepancy in their length, expressed in higher values of their dispersity index \bar{D} .^[19] Along with the molecular weight, the dispersity has a significant impact on the mechanical and physical properties of polymer chains.^[20] In broad distributed polymers, short and long chains contribute collectively to the overall characteristics of the polymer system. For instance, short chains reduce the brittleness, which improves the processability of the polymer, whereas longer chains increase the impact strength for better mechanical properties.^[21] However, certain applications require precision polymers of exact lengths and defined properties, e.g. as polymer standards for size exclusion chromatography (SEC) measurements (refer to Chapter 2.4.1). For this reason, extensive effort is invested in the synthesis of narrowly distributed polymer chains, of which some developed methods are discussed in the following chapters.

The most versatile polymerization technique, belonging to the class of chain-growth polymerization, is the **Free Radical Polymerization (FRP)**. In FRP, molecules featuring unpaired electrons (radicals) react with monomers bearing a unsaturated vinyl unit. An example is given in Scheme 2.1, in which the initiator AIBN (azobisisobutyronitrile) decomposes into two radicals upon thermal treatment. The subsequent reaction with a monomer forms a chain-initiating radical (example A and B). In the following propagation reaction, monomers add to the macro-radical (C).

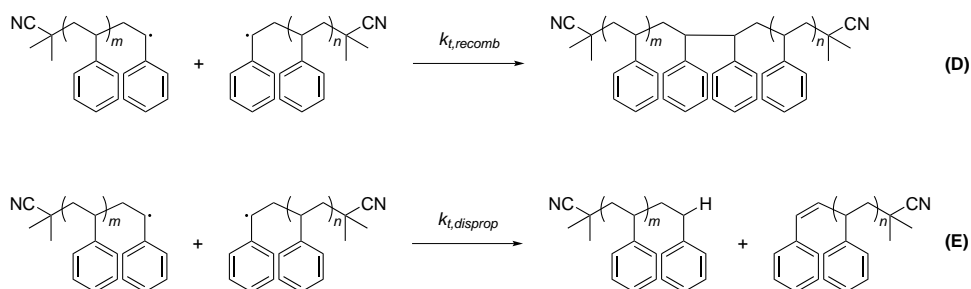


Scheme 2.1: Decomposition of the thermo-labile initiator AIBN through effect of heat into two radicals (A), ready to initiate polymerization. Upon reaction of the radical with a monomer, a macro-radical is formed (B). Further monomer is added in the propagation reaction (C).

In dependency of the concentration of monomer $[M]$, the radical species $[R\cdot]$ and the coefficient for chain propagation k_p , the reaction rate v_p for propagation is defined as:

$$v_p = k_p [M] [R\cdot]$$

The undesired termination reactions of propagating chains often proceed *via* the two following mechanism: recombination (D) or disproportionation (E), depicted in Scheme 2.2. While for recombination one saturated polymer chain as the final structure is formed, disproportionation simultaneously generates a saturated and an unsaturated macromolecule.



Scheme 2.2: Two possible termination reactions of propagating chains: recombination (D) and disproportionation (E).

Considering the coefficient for the termination reaction k_t , analogous to the propagation coefficient, the reaction rate v_t for termination is described as:

$$v_t = 2k_t [R\cdot]^2$$

The success of the FRP method can be related to the non-specific nature of radicals, which tolerates a wide variety of monomers for polymerization, thus enabling the synthesis of various soft matter materials. This functional group tolerance combined with a relatively low sensitivity to impurities makes FRP the most commonly used polymerization technique in industry, accounting for more than 50 % of all industrially produced polymers.^[22]

For the thermodynamics of a polymerization, the **Gibbs Free Energy Equation** is central, connecting the enthalpy H , the temperature T and the entropy S :

$$\partial G = \partial H - T\partial S$$

The essential condition for a successful chemical reaction is a reduction of the free energy G , hence $-\partial G$. Consequently, the following must apply: $\partial H > T\partial S$. In polymerizations, the change of the enthalpy ∂H is always negative, since the bond formation between monomers is an exothermic reaction. Simultaneously, the process of chain propagation results in an overall decrease of entropy, due to a reduction of the number of microscopic configurations. Therefore, the pivotal factor is the temperature. Exceeding the critical temperature, the **Ceiling Temperature** T_c , the system reaches an equilibrium $\partial G = 0$ without tendency for polymerization.^[23]

A major disadvantage in conventional FRP is the generation of polymer chains with broad distributed chain lengths. As a consequence, mechanisms to control the molecular weight and the distribution of polymers have been developed and are presented in the following sections.

2.1.1 Reversible Deactivation Radical Polymerization (RDRP)

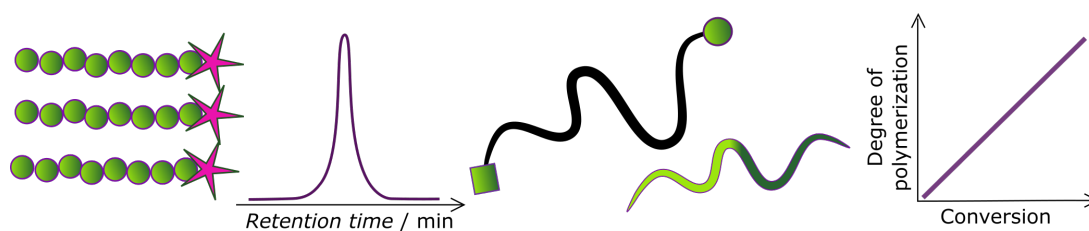


Figure 2.1: Reversible Deactivation Radical Polymerization (RDRP) combines a non-demanding synthesis procedure with facile control over the molecular mass of narrowly distributed polymer chains. The reason is a simultaneous initiation of all chains and the minimization of termination and transfer reactions. The linear increase of the polymerization degree with conversion allows the predetermination of the molecular mass. Permanent active chain ends open the possibility to restart propagation or functionalize chain ends. In conclusion, RDRP enables the synthesis of advanced macromolecular structures such as block copolymers, star or grafted polymers.

Of particular interest for scientists in polymer chemistry was the synthesis of polymer chains with predictable, narrowly distributed chain lengths. However, such a control over the polymerization was found impossible for a long time, due to asynchronous chain initiation followed by inevitable termination and chain transfer reactions. Consequently, the development of anionic polymerization by Michael Szwarc and coworkers in 1956 had a remarkable effect on the research in the field of polymer chemistry. Their method, anionic polymerization, exhibited a termination- and transfer-free nature, opening the door for facile synthesis routes yielding well-defined polymers of uniform chain lengths.

Central in their work was the use of carbanions as initiators, which rapidly triggered the subsequent chain propagation.^[24] Provided the exclusion of any impurities, including oxygen and moisture, the anion stayed constantly active until deliberate termination reactions. Thus, polymers of predictable molecular weight with narrow dispersity were produced. Szwarc described the polymerization method as ‘**Living Polymerization**’, thereby referring to the fact that the chain ends did not terminate and were able to repropagate upon further monomer addition.^[25]

As mentioned, the anionic polymerization technique is highly sensitive towards impurities and therefore requires a high purity of all participating reactants. This is necessary to prevent undesired reactions with the reactive anionic polymerization center. For the same reason, anionic polymerization has a limited tolerance towards numerous functional groups, limiting the application scope of the, so far, investigated living polymerization.

A solution was found in 1982, when Takayuki Otsu established a novel way of free radical polymerization that combined the simple handling of free radical polymerization with the advantages of anionic polymerization: an easy-to-operate synthetic procedure, a high tolerance of functional groups and the possibility to control the molecular mass of narrowly distributed polymer chains

(Figure 2.1).^[26] The solution for the (almost complete) elimination of termination reactions was an exchange process between the propagating radicals and a dormant species.^[27] In this respect, the central element was a dynamic equilibrium in which the propagating radicals were reversibly trapped and reactivated. The feature of having a **Persistent Radical** was henceforward investigated and led to different methodologies of living free radical polymerization. Their common characteristic is an equally distributed propagation probability over all chains and the termination reaction is reduced to a minimum. An alternative approach involves the reversible transfer of the propagating radicals, termed **Degenerative Exchange Process**.^[28]

In total, such **Reversible Deactivation Radical Polymerizations** (RDRP) feature a simultaneous initiation of all chains, a minimization of termination reactions, a thereof resulting linear increase of the polymerization degree with conversion and active chain ends, ready to restart polymerization or being functionalized.

Today, various techniques of the RDRP method exist, resulting in polymer chains of uniform chains lengths with a high tolerance towards functional groups. The following two chapters are dedicated to the two methods, which were employed in the current thesis.

One method reduces the termination reaction of the propagating chain by the usage of a scavenger, which reversibly traps the radical, thus allows reactivation. Well-known scavengers for transient carbon-centered radicals are nitroxides, a class of stable organic free radicals, which were eponymous for the technique **Nitroxide Mediated Polymerization**.

The other procedure does not reduce the overall radical concentration, yet alternately traps and releases radicals following a radical transfer mechanism. This method is termed **Reversible Addition Fragmentation Chain Transfer**.

2.1.2 Nitroxide Mediated Polymerization (NMP)

The nitroxide mediated polymerization (NMP) is categorized as a reversible deactivation radical polymerization. In contrast to conventional FRP, NMP enables the synthesis of polymers of uniform chain lengths and gives excellent control over the molecular weight.^[29] As a result, NMP allows the design of advanced polymer architectures such as block or graft copolymers^[30] and ensures access to polymers equipped with tailor-functionalized end groups.^[31, 32]

The living nature of NMP originates from its key component, a particularly stable and long-lived **Nitroxide Radical**. Initially studied as a radical trap for methyl acrylate polymerizations, nitroxides were discovered as effective compounds to selectively scavenge carbon-centered radicals and form stable alkoxyamines.^[33] In further investigations, it was found that the C–O bond between a nitroxide and a carbon is thermally labile and thus can be reversibly cleaved. First ideas and concepts were generated to intentionally trap the propagating radical *via* nitroxides and subsequently release the active radical species. Accordingly, the majority of the propagating chains remained in a dormant state, hence reducing the overall radical concentration. Consequently, the propagation rate is reduced linearly (refer to the rate equation in Chapter 2.1). However, and more importantly, the termination rate is affected quadratically, thus minimizing termination reactions.

Nitroxides are well-known for their radical scavenging properties of carbon-centered radicals, however, they do not self-initiate polymerizations, neither self-dimerize. The characteristics of the so-called **Persistent Radicals** are caused by the high resonance energy of the two main mesomeric structures, in which an unpaired electron is delocalized between the nitrogen and oxygen atom, forming a stable 2-center 3-electron system. As an example, the mesomeric structure of the nitroxide 2,2,6,6-tetramethylpiperidin-1-yl)oxyl (TEMPO) is depicted in Figure 2.2.^[34, 35]

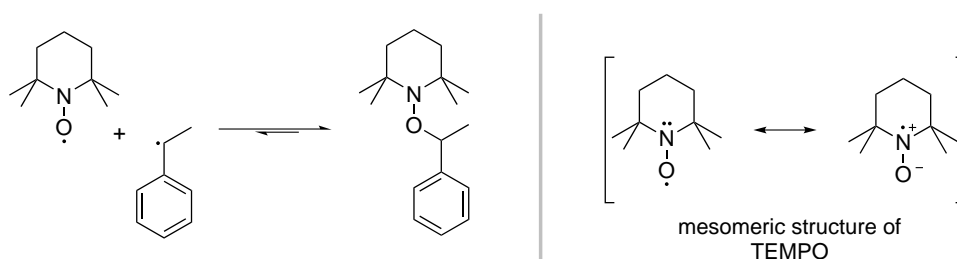
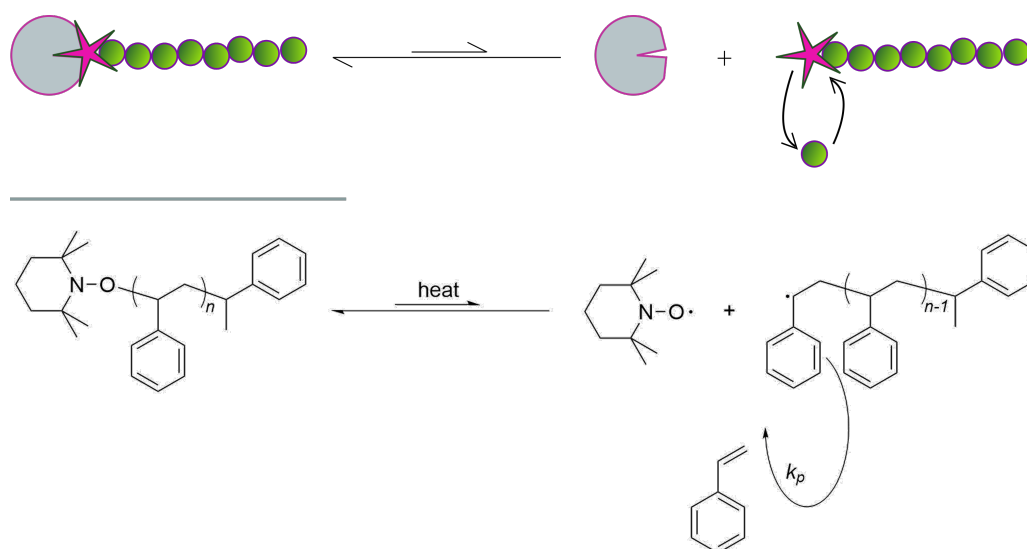


Figure 2.2: *Left:* A nitroxide reacts reversibly with a carbon-centered radical to form a stable alkoxyamine. *Right:* Due to mesomeric structures, TEMPO has a high resonance stabilization energy. The combination with space-demanding methyl groups makes TEMPO a persistent radical, perfectly designed for its application in NMP.

Advantageously, radical coupling between the nitroxides is suppressed due to a higher resonance energy of the radicals than the energy gain of a hypothetical O–O bond formation. The dimerization of the nitroxides can additionally be inhibited by bulky side groups close to the radical center.

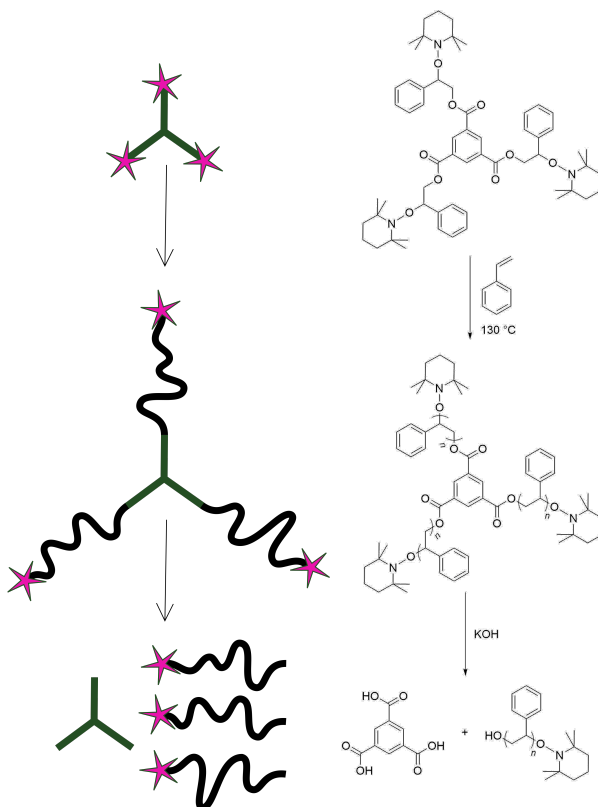
In the years between 1970 and 2000, various approaches were performed to establish the most suitable chemical structure of the scavengers and to perfectly tune the reaction conditions for a controlled polymerization *via* nitroxides.^[36] In first attempts, the polymerization was initiated by traditional free radical initiators, such as AIBN, and the nitroxide species was additionally added. However, a study of Rizzardo and Hawker in 1996 led to new perceptions about ideal reaction conditions.^[37] Their results suggested the application of identical amounts of nitroxide and initiator. These findings resulted in the design of alkoxyamines, which dissociate at high temperatures into both the nitroxide and the initiating radical.

Commonly used alkoxyamines were based on the nitroxide TEMPO, due to its low cost, easy storage and its remarkable control over the polymerization of styrene and its derivatives. The key reaction step in the NMP mechanism is depicted in Scheme 2.3.



Scheme 2.3: Illustration and example of the key reaction step in nitroxide-mediated polymerization (NMP). Stable nitroxide radicals form thermally labile bonds with reactive carbon-centered radicals, resulting in a macromolecular alkoxyamine, the dormant species (*left*). Upon dissociation at elevated temperatures, the re-activated radicals react with monomer thus undergoing chain propagation (*right*). The repetitive activation and deactivation reaction step of the propagating chain suppresses undesired chain terminations and yields well-defined, narrowly distributed polymer chains.

The easy handling of NMP is presented by an example of the work of Hawker, describing the precise control over star polymers *via* the NMP technique.^[38] Trifunctional initiators were developed, containing three initiating alkoxyamine groups. A simultaneous initiation of all three arms resulted in the formation of polymer branches, very similar in chain length. After cleaving off the arms under basic conditions, the narrow molecular weight distribution of the single arms was confirmed (Scheme 2.4).



Scheme 2.4: A core structure composed of three alkoxyamine functional groups was designed, allowing each arm to propagate. After the polymerization, the arms were cleaved off under basic conditions, thus enabling the analysis of the single polymer chains. As reported, high molecular weight polymers of uniform chain lengths were obtained.

However, TEMPO-based alkoxyamines require elevated reaction temperatures (over 100 °C) to decompose into the nitroxide and the corresponding alkyl-radical. In reactions with non-styrene based monomers, such as methyl methacrylates, stability issues have an even larger influence, since the homolysis of the C–O bond is too slow, resulting in poor control over the propagating chains.^[39] For this reason, more versatile nitroxides have been developed, such as 2,2,5-trimethyl-4-phenyl-3-azahexane-3-oxy (TIPNO) or *N*-tert-butyl-*N*-[1-diethylphosphono-(2,2-dimethylpropyl)] nitroxide (SG1), suitable for the polymerization of a vast array of monomers, such as acrylates and acrylamides (refer to the corresponding chemical structures in Figure 2.3).^[40, 41]

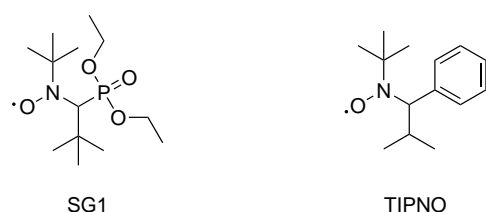


Figure 2.3: While TEMPO mediates mainly the polymerization of styrene and its derivatives, the nitroxides SG1 and TIPNO control precisely the propagation of monomers such as acrylates or acrylamides.

Today, various alkoxyamines have been developed, which provide excellent control over a broad spectrum of monomers employing the NMP technique. Already several NMP alkoxyamines are commercially available. At the same time, laboratory research focuses on pushing the boundaries of the capabilities of NMP, including the use of chiral nitroxides or cyclic alkoxyamine initiators. An example for a polymerization of styrene or acrylates *via* a cyclic alkoxyamine is depicted in Figure 2.4, yielding cyclic polymer chains with various amounts of alkoxyamine functionalities.

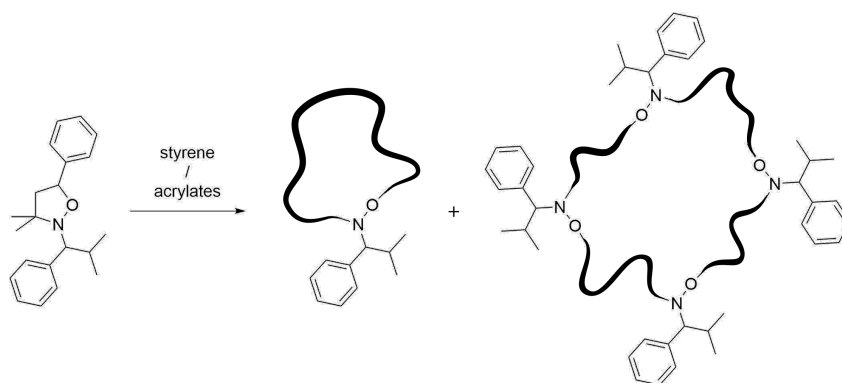


Figure 2.4: A five-membered cyclic alkoxyamine is able to polymerize styrene (derivatives) or acrylates, resulting in cyclic polymers with various content of incorporated alkoxyamine functional groups.

The versatility and tolerance of the NMP method towards various functional monomers was the decisive factor to utilize this technique for the synthesis of the functionalized co- and terpolymers, employed in the current thesis (Chapter 3, 4, 5 and 6). The robustness and resistance at elevated temperatures of the alkoxyamines and the immunity towards metal incorporation made NMP the most attractive polymerization strategy for the purpose of metal-complexed single-chain nanoparticles.

2.1.3 Reversible Addition Fragmentation Chain Transfer Polymerization (RAFT)

In the process of developing novel techniques to control the degree and dispersity of polymer chains, an essential idea was the creation of a method, in which the product of the chain transfer is also a chain transfer agent. Based on this concept, in 1998, Rizzardo, Moad and colleagues presented for the first time the mechanism of reversible addition fragmentation chain transfer polymerization (RAFT).^[42] In the same time frame, an analogous model was developed by the group of Zard limiting side product formation in radical chain polymerizations by a degenerative transfer of radical species to a xanthate.^[43, 44] The concept of the so-called MADIX technique (macromolecular design *via* the interchange of xanthates) is closely related to the RAFT process, which is why in the following chapters only the term RAFT is utilized.

Central in the RAFT mechanism is the so-called **RAFT Agent**, a thiocarbonylthio compound, which maintains an equilibrium between active and dormant species *via* the **Degenerative Effect** as a chain transfer agent.^[45] Thereby, polymer chains of a predictable molecular weight with narrow dispersity are obtained without lowering the overall radical concentration. The combination of high end group fidelity, tolerance to a broad range of monomers and the capacity to restart chain growth for the synthesis of block copolymerizations, makes RAFT one of the most versatile processes to engineer complex macromolecular architectures.^[46, 47]

RAFT polymerization consists of three basic components, *i.e.* a radical source, monomer and the RAFT agent. As a radical source, standard initiators, established in conventional FRP, are commonly employed, such as AIBN. The high adaptability of the RAFT agent, enables the use of a wide range of functional monomers in the RAFT process. Depending on the reactivity of the vinyl unit in the monomer, two groups of monomers are differentiated: **More Activated Monomers** (MAMs) and **Less Activated Monomers** (LAMs) (examples are given in Figure 2.5). Common examples for MAMs are monomers with an vinyl bond, which is adjacent to either a double bond, an aromatic ring, a carbonyl bond or a nitrile (*e.g.* butadiene, styrene, (meth)acrylates/acrylamides or acrylonitrile, respectively). In LAMs the vinyl unit is conjugated to an oxygen, a nitrogen or a halogen atom, to sulfur ion pairs or saturated carbons (*e.g.* vinyl acetate, *N*-vinylpyrrolidone, vinyl chloride, 1-alkenes).

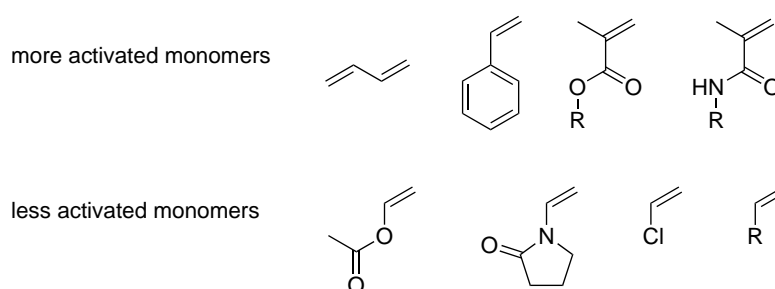


Figure 2.5: Depending on the reactivity of the vinyl unit in the monomer, two classes of monomers are differentiated: more activated monomers and less activated monomers. Examples for both classes are depicted.

The key component is the RAFT agent, which is depicted in its basic structure in Figure 2.6, *top*. The chain transfer agent comprises a reactive C=S double bond, which is connected to a so-called Z-group, and a weak C–S bond, to which a group termed R-group is attached.

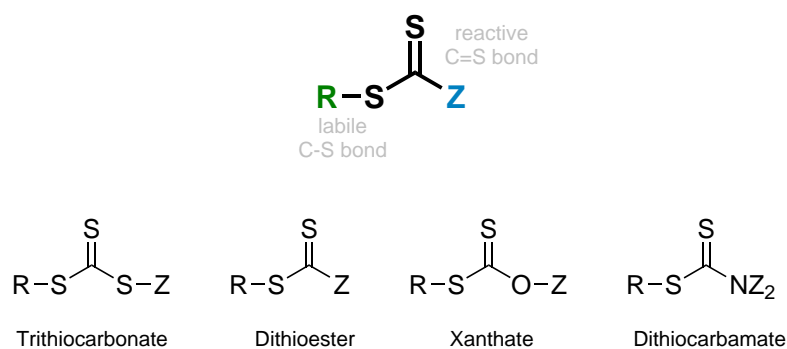


Figure 2.6: *Top:* Core structure of a RAFT agent. *Bottom:* Chemical structure of four types of RAFT agents: trithiocarbonate, dithioester, xanthate and dithiocarbamate. Depending on the employed monomer, the appropriate RAFT structure is selected and suitable R- and Z-groups are chosen.

Both the R- and the Z-groups account for the efficiency of the chain transfer agent and have to be carefully selected, dependent on the employed monomer. The **Z-Group** mainly influences the reactivity of the C=S bond. Using more activated monomers, such as styrene or acrylates, Z-groups are necessary to stabilize the intermediate radical, as found for trithiocarbonates or dithiobenzoates (Figure 2.6, *bottom*). In comparison, less activated monomers require less stable intermediate radicals, achieved by RAFT agents of the xanthates type (Z = O-alkyl) or dithiocarbamates (Z = N-alkyl). Thereby, the nitrogen or oxygen atom destabilizes the C=S bond of the RAFT agent through their delocalized electron pairs. This favors fragmentation of the intermediate radical, preventing the RAFT agent from being a radical sink.

The **R-Group** has a more complex role, responsible for maintaining a good balance between the stability of the intermediate radical and the chain radical. Therefore, the R-group has to fragment easily from the intermediate radical and be sufficiently reactive to rapidly reinitiate propagation.^[48]

Typically, a good compatibility of the RAFT agent is achieved by R-groups of similar structure than the applied monomers. Examples for Z- and R-groups and the corresponding monomers are given in Figure 2.7.

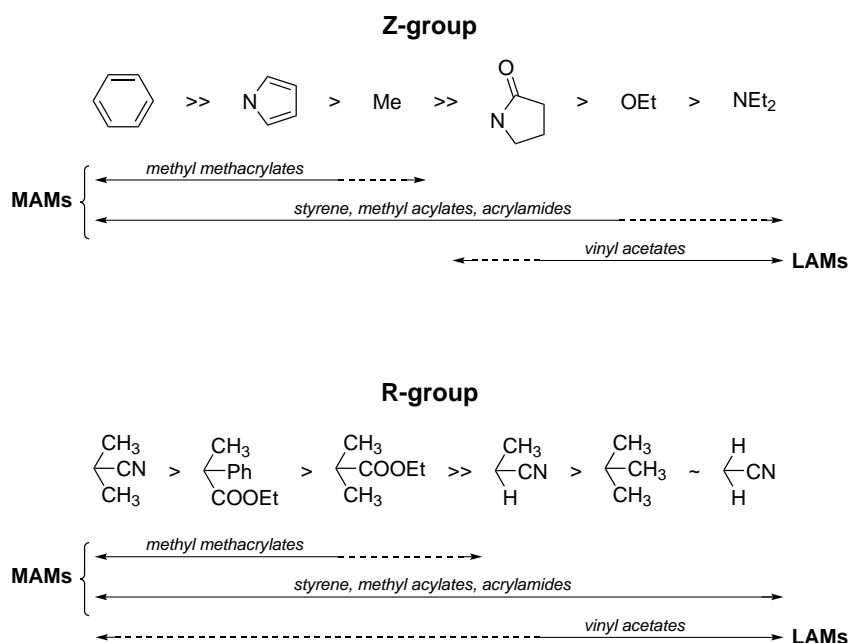


Figure 2.7: *Top:* Examples for the structure of the Z-group in RAFT agents and the related suitable monomer functionalities. The appropriate selection of the Z-group guarantees a good control over the polymerization of the particular monomer. From left to right the addition rate decreases, while the fragmentation rate increases for the corresponding RAFT structures. *Bottom:* Chemical structures of the R-group in RAFT agents for a suitable match with the corresponding monomers. The fragmentation rate for the depicted structures decreases from left to right.

One of the reasons why RAFT attracts significant interest is its ability to polymerize a vast array of monomers. Only functionalities that show potential for side reactions with the thiocarbonylthio group in the RAFT agent, such as nucleophilic substituents, are excluded. The careful selection of the RAFT agent with deliberately chosen R- and Z-groups enables numerous monomers to result in narrowly distributed, high molecular weight polymers.

The RAFT process starts with the activation of the initiator, forming a radical species, which reacts with the RAFT agent, thereby initiating the transfer reaction. In an equilibrium between active and dormant species, the macroRAFT agent simultaneously releases and traps the propagating chains (Figure 2.8). Keeping the rate of **Addition/Fragmentation Equilibrium** on a higher level than the propagating step, less than one monomer is added to the chain during one activation cycle. A higher addition rate to the macroRAFT agent is achieved by a higher activity of the C=S bond in the RAFT agent towards radical addition, compared to the activity of the C=C bonds in the monomers. Thus, without lowering the overall radical concentration, termination reactions are (almost) eliminated,

causing the chains to have identical probabilities to propagate and thus results in polymers of uniform chain length.^[49]

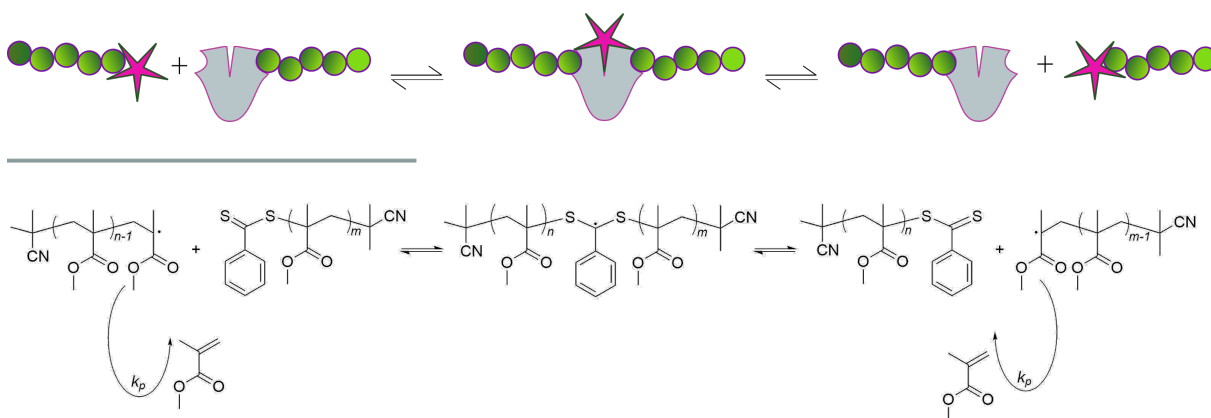


Figure 2.8: Key reaction step in the RAFT process: The equilibrium between free propagating chains and their trapped version as an intermediate macroradical enables the synthesis of polymers with predictable molecular weights and a narrow dispersity.

Interesting for post-modifications of polymer chains is the convertible thiocarbonylthio end group functionality.^[50] Easily, the thiocarbonylthio group can be converted into a thiol *via* aminolysis or hydrolysis, offering numerous possibilities for further nucleophilic attacks and thus conversion into the desired **End Group Functionality**. Another simple method to remove the end group is *via* thermolysis (150–230 °C), introducing an alkene at the chain end. A potential alternative to alter the RAFT group is a radical induced transformation, generating *in situ* a radical, which is subsequently trapped by a functional group. Instead of removing the RAFT group, the thiocarbonylthio unit can also be considered as a dienophile, reacting in a hetero Diels–Alder reactions with dienes, which opens avenues for the generation of diblock-copolymers. Among the stated possibilities, there are further methods discussed in several review articles.^[51, 52] The described examples for a functionalization of the end groups in RAFT-steamed polymers are depicted in Figure 2.9.

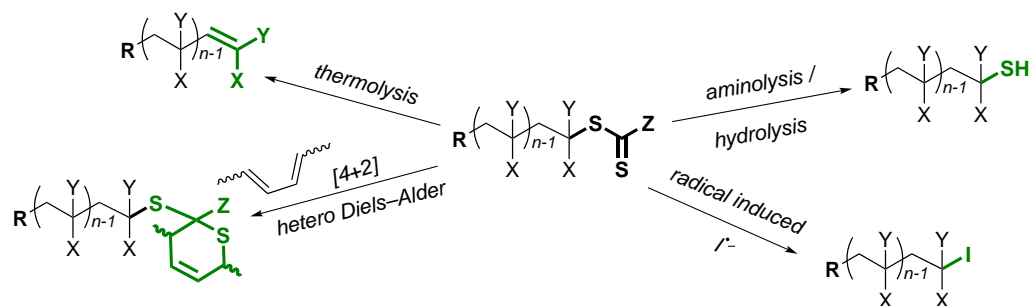


Figure 2.9: The thiocarbonylthio functionality in RAFT agents offers various possibilities to be converted into desired end group functionalities. Selected examples are depicted, including aminolysis, thermolysis, a radical induced transformation and a hetero Diels–Alder reaction with an activated diene.

In an approach described by Rubio-Cervilla *et al.*, the particular feature of dienophil activity of the RAFT agent was employed to perform a ring-closure reaction. For this purpose two functionalities, α -methylbenzaldehyde and a dithioester, were placed on each side of the chain ends. Subsequently, the chain ends reacted with each other *via* the photoactivated hetero Diels–Alder (HDA) ring-closure reaction. Utilizing appropriate reaction conditions, such as high dilution, the chain ends of the same chain connected and single-chain rings were formed. Such artificial cyclotides are of emerging interest for mimicking small cyclic polypeptides, since they exhibit, due to their exclusive ring structure, a high stability against enzymatic degradation. In the described procedure, the rings were even further collapsed *via* intra-ring copper (I) catalyzed azide–alkyne cycloaddition (CuAAC) reactions, resulting in single-ring nanoparticles (Figure 2.10).^[53]

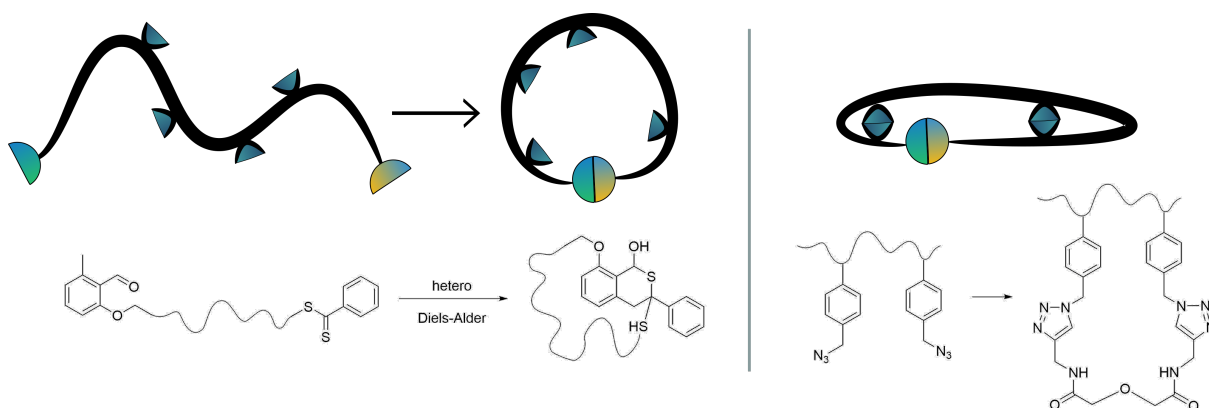


Figure 2.10: The thiocarbonylthio functionality of the RAFT agent in a polymer underwent hetero Diels–Alder (HDA) reaction with α -methylbenzaldehyde. The placement of the functionalities at each end of the chain and the performance of the HDA reaction under high dilution, resulted in the closure of single-rings. Subsequently performed CuAAC reaction caused a collapse of the rings and led to single-ring nanoparticles.

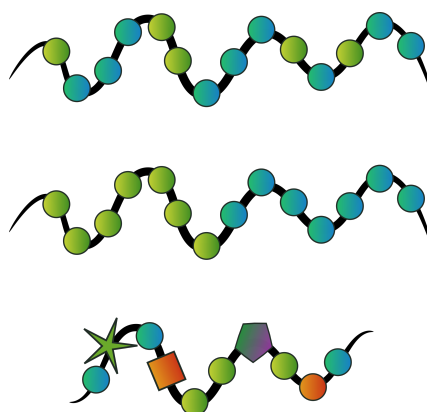
Previously, RAFT was considered to control distributions of only low molecular weight polymers. Yet, recent advances such as the performance of the polymerization at low temperatures or the initiation *via* microwave irradiation, give access to polymer chains of a molecular weight of up to $10^6 \text{ g} \cdot \text{mol}^{-1}$. Furthermore, the adjustment of the RAFT agent towards the respective reaction conditions even allows its performance in aqueous medium. Other possibilities include a lower sensitivity of the agent towards oxygen, facilitating synthesis protocols. Today, the facile synthesis procedure in different reaction media, without excessive need for purification and the good scalability of RAFT reactions make the technique relevant for industrial applications.^[54]

2.1.4 Copolymerization

Copolymerization describes, as a general term, the polymerization of more than one type of structural unit.^[55] The interest in the synthesis of copolymers is especially related to their unique trait, tuning their properties as a function of monomer type and composition. Thus, copolymers with widely varying properties can be synthesized, obtained by the incorporation of various monomers in different ratios.^[56]

Dependent on their structural arrangement, copolymers can be classified into four categories. Copolymers in which the monomers are randomly distributed in no particular order are defined as **Statistical Copolymers** (..ABBABAAABA...). If a copolymer has regularly ordered monomers, it belongs to the class of **Alternating Copolymers** (..ABABAB..). In **Block Copolymers**, long sequences contain the same type of monomer (..AAAABBBB..). Part of the category of non-linear copolymers are branched or grafted copolymers in which the main chain consists of one monomer-type and side chains are formed by the other monomer (refer to Figure 2.11, depicting examples for a statistical and a block copolymer).^[56]

Figure 2.11: Copolymers consist of more than one type of monomer. Depending on the structural arrangement, distributed copolymer chains or block copolymers with sequences of the same monomer are distinguished. The relative amount of each monomer in a polymer can be determined applying the Mayo–Lewis equation. The last example refers to recent investigations exploring the controlled placement of functional moieties in the chain.



In this section, particular focus is placed on statistical copolymers, since all synthesized and employed copolymers of the current thesis belong to this class. As the name indicates, the sequence of monomers in this category follows a statistical rule. Still, there are relevant parameters influencing the composition of the polymer. One regards the relationship between monomer feed ratio and polymer composition, often not being linear. The reason is the non-equal reactivity ratio of each component. Such reactivity ratios define, whether one type of monomer favors the reaction with its own kind or with another type of monomer. A possibility to describe the procedure of monomer addition is the **Terminal Model**, narrowing that only the last segment in a propagating chain affects the subsequent monomer addition.

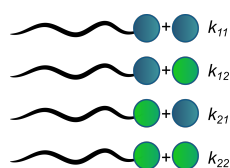


Figure 2.12: The terminal model describes the addition of a monomer to the propagating chain as an affection by the last segment in the chain. For a two component system with the monomers M_1 and M_2 , four reactions can occur. The reactivity ratio for each component is calculated by the ratio of the rate constants k_i .

For a two component system (Figure 2.12) with monomer M_1 and M_2 , four potential reaction steps occur at the chain end of a macromolecule: $M_1 + M_1$, $M_1 + M_2$, $M_2 + M_1$ and $M_2 + M_2$. Based on the rate constant k_i of each reaction, the reactivity ratios r_i of the participating monomers are calculated.

$$r_1 = \frac{k_{11}}{k_{12}} r_2 = \frac{k_{22}}{k_{21}}$$

Knowing the reactivity ratios r_1 and r_2 , the mole fraction F_1 of monomer M_1 in the copolymer can be calculated *via* the **Mayo–Lewis Equation**, the copolymerization equation.^[57] The mole fractions of M_1 and M_2 in the monomer feed are labeled f_1 and f_2 , respectively.^[58] Similarly, the Mayo–Lewis Equation can equally be calculated applying the monomer concentrations.

$$F_1 = \frac{r_1 f_1^2 + f_1 f_2}{r_1 f_1^2 + 2 f_1 f_2 + r_2 f_2^2}$$

An even preciser approximation for the monomer composition in the polymer is obtained applying the **Penultimate Model**. Here, the two last segments of a polymer chain are considered as well. However, applying this model in a two component system, there are already eight different rate constants and consequently six reactivity values to consider, increasing significantly the level of complexity. Therefore, for most of the systems, the application of the terminal model is completely sufficient.

Today, scientists investigate the exquisite, controlled placement of functional units along the polymer chain (last example in Figure 2.11). Such **Sequence-Controlled Polymers** consist, to some extent, of intentionally ordered monomer units.^[59] In its easiest form, an alternating polymer is a sequence-controlled polymer. Yet, such polymers do not necessarily have a uniform chain length. Exact chain length and perfectly defined sequences are only realized in **Sequence-Defined Polymers**.^[60, 61] However, the synthesis protocols for fully sequence-controlled polymer materials are still high demanding and often limited to the synthesis of short oligomers *via* iterative steps.^[62]

2.2 Supramolecular Metallopolymers

A class of supramolecular architectures, which warrants particular mention, are **Metallopolymers**, which combine the mechanical properties and processing advantages of polymers with functional metal ions. The resulting materials are of high diversity in structure and dynamics, providing access to luminescent or magnetic properties, or catalytic function.^[63–65] The overall term "metallopolymers" comprises any combination of metal ions with polymeric material. However, in the current context, it refers to a macromolecular construct, which exists in a stable form as a solid and also in a dissolved state. Thereby, the metal ions are either an integral part of the backbone or implemented in the repeating units in the side chain (refer to Figure 2.13).^[66, 67]

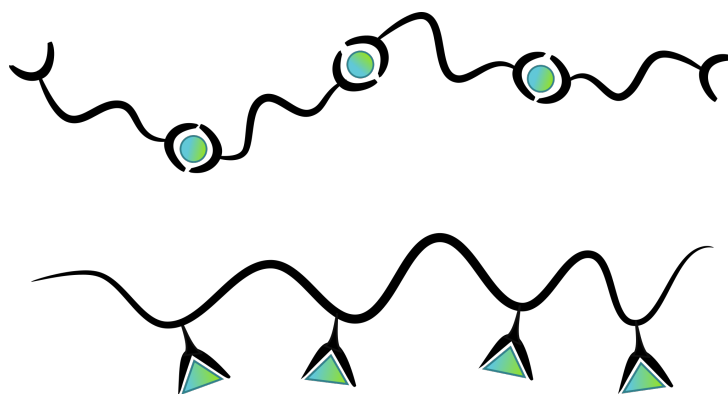
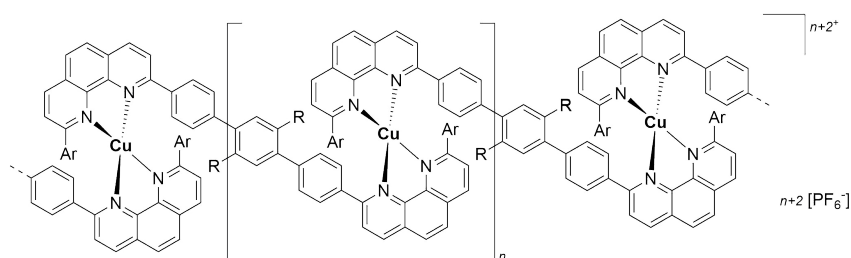


Figure 2.13: Schematical structures of supramolecular metallopolymers. *Top:* One approach employs metal ions as independent monomers in the backbone, opening avenues for a myriad of applications, such as data storage, superconductors or as framework for the synthesis of stimuli-responsive material.^[68] *Bottom:* Alternatively, the metal ions are part of the repeating units, located in the side chain.

In earlier years, the synthesis protocols for a direct polymerization of metallic monomer units were limited due to side reactions entailed by metal ions. However, today many procedures have been developed, tolerating the presence of metal compounds. An extensively studied subclass are polymetalloenes, for instance based on ferrocene, interesting as redox-responsive material.^[69] For their synthesis, strained ferrocenophane monomers are polymerized *via* ring-opening polymerization to result in material of stable, covalent Fe–Cp interactions.^[70] In comparison, supramolecular material of more dynamic behaviour is produced by employing nickelocene instead of ferrocene. Due to the weaker Ni–Cp interactions, monomer and cyclic oligomeric material form a reversible, dynamic equilibrium.^[71] Such systems are particularly interesting, when speaking about self-healing and stimuli-responsive properties.^[7, 68, 72]

Another approach utilizing metal ions as independent monomers was reported by Velten and Reahn,^[73] developing a strategy to stabilize kinetically unstable metal complexes. Often, this class

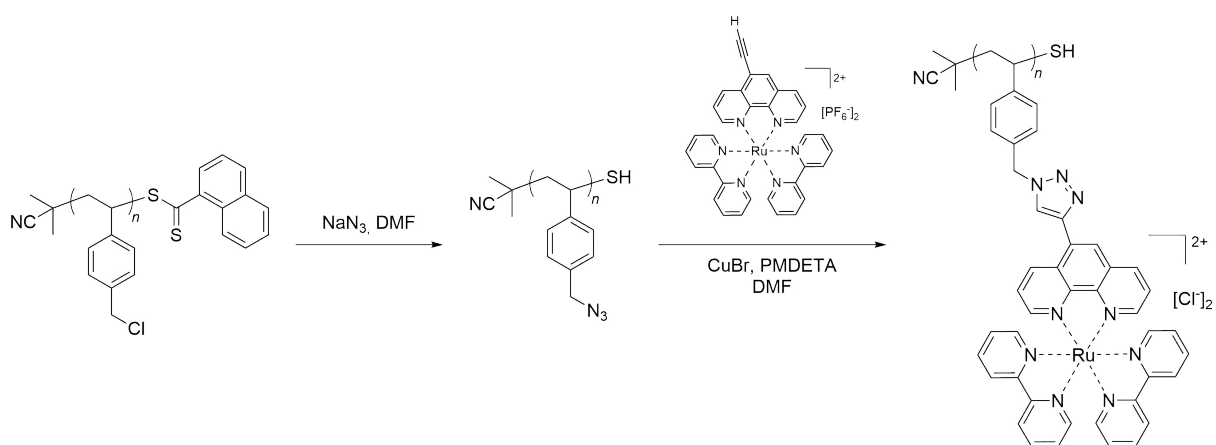
of metallopolymers easily decomposes, due to coordination to competitive ligands. However, their realization would allow access to supramolecular structures, such as polycatenanes. In the presented study, the applied monomer units were σ -phenanthroline derivatives, coordinating to copper(I) in the solvent 1,1,2,2-tetrachloroethane. Thus, high molar mass polymer of up to approx. $45\,000\text{ g} \cdot \text{mol}^{-1}$ was obtained. The structure of the metallopolymer is depicted in Scheme 2.5.



Scheme 2.5: Linear supramolecular metallopolymers are formed *via* coordinative linkages of σ -phenanthroline ligands with copper(I) ions. The performance of the synthesis in 1,1,2,2-tetrachloroethane enables metallopolymers consisting of kinetically unstable metal complexes.

In a more elaborate approach, metallopolymers are accessed by employing the method of subcomponent self-assembly. Inspired by natural DNA, two conjugated helical ligand strands are formed *via* copper(I) directed imine bond formation. This topic is of great interest for the field of polyelectrolyte electroluminescent devices.^[74]

In comparison to the so far presented methods, there are also many systems, in which metal complexes are part of pendent side chains in polymers. Widely used are ruthenium ions, forming high stability complexes with various application possibilities in the field of light emitting materials.^[75] The implementation of metal ions into polymer chains is often carried out by a postmodification of already existing polymer chains, as done in the work of Schanze and coworkers. After having synthesized monodispers polymer chains *via* RAFT, the chloride side group of the monomers was modified to an azide. Subsequently, the azide reacted with an alkyne, which contained a ruthenium complex. The resulting Ru(II) metallopolymers were found to be efficient light-harvesting material (Scheme 2.6).^[76]



Scheme 2.6: An example for the synthesis of a metallopolymer with metal complexes in the pendent side groups. After RAFT polymerization of 4-vinylbenzylchloride, the RAFT group was removed from the polymer chain while the chloride in the side chain was simultaneously transformed into an azide unit. In the last step, a ruthenium precursor complex was grafted onto the chain *via* a click reaction, resulting in Ru(II) metallopolymers.

2.3 Single-Chain Nanoparticles (SCNPs)

Parts of the section are reproduced from Rothfuss*, H; Knöfel*, N. D.; Roesky, P. W.; Barner-Kowollik, C. *J. Am. Chem. Soc.* **2018**, *140*, 5875-5881. Copyright 2018 American Chemical Society.

2.3.1 General Remarks on SCNPs

Intriguing in the field of polymer science is the development of smart materials with novel properties. Thereby, the synthesis of sophisticated architectures, molecular machines or natural occurring biomacromolecules *via* artificial polymer synthesis is targeted.^[77-80] A long sought-after goal of polymer chemists has been to artificially replicate the conformation and composition of complex natural enzymes, outstanding examples for a structure-function relationship. One avenue to realize the creation of such ambitious, three dimensional nanoreactors is the synthesis of single-chain nanoparticles (SCNPs), displaying exceptional diversity in structure and dynamics.

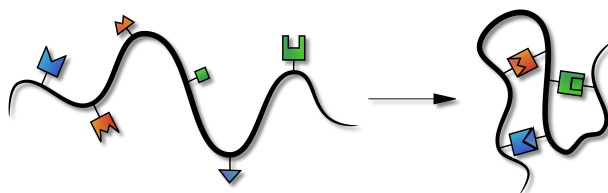


Figure 2.14: Schematic depiction of a collapse of a single-chain into a compact nanoparticle *via* an external trigger. The depicted process follows the selective point folding approach. Hereby, orthogonal units are placed judiciously along the polymer chain and react only with their corresponding partner. This allocation of reaction partners provides a high control over the structure of the nanoparticle. However, the synthesis of such a precursor polymer requires high synthetic effort.

Single-chain nanoparticles are polymer chains that are collapsed *via* an external trigger into compact nanoparticles (Figure 2.14). Specifically, intramolecular linkages within the chain result in small, sub-component, soft colloids with a diameter between 3 to 30 nm, close to the size of metalloenzymes.

The concept and synthesis of SCNPs is inspired by the highly structured, sophisticated architectures of natural enzymes.^[81] In early approaches, intramolecular linkages based on hydrogen bonds were employed to mimic the well-organized molecular entities of such biomacromolecules. However, the range of chemical bond formation for a chain collapse has been expanded to include other crosslinking mechanism.^[82] Today, the collapse of polymer chains into nanoparticles is triggered *via* non-covalent, covalent or even coordinative intrachain linkage formation.^[1-4] Simultaneous with the expansion of synthetic methods, SCNPs have rapidly attracted significant interest, due to their comprehensive application possibilities as smart adaptive materials. SCNPs complete complex tasks in various areas, such as sensing,^[5] drug delivery,^[6] as healable materials^[7] and in catalysis.^[8]

From a synthetic point of view, SCNPs can be categorized into two groups depending on their folding mechanism: **Selective Point Folding** and **Repeat Unit Folding**. In the **Selective Point Folding** approach, orthogonal units are placed along the chain. Upon triggering the collapse, only the corresponding reaction partners form linkages between each other, as shown in Figure 2.14. Examples for complementary recognition motifs include hydrogen bond formation in the six-point cyanuric acid–Hamilton wedge system or the association of adamantane into β -cyclodextrine.^[83] Despite the advantage of a predetermined chain collapse, the concept of selective point folding requires high synthetic effort and the variety of applicable motifs is limited.

Easier to realize is the **Repeat Unit Folding** approach, in which functional groups are randomly distributed along the chain, as depicted in Figure 2.15. During the folding process, linkages between functional units are formed almost arbitrarily. Most of the dependent variables are physical constraints, for instance, chain stiffness, which requires a minimum loop-size. Although the dense coils are probably folded without order, the current approach provides easy folding protocols and gives almost unlimited choice of chemical reactions to trigger the collapse.^[84]

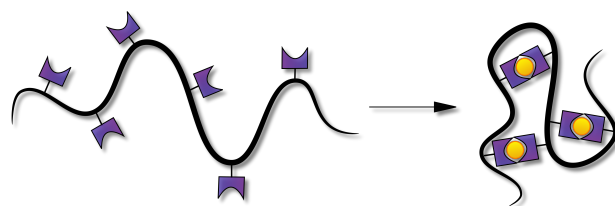


Figure 2.15: Single-chains collapse into compact nanoparticles *via* the addition of external linker molecules. The depicted process follows the repeat unit approach, in which the same type of functional units are distributed statistically along the chain. During the folding process, all units are able to interact with each other and form linkages.

Independent of the folding mechanism, most importantly is the exclusive formation of intramolecular bonds, implying the collapse of a single-chain. Whereas multiple-chain folding harbours the risk of insoluble network formation, only single-chain folding permits access to well-defined nano-objects with confined local pockets (refer to Section 2.3.2). For this reason, a general requirement for the synthesis of SCNPs is the suppression of intermolecular bond formation. Whereas some approaches simply perform the nanoparticle formation under highly diluted conditions, often achieved by application of a syringe pump,^[85] there are also advanced synthesis procedures. For instance, Pomposo *et al.* developed a solvent based strategy to prefold single-chains, by exploiting the different solubility behavior of the applied monomer units in the polymer.^[86] Providing a close proximity of the reaction partners, the process of folding chains into nanoparticles could be performed at higher concentrations than in common synthesis protocols. Recently, the **Proximity Effect** was further exploited by Frisch

et al., folding single-chains at exceptionally high concentrations (approx. 10 times higher than reported normally). In his work, styrylpyrene units were placed along the chain, creating a confined environment. The subsequent light induced linkage formation *via* a [2+2] photocycloaddition of styrylpyrene has proved successful for a precise temporal and spatial control of the single-chain compaction.^[87]

While SCNPs can be distinguished by the process of chain collapse, they can also be differentiated by the **Nature of Chemical Bonds** within the chain, refer to Figure 2.16. Due to the growing interest in the field of SCNPs technology, the toolbox for novel, refined intrachain crosslinking procedures has expanded.

In the class of covalent bond formation, many folding routes have been established, such as light-induced dimerization or thermal induced [4+4] cycloadditions of pendant groups (example a + b),^[3, 87–90] nitroxide reactions or disulfide bond formation *via* externally added linker molecules (examples c + d),^[91, 92] UV light induced imine-mediated tetrazole-ene cycloaddition (example e),^[93, 94] Diels–Alder reactions,^[95] or ring-opening polymerization of epoxide side chains.^[96]

One concrete example is the photoinduced [4+4] dimerization of anthracenes, as described by Berda and coworkers.^[90] The particular feature of this study is the formation of covalent C–C bonds between anthracene units, allowing the reopening *via* UV light or at elevated temperatures.

Such a reversibility of intrachain linkages, enabling to rearrange the architecture, is a key principle in natural enzymes enabling their easy adaption towards changing reactions conditions.

An easier access to structurally dynamic materials is given by employing reversible bond formation *via* weak, non-covalent linkages, such as hydrogen bonds or π - π stacking (example f).^[2] A new type of non-covalent bonds for SCNP formation was recently reported by the group of O'Reilly presenting a promising pathway towards SCNP systems utilizing ionic liquids (example g) with broad potential in catalysis. Based on imidazolium units, catalytically active *N*-heterocyclic carbenes are generated at high temperatures. Acidic side groups in the same polymer chain serve as counter ions for electrostatic interactions, thus creating defined SCNP pockets.^[97]

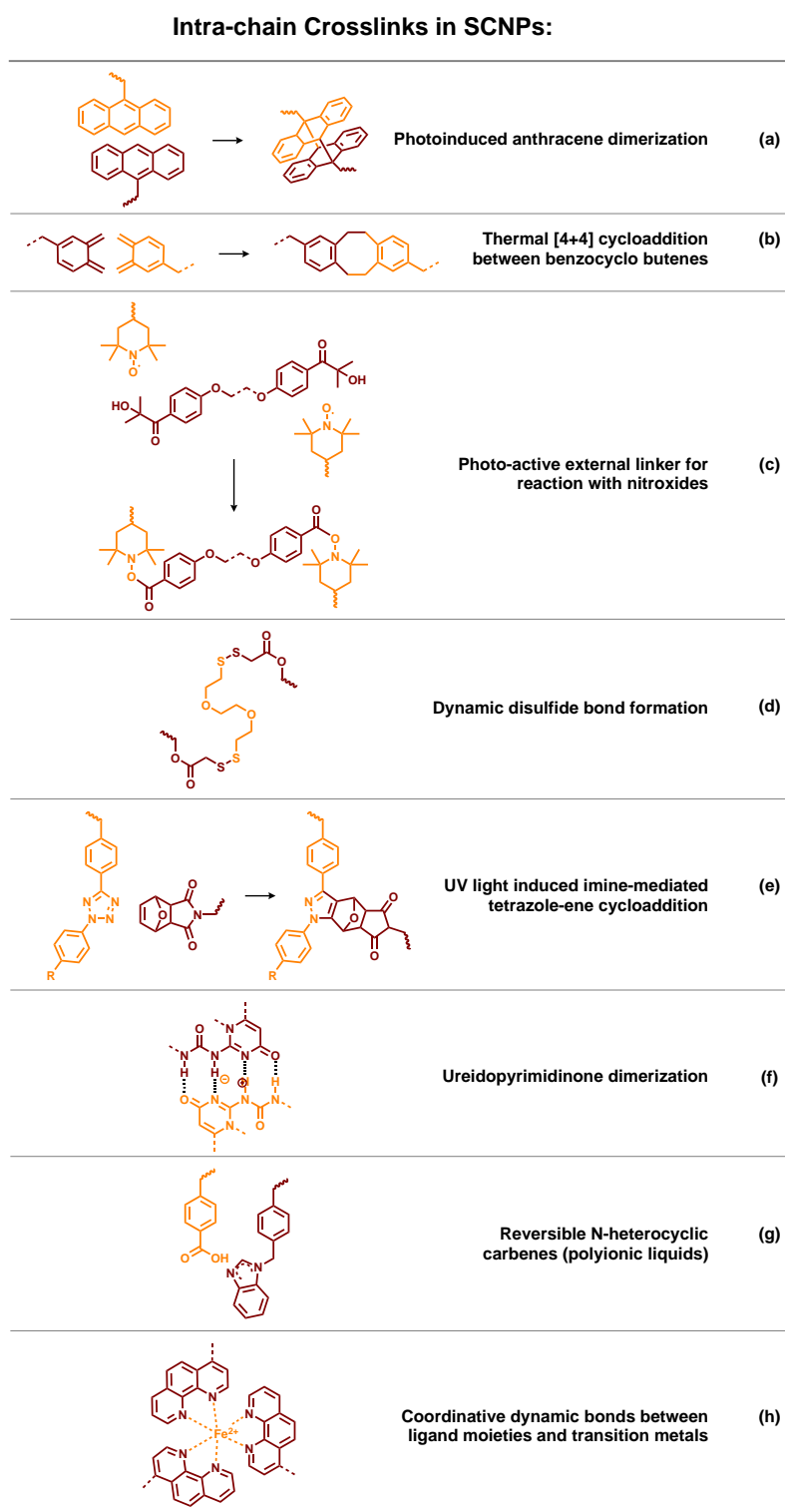


Figure 2.16: A vast array of chemical reactions can be employed to form intramolecular crosslinks within single-chains, yielding SCNPs.

A combination of two different non-covalent binding principles for SCNP formation has been described by Meijer and coworkers (Figure 2.17).^[98] In their work, they emulated helical threads *via* helical stacking of chiral benzene-1,3,5-tricarboxamide (BTA) units, stabilized by hydrogen bonds. In detail, a terpolymer was synthesized consisting of BTA units, poly(ethylene glycol) (PEG) moieties and a third functionality with a *L*-proline motif. While the PEG units ensured a solubility of the terpolymer in aqueous media, the *L*-proline groups provided catalytic functionality in an aldol reaction. In a similar system, the same group employed pendant phosphine groups instead of the *L*-proline motif.^[99] After the chain folding *via* the BTA units, the phosphine groups coordinated to ruthenium(II) ions, resulting in catalytically active SCNPs.

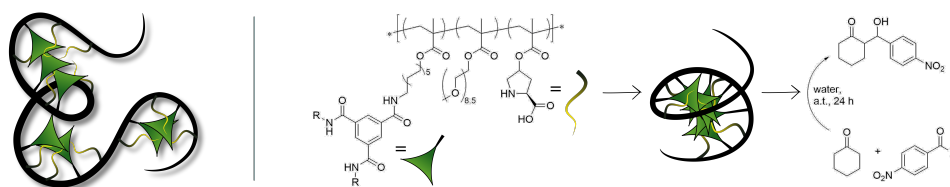


Figure 2.17: Meijer and coworker developed the synthesis of a terpolymer, consisting of BTA units, PEG functionalities and pendent *L*-proline groups. In the polymer, each monomer has a characteristic role, contributing to the overall properties of the polymeric lattice: The BTA units stack helically onto each other, generating hydrogen bonds between each layer. The PEG units ensure a good solubility of the whole macromolecular construct in polar solvents, enabling the *L*-proline units to be catalytically active in an aldol reaction. Adapted from [8] with permission of the American Chemical Society.

Although in the aforementioned example the chain collapse was not triggered by metal ions, certainly metal–ligand coordination serves as a powerful avenue for SCNP formation (example h in Figure 2.16). Numerous experiments focus on the creation of **Metal-Complexed Nanoparticles** as an appealing pathway to combine single-chain collapse and function implementation.^[100] Due to the high relevance of the last class of SCNPs in the context of the current thesis, Section 2.3.2 is devoted to metal-complexed SCNPs.

2.3.2 Metal-Complexed SCNPs

With the evolving topic of single-chain nanoparticles, interests grew enhancing their diversity in structure and dynamics. Therefore, the combination of metal ions with a polymer lattice seems appealing. This approach links the easily adjustable characteristics of polymeric materials with metal ion induced properties ranging from magnetic to optical or catalytic areas. The resulting hybrid materials are smartly adaptive and open up a variety of potential applications, exhibiting unrivaled traits in diverse categories, such as selectivity, stabilization or recyclability.^[8] Moreover, the encapsulation of metal ions in SCNPs entails, for instance, a local separation of metal ions, thus suppressing their aggregation and potential deactivation.^[101] In addition, compartmentalized three dimensional structures allow local concentrations of active species, stabilized by the polymer lattice, which can even enhance their activity.

Before describing the existing synthetically techniques to incorporate metal ions into SCNPs systems, two examples of early work in the field of metal-complexed SCNPs are presented, emphasizing the importance of polymer-encapsulated metal ions.

A milestone is the work of Perez-Baena *et al.*, who introduced **Gadolinium(III)-Decorated SCNPs** as contrast agents for magnetic resonance imaging (MRI).^[102] Being one of the few examples employing lanthanide ions in SCNP chemistry, their study additionally demonstrates the necessity of nanoparticle formation in contrary to linear metallopolymers. For a successful enhancement of sensitivity in MRI, high relaxivity values are required for the contrast agent. However, such values can not be reached by simple linear metallopolymers due to their high chain flexibility. To decrease the internal flexibility, the chains are intramolecularly crosslinked *via* Gd(III)-containing bifunctional linker molecules (Figure 2.18). As a result, Gd(III)-decorated SCNPs are obtained, limited in agility and thus suitable for MRI technique.



Figure 2.18: Gadolinium(III)-decorated linear metallopolymers vs Gd(III)-SCNPs. For their suitability as contrast agents for magnetic resonance imaging, the Gd(III)-containing substances require reduced internal flexibility, achieved by crosslinking the chains into nanoparticles.

In a further approach, Paik and coworkers described how a polymer based support can improve application aspects of former molecular structures. Due to the π – π -stacking of the aromatic rings, **Copper Metallated Phthalocyanines** tend to form non-soluble aggregates, limiting their usage as chromophores in light-emitting devices. A solution was the physical separation of the copper units *via* embedding them in polymer chains. Therefore, phthalonitrile units in the polymer chain enable intramolecular macrocyclization upon CuCl addition and molecular phthalonitrile addition. The resulting Cu(II)-SCNPs were soluble in various organic solvents, offering access to solution processable Cu(II) phthalonitrile dyes.^[103]

Applying the techniques of modern polymer chemistry, there are three synthetic methodologies to incorporate metal ions into a SCNP system: i) Already collapsed single-chains featuring additional functional groups ready to coordinate to subsequently added metal ions. ii) One single metal-containing site is attached to the polymer system prior or after the collapse, non-participating in the folding process. iii) Metal ions induce the chain collapse into nanoparticles, forming dynamic coordinative crosslinks within the chain. The chain collapse, induced by externally added metal ions is schematically depicted in Figure 2.19 (explanation and description of the other two approaches are presented later).

Whereas approaches i) and ii) follow the conditions for a "regular" single-chain folding, the pathway of triggering the intramolecular collapse *via* metal ions needs some synthetic considerations.

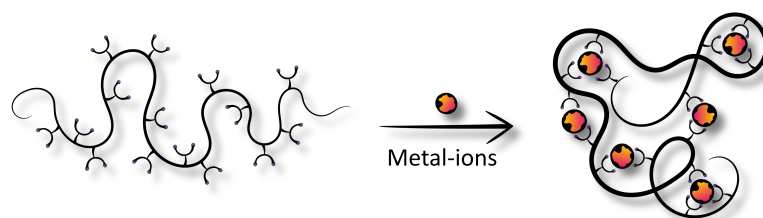


Figure 2.19: Synthesis of single-chain nanoparticles by coordinating externally added metal ions to ligand moieties in the polymer chain. This process leads to single-chain folding with concomitant functional unit insertion.

For a successful metal-induced collapse of a polymer chain, a minimum ligand-to-metal ration of $\geq 2:1$ is required. The precursor metal complexes either have to feature free coordination sites or readily replaceable ligand moieties, leaving the precursor complex upon polymer addition. In case of a substitution by the polymer, the ligand moieties in the chain have to bind stronger to the metal ion than its initial ligands. In addition to the binding constants, the steric demand has to be considered. The coordination of the functional motifs in the polymer can lead to strains in the backbone. Thus, especially in polymers with rigid backbone, the functional units within the chain should be arranged with a sufficient amount of spacer monomers. Space demanding side groups in

the polymer might limit the accessibility of the intended ligand moieties and have a negative influence on a metal incorporation.

In all approaches, independent of the mechanism of metal embedding, the polymer chain forms local pockets around the metal ion cores, generating confined entities with potential catalytic activity. Provided that the polymeric material is only loosely collapsed around the metals, the thus formed catalytic centerpiece mimics the active site of **Metalloenzymes**. This is of significant interest, since more than one third of all proteins are metalloproteins,^[104] showing tailor-made catalytic cavity for an efficient substrate-to-product transformation. Metalloenzymes are outstanding in their structure-function relationship, which is still only scarcely replicated in the laboratory.

Although not close to natural perfectness, interesting effects have been observed for catalytic SCNPs, regarding substrate specificity, product selectivity or increased stability, when encapsulating metal ions into a polymeric scaffold.^[8]

Thus, the present thesis highlights in particular the first steps towards metal-complexed SCNPs as catalytic nanoreactors, mimicking natural enzymes.

One of the first approaches for a chain collapse *via* metal ions and a simultaneous functionalization of the nanoparticles was described by the group of Lemcoff.^[105] Employing rhodium(I) ions, these authors reported the reaction of $[\text{RhCl}(\text{C}_2\text{H}_4)_2]_2$ with a polymer of **Polycycloocta-1,5-Diene** by direct exchange of the labile C_2H_4 . In similar reaction procedures, Ni(II) ions and Ir(I) ions were separately embedded into polymer scaffolds. In one attempt, even both Rh(I) and Ir(I) ions were embedded into the same structure. Thereby, the amount of each type of metal ion was defined by the ratio of the applied precursor complexes. Although employing only one ligand in the polymer chain, **Bimetallic SCNPs** were obtained. In subsequent experiments Lemcoff *et al.* showed the catalytic activity of the **Rh(I)** and **Ir(I) SCNPs**, described in the following paragraph.

In a detailed study, these authors compared the catalytic activity of metal-complexed SCNPs with molecular model complexes. Highly relevant are the results of the cross-coupling reaction between 4-nitrobenzaldehyde and phenyl boronic acid, catalyzed either by Rh(I)-SCNPs or the molecular analogue $[\text{Rh}(\text{I})\text{Cl}(\text{cod})]_2$, respectively (refer to Figure 2.20). Applying the molecular catalyst, a product mixture of homo- and hetero-coupled substances was obtained. In comparison, only the homo-product was obtained for the Rh(I)-SCNPs (>99 %). As shown in further experiments, this product selectivity is most likely a result of the closely packed environment around the Rh(I) ions in the SCNP units.

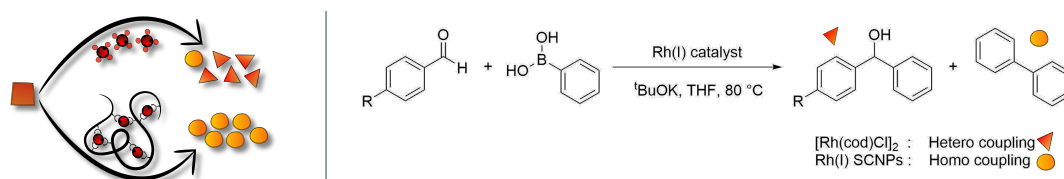


Figure 2.20: Conceptual difference between a molecular catalyst and catalytically active SCNPs: A significant impact on the product ratio is observed when a molecular catalyst $[\text{Rh}(\text{cod})\text{Cl}]_2$ is substituted by Rh(I)-SCNPs. Adapted from [8] with permission of the American Chemical Society.

The above study did not only introduce for the first time different types of metal ions into one polymer system and thus trigger the chain collapse, even more important, an influence on the catalytic activity was observed when applying SCNPs instead of molecular catalysts.

A further example for the interference of the polymer lattice of **Cu(II)-SCNPs** in catalytic process's was reported by Sanchez-Sanchez *et al.*^[106] In a facile synthesis route, copper-containing SCNPs were accessed *via* coordination of $[\text{Cu}(\text{OAc})_2]$ to β -Ketoester ligand moieties in a 1:2 ratio. When employing the resulting Cu(II)-SCNPs as catalysts in the coupling reaction of terminal acetylenes into 1,3-diynes, unexpected results were obtained. From a mixture of terminal acetylenes, the Cu(II)-SCNPs transformed exclusively one starting compound into its 1,3-diyne product, as depicted in Figure 2.21. This unprecedented selectivity was only observed for the Cu(II)-SCNPs, neither one of the compared molecular catalysts, such as $[\text{Cu}(\text{OAc})_2]$ or $[\text{Cu}(\text{acac})_2]$ were found to be selective. A hypothesis for this behavior is the formation of an optimum transition state of the specific starting compound caused by the polymer chain, favoring its substrate binding and subsequent transformation.

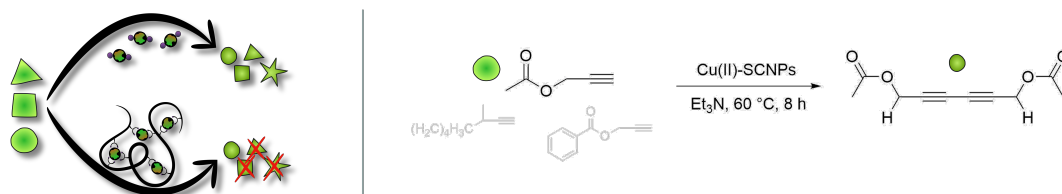


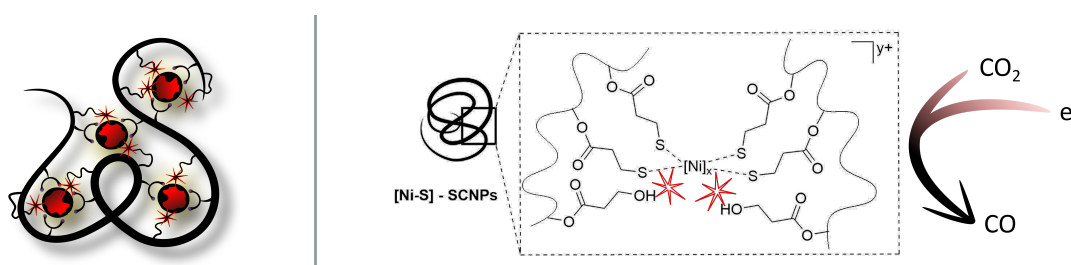
Figure 2.21: Cu(II)-SCNPs as catalysts show unique substrate specificity in an oxidative coupling of terminal acetylenes. In comparison with the molecular analogue, a product mixture is obtained. Adapted from [8] with permission of the American Chemical Society.

The importance of a stable metal incorporation, when using metal-complexed SCNPs for catalysis was revealed in the work of Willenbacher *et al.*^[9] In a straightforward synthetic route, palladium(II) ions crosslinked intramolecularly phosphine-containing copolymers, yielding **Pd(II)-SCNPs**. However, although the Pd(II)-SCNPs were successfully employed as catalysts in a Sonogashira cross-coupling reaction, the harsh reaction conditions led to leaching of the metal ions, thus only linear chains

without catalytic function remained. A plausible reason is a change in the oxidation state of the metal ions, weakening the phosphine–palladium bond.

The challenge of metal-leaching and the corresponding recyclability of SCNPs-catalysts was further investigated in own experiments, refer to Chapter 3.

Under different circumstances the encapsulation of metal ions by polymer chains can also increase the stability of a complex. This was shown in the recent study of He and coworkers, by creating **Ni(II)-SCNPs** of enhanced stability for photo-reduction of CO₂ at higher temperature.^[107] Therefore, these authors used **Thiols** as binding motifs in their precursor polymers. Upon complexation with transition metal ions, such as Ni²⁺, Zn²⁺ or Co²⁺, metal-thiolates are formed, mimicking active units of metalloenzymes for the metabolism of CO₂. This, originally biological transformation, is of high interest for the conversion of CO₂ into carbon-based fuel. One way for its technical realization is to mimic the metalloenzymes by metallofoldamers, whereby polymer chains imitate the protein framework. In their work, the embedding of the ions into a polymer lattice was essential to stabilize the metal-thiolates and to promote the selectivity of the catalytic unit. With novel synthetic strategies, the group of He created a terpolymer based on methacrylates with thiol-functional groups, depicted in Scheme 2.7. The monomer contained hydroxyl groups as local proton sources, supporting the activation of CO₂. Ni(II)-SCNPs are formed *via* the addition of Ni(II) ions, and subsequently employed in the photoreduction of CO₂. Unexpected results were obtained, showing a higher stability of the Ni(II)-SCNPs than the metalloenzymes at elevated temperatures (80 °C instead of ambient temperature), thus allowing higher turn-over-frequencies. Discussed is a positive synergism between the Ni(II) centers and the polymer framework, promoted by the hydroxyl groups in the side chain.



Scheme 2.7: Synthesis of Ni(II) foldamers *via* coordination of NiCl₂ to thiol-functionalized chains, employed in the photoreduction of CO₂. The embedding of metal ions into the polymeric scaffold stabilized the complex and thus allowed the performance of the catalytic reaction at higher temperatures than the biological Ni(II) metalloenzymes, resulting in higher turn-over frequencies. Additional hydroxyl side chains in the polymer are discussed to positively influence the catalytic selectivity. Adapted from [8] with permission of the American Chemical Society.

Those additional binding sites contribute to the so-called **Secondary Coordination Site Effect**, in which compounds, not directly part of the catalytic unit, influence the catalytic activity. Factors include the stabilization *via* tailor-made polymeric cavities or substrate binding sites in close proximity

to a reactive metal center. The "protection" of catalytic centers becomes increasingly important, when SCNPs actually replace metalloenzymes and operate inside living cells. The biological conditions, such as changing pH-value, temperature and various substrates, demand for a protein-like shell, realized by polymer chains.

Putting this into practice, Zimmermann and colleagues synthesized **Cu(II)-SCNPs** for a copper-catalyzed alkyne-azide cycloaddition (CuAAC) inside living cells.^[108, 109] For the emulation of metalloenzymes, the SCNPs needed to be water-soluble, catalytically active and containing additional binding sites for hydrophobic substrates. Those needs were addressed by a copolymer with imidazolium units for facile solubility, long alkyl chains for the binding sites and amino acids for complexing the catalytic unit copper(II). The embedding of metal ions transferred the polymer coils into compact particles, sufficiently small to enter living cells and to perform the CuAAC reaction. It was assumed that the low catalyst loading of copper does not intoxicate the cell, however the metal-leaching was not investigated.

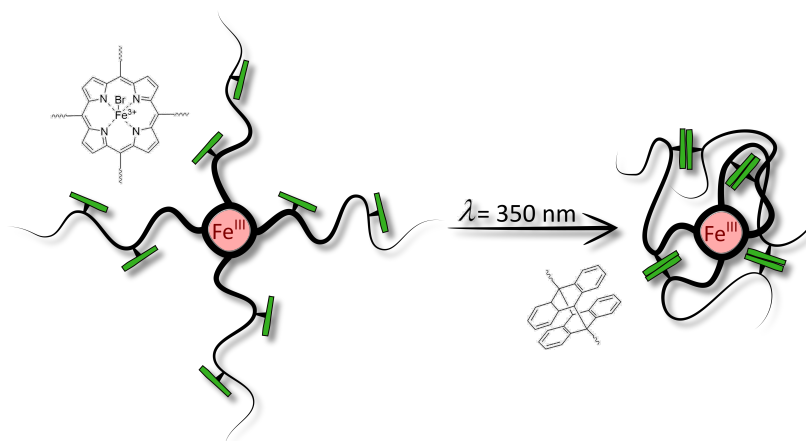


Figure 2.22: A four-armed star polymer exhibits a porphyrine heme core and anthracene side groups. After phototriggered dimerization of the anthracene groups, the polymer chains form a macromolecular environment around the metal ion. The polymer pocket around the metal center is most likely the reason for its high activity and stability.

A fundamentally new route to investigate the influence of a macromolecular environment in catalytic systems was proposed by the groups of Berda and Pazicni. In two studies, these authors re-constructed the active site of naturally occurring enzymes in SCNPs, the hydrogenase with an active **[FeFe]** unit and a model **Fe(III)-Heme** core.^[110, 111] In both systems, the chain collapse was not triggered by the metal ion, yet instead performed by a photo-induced dimerization of anthracene containing side groups. Whereas in the **[FeFe]** study the active site is attached to the polymer chain end, in a more

developed version, the porphyrine heme core sits in the center of the four armed polymer chain, as depicted in Figure 2.22. This ensures a complete encapsulation of the Fe(III) heme core model after nanoparticle formation and most likely attributes to its stability towards undesired side reactions. In comparison to native heme proteins, the model complex exhibited similar reactivity.

However, metal ions can just as well be incorporated into polymeric structures after the chain collapse. The presence of at least two different functional moieties in the polymer chain is required, one to perform the chain collapse and another one to build the metal complexing unit, as schematically depicted in Figure 2.23.

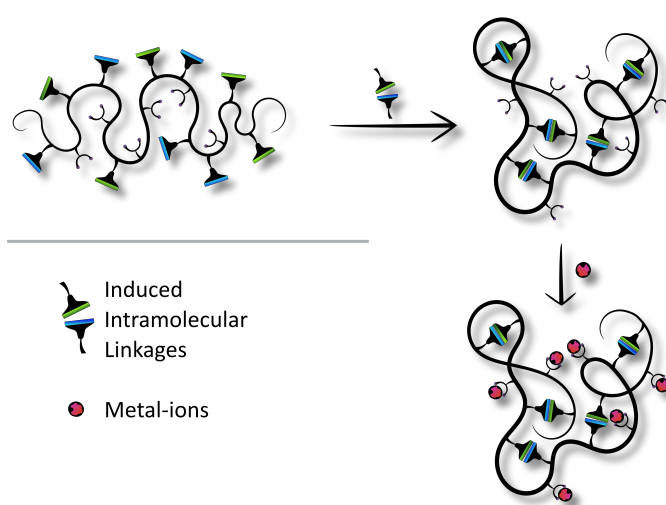
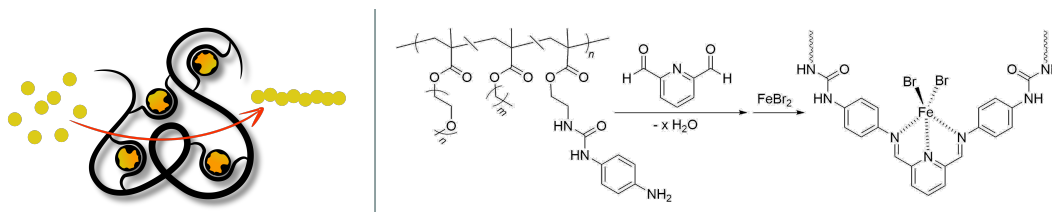


Figure 2.23: Synthesis of single-chain nanoparticles without involvement of metal ions, which are incorporated after the collapse. Necessary are at least two functional units in the polymer chain to allow chain folding and metal ion coordination.

Following such an approach, Sawamoto and coworkers first intramolecularly crosslinked amphiphilic copolymers into nanoparticles. Subsequently, **Fe(II) ions** were encapsulated into the generated ligand cavities (Scheme 2.8).^[112] While the element iron exists in a high abundance on earth and has potentially low toxicity, its drawback is its low stability and tolerance of polar groups. However, the coordination of Fe(II) ions to **Bis(imino)pyridine** ligands was sufficiently strong enough to allow their further application as a catalyst in living radical polymerization. The specific structure of the catalyst even allowed its recyclization. Due to hydrophilic poly(ethylene glycol) side groups in the copolymer, the catalyst remained in solution, while the newly formed polymer precipitated in MeOH.

Exploiting the structural and material facets of polymers, Meijer and colleagues reported a supramolecular SCNP-based system with compartmentalized, catalytically active cavities. The basis is an amphiphilic terpolymer containing hydrophilic side groups, phosphine units and 1,3,5-



Scheme 2.8: The crosslinking of the copolymer creates ligand cavities, tailor-made for a subsequent coordination of Fe(II) ions. Stabilized by the surrounding polymer construct, the iron moieties are sufficiently stable enough to be employed as catalysts for living radical polymerization.

tricarboxamide (BTA) units. The latter induces chain collapse *via* three-fold hydrogen bonds and pendant phosphine units subsequently coordinate to **Ru(II)**, thereby creating a catalytic core inside the hydrophobic compartments of the tricarboxamide motifs.^[113] In a transformation of cyclohexanone to cyclohexanol, performed in water, a high activity of the catalyst was observed. This was attributed to the need of the starting material to enter the hydrophobic cavities, where the catalytic units were placed. In similar approaches, the group synthesized terpolymers with **Organic Catalysts**, namely **L-Proline**. In a comparative study, both catalytic systems, either with Ru(II) or with *L*-proline, were synthesized without the BTA units, revealing especially for the *L*-proline species the need of hydrophobic cavities to be fully catalytically active.^[114]

Although currently the explicit impact of a polymeric scaffold on the catalytic activity of metal ions is still not completely understood, it clearly plays a key role when developing novel catalyst properties. While substituting molecular ligands by polymeric material enhances the stability, second coordination site effects, caused by additional side groups, may lead to an increased activity or better substrate binding. The accessibility and selectivity for substrates is apparently positively influenced by the loosely collapsed state of SCNPs, offering optimum prerequisites for starting compounds and products to enter and leave the cavity.

A different concept for unidirectional, stepwise self-assembly into SCNPs was described by the group of Cai, creating **Locally Orthogonal Systems**. For this purpose a terpolymer (ABC) of imidazolium motifs (A), hydroxyl groups (B) and NH_3^+ (C) was synthesized and subsequently dissolved in an aqueous solution of Cu(II) ions. At a pH value either below 4.4 or higher than 5.3, the deprotonated imidazolium motifs and the NH_2 units in the A and C block coordinated to Cu(II) ions, leading to a discrete, local collapse of the terminal blocks imbuing the polymer with a dumbbell-shaped morphology (refer to Figure 2.24).^[115] In further studies the group presented the unidirectional disassembly of the C block in the dumbbell-shaped SCNP, when the cupric centers were reduced to Cu(I). On the contrary, the strong imidazole bonds towards Cu(II) in block A did not release the metal ion upon

its reduction to Cu(I), resulting in tadpole shaped SCNPs. In the last step, the Cu(I) ions were re-oxidized to Cu(II) and thereby re-coordinated to the NH₂ units in block C, completing the circle of unimolecular molecule shuffling.^[116]

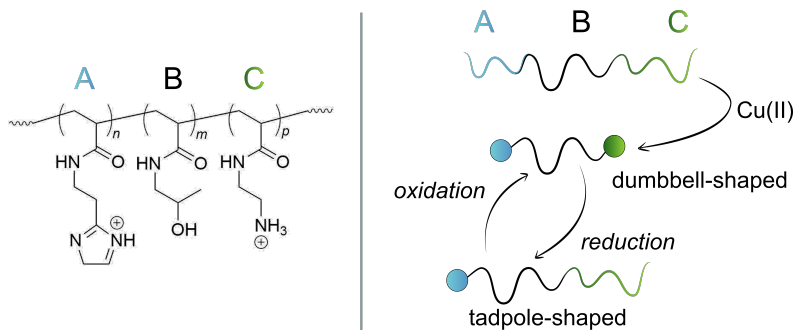


Figure 2.24: A terpolymer consisting of the monomer blocks A, B and C forms dumbbell-shaped SCNPs upon coordination to Cu(II) ions by the monomer units in block A and C. The reduction of the copper ions to Cu(I) causes their release from the polymer scaffold in block C, whereas strong coordinative bonds in block A continue to encapsulate Cu(I) ions. The resulting tadpole-shaped SCNPs can regenerate its dumbbell shape upon subsequent metal oxidation to Cu(II).

Regardless of the challenging synthesis, today a number of metal-incorporated SCNPs were synthesized, analyzed and occasionally applied as catalytic nanoreactors. In on-going research projects, novel ligand moieties for a broader choice of metal ion encapsulation are designed. Simultaneously, routes towards a combination of different chain collapse mechanism in one system are developed and their mutual impact to each other investigated.^[117, 118]

In addition, various analysis methods are adapted to allow detailed insight in the folding process and chain collapse, for instance *via* high resolution mass spectrometry or atomic force microscopy.^[96, 119] Recent research aims for a closer insight into the role of chain stiffness of the backbone.^[120] A further focus of interest is the reversible embedding of metal ions, for instance *via* different pH values.^[115] Consolidating future efforts, scientists might accomplish the planned design of 3D defined polymer units, exhibiting desired catalytic functions as presented by natural enzymes.

2.4 Characterization of SCNPs

The two major tasks in the field of SCNPs chemistry are evidencing the formation of intramolecularly formed compact nanoparticles and detailing the actual folding motif, the crosslinking section.

Often the collapse into a nanoparticle involves a change in the chemical structure as a result of a reaction between functional groups, external linker molecules or the incorporation of metal ions. Such chemical modifications, caused by intrachain bond formation, can be investigated and displayed by common analytic techniques, established in organic synthesis, *e.g.* shifted or new sets of resonances in NMR spectra or appearing and disappearing bands in IR spectra. Consequently, there are many possibilities to depict the actual folding motif.

However, such variations in the chemical structure do also occur for multi-chain or intermolecular linkage formation. For this reason, a greater challenge is the analysis of the morphological structure concomitant to a verification of a single-chain compaction.

In the following sections, selected examples about the investigations in the field of SCNPs on an analytical and practical level are described, before explaining in an overview three analytic techniques, valuable to evidence single-chain nanoparticle formation.

Tracing the Single-Chain Folding Process

In the first experiments synthesizing single-chain nanoparticles, no-one knew about the mechanism of the chain collapse. Although today this intricate process is still not completely understood, the elaborate work of numerous scientists has enabled insight and disclosed information about the procedure.

One approach to image the folding of single-chains into nanoparticles was postulated by Steinkönig *et al.*^[96, 121] In his work, polymer chains were synthesized, small enough to allow their analysis *via* high resolution mass spectroscopy. After the crosslinking reaction of the single-chains, the linear precursor polymer and the corresponding SCNPs were imaged by characteristic mass changes. Of high interest was the possibility to differentiate between two modes of intrachain linkage formation, presenting a potential technique to enclose the sophisticated chain collapse process.

A way to deduce the morphology of SCNPs *via* atomic force microscope (AFM) was presented by Meijer and coworkers.^[119] Therefore, SCNPs were stretched by an AFM cantilever, unfolding mechanically the crosslinks in the collapsed matrix. The measurement of the force-extension profile

during the stretching monitored consecutive peaks, attributed to rupture events, and thus providing insight into the internal structure of SCNPs.

Another work proposed by the group of Pomposo retraced the collapse through extensive computer simulations. Interestingly, the results indicated that the collapse of polymer chains into SCNPs does not necessarily lead to compact nanoparticles. Much more likely are linkages between reactive groups at short distances, thus creating only local compaction. This is probably caused by the self-avoiding character of polymers. Only at high crosslinking degrees, long-range loops are formed. However, for the mimic of natural, globular nanoparticles, the conformation of such long-range loops is essential.^[122, 123]

The issue of globular SCNP formation was further addressed by the same group in a solvent-assisted procedure.^[124] In doing so, polymer precursors were anchored on a surface and subsequently collapsed, resulting in highly crosslinked, globular SCNPs. In another approach, they postulated access to higher levels of crosslinking *via* orthogonal linkers, employing the selected point folding approach.^[125]

Further reports in the literature investigated the collapsed status of SCNPs in comparison to the linear precursor complexes by small-angle scattering experiments by neutrons (SANS) and X-rays (SAXS), supported by molecular dynamics (MD),^[126] or imaging techniques, such as transmission electron microscopy (TEM) and cryo-TEM.^[127]

The Non-Predictable Collapse of Single Polymer Chains

The reason for a non-predictable collapse during SCNP formation has its origin in the statistical distribution of functional units along the precursor chain. Even in the same batch of precursor polymers, every chain varies in the localization of its functional units. The order of similarity further decreases in the final nanoparticles, as so far no pre-organized or preferential folding process could be established and thus SCNPs of different topologies are created. The resulting differences in shape and functionalization of the SCNPs hamper the development of future applications, *i.e.* for catalytic systems.^[8] Therefore, the next level in SCNP chemistry is the exact placement of functional units along the chain and a better control of the folding procedure. First steps have already been carried out, employing sequence-defined (co)polymers, which contain intentionally placed functional units (refer also to Chapter 2.1.4).^[61, 128, 129] Developing such synthesis protocols will finally enable scientists to gain control over the degree of compactness and minimize micro structural defects.

While not having reached the point of perfection in polymer synthesis, two groups ascertained alternative pathways to handle unequal nanoparticle formation:

On a theoretical basis, in a joint project between chemists and physicists, the statistical knowledge of the precursor polymer batch was employed to establish a mathematic connection between the global compaction degree, the size and the number of local domains generated upon SCNP formation at high dilution.^[130]

A completely different pathway is the approach of Jiang *et al.* addressing the point of simultaneous single-chain and multi-chain formation and their subsequent separation. Therefore, at first single-chain Janus particles (SCJPs) were generated from a diblock precursor polymer. Janus particles are anisotropic particles, exhibiting distinct physical properties in one compound. In further steps, the SCJPs were isolated from likewise formed irregular and multi-chain nanoparticles. This was feasible by the establishment of central conditions leading to the exclusive self-assembly of the SCJPs in a crystal-like appearance. Consequently, the assembled SCJPs precipitated from the solution, which enabled their facile isolation. Astonishingly, the obtained SCJPs were uniform in size and shape.^[131]

In the current thesis all synthesized single-chain nanoparticles were obtained *via* metal-incorporation. Whereas the concomitant changes in the chemical structure were evidenced by NMR, IR and Raman spectroscopy as well as UV/Vis measurements, the collapse into compact nanoparticles was analyzed *via* SEC, DLS and DOSY measurements.

Those analytical methods were suitable to distinguish single-chain and multi-chain collapse, provided that the size of the precursor polymer decreased upon nanoparticle formation.

2.4.1 Size Exclusion Chromatography (SEC)

Size exclusion chromatography (SEC), also known as gel permeation chromatography (GPC), is a liquid column chromatography technique to sort a mixture of macromolecules by their size, or technically their **Hydrodynamic Volume**.^[132] It is a convenient standard technique for the analysis of polymeric material. In a classical measurement, values for the molecular weight and the molecular mass distribution of the sample are obtained. Both information is relevant, since they are directly influenced by the polymer's properties, such as brittleness, toughness or elasticity.^[133]

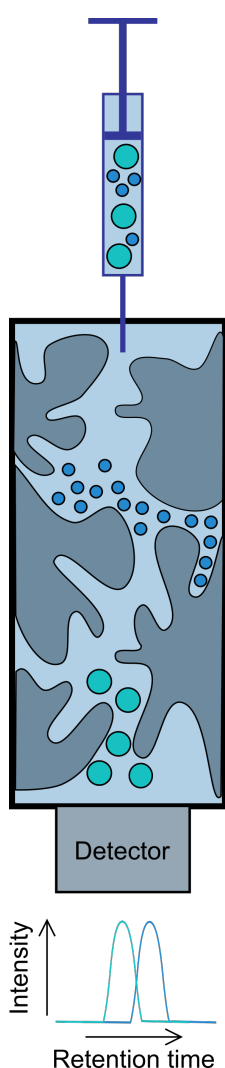


Figure 2.25: SEC separates molecules regarding to their hydrodynamic volume.

The benefits of SEC analysis include a simple, rather affordable and fast (< hour) procedure, which requires only small amounts of sample material. On the downside, there is only a limited number of peaks that can be resolved in a multicomponent mixture, requiring a minimum mass difference of particles.^[134] In addition, obtained values might be calculated relative to a standard, depending on the applied calibration.

The basic idea in SEC is the transport of dissolved macromolecules through a porous column. Depending on the hydrodynamic volume of the particles, they elute at a size-specific volume.

The column is packed with a gel of different pore sizes (stationary phase). Requirement for the gel material is the absence of ionizing groups to prohibit any interaction with the sample molecules. Typical gels consist of crosslinked polystyrene, divinyl benzene, dextrane, polyacrylamides and acrylates or cellulose.^[134] The column is continuously flushed with a solvent, the eluent (mobile phase) *via* a pump. For the analysis of a sample, the analytes are dissolved in the same solvent as the eluent, filtered and injected to the system.

The separation of molecules or particles of different hydrodynamic radii takes place, since they need different time periods to traverse the column. Smaller particles can enter (almost) every pore and remain for a longer time in the column, resulting in increased retention times. On the contrary, larger particles elute more quickly. However, there is an elution limit in every column for molecules below or above a determined size.

The total volume, the internal column volume V_c , is defined as:

$$V_c = V_d + V_p + V_0$$

where V_d is labeled as the volume of the stationary phase (gel), V_p as the inner volume of the gel and V_0 as the volume between the gel particles.^[135] Particles, which are too large to enter any pore and therefore elute without a delay, have a retention volume V_R , which is equivalent to V_0 , hence $V_R = V_0$. In an analogous manner, very small molecules, which access every pore, have a retention volume of: $V_R = V_p + V_0$. The size variation of molecules below or above this limit can not be determined. However, molecules accessing only a *fraction* K_{SEC} ($0 < K_{SEC} < 1$) of the pores, can be analyzed and their retention volume V_R is determined *via* the **SEC Equation**:

$$V_R = V_0 + K^{SEC}V_p$$

The constant K_{SEC} is dependent on various factors: The strongest impact has the size and the shape of the analyzed particles. In addition, various other parameters need to be considered, such as the type of solvent, the material of the stationary phase and the temperature. Consequentially, a calibration of the SEC system is necessary.

Various options exist to calibrate a SEC system, in here, only two possibilities are mentioned. More information can be found in the literature.^[136]

- The calibration *via* **Narrow Molecular Weight Standards**: The molecular mass of the unknown sample is quoted relatively to the molecular weight of a standard sample, often linear polystyrene (PS) or polymethylmethacrylate (PMMA).
- The application of a **Universal Calibration**:^[137] Applying the **Mark–Houwink Equation**, the relation between the intrinsic viscosity $[\eta]$ of the solution, containing the dissolved sample, and its molecular weight is described by:

$$[\eta] = KM^\alpha$$

The Mark–Houwink parameter K and α are dependent on the polymer-solvent system. Knowing the values for a standard polymer sample and assuming that the polymer-solvent systems have the same intrinsic viscosity, the molecular weight of an unknown polymer sample can be determined by:

$$K_1M_1^{1+\alpha_1} = K_2M_2^{1+\alpha_2}$$

In the field of SCNPs, SEC analysis is an optimal tool to distinguish a single-chain collapse from multi-chain aggregation. For successful SCNP formation, the SEC trace of the SCNPs is shifted towards longer retention times in comparison to the precursor polymer. The general assumption that a longer retention time corresponds to a smaller molecular weight is incorrect when regarding SCNPs. Instead, it implies a reduction in the hydrodynamic radius of the single-chain upon chain collapse. The actual molecular weight of the SCNPs can even increase, for instance, *via* the incorporation of metal ions in the case of metal-complexed SCNPs.

The application of SEC as a tool for the analysis of SCNPs was further investigated by various research groups. In particular, the group of Pomposo dedicated themselves to examine the relations between the shape and compaction degree of SCNPs with parameters obtained from SEC analysis. For instance, the group mathematically modeled the compactness of nanoparticles, hence the formation of sparse or globular SCNPs, based on SEC data of real existing systems.^[138]

Of specific interest to the current thesis was one project from this group,^[139] where they developed an equation to predict the size reduction of SCNPs on the basis of the SEC data of the precursor polymer. Including the results of Fetters *et al.*,^[140] the hydrodynamic radius r_H^{SEC} of the precursor polymer was calculated from its molecular weight, determined *via* SEC analysis. Preconditions for these measurements were THF as solvent and the use of a polystyrene calibration.

$$r_H^{\text{SEC}} = 1.4410^{-2}(M_w)^{0.561}$$

In the next step, the calculated hydrodynamic radius r_H^{SEC} of the precursor polymer was defined as $r_0 \rightarrow r_0 = r_H^{\text{SEC}}$. Knowing the *fraction* x of functional groups participating in intramolecular linkages, the hydrodynamic radius r_H of the nanoparticles can be estimated:

$$r_H = r_0(1 - x)^{0.6}$$

A comparison of theoretical and experimental data is reported to be in good agreement. However, when applied to our systems, the results were sparsely in good agreement (refer for instance to the analysis of Pt(II)-SCNPs, Chapter 3.5). The influence of parameters such as size and shape of the linker molecules could be the cause of the deviation from the theoretical model. Moreover, the equation assumes that two functionalities in the polymer build up one linkage in the polymer chain. However, in the specific case of metal-SCNPs, a ratio between metal ions (=linker) and ligands (=functional groups in the polymer) of more than 1:2 is no exception. Therefore, higher levels of chain compaction are expected than are calculated with the aforementioned equations.

2.4.2 Diffusion Ordered Spectroscopy (DOSY)

The translational motion of molecules in solution is known as Brownian molecular motion or **Diffusion**. Dependent on the molecule's size, shape and the solvent's temperature and viscosity, a diffusion coefficient for a molecule can be determined.

A satisfactory method for measuring the diffusion coefficient of molecules is the 2D NMR experiment **Diffusion Ordered Spectroscopy (DOSY)**. Based on a pulse field gradient stimulated-echo pulse sequence, spatial information about the molecules in a sample is encoded. Therefore, the spins of the molecules are spatially labeled and their change in position after a certain time, called diffusion time, is detected.

For each NMR resonance in the sample, the intensity I is determined in relation to the reference intensity I_0 . In dependency of additional parameters, such as the diffusion time, the gradient parameter of the instrument and the gyromagnetic ratio, which are all collocated in q , the diffusion coefficient D can be calculated *via* the Stejskal–Tanner equation.^[141, 142]

$$I = I_0 e^{-Dq^2}$$

Typically, NMR resonances belonging to the same molecule exhibit the same diffusion coefficient. Simultaneously, molecules of different sizes differ in their coefficients, which are inversely proportional to their hydrodynamic radius. Thus, small molecules move faster than large molecules, along with a faster reduction in the intensity of their NMR resonances.

The correlation between the diffusion coefficient and the hydrodynamic radius r_H of the material is described for spherical particles by the **Stokes–Einstein Equation**.^[143]

$$D = \frac{kT}{6\pi\eta r_H}$$

Thereby, k is referred to as the Boltzmann constant, T for the temperature in Kelvin and η describes the viscosity of the solvent.

In terms of instrumentation and theory, DOSY experiments are a complex topic and explained more in detail in the literature.^[144] However, the technique of DOSY measurement, originally invented to identify different components in a mixture, is today an often employed method in the field of SCNP chemistry.^[84] Thereby, a more compact structure of the SCNPs than in the prior polymer system is assumed, similar as in SEC measurements.

In association with the current topic in which metal cores were implemented into the polymer structure, nevertheless a smaller hydrodynamic radius for the resulting SCNPs was inferred. Hence, even though the actual molecular mass of the SCNPs increased in comparison to the polymer system, the SCNPs exhibited a higher diffusion coefficient. The obtained values for the diffusion coefficients were therefore not taken as absolute values, yet the measurements of polymer chains and SCNPs under the same conditions allowed a relative comparison between the linear polymer chain and the collapsed nanoparticles.

The relation between the diffusion coefficient and hydrodynamic radius r_H is of high interest in the determination of the compaction of a polymer chain upon single-chain nanoparticle formation and reported for various projects, including the current thesis.^[4, 145]

2.4.3 Dynamic Light Scattering (DLS)

Dynamic light scattering (DLS), also termed photon correlation spectroscopy, is a major source to gain information about the size and shape of particles in suspension or solution. It is an often employed analysis technique, favorable due to its non-invasive character.^[146–150]

In the process of measuring, the beam of a monochromatic light source, usually a laser, is shot through the analyzing sample causing the light to scatter. Given that the diameter d of the investigated particles is smaller than the wavelength λ of the light source, $d < \frac{\lambda}{20}$, the scattering of the light is isotropic, *i.e.* equal in all directions. The majority of the light is scattered elastically, termed **Rayleigh Scattering**, hence at the same frequency as the laser beam. This phenomenon is caused by the oscillating electromagnetic field of the laser light, exciting the electrons of the particles to oscillate at the same frequency. The net scattering intensity is finally recorded at a detector, consisting of many individual scattered waves from the particles.

The scattered light of a particle interferes with the scattered light of neighboring particles, resulting in constructive or destructive interference, measured by a change in intensity. Due to the Brownian motion, the particles diffuse in solution, leading to a **Fluctuation of the Intensity**. The detector compares the light intensity at each spot at short time intervals, measuring the rate at which the intensity of the scattered light fluctuates. The intensity fluctuation contains information about the scale of movement of the scattering particles, hence depends on the size of the particles.

At short time delays ($t + \delta t$) there is a high correlation, because the particles did not move to a great extent, meaning that the signals are unchanged when compared to each other. Over a longer delay time, the correlation decays exponentially, since the particles moved away and no correlation between the scattered intensity at the initial and the final states is found. The decay of intensity is mathematically described with the so-called **Auto-Correlation Function** $C(q, \tau)$, which is dependent on the delay time τ and the diffusion coefficient D :

$$C(q, \tau) \sim e^{-Dq^2\tau}$$

In the equation, q stands for the wave vector, related to the refractive index n_0 , the wavelength of the laser λ and the angle of the detector Φ and defined as:

$$q = \frac{4\pi n_0}{\lambda}$$

Applying the Stokes–Einstein Equation (also applied in DOSY) enables the calculation of the hydrodynamic radius r_H of the particles:

$$D = \frac{kT}{6\pi\eta r_H}$$

Further amendments regard the dispersity of systems, developing a probability-density function for an auto-correlation function for disperse samples.

Caution should be exercised when applying the described procedure for the analysis of polymeric material.^[145] Generally, the described system anticipates the shape of the analyzing sample as spherical, hard particles. For non-spherical particles, the rotational motion in the above-described system is not considered, yet the scattering is dependent on the orientation of the particle in question. In addition, the determined hydrodynamic radius r_H does not consider the true nature of the dissolved polymer particles, refer to Figure 2.26.

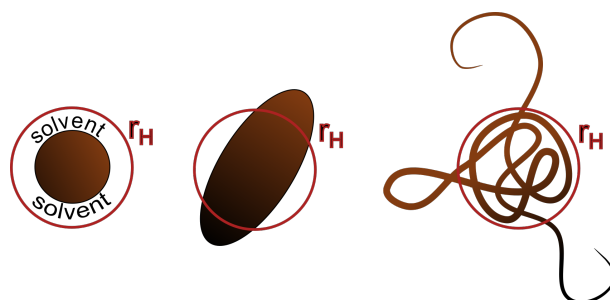


Figure 2.26: DLS anticipates the analyzed sample as a hard, spherical particle. In doing so, the actual size of the particles is neglected. As depicted, the determined hydrodynamic radius r_H for polymeric samples does not necessarily match the dissolved status.

Another concern is the analysis of a mixture of particles of different sizes. As derived from the Rayleigh approximation, the intensity of the scattering is correlated to the diameter of the particles:^[151]

$$I \sim d^6$$

This implies that larger particles contribute to a higher extent to the measured intensity. It is therefore necessary to select the appropriate method when calculating the size distributions in a sample.^[152] At first, the intensity decay of the correlation function is fitted to obtain the distribution of the particle sizes → **Intensity Size Distribution**. In case of multiple signals or signal tailing, pointing towards a multi-modal distribution, the intensity distribution can be converted into a **Volume Distribution**. A further step calculates the **Number Distribution**, the best representation for the situation within a polymeric sample.

However, in disperse samples, the strong scattering of larger particles can suppress the signal of smaller particles, producing less amount of scattering.^[153] This phenomenon therefore can potentially make the acquisition of the accurate r_H data on SCNPs challenging.

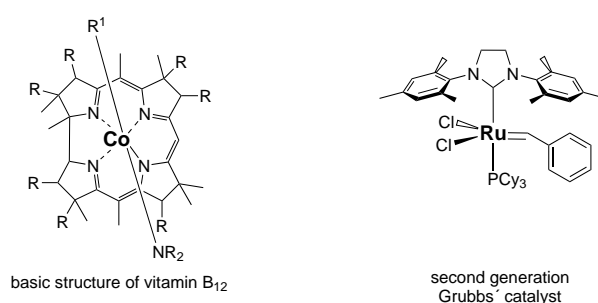
In general, the complexity of single-chain nanoparticles, which is even enhanced when encapsulating another species such as metal ions, requires thorough analysis combined with critical evaluation of the obtained data, before uniting the information for a complete picture of the generated (metal-)SCNPs.

2.5 Coordination Complexes

The central topic of the current thesis is the incorporation of metal cores into polymer chains *via* coordinative bonds to pendent ligand moieties. Depending on the ligand-to-metal ratio, metallopolymers or metal-complexed single-chain nanoparticles (SCNPs), exhibiting metal cores as folding units, are obtained. Therefore, an understanding of complex formation and metal-to-ligand interaction is essential for the selection of ligand functionalities in the polymers and the appropriate precursor metal complexes. A suitable combination is especially important when aiming for **Orthogonal Metal Incorporation**. This implies the simultaneous existence of two ligand moieties and two precursor metal complexes, in which always only two counterparts form a **Metal–Ligand Pair** (refer to Chapter 6). For this purpose, the preference of a class of metals towards certain types of ligands needs to be considered. The following sections provide an overview of the commented topics.

2.5.1 General Remarks on the Formation of Transition Metal Complexes

Metal complexes and transition metal complexes in particular are a key element in modern chemistry and have been analyzed, isolated, studied and purposeful synthesized. Due to their diversity in structure and function, metal complexes have a wide array of applications. Selected examples include active units in natural enzymes such as the co-factor vitamin B₁₂, molecular dyes, for example cobalt based polypyridyl-based electrolytes, or as catalysts in homogeneous reactions, such as the famous Grubbs' catalyst (Figure 2.9).^[154–156]



Scheme 2.9: Selected examples of remarkable metal complexes: The corrin ring with a central placed cobalt atom is the key component in the co-factor vitamin B₁₂, *left*. Popular in organic synthesis is the Grubbs' catalyst, a ruthenium complex for olefin metathesis reactions, *right*.

A monomeric metal complex consists of a metal core and its surrounding, coordinating ligands. Depending on various parameters, such as the type of metal, its oxidation state and the nature of the ligands, a certain number of ligands arrange in a characteristic geometry around the metal center.

The ligands can be categorized according to their charge, size, identity of the coordinating atom or denticity, if various functionalities in one ligand bind to the same metal center. Multiple dentate ligands employed in the current thesis include the bidentate phenanthroline ligand (Chapter 2.5.3), coordinating with both nitrogen atoms to the same metal core, and carboxylates, exhibiting mono and bidentate properties (Chapter 2.5.4). The classification *via* their donating and accepting character is described in detail in Chapter 2.5.2.

In transition metal complexes, predominantly the d-orbitals of the metal atom interact with the orbitals of the ligands. Thereby, the originally degenerated five d-orbitals of the isolated metal are affected by the ligand sphere. Orbitals pointing directly towards the ligands are shifted towards higher energy. In contrast, d-orbitals with less interaction with ligands, are decreased in their energy. The resulting orbital diagram and the energy difference between the sets of energetically elevated and lowered d-orbitals is an indication of the electronic structure and stability of the complexes. One of the most common geometries are octahedrons, where six ligand moieties participate. Other arrangements are square-planar or tetrahedral complexes, with four coordinating ligands. The structure of an octahedral complex and the resulting d-orbital splitting is depicted in Figure 2.27.

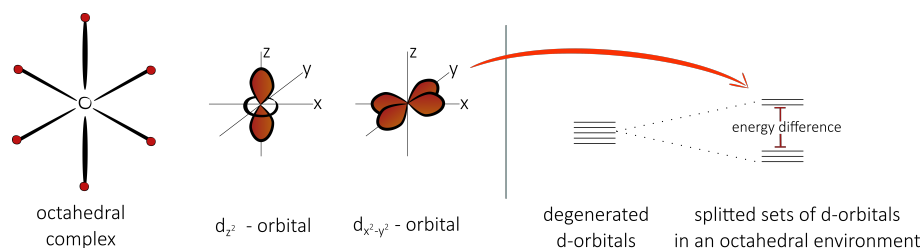


Figure 2.27: The interaction of the orbitals of the ligand molecules with the orbitals of the metal core splits the d-orbitals of the metal atom in sets of raised and lowered d-orbitals. In the example of an octahedral complex, the $d_{x^2-y^2}$ and d_{z^2} orbitals point directly towards the ligands and are raised in their energy.

The bonds in metal complexes form their own class of linkages, the so-called coordinative bond. Discussed in various theories, the most common model describes the bonding as a combination of atomic orbitals (AOs) of the participating molecules, resulting in molecular orbitals (MOs), therefore termed **MO Theory**.^[157] From a set of AOs, an equal amount of MOs is formed. In the process, two atomic orbitals generate two MOs: A bonding MO, constructive and with an energy lower than the AOs, and one anti-bonding MO, deconstructive and with a higher energy than the AOs. AOs without a suitable partner result in non-bonding orbitals, maintaining the same energy. The obtained MOs are distinguished by their molecular orbital symmetry, for instance, having a σ - or a π - character, as depicted in Figure 2.28.

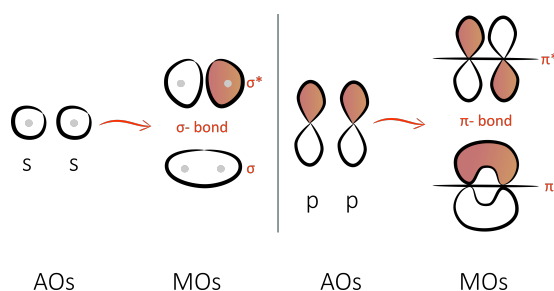
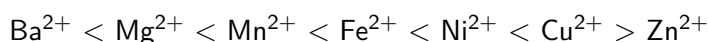


Figure 2.28: Molecular orbitals (MO) are categorized according to their molecular orbital symmetry. σ bonds are symmetrical with regard to rotation about the connecting bond (*left*). In comparison, π bonds have a shared plane, crossing their nuclei (*right*). Independent of the symmetry, in each bond formation, two MOs are formed, either bonding or antibonding. The latter is labeled with a star *.

Studying the stability of complexes, the scientists Irving and William noted a trend in the stability of octahedral complexes when changing the central metal ion in the same ligand field. Based on their results, they established the **Irving–William Series** of relative complex stability.^[158]



The reason for the above relation is assumed to be an electrostatic effect, reducing the ionic radius from left to right. However, complexes of different stability were formed from the same metal core by altering the binding donor atoms (O, N and S) of the ligands. For transition metals, another trend was observed: Light transition metals in high oxidation states form stable complexes preferentially with N or O donor atoms, whereas the heavy homologues favor complex formation with phosphines and thiol ethers.^[159]

Soft acids	Soft bases	Borderline acids: Cu²⁺, Fe²⁺, Zn²⁺
Cu ⁺ , Ag ⁺ , Au⁺ , Pd ²⁺ , Pt²⁺	RS ⁻ , R₃P , CO	
Hard acids	Hard bases	Borderline bases: pyridine , aniline
Na ⁺ , K ⁺ Ln³⁺, Zr⁴⁺	NH ₃ , CH₃COO⁻ , PPh₃=O	

Figure 2.29: Bonding in metal complexes as described with the Lewis model: Ligand and metal ions are categorized as hard and soft acids and bases. Typically, pairs of soft-soft or hard-hard acids and bases form strong bonds. Metal ions and ligands, which are utilized in the course of the current thesis are marked in bold.

This concept was fine-tuned by Pearson, describing the bonding in metal complexes with the **Lewis Model**.^[160] He proposed that metal complex formation can be regarded as an interaction of metal ions with a vacant orbital as Lewis acids and ligands with an donating pair of electrons as Lewis bases. Investigations showed that the softer the ligands, the higher their HOMO and the harder the metal center the higher their LUMO. As a consequence, in a reaction of a soft acid (metal center) and a soft base (ligand), the participating HOMO and LUMO orbitals are in close proximity and form a covalent bond. In contrast, in a pair of hard acids and bases, the energy difference between HOMO and LUMO is significantly

high, inhibiting the formation of covalent bonds. Instead, the locally separated charge of metal core and ligand yields in coulomb energy, hence high electrostatic interaction energy.

Consequently, a high complex stability is obtained either for the interaction of soft–soft or hard–hard acid and base pairs, due to covalent or ionic contributions to the bond strength, respectively.^[159]

Furthermore, a low LUMO in ligands can participate as an accepting orbital for an interaction with high electron density metal centers. Such **Backbonding** into anti-bonding orbitals of the ligands enable even weak Lewis bases to form stable complexes.

As depicted in the example for the coordinated CO ligand in Figure 2.30, three common bondings can occur in metal complexation: A) σ -bonding, a donation of two electrons from the ligand to the metal ion; B) π -bonding, an electron donation of the ligand towards the metal center (usually of insignificant contribution); C) π -backbonding, a transfer of electron density from the metal core to the, so-called, π -acceptor ligand. The intake of charge into antibonding CO orbitals, in turn, weakens the C=O bond. Hence, meaningful data on the acceptor character of ligands can be obtained *via* IR spectroscopy, detecting the shifts of the frequency of the C–O stretching vibration (further described in Chapter 2.5.2).^[161]

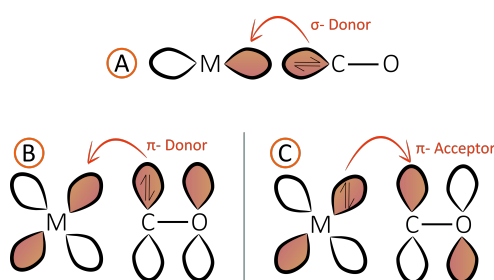


Figure 2.30: Possible bonding modes in metal complexes, shown for a metal–CO–moiety. Typically, ligands donate electrons into empty orbitals of the metal center (A+B). However, also backdonation from the occupied metal orbitals into free (antibonding) orbitals of the ligand can occur, strengthening the complex stability (C).

The following sections outline relevant information about three different ligand moieties, **Phosphine**, **Nitrogen Ligands** and **Oxygen Ligands**. In accordance with the topics of the current thesis, the section about phosphines focuses on triphenylphosphine units, employed for the synthesis of Pt(II)-SCNPs and orthogonal, heterometallic Eu(III)/Pt(II)-SCNPs (refer to Chapter 3 and 6). For the same reason, the section on nitrogen ligands focuses on the specific heteroaromatic phenanthroline ligand as applied for phenanthroline-containing SCNPs and metallopolymers (refer to Chapter 4). Lastly, the section of oxygen ligands elucidates the group of carboxylate units, investigated for the generation of paddlewheel structures in SCNPs and Au(I)/Cu₂(II) heterometallic systems (refer to Chapter 5 and 6).

The last section provides a separate summary about **Lanthanide Complexes**, as this class of metals behaves differently from transition metals. Their luminescent properties in combination with aromatic, space demanding ligands are of special interest, as investigated in the current thesis in Chapter 4.9 and Chapter 6.4.

2.5.2 Phosphine Ligands – Triphenylphosphine

In accordance with the **Covalent Bond Classification**, three types of ligands Z, X and L are identified.^[162] The classification of the ligands is based on their electron donating or accepting character, independent from the oxidation state of the metal center. A Z-ligand is a strong electron acceptor, which withdraws two electrons from the metal core. In contrast, if the ligand and the metal core each donate one electron for the bond, the ligand is categorized as an X-ligand. The last group are L-type ligands, corresponding to a two electron donor ligand.

Phosphine ligands belong to the group of L-type ligands, exhibiting as their predominant interaction the donation of their lone-pair of the phosphorous atom to an empty d-orbital in the metal.^[163]

Common phosphine ligands have a PR_3 structure with a varying donor strength and steric demand, depending on the electronic nature of the R-group (Figure 2.31). A possibility to define the strength of the electron donating or withdrawing capability of a PR_3 ligand, now in total termed ligand L, is the measurement of the **Tolman Electronic Parameter**.

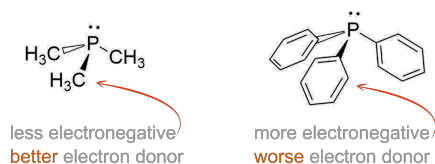


Figure 2.31: The electronic nature of the R-group in PR_3 ligands is decisive for the electron donating strength of the phosphorous atom.

Therefore, the frequency of the vibrational mode of A_1-CO in the model complex $[LNi(CO)_3]$ is measured *via* infrared spectrometry (refer to Figure 2.32, *left*). Not covered by other frequencies and thus isolated in the spectrum, shifts of the A_1-CO frequency, originating from symmetric stretching, can easily be detected. In accordance to an increase or decrease of the electron density at the Ni(II) center, caused by the ligand L, less or stronger π -backbonding from the Ni(II) center to the CO bond occurs. The corresponding weaker or stronger CO-bond results in higher or lower vibrational frequencies, traceable in the IR spectrum.^[164]

Another important characteristic of phosphines is their steric bulk in metal complexes, measured by the **Ligand Cone Angle**. Therefore, a theoretical cone is placed into the chemical structure of the complex with the metal at the vertex and the outmost radius at the edge of the van-der-Waals spheres of the ligand atoms (refer to Figure 2.32, *right*). Described originally for tertiary phosphines, it is adaptable to any ligand. Knowing the steric bulk of phosphines (ligands) is particularly interesting when applying the complex as a catalyst, since the steric demand strongly influences the selectivity of the catalyst.^[164]

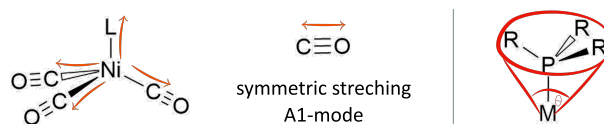


Figure 2.32: *Left:* The model complex $[\text{LNi}(\text{CO})_3]$ allows the determination of the electron donating or withdrawing character of the ligand L by measuring the shifts of the frequency of the A_1 mode. *Right:* The steric bulk of ligands in metal complexes is measured *via* the ligand cone angle, placing the metal at the vertex and the outmost radius at the edge of the van-der-Waals spheres of the ligand.

Narrowing the section to **Triphenylphosphine** ligands (and their derivatives), PPh_3 compounds belong to the class of soft bases, predestined for stable soft-soft matching with middle and late transition metals, for instance the platinum group (Au, Ag, Pd, Pt).^[159] Thereby, PPh_3 ligands do not only exhibit strong σ -bonding *via* donation of the lone pair of the phosphorous atom, yet also show high π -accepting character for backbonding into the $\text{P}-\text{C}$ σ^* anti-bonding orbital. While less electronegative R -groups enhance the electron donor ability of the phosphorous, electron withdrawing groups stabilize the negative charge easier, thus facilitating the backbonding. The combination of their lipophilic character, which allows facile solubility in organic solvents, and their compatibility with metals in various oxidation states, make phosphines prominent ligands in homogeneous catalysis.

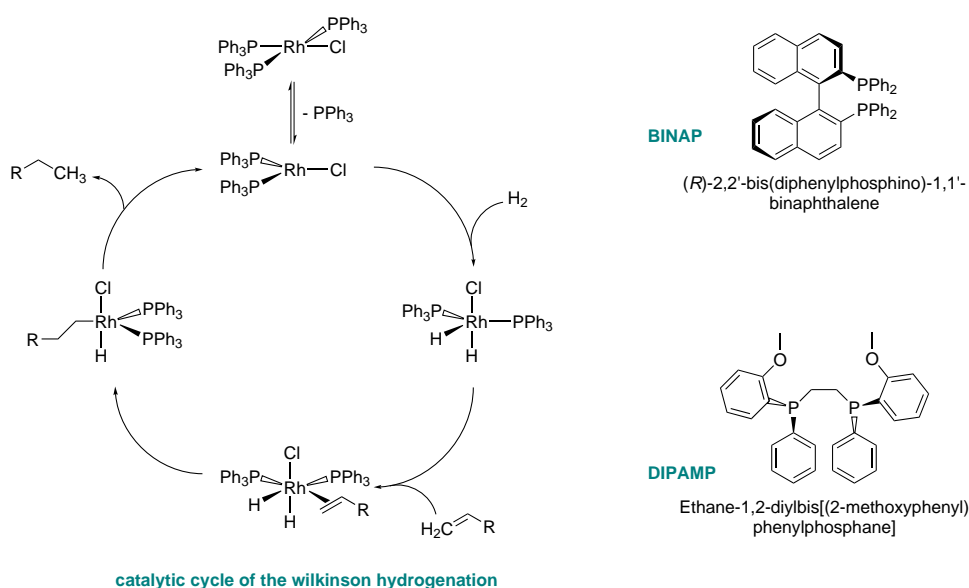


Figure 2.33: The Wilkinson catalyst $[\text{RhCl}(\text{PPh}_3)_3]$ is known for its excellent performance in hydrogenating olefins. The mechanism involves the ongoing oxidation and reduction of the central rhodium ion from +1 to +3. Replacement of PPh_3 by chiral phosphines, such as BINAP or DIPAMP, enables asymmetric catalysis.

Particular attention must be given to the rhodium complex $[\text{Rh}(\text{PPh}_3)_3\text{Cl}]$, the **Wilkinson Catalyst**. This complex is a prime example for metal complex catalysts, known for its highly efficient hydrogenation of olefins (Figure 2.33). Centerpiece in the Wilkinson catalyst is a $\text{Rh}(\text{I})$ core, which,

after release of one phosphine ligand, is oxidized to Rh(III) *via* H₂ addition. Following reaction steps include the coordination of an olefin to the complex and a hydride transfer. Subsequently releasing the alkane from the metal center *via* reductive elimination completes the catalytic circle and regenerates the Rh(I) unit (refer to Figure 2.33, *left*).^[165]

Moreover, the replacement of the ligand PPh₃ by chiral phosphine ligands, such as BINAP (2,2'-bis(diphenylphosphino)-1,1'-binaphthalene), enables enantioselective H-transfer reactions and laid the foundation for modern asymmetric catalysis.^[166] The reason why BINAP forms stereoisomers is atropisomerism, which is a hindered rotation around a single bond.^[167] A further development reported by Knowles, was DIPAMP (ethane-1,2-diylbis((2-methoxyphenyl)phenylphosphane)), enabling the first industrial asymmetric hydrogenation and awarding him in 2002 with the nobel prize in chemistry (Figure 2.33, *right*).^[168]

A spectroscopic advantage of using phosphines is their NMR active ³¹P nuclei, allowing facile monitoring of their assembly. With an abundance of 100 %, a relatively high gyromagnetic radius, and a nuclei spin of 1/2, ³¹P NMR spectroscopy is a commonly applied technique with easy to interpret spectra. Upon coordination to metal ions, the resulting bound phosphines reveal characteristic resonances in the spectra, even sensitive to geometrical arrangements.^[169]

Phosphines are easily oxidized, which is often exploited as the driving force in organic reactions, for instance in the Appel Reaction.^[170] The oxidation of triphenylphosphine into triphenylphosphine oxide (TPPO) O=PPh₃ leads to an important change in the ligand character: While PPh₃ preferentially forms coordinative bonds to soft metal centers, TPPO favors coordination to hard acids. The reason is the switch from phosphorous as a donor atom to the hard, electronegative oxygen. As reported in recent studies, the P=O formal double bond even displays significant ionic character. The double bond is therefore better described as a R₃P⁺-O⁻ unit, in which the oxygen is negatively charged.^[171] As a consequence, TPPO favors, for instance, the coordination to the positively charged oxophilic lanthanide(III) ions, further described in Chapter 2.5.5.

The counteractive behavior of PPh₃ and TPPO was exploited in the current thesis for the preparation of selective-coordinated heterometallic SCNPs. To this effect, both ligand moieties were incorporated into the same polymer system. In a one-pot reaction transition metal complexes of the class of soft acids and lanthanide complexes as hard acids coordinated target-oriented either to the phosphine or TPPO moieties. A detailed description of selectively reacting systems is presented in Chapter 6.

2.5.3 Nitrogen Ligands – Phenanthroline and Derivatives

Within the wide class of nitrogen ligands, the current chapter focuses on pyridine-based compounds, especially on **1,10-Phenanthroline** (Phen) and its derivatives. Along with the closely related structure of bipyridine (bipy), both ligand types play an important role in coordination chemistry, forming stable complexes with almost every transition or lanthanide metal. Of considerable interest are the photo-physical properties of Phen. As a **Triplet-State Sensitizer**, Phen supports the population of excited states in poorly absorbing atoms, such as lanthanides (refer to Chapter 2.5.5).

Like most nitrogen ligands, Phen and its derivatives belong to the class of L-type ligands. Although donating two electrons, N-heteroaromatic ligands are poor electron donor substituents. The low donor ability is compensated by a high π -acceptability. Caused by the π -electron deficiency in the nitrogen-containing ring, the low-energy π^* orbitals enable strong metal-ligand charge-transfer (MLCT) complexes, stabilizing metals in low oxidation states.^[172]

The high stability of Phen complexes is additionally attributed to an enhanced affinity of metal centers towards **Chelate Type** ligands in comparison to non-chelating ligands. The stabilizing effect is caused by the rigid character of Phen, holding the two coordinating nitrogen atoms in juxta position. Thus, after coordination of the first nitrogen atom to a metal core, the statistical probability for a second bonding site is enhanced. This pre-organization gives entropic and enthalpic advantages over other bidentate ligands, such as bipy or ethylenediamine.^[173, 174]

A well-studied example is the chiral, octahedral $[\text{Ru}(\text{bipy})_3]^{2+}$ complex, with the counter ions $[\text{Cl}]_2^{-1}$ or $[\text{PF}_6]_2^{-1}$, known to perform photoinduced redox processes.^[175] A good precondition for such reactions is a broad absorption band of the complex in the visible and ultraviolet light. The process is illustrated in Figure 2.34 and the depicted structures are related to the text by color indication in brackets behind the corresponding complexes. The process starts with a metal-to-ligand charge transfer reaction, resulting in easy excitation of the complex $[\text{Ru}(\text{bipy})_3]^{2+}[\text{PF}_6]_2^{-1}$ (red) into its transition state $[\text{Ru}(\text{bipy})_3]^{2+*}$ (purple). At first, the singlet state is populated, followed by an intersystem crossing, which yields a long-lived luminescent triplet state. Due to the complex's specific structure, a local charge separation can take place, $[\text{Ru}^{3+}(\text{bipy})_2(\text{bipy})^{-1}]^{2+}$ (purple). Depending on the surrounding molecules, the ruthenium ion triggers either photo-reduction or oxidation (orange and pink).^[176–178]

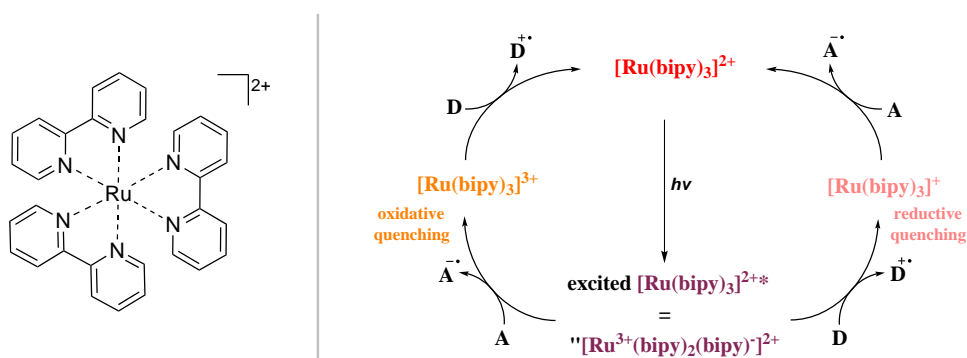


Figure 2.34: $[\text{Ru}(\text{bipy})_3]^{2+}$ is a well-studied example for photoinduced redox processes *via* visible light. After excitation, the ruthenium ion triggers either reduction or oxidation, dependent on the surrounding molecules.

A potential candidate to replace the expensive $[\text{Ru}(\text{bipy})_3]^{2+}$ complex is the cheaper copper based $[\text{Cu}(\text{dimethyl-Phen})_2]^+$ complex, promising as a photocatalyst and photosensitizer in solar energy conversion.^[179]

Recently, Phen derivatives attracted high attention as ligands in sophisticated 3D architectures with novel molecular topology. The reason was the intention of Sauvage and coworkers to develop a direct synthesis route for catenanes, mechanically interlocked rings.^[180] In contrary to existing synthesis protocols, Sauvage took advantage of the metal-induced **Template Effect**, in which ligands assemble in a predictable geometry. In detail, two equivalents of Phen-containing diphenols formed a stable 2:1 complex with copper(I) ions, stable enough to allow ring-closure reactions of each diphenol. After decomplexation, the catenane was formed (Figure 2.35). Due to this reaction and following developments in the area of molecular machines, Sauvage was awarded with the nobel prize in chemistry in 2016.

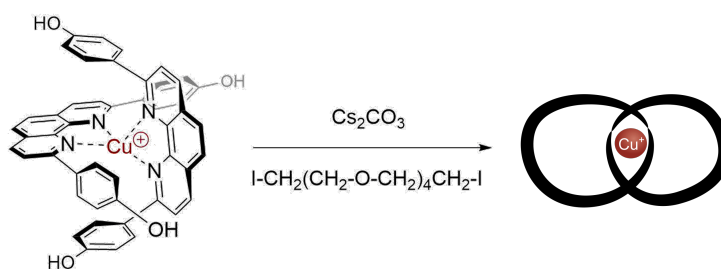


Figure 2.35: Short and convenient synthesis pathway for a metal template supported catenane formation. Two diphenols coordinate to a copper(I) center, forming a complex, which is stable enough to withstand a subsequent ring-closure reaction.

In conclusion, the nitrogen-based molecule Phen is widely applied as a building block in supramolecular architectures or as a coordinating ligand in metal complexes. As a triplet-state photosensitizer, Phen can enhance the catalytic activity of the metal center, for instance in the case of ruthenium or

copper, or induce luminescent properties, as for the lanthanides. Moreover, the strong coordinating nature of Phen can be used to synthesize biomimetic model complexes of metalloenzymes to provide insight into their operating mechanism. In addition, the modification of Phen into chiral ligands gives access to stereo- and enantioselective catalysis.^[181] At present, the application of Phen in polymer systems is only sparsely reported, yet is discussed in the current thesis in Chapter 4.

2.5.4 Oxygen Ligands – Carboxylates

Among the various types of ligands which coordinate *via* oxygen atoms toward metals, this section focuses on carboxylate ligands. The donor atom oxygen is relatively compact and less polarizable. Regarding the **Pearson Classification**, carboxylates are hard donor ligands.^[160] Their versatility is reflected by the wide range of possible applications, caused by the presence of lone-pairs of electrons, available for metal binding. In metalloenzymes, carboxylates play an important role as ligands for 3d metals forming complexes catalyzing electron transfer reactions or dioxygen metabolism.^[182]

Carboxylates offer a wide range of bonding modes, reaching from ionic to covalent binding character and mono- and bidentate coordination. Additionally, numerous options of chelating and bridging modes are known. Examples for the respective binding modes are depicted in the table in Figure 2.36. Among these various types of bonding modes, most striking are bridging modes, in particular, the *syn-syn* mode. Due to its capability to form metal complexes with metal atoms in close proximity, the *syn-syn* mode is of high interest and was extensively studied.

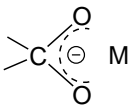
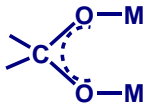
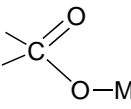
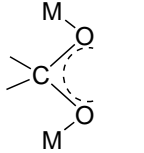
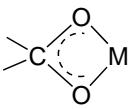
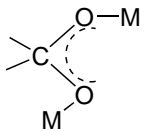
Unidentate and Chelate Carboxylate Oxygen Atom Coordination		Bridging Carboxylate Oxygen Atom Coordination	
Type	Description	Type	Description
	ionic		<i>syn-syn</i>
	unidentate		anti-anti
	chelate		anti-syn

Figure 2.36: Carboxylate ligands form a wide range of binding modes in metal complexes. The bridging mode in bimetallic complexes can be sub-divided into symmetric and asymmetric coordination. Of specific interest are *syn-syn* bridging carboxylates to study metal-metal interactions.

Most common are dimetal complexes, organized in so-called **Paddlewheel** structures, or triangular arrangements. The need to understand the nature of such metal-metal interactions entails extensive structural and physiochemical studies.^[183]

The basic structure in paddlewheel complexes consists of four carboxylates with two metal cores, termed tetrakis(carboxylato)dimetal complexes (refer to the model complex in Figure 2.37). Such complexes were prepared first in 1944 with chromium(II) cores. Shortly after, similar geometries were found for the transition metals Cu(II), Re(III), Mo(II) and Rh(II).^[184] A striking feature of such complexes is their ability to form metal–metal bonds, favored by metals with unpaired electrons. A paradigm for multiple-bonded M_2 structures are molybdenum(II) complexes, exhibiting quadruple bonded Mo–Mo atoms.^[185]

In contrast, no metal–metal bond is formed in bimetallic copper(II) compounds. However, the exchanged coupled paramagnetic centers are of considerable interest for the study of their electronic and magnetic behavior.^[186]

The possibility to implement such paddlewheel structures as linking motifs in SCNPs was investigated in the current thesis in Chapter 5. Thereby, carboxylates act as bidentate bridging ligands between two metal cores, allowing the incorporation of two metal ions in each crosslinking unit. Employed were metal cores of copper(II) and molybdenum(II). For each system, model complexes were synthesized of which the molybdenum type, crystallized in DMSO, is depicted in Figure 2.37 to illustrate the intricate paddlewheel structure.

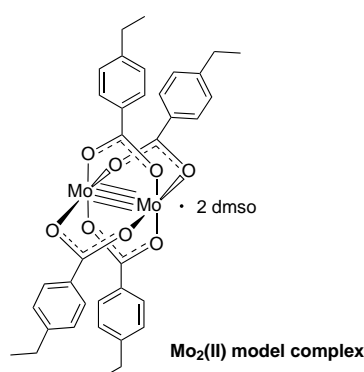


Figure 2.37: Solid state structure of a Mo_2^{4+} -paddlewheel complex, crystallized in DMSO. The depicted structure was synthesized in the current thesis as a molecular model complex for further creation of such structures as crosslinking units in SCNPs.

2.5.5 General Remarks on Lanthanide Complexes

A considerable part of the present thesis involves the complex formation with metals of the f-block in the table of elements, the lanthanides (Ln).^[187]

The chemistry of lanthanides is dominated by ions in the oxidation state +3, their most stable oxidation state.^[188] Such Ln(III) centers are strongly electropositive, thus reacting as hard Lewis acids with hard Lewis bases *via* ionic bonding interactions. Hence, a coordination to ligands containing nitrogen or oxygen donor atoms is favored. Typical coordination numbers for the large Ln (III) cations range between 8 to 10.^[189] Regarding industrial applications, Ln(III) ions are applied as active, luminescent species in optoelectronic devices or as diagnostic tools for anticancer or drug discovery studies.^[190, 191] Recently, lanthanide compounds drew attention as superconductors at high temperatures.^[192]

Characteristic for most of the trivalent lanthanides is the presence of unpaired electrons in f-orbitals, shielded by the filled 5s and 5p sub-shells.^[193] Consequently, in emission spectroscopy 4f–4f transitions endow sharp, easily recognizable emission bands and are almost insensitive to the chemical environment of the metal center. According to IUPAC rules, such emissions are categorized as fluorescence if they occur without a change in the spin or phosphorescence, which involves a change in spin.^[194] However, such 4f–4f electric dipole transitions are parity forbidden, as described by the **Laporte Rule**.^[161] This spectroscopic selection rule applies to electric dipole transitions of molecules with an inversion centre. It states that in such centrosymmetric molecules, electron transitions must involve a change in parity of the wavefunctions of the orbitals, meaning either $u \rightarrow g$ or vice versa ($u = \textit{ungerade}$ (odd), $g = \textit{gerade}$ (even)). The prohibition of 4f–4f transitions impedes a direct excitation of the Ln(III) cores, yet once an electron has been excited, its decay to the ground state is slow, from micro- to milliseconds.^[195] This property makes lanthanides suitable for applications in laser technology.^[190]

Instead of direct f-electron excitation, a more facile alternative to activate lanthanides is the sensitization by external chromophores (ligands), termed **Antenna Effect**. Such a sensitization process consists of numerous steps, from the excitation of the ligands to an energy transfer to the lanthanide ions, as illustrated in Figure 2.38. At first, the antenna ligand in the complex (${}^0\text{Ligand-Ln(III)}$) is excited from the ground state S_0 to the singlet-excited state S_1 (${}^1\text{Ligand-Ln(III)}$). Now, either a deactivation to the ground state can occur, or, in the presence of spin-orbit coupling, the triplet-excited state T_1 (${}^3\text{Ligand-Ln(III)}$) is populated. The latter process is promoted by the heavy nature of the lanthanide atom and proceeds *via* so-called intersystem crossing (ISC). If no quenching takes place, the energy is transferred to the excited state of the lanthanides, Ligand-Ln(III)^* .

This reversible process either follows the **Dexter Energy Transfer**, a transfer through bonds *via* overlapping of orbitals, or the **Förster Energy Transfer** through space, where the antenna ligand induces a dipole in the lanthanide ion. Lastly, in the absence of ligands containing N–H or O–H units, which deactivate the excited state *via* vibrational quenching, lanthanide emission occurs.^[196]

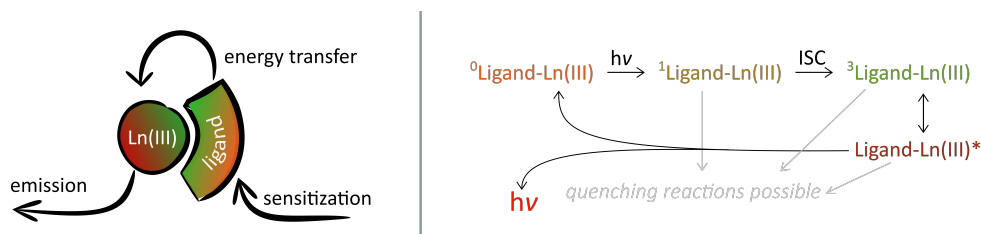


Figure 2.38: The direct excitation of lanthanide ions implies 4f–4f transitions and is therefore spectroscopically forbidden. A solution is the use of coordinating ligands, which functions as antennas. After excitation of the singlet state of the ligand, intersystem crossing (ISC) can occur, populating the triplet state. In the final step, energy is transferred from the ligands to the excited state of the lanthanide. Relaxation to the ground state results in lanthanide luminescence. Deactivation or quenching is possible in every intermediate step.

The choice of antenna ligands is highly dependent on the energy level of the triplet state of the ligand and the excited state of the lanthanide.^[197] An energy level of at least 1700 cm^{-1} above the Ligand-Ln(III)^* level is required to achieve sufficiently high population without the thermally initiated back transfer process. In addition, ligands such as water, which have vibrational modes that closely match the energy of the excited state Ligand-Ln(III)^* and thus quench the luminescence, have to be replaced. Mono-dentate ligands are often too weak to displace already coordinated water molecules, therefore chelating ligands are preferred. Indeed, multidentate and additionally space-demanding ligands are commonly used to shield the lanthanide center. Examples include cryptates, 1,3-diketones or phenanthrolines and their derivatives to transform poorly absorbing lanthanides into luminescent material.^[196, 198, 199]

Among the lanthanides, europium and terbium are the most intriguing elements, due to their emission in the visible region (550–750 nm for Eu(III) and 450–650 nm for Tb(III)). In addition, the energy gap of complexes with judicious selected ligands is sufficiently large to allow excellent population of the excited state, followed by transitions from $^5\text{D}_0 \rightarrow ^7\text{F}_6$ for Eu(III) and $^5\text{D}_4 \rightarrow ^7\text{F}_0$ for Tb(III) .^[196] The low toxicity of europium and terbium in combination with significant luminescence, entails numerous applications in life science assays such as drug discovery and imaging applications.^[200, 201]

In the present thesis in Chapter 4, the aforementioned enhancement of luminescence upon replacement of water molecules in lanthanides is investigated and described.

Platinum(II)-SCNPs as Homogeneous, Recyclable Catalysts

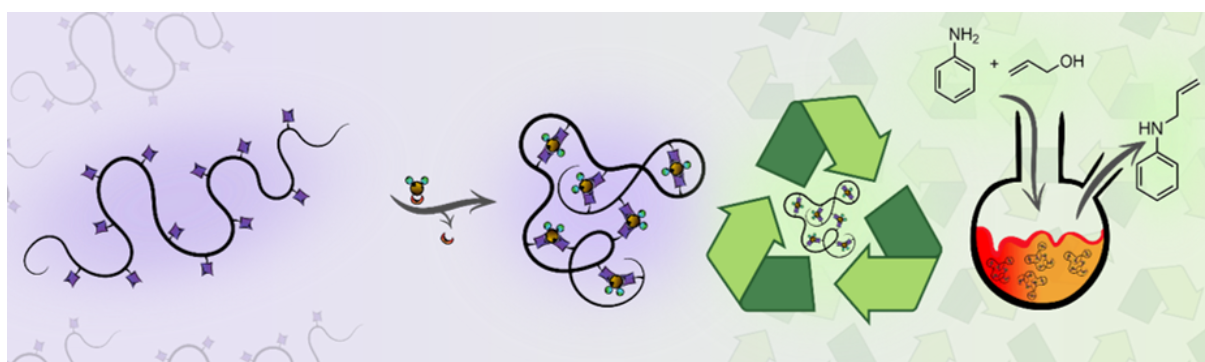


Figure 3.1: Phosphine-containing polymer chains collapse into metal-complexed SCNPs upon platinum(II) incorporation. Afterwards, the high activity of the Pt(II)-SCNPs as homogeneous catalysts is demonstrated in the amination of allyl alcohols. The specific structure of the nanoparticles enables their subsequent, facile isolation from the reaction mixture, allowing for their reuse in a second catalytic cycle.

3.1 Motivation

The present project explored catalytically active single-chain nanoparticles (SCNPs), retaining their form and function during catalysis *via* stable metal encapsulation. Particular focus was placed on the improvement of catalyst isolation and their reuse, while maintaining a high catalytic activity. Whereas molecular organometallic complexes are considered to be the most effective homogeneous catalysts for a wide range of chemical reactions, their subsequent separation from the reaction mixture remains a highly challenging task. Instead, heterogeneous catalysts allow facile separation, yet exhibit lower catalytic activity. To bridge the gap between homogeneous activity and heterogeneous recyclability, a catalytic SCNP system was developed, which switches on demand between homogeneity in-phase or heterogeneity for facile isolation.

In preliminary studies, described by our group, triarylphosphine-functionalized polymer chains formed nanoparticles upon coordination to palladium(II) ions.^[9] The resulting Pd(II)-SCNPs were applied as catalysts in a subsequently performed Sonogashira cross-coupling reaction. However, the Pd(II)-SCNPs unfolded during catalysis and only the bare polymer chains without metal ions were recovered. The reason for the metal leaching was probably a reduction of Pd(II) to Pd(0) during the catalytic process. Thereby, the metal-to-ligand bonds cleaved and released the palladium. As a result, the catalyst could not be recycled or reused.

Instead of palladium, herein platinum(II) ions were employed, expected to form more stable complexes with phosphine ligands even at elevated temperatures. Moreover, Pt(II) ions are known for efficient catalysis in numerous transformations, such as hydrations and hydrosilations.^[202–204] From an analytic point of view, the use of Pt(II) ions in phosphine systems allows for in-depth solution studies *via* ³¹P NMR and ¹⁹⁵Pt NMR spectroscopy.^[205]

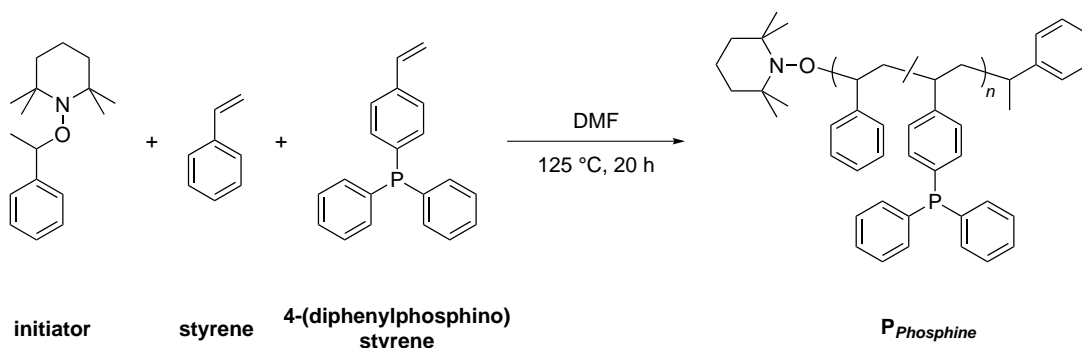
The following sections report the synthesis of a phosphine-containing polymer and its subsequent transformation in Pt(II)-SCNPs. After demonstrating the exclusive formation of Pt(II)-SCNPs, the catalytic activity and stability of the nanoparticles were investigated. As an example, the amination of allyl alcohols catalyzed by Pt(II)-SCNPs was examined. Refer to Figure 3.1 for a graphical overview of the present project.

The synthesis of the polymeric structures and the catalysis was performed in cooperation with N. Knöfel. The ¹⁹⁵Pt NMR spectrum of the Pt(II)-SCNP was measured by H. Berberich. J. Willenbacher is thanked for fruitful discussions and support. C. Barner-Kowollik and P. W. Roesky motivated and supervised the project. This chapter is adapted from Knöfel*, N. D.; Rothfuss*, H.; Willenbacher, J.; Barner-Kowollik, C.; Roesky, P. W. *Angew. Chem. Int. Ed.* **2017**, *56*, 4950–4954, with permission from John Wiley and Sons.

3.2 Synthesis of a Phosphine-Containing Polymer

Alerted by the high cost of precious metals and their inherent cell toxicity,^[206] there is an increasing demand for the generation of reusable metal-based catalysts, which are easy to isolate from the reaction compounds. Thus, the incorporation of metal ions within polymeric scaffolds is a promising approach with respect to various chemical design strategies in polymer chemistry, and easily adjustable properties of the polymer chains.

In analogy to the reported Pd(II)-SCNPs, platinum(II) ions form stable complexes *via* dynamic coordination to phosphines in a metal–ligand ratio of 1:2. Hence, a linear polymer had to be synthesized with multiple phosphine ligands along the polymer chain for subsequent metal complexation. A polymer chain, consisting of only phosphine units was considered to be less beneficial, considering the steric demands of the phenyl groups and an oversupply of coordination ligands in the subsequent metal complexation. For this reason, the commercially available monomers 4-(diphenylphosphino)styrene and styrene, serving as a comonomer, were selected. Following the repeat unit approach (refer to Chapter 2.3.1), both monomers were statistically copolymerized *via* nitroxide mediated polymerization (NMP) to ensure a narrow molecular weight distribution with predictable chain lengths (Scheme 3.1).



Scheme 3.1: Synthesis of the copolymer $P_{\text{Phosphine}}$ *via* NMP, which consists of the monomers styrene and 4-(diphenylphosphino)styrene. Adapted from [207] with permission from John Wiley and Sons.

In numerous reactions, performed during the master thesis (*Single-Chain Nanoparticles via Platinum(II) Complexation*, Rothfuss, H., 2015, KIT), a content of approx. 5 % of phosphine units and a polymer chain length with a minimum molecular weight of $25\,000\text{ g} \cdot \text{mol}^{-1}$ were found to be optimal for subsequent SCNP formation. Higher contents of functional units allowed for too many crosslinking possibilities, and thus the size reduction after chain collapse was less obvious. Simultaneously, a lower amount of functional units limited possible intrachain crosslinking reactions, probably due to the rigid structure of the backbone of the polymer chain. Furthermore, the analysis of SCNPs, originating

from chains of a molecular weight below $25\,000\text{ g}\cdot\text{mol}^{-1}$ was challenging, due to their compact nature and small size, significantly below $< 10\text{ nm}$ (refer to Chapter 2.4.3).

In agreement with the aforementioned criteria, the copolymer $P_{\text{Phosphine}}$ was selected as a precursor macromolecule, most suitable for subsequent single-chain folding with regards to chain length, polydispersity and functional group distribution. The copolymer composition was determined via ^1H NMR spectroscopy, comparing the integrals of the aromatic resonances of the two monomers (Figure 3.2). A monomer ratio of 21:1, regarding the higher amount to styrene, was identified. This ratio is close to approx. 5 % of phosphine units. The incorporation of phosphine units into the polymer chain was verified via $^{31}\text{P}\{^1\text{H}\}$ NMR spectroscopy, detecting a resonance for triarylphosphine at $\delta = -6.2\text{ ppm}$ (Figure 3.3, right). Inevitable was the partial oxidation of some triarylphosphine groups, apparent at $\delta = 29.0\text{ ppm}$. Noteworthy, the employed monomer already contained approx. 3 % of oxidized species. During polymerization, the amount of oxidized triarylphosphine increased to $\sim 7\%$ (in comparison to the main signal).

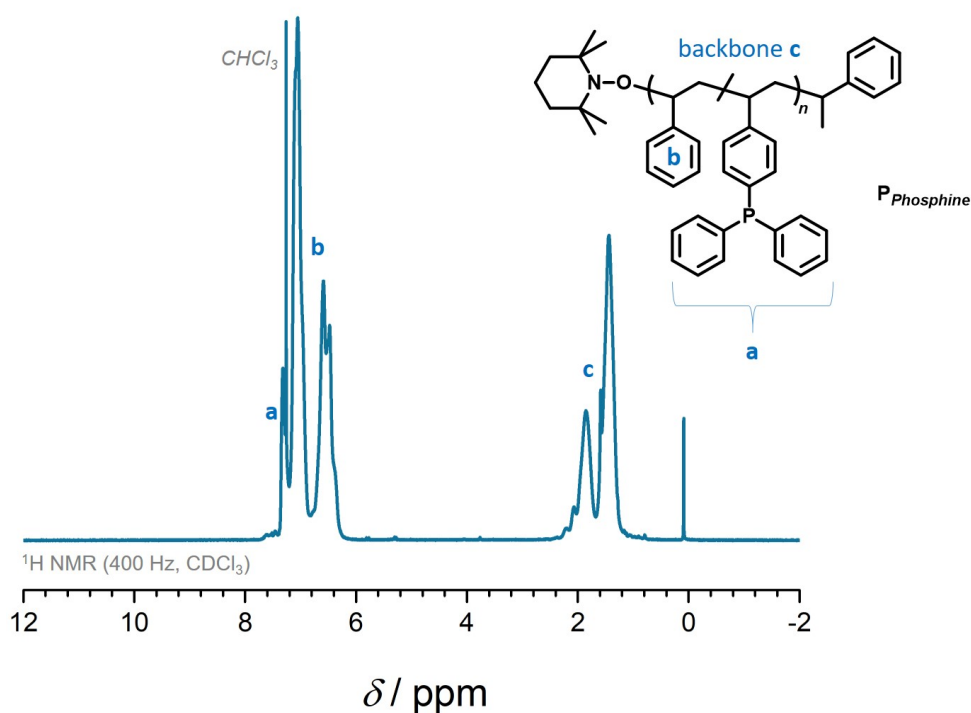


Figure 3.2: Analysis of the copolymer $P_{\text{Phosphine}}$ via ^1H NMR spectroscopy, detecting resonances for the aromatic and aliphatic protons of both employed monomers. A monomer ratio in the copolymer of 1:21, equivalent to 5 % phosphine units, was determined.

Size exclusion chromatography (SEC) measurement in THF (RI detector) indicated for $P_{\text{Phosphine}}$ a molecular weight of M_n close to $40,600\text{ g}\cdot\text{mol}^{-1}$ with a narrow dispersity index of $D = 1.15$.

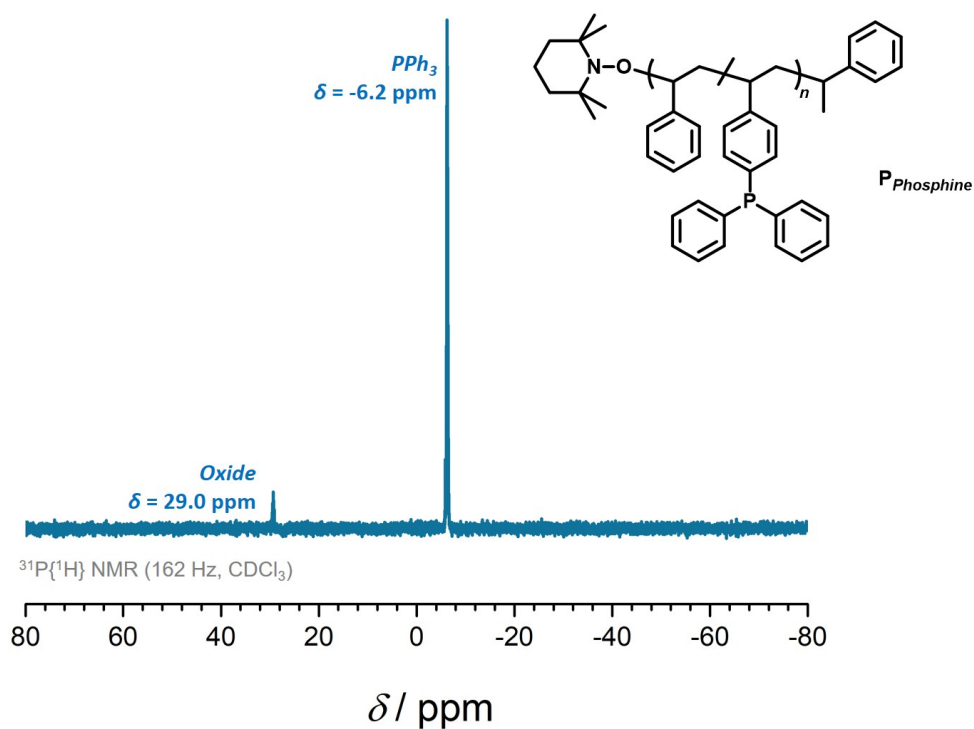


Figure 3.3: The incorporation of phosphine units in $\text{P}_{\text{Phosphine}}$ was confirmed by $^{31}\text{P}\{^1\text{H}\}$ NMR spectroscopy, showing resonances for triarylphosphines at $\delta = -6.2$ ppm and its oxidized species at $\delta = 29.0$ ppm. Adapted from [207] with permission from John Wiley and Sons.

3.3 Synthesis of Pt(II)-SCNPs

One of the main requirements for the preparation of SCNPs is the exclusive intrachain crosslinking without any intermolecular linkages. Otherwise, disordered macromolecules or insoluble networks are formed. Hence, working under high dilution is essential, ensuring a low concentration of active groups in close spatial proximity. Therefore, the precursor metal complex is dissolved in high amounts of the respective solvent. To maintain an overall low concentration without excessive use of solvent, the precursor polymer is added dropwise to this salt solution *via* a syringe pump. A low addition rate, typically $1 \text{ mL} \cdot \text{h}^{-1}$, ensures that each aliquot polymer has already reacted before the next aliquot of polymer solution is added to the mixture.

A specific prerequisite for working with phosphine compounds is the suppression of phosphine oxidation. The resulting phosphine oxides have a different coordination behavior and will no longer form complexes with platinum(II), as described in the Chapter addressing phosphine ligands and lanthanides, 2.5.5 and 2.5.3. Therefore, all reactions involving phosphine moieties were performed under the exclusion of oxygen in an argon or nitrogen atmosphere.

Important on a molecular level are free coordination sites on a metal ion or readily replaceable ligands. For the coordination of phosphine-to-platinum, the precursor complex $[\text{PtCl}_2(\text{cod})]$ was employed. This complex was selected due to its labile ligand 1,5-cyclooctadiene (COD), which can be readily substituted by two phosphine moieties.^[208]

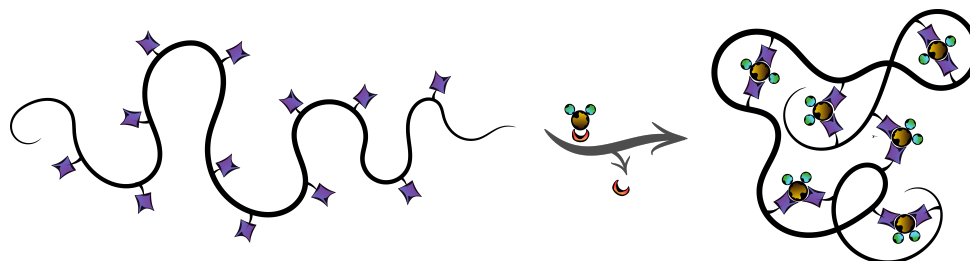
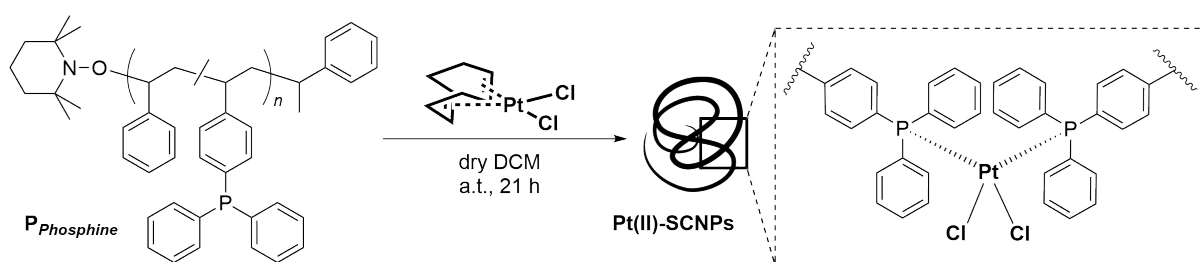


Figure 3.4: A single polymer chain collapses into a nanoparticle triggered by the addition of metal ions.

The ratio between ligands and metal ions of 2:1 pointed towards a chain collapse, as schematically shown in Figure 3.4 and with chemical structures in Scheme 3.2. After isolation and purification of the presumed nanoparticles, the change of polymer architecture, from the unfolded to the folded state, as well as the folding motif were carefully analyzed.

First evidence for a reduced hydrodynamic radius was provided by SEC measurements (THF, RI). In comparison to the precursor polymer $P_{\text{Phosphine}}$, the SEC trace of the nanoparticles is shifted towards a higher, prolonged retention time with a small dispersity index of $\mathcal{D} = 1.2$ (Figure 3.5, *left*). Although the molecular weight of the metal-doped polymer system had slightly increased upon platinum(II)



Scheme 3.2: Reaction scheme for the formation of Pt(II)-SCNPs utilizing the precursor complex $[\text{PtCl}_2(\text{cod})]$ and the copolymer $\text{P}_{\text{Phosphine}}$. The replacement of the labile coordinated COD ligand by two polymer-derived phosphine ligands resulted in the incorporation of platinum(II) ions into the polymer scaffold. By working under high dilution, the 2:1 ratio between ligands and metal ion induced a single-chain collapse, thus Pt(II)-SCNPs are formed. Adapted from [207] with permission from John Wiley and Sons.

complexation, a smaller hydrodynamic radius was detected, pointing towards the exclusive formation of SCNPs (refer to the Chapter about SEC analysis 2.4.1).

The formation of Pt(II)-SCNPs was additionally confirmed by diffusion ordered spectroscopy (DOSY), distinguishing molecules according to their diffusion coefficient (refer to Chapter 2.4.2). The correlation between the diffusion coefficient D of a molecule and the hydrodynamic radius r_H is given by the Stokes–Einstein Equation.

Table 3.1: Diffusion coefficients D and the corresponding hydrodynamic radii r_H of the linear copolymer $\text{P}_{\text{Phosphine}}$ and the Pt(II)-SCNPs, determined *via* DOSY. The shown values are averages of the diffusion coefficients of resonances of the backbone and side chains. Based on the diffusion coefficients, the hydrodynamic radii r_H of the compounds were calculated applying the Stokes–Einstein Equation.

Substance	D [m^2s^{-1}]	Error	r_H [nm]
Copolymer $\text{P}_{\text{Phosphine}}$	5.46×10^{-11}	0.9×10^{-13}	7.4
Pt(II)-SCNPs	8.82×10^{-11}	2.9×10^{-12}	4.6

For a comparison between $\text{P}_{\text{Phosphine}}$ and Pt(II)-nanoparticles, DOSY measurements of both polymer structures were performed (refer to Table 3.1). To ensure a representative value, numerous NMR resonances from the backbone and the side chains were selected and their diffusion coefficients were determined. The precursor polymer and the nanoparticles were analyzed in CDCl_3 , employing a dynamic viscosity of $\eta = 0.5418 \cdot 10^{-3} \text{ Nsm}^{-2}$ (at 25 °C).^[209] The mean hydrodynamic radius of $\text{P}_{\text{Phosphine}}$ resulted in $r_{H,\text{DOSY}} = 7.4 \text{ nm}$, while a radius of $r_{H,\text{DOSY}} = 4.6 \text{ nm}$ was calculated for the Pt(II)-SCNPs.

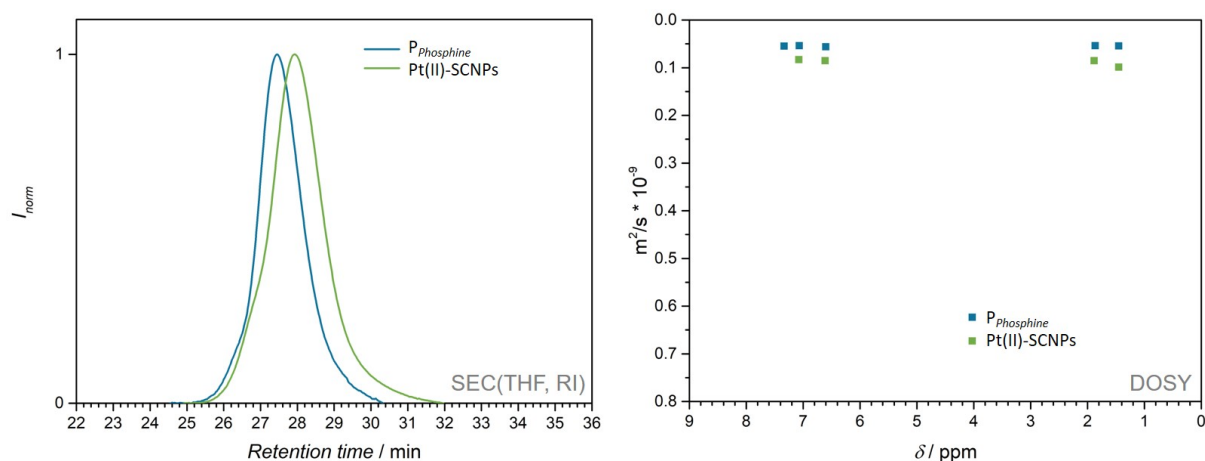


Figure 3.5: Evidence for a reduced hydrodynamic radius of the Pt(II)-SCNPs was provided by SEC analysis (THF, RI detector), *left*. The trace for the nanoparticles is shifted completely towards higher retention times, indicating a smaller radius. A single chain collapse of $P_{\text{Phosphine}}$ into nanoparticles was further confirmed *via* DOSY measurements, *right*. Adapted from [207] with permission from John Wiley and Sons.

The polymer compaction upon metal salt addition was further demonstrated by dynamic light scattering (DLS). For the precursor $P_{\text{Phosphine}}$, a hydrodynamic diameter of $d = 15.2$ nm was obtained, while a diameter of $d = 8.5$ nm was observed for the Pt(II)-SCNPs. However, the determination of the hydrodynamic radius *via* DLS invokes critical assumptions. The analyzed molecules are treated as hard, spherical particles with a homogeneous density, not considering the actual conformation of the analyzed particles. This may cause significant discrepancies for disperse polymer chains and nanoparticles when analyzing them *via* DLS.^[145]

In conclusion, the decrease of the hydrodynamic radius of the Pt(II)-SCNPs was determined by the characterization methods SEC, DOSY and DLS measurements. All mentioned characterization techniques confirmed the successful collapse of the single-chains into nanoparticles.

In the next step, the implementation of Pt(II) ions and the actual folding motif in the SCNPs were carefully analyzed.

The analysis of the Pt(II)-SCNPs *via* ^1H NMR spectroscopy indicated the expected resonances for the aromatic and aliphatic protons in the polymer structure. A linkage of COD to platinum could be ruled out, since no resonance for the free or coordinated COD ligand was detected (COD: $\delta = 5.6, 2.0$ ppm; $[\text{PtCl}_2(\text{cod})]$: $\delta = 5.5, 2.7\text{--}2.1$ ppm).^[210, 211] In comparison with the ^1H NMR spectrum of $P_{\text{Phosphine}}$, the resonances of the aromatic protons of the 4-(diphenylphosphine)styrene monomer were shifted towards down-field, caused by the vicinity to the platinum ions (Figure 3.6).

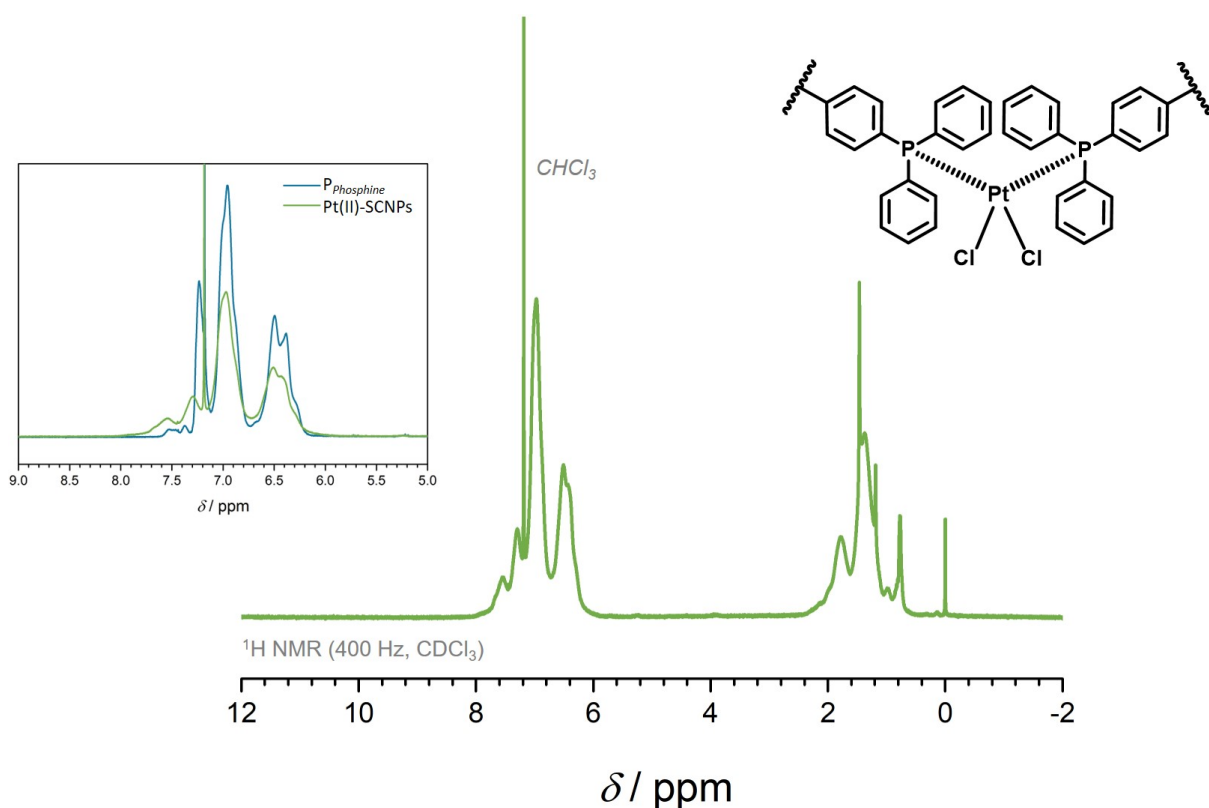


Figure 3.6: Analysis of the Pt(II)-SCNPs via ^1H NMR spectroscopy, depicting the expected resonances of the aromatic and aliphatic protons. No resonance for free or coordinated COD was detected, pointing towards a complete substitution and sufficient purification. Upon platinum(II) coordination, the corresponding aromatic protons are shifted towards low field, compared to the former precursor $P_{\text{Phosphine}}$, zoomed in spectrum, left. Adapted from [207] with permission from John Wiley and Sons.

A benefit in employing platinum is its NMR active core in the isotope ^{195}Pt . With a spin of $I = 1/2$ and an abundance of 33.4 %, the measurement of ^{195}Pt NMR is enabled.^[212] Moreover, the cores of ^{195}Pt and ^{31}P have a scalar coupling, provided that the atoms are connected via a binding electron pair.^[213] This coupling results in characteristic platinum satellites in a ^{31}P NMR spectrum.

Regarding the geometrical arrangement in the folding unit, Pt(II) ions are known to form complexes of square planar coordination. Thus, with the two pairs of ligand moieties, chloride and phosphines, two stereoisomers are possible: the *trans* and *cis* isomers, which are depicted in Figure 3.7. In such a square planar geometry, the magnitude of the coupling between the ^{195}Pt and ^{31}P nuclei is very sensitive to the stereochemistry of the ligands. The aforementioned *cis* or *trans* geometry can therefore be differentiated by the resonance shifts of the phosphine species in the ^{31}P NMR spectrum. In addition, the ligand environment and geometrical arrangement supply characteristic coupling constants. For the molecular complex $[\text{PtCl}_2(\text{PPh}_3)_2]$ a coupling constant of $^1J_{\text{Pt}, \text{P}} = 3800$ Hz is distinctive for a *cis*-species and a coupling constant of $^1J_{\text{Pt}, \text{P}} = 2600$ Hz for *trans*-coordination.^[214]

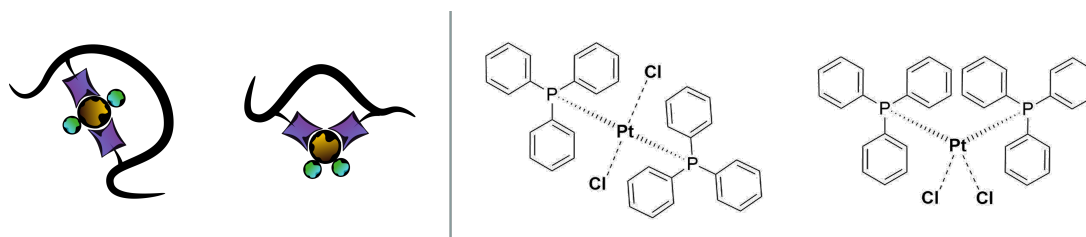


Figure 3.7: Platinum(II) ions typically form complexes of square planar coordination. In a combination of two pairs of ligands, *trans* or *cis* complexes are received (left and right, respectively). During synthesis of the complex, both arrangements can be formed. Since each geometry causes characteristic resonances in the ^{31}P NMR spectrum, the *cis/trans* ratio in a mixture can easily be determined.

The coupling between ^{195}Pt and ^{31}P is reciprocal, hence phosphine units cause a splitting of the ^{195}Pt resonances in the corresponding ^{195}Pt NMR spectrum. However, ^{195}Pt NMR spectroscopy is rarely employed, due to the necessity of large amounts of analyte and elaborate measurement procedures, since the resonances for platinum species shift over a wide range (approx. 13 000 ppm).^[212] Aggravating is the fact that the shifts appear without direct relation to oxidation state or coordination number.

The properties of structural arrangement in molecular complexes can directly be transferred to the geometry in the Pt(II)-SCNPs.

On a molecular level, the complete coordination of phosphine units in $P_{\text{Phosphine}}$ was confirmed via $^{31}\text{P}\{^1\text{H}\}$ spectroscopy (Figure 3.8). Importantly, no resonance at $\delta = -6.2$ ppm of the formerly triarylphosphine species was detected. Instead, new sets of signals appeared in the downfield region. The most intense resonance at $\delta = 13.4$ ppm was assigned to the triarylphosphine-Pt(II) *cis*-coordination accompanied by characteristic ^{195}Pt satellites ($d, {}^1J_{\text{P,Pt}} = 3706$ Hz). The coupling constant of the satellites, as well as the shift of the complexed phosphine moieties are in close agreement with data of the literature-known complex *cis*- $[\text{PtCl}_2(\text{PPh}_3)_2]$ ($\delta = 14.3$ ppm; ${}^1J_{\text{P,Pt}} = 3673$ Hz).^[214] Less intense is the resonance for the *trans*-species at $\delta = 19.5$ ppm and the corresponding satellites ($d, {}^1J_{\text{P,Pt}} = 2700$ Hz), consistent with the analogous complex *trans*- $[\text{PtCl}_2(\text{PPh}_3)_2]$ ($\delta = 19.8$ ppm; ${}^1J_{\text{P,Pt}} = 2637$ Hz).^[214] The preference for a *cis*-coordinated phosphine–platinum unit is presumably due to the predetermined geometry of the *cis*-configuration of the starting material $[\text{PtCl}_2(\text{cod})]$. As observed already for $P_{\text{Phosphine}}$, a resonance for oxidized phosphine units is allocated at $\delta = 29.1$ ppm. Within the experimental accuracy of NMR spectroscopy, a *cis/trans*-configuration ratio of 9:1 was determined for the Pt(II)-SCNPs.

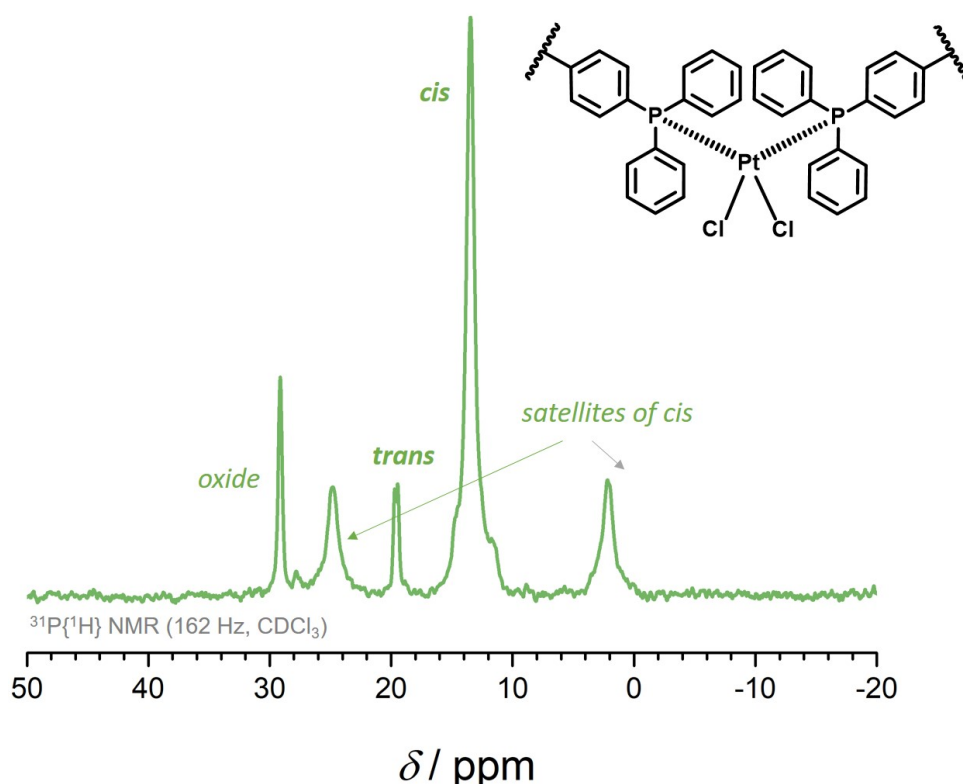


Figure 3.8: Pt(II)-SCNPs exhibit characteristic resonances in the $^{31}\text{P}\{^1\text{H}\}$ NMR spectrum for the *cis* and *trans* species, pointing towards a successful implementation of platinum(II) ions in the polymer scaffold. The higher amount of *cis*-species is explained by the use of a *cis*-coordinated precursor complex. The scalar coupling between the NMR active cores of ^{195}Pt and ^{31}P causes platinum satellites in the $^{31}\text{P}\{^1\text{H}\}$ NMR spectrum. Adapted from [207] with permission from John Wiley and Sons.

The data, obtained from the $^{31}\text{P}\{^1\text{H}\}$ NMR analysis, was further confirmed by ^{195}Pt NMR spectroscopy (Figure 3.9). As expected, two sets of resonances were detected in the spectrum. The dominant resonance at $\delta = -4413$ ppm ($t, {}^1J_{\text{Pt,P}} = 3694$ Hz) was assigned to the *cis*-coordinated platinum moiety. The less intense resonance at $\delta = -4033$ ppm ($t, {}^1J_{\text{Pt,P}} = 2648$ Hz) was associated with the *trans*-species. For comparison, the same observations were made for the previously described molecular complex $[\text{PtCl}_2(\text{PPh}_3)_2]$ and reported for molecular complexes of similar structure.^[205]

In conclusion, the collapse of single-chains into platinum(II)-nanoparticles upon Pt(II) ion addition was explored and verified *via* SEC, DOSY and DLS measurements. The implementation of Pt(II) ions and the analysis of the folding motif were depicted by ^1H , $^{31}\text{P}\{^1\text{H}\}$ and ^{195}Pt NMR spectroscopy. Characteristic resonances were identified, being in good agreement with literature-known values for analogues molecular complexes.

The successfully synthesized Pt(II)-SCNPs were further investigated in their activity as homogeneous, recyclable catalysts in an organic model reaction.

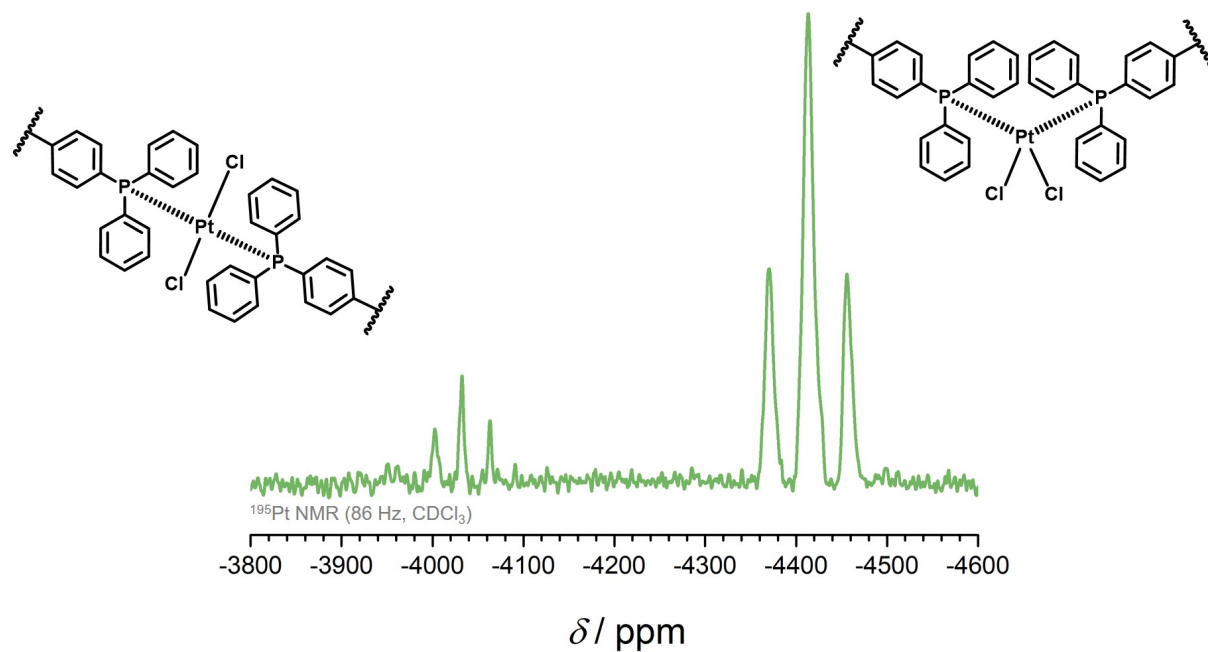


Figure 3.9: The incorporation of NMR active ^{195}Pt cores allows for ^{195}Pt NMR analysis of the Pt(II)-SCNPs. In the spectrum, two triplets for the *cis* and *trans* arrangement in the nanoparticles appear. Their shifts and coupling constants are in good agreement with values for a platinum core in a square-planar surrounding of phosphine ligands. As observed already in the $^{31}\text{P}\{^1\text{H}\}$ NMR spectrum, herein the dominant resonance at $\delta = -4413$ ppm belongs to the *cis*-species. Adapted from [207] with permission from John Wiley and Sons.

3.4 Application of Pt(II)-SCNPs as Homogeneous, Recyclable Catalysts

The aim when generate Pt(II)-SCNPs was the possible synergy of the high activity of a homogeneous catalyst with the recyclability of heterogeneous systems. This ability is enabled by a switch in the solubility of the polymer chains, dependent on the solvent polarity. Due to the styrene moieties in the polymer scaffold, the SCNPs easily dissolve in non-polar organic solvents, yet precipitate in polar media. This characteristic of the nanoparticles allows their isolation and reuse after catalysis, adjustable by the decisive change of the polarity of the solvent.

Compared to typical molecular metal-organic complexes employed as homogeneous catalysts, this is a significant advantage. Often, their separation from the reaction mixture after catalysis requires elaborate purification methods, causing them to remain in the product.

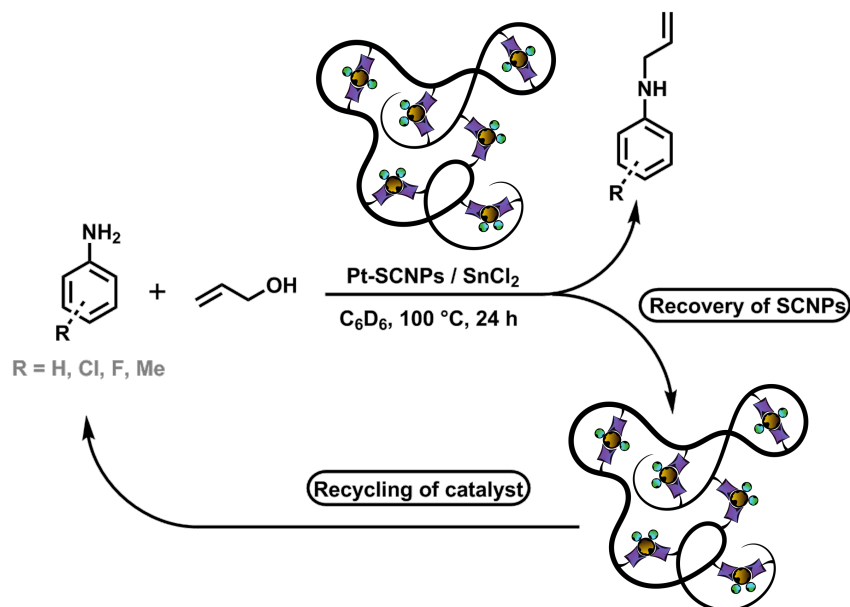


Figure 3.10: Pt(II)-SCNPs retain their folded structure and catalytic activity in the catalytic cycle of the amination of allyl alcohol. Due to the characteristics of the polymeric scaffold, the SCNPs could readily be heterogenized after the reaction, allowing their isolation and application in a second catalytic cycle. Adapted from [207] with permission from John Wiley and Sons.

The catalytic activity of the Pt(II)-SCNPs was investigated in a reaction of allyl alcohol with different aniline derivatives, known to be catalyzed by Pt(II) ions.^[10, 215] This reaction type has been in the focus of scientific research lately, since it is an atom economic reaction to synthesize various amines, with water being the only side product.

Described in detail in the Experimental Section, Figure 3.11 depicts the equation for the reaction of aniline with propenol, catalyzed by Pt(II)-SCNPs. Below, the corresponding proton NMRs at time

zero and after 24 hours clearly depict the consumption of the starting material and the formation of the product allylaniline. All catalytic experiments were carried out in benzene (C_6D_6) to allow immediate conversion and yield determination *via* NMR analysis. Further reaction conditions entailed a reaction temperature at 100 °C, 24 hours and the application of tin(II) chloride ($SnCl_2$) as a co-catalyst. Nascent water was absorbed by added molecular sieves (3 Å).

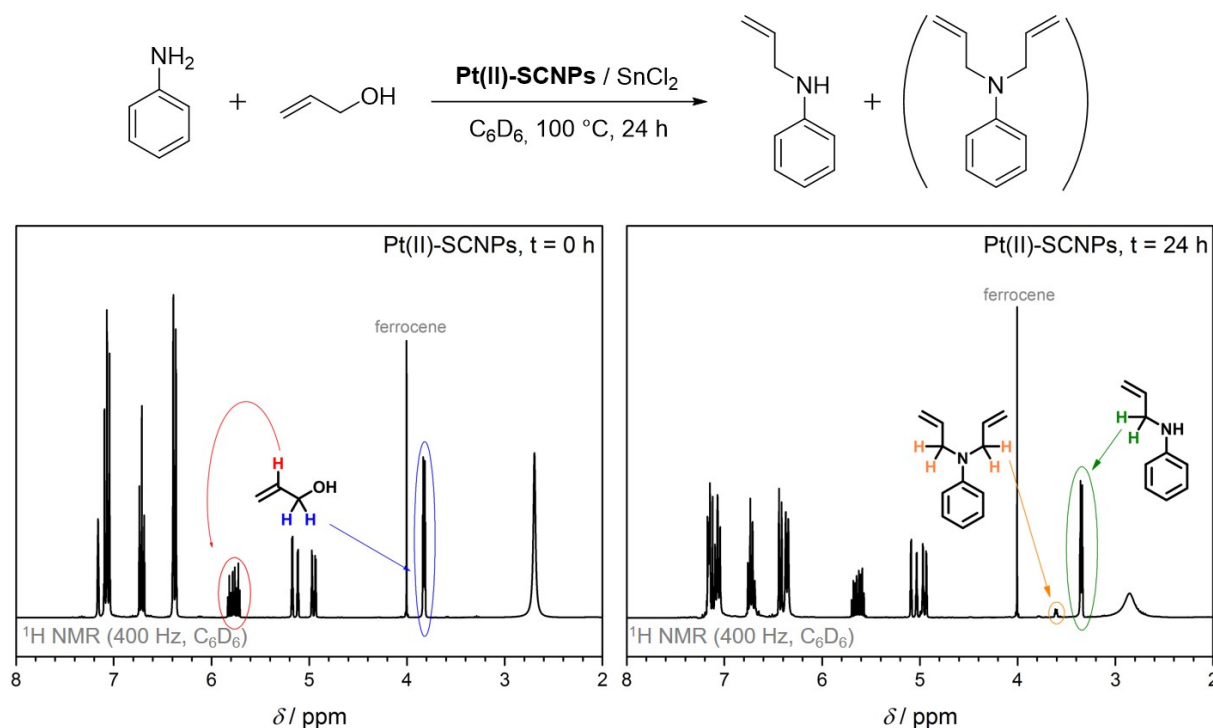


Figure 3.11: Pt(II)-SCNPs demonstrated their catalytic activity in the amination of allyl alcohols. *Below:* The ¹H NMRs of the reaction mixtures at time zero and after 24 hours. Marked in color are the replacements of the resonances of the starting material by the resonances of the product. Adapted from [207] with permission from John Wiley and Sons.

The conversions and selectivity of the presented and the following reactions were determined by ¹H NMR spectroscopy, applying ferrocene as additionally added standard. Therefore, the ratio between ferrocene ($\delta = 4.0$ ppm), the starting material allyl alcohol and the product(s) was calculated by a comparison of the integrals of the corresponding proton resonances $-CH_2$ and $=CH$, respectively. In additionally performed control reactions, the catalytic activity of the other metal-containing substances in the reaction mixture was excluded. Neither ferrocene, nor the co-catalyst tin(II) chloride showed any catalytic activity themselves in this specific reaction.

Interestingly, applying only 0.24 mol % of catalyst, high conversions of the alcohol of over 90 % were observed after 24 hours. The reaction of aniline with propenol was furthermore followed *via* proton NMR over the complete reaction time of 24 hours to monitor the conversion. Samples in intervals of 30 minutes, 1 hour and two hours were taken. The NMR data of the first 12 hours are

provided in Figure 3.12, showing the fast consumption of the starting material and the generation of product.

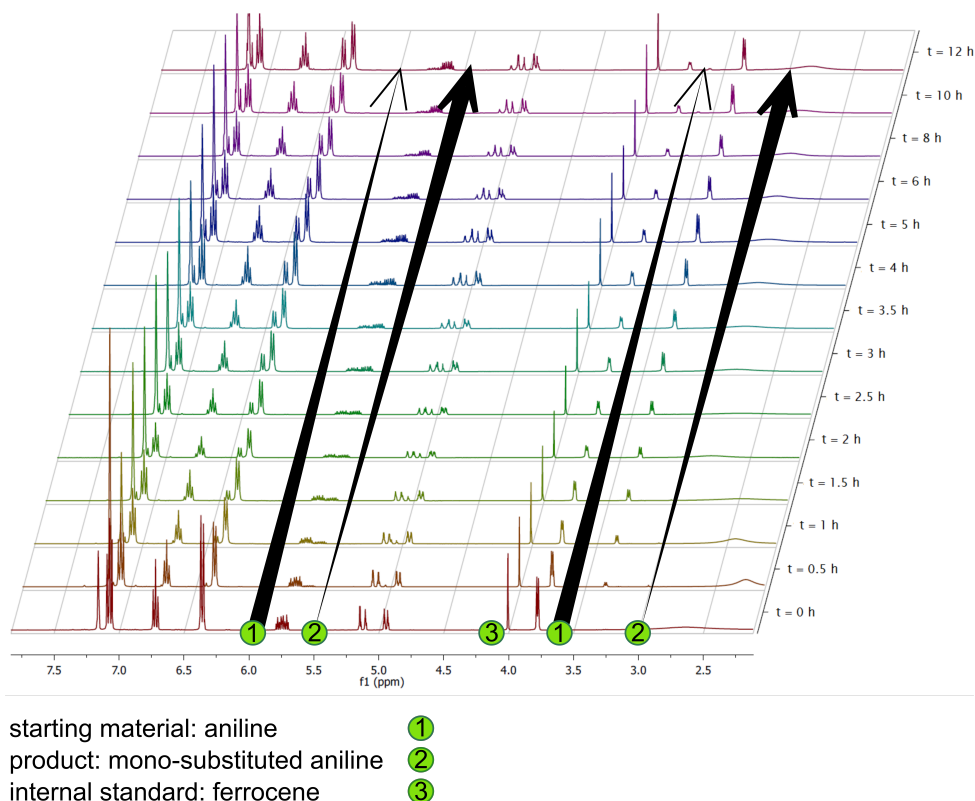


Figure 3.12: To follow the amination of allylic alcohol catalyzed by Pt(II)-SCNP, samples were taken and analyzed via ^1H NMR spectroscopy over a time period of 24 hours. Depicted here are the first 12 hours. The measurement was performed in C_6D_6 ($\delta = 7.16$ ppm), with ferrocene ($\delta = 4.0$ ppm) as an internal standard. Adapted from [207] with permission from John Wiley and Sons.

To demonstrate the functional group tolerance of the catalyst, various aniline derivatives were employed as starting materials (refer to Table 3.2 and Appendix; here presented numbers do only refer to the referred table and not to the numbering in the Experimental Section). In most of the reactions, the allyl alcohol was converted nearly quantitatively within 24 hours. Starting with aniline, the main product was the mono-substituted amine (1b) obtained in a yield of 91 %, whereas the di-substituted version (1c) was only formed up to 4 %. The conversion of the halide-substituted aniline derivatives 3-chloroaniline, 3-fluoroaniline and 4-chloroaniline (2a-4a) was consistently high (91–98 %) with nearly identical yields for the corresponding products 2b–4b (79–86 %). Employing 2,6-dimethylaniline (5a) as starting material, the conversion and the yield of the allyl alcohol decreased significantly to approx. 35 %. The reason was probably steric hindrance, caused by the two methyl groups in *ortho*-position of the amine group.

3 Platinum(II)-SCNPs as Homogeneous, Recyclable Catalysts

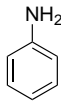
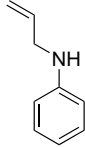
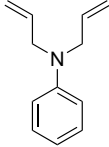
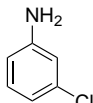
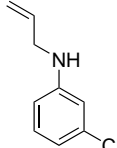
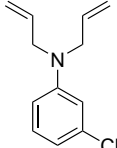
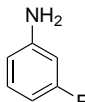
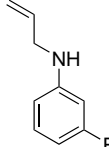
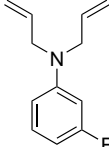
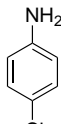
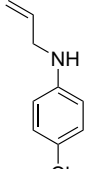
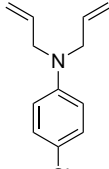
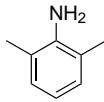
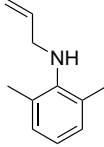
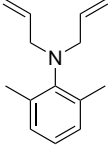
Subst. ^[b]	Catalyst	Conversion [%] ^[c]	Product	yield [%] ^[c]	Side-product	yield [%] ^[c]
 1a	Pt-SCNPs	99	 1b	91	 1c	3.8
	[Pt(PPh ₃) ₂ Cl ₂]	97		85		3.2
 2a	Pt-SCNPs	96	 2b	86	 2c	2.8
	[Pt(PPh ₃) ₂ Cl ₂]	92		79		2.4
 3a	Pt-SCNPs	98	 3b	79	 3c	3.3
	[Pt(PPh ₃) ₂ Cl ₂]	90		82		2.6
 4a	Pt-SCNPs	91	 4b	79	 4c	2.5
	[Pt(PPh ₃) ₂ Cl ₂]	96		84		3.0
 5a	Pt-SCNPs	35	 5b	32	 5c	-
	[Pt(PPh ₃) ₂ Cl ₂]	34		22		-

Table 3.2: Amination of allyl alcohol, catalyzed by Pt(II)-SCNPs and *cis*-[Pt(PPh₃)₂Cl₂].^[a] [a] Conditions: 0.24 % catalyst, SnCl₂ (0.96 mol%), C₆D₆, 24 hours, 100 °C, molecular sieves (3 Å). [b] Aniline derivatives were used in excess (2 equiv.). [c] Calculated by ¹H NMR spectroscopy with ferrocene as internal standard.

To quantify the catalytic activity of the Pt(II)-SCNPs, analogous reactions were performed with the molecular catalyst *cis*-[PtCl₂(PPh₃)₂]. Interestingly, the mono-molecular complex showed similar conversions and yields as the Pt(II)-SCNPs, 90–97 % for 1a–4a and 79–85 % for 1b–4b, respectively. Clearly, the platinum-centers, although anchored on a polymer support, were not limited in their activity and selectivity. Hence, the polymer-created pockets had no negative influence due to undesired shielding. A facile access of the reaction partners to the catalytic platinum centers can therefore be assumed.

For the recovery of the Pt(II)-SCNPs, various purification methods were tested. In general, the small amounts of employed catalysts required careful purification to avoid any loss of material. At first, small particles in the solution, probably due to scrapping between the stir bar and the molecular sieves, had to be filtered off. In a subsequent addition of methanol to the reaction mixture, a white precipitate, likely polymeric material, was observed. However, the dispersed nanoparticles precipitated as colloids, complicating filtration.

The best pathway proved to be purification *via* dialysis. Therefore, the entire reaction mixture was transferred into a dialysis tube and rinsed for four days with methanol. Subsequent filtering of the solid allowed a quantitative recovery. The absence of catalyst in the products was evidenced by ³¹P{¹H} NMR spectroscopy, where no phosphine resonances were detected. To determine the post-catalytic structure of the isolated Pt(II)-SCNPs, they were further analyzed by SEC (DMAc, RI) and ³¹P{¹H} NMR spectroscopy.

As depicted in Figure 3.13, the SEC traces of the Pt(II)-SCNPs before and after catalysis overlap closely, indicating a still folded structure of the nanoparticles. In repeated reactions and subsequent measurements even a shrinking of the recycled SCNPs was observed *via* SEC analysis. In accordance with the corresponding ³¹P{¹H} NMR spectrum, resonances for a Pt–phosphine species in *cis* and *trans* configuration were detected. Moreover, no resonance for a free phosphine moiety appeared.

The combination of both analyses methods pointed towards a still folded nanoparticle structure with quantitative coordination of the phosphine ligands to the platinum ions.

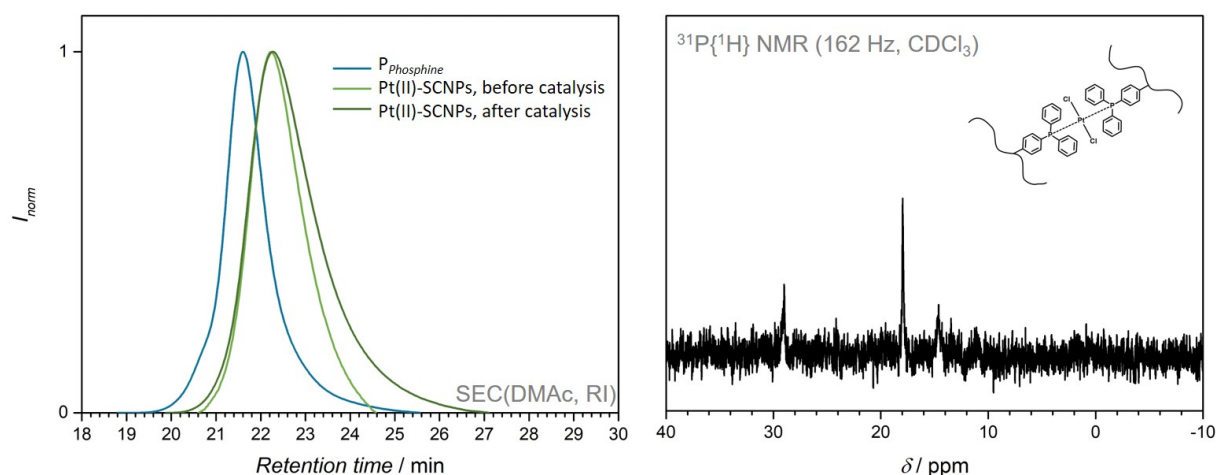


Figure 3.13: SEC measurements (DMAc, RI) and $^{31}P\{^1H\}$ NMR spectroscopy demonstrate the folded structure of the Pt(II)-SCNPs after catalysis. The SEC traces of the SCNPs before and after catalysis overlap, *left*. Resonances for a Pt–phosphine species in *cis* and *trans* geometry are detected in the $^{31}P\{^1H\}$ NMR spectrum. Adapted from [207] with permission from John Wiley and Sons.

Interestingly, the $^{31}P\{^1H\}$ NMR spectrum indicated a change in the *cis/trans* coordination ratio. In comparison to the former $^{31}P\{^1H\}$ NMR spectrum, here, the most intense resonance appeared at $\delta = 17.9$ ppm, most likely associated with a *trans*-coordination of the platinum(II) ions to the phosphine groups. To investigate the origin of the change in geometry further reactions were performed. Likely seemed a temperature-related reason. Therefore, non-used Pt(II)-SCNPs, predominately in *cis*-configuration, were heated in C_6D_6 at 100 °C for 24 hours. No other substances were added to the solution. Subsequently performed $^{31}P\{^1H\}$ NMR analysis revealed the transformation into a primarily *trans*-configuration (Figure 3.14).

Having confirmed the geometry change as a temperature-induced reaction, the *trans*-Pt(II)-SCNPs were applied as catalysts. Applying aniline (1a), the reaction was carried out as described before. The determination of the allyl alcohol conversion (94 %) as well as product formation of 1b (85 %) and 1c (3 %), identified only a slightly reduced catalytic activity of the *trans*-configured Pt(II)-SCNPs in comparison to the mainly *cis*-configured Pt(II)-SCNPs (1b: 91 %). Obviously, the isomerization of the Pt(II)-to-phosphine unit did not significantly influence the catalytic activity of the Pt(II)-SCNPs. Moreover, the experiment evidenced the temperature stability of the SCNPs. Neither free phosphine, nor oxide were detected in the NMR, and the *trans*-coordinated Pt(II)-SCNPs did not suffer a significant loss of activity.

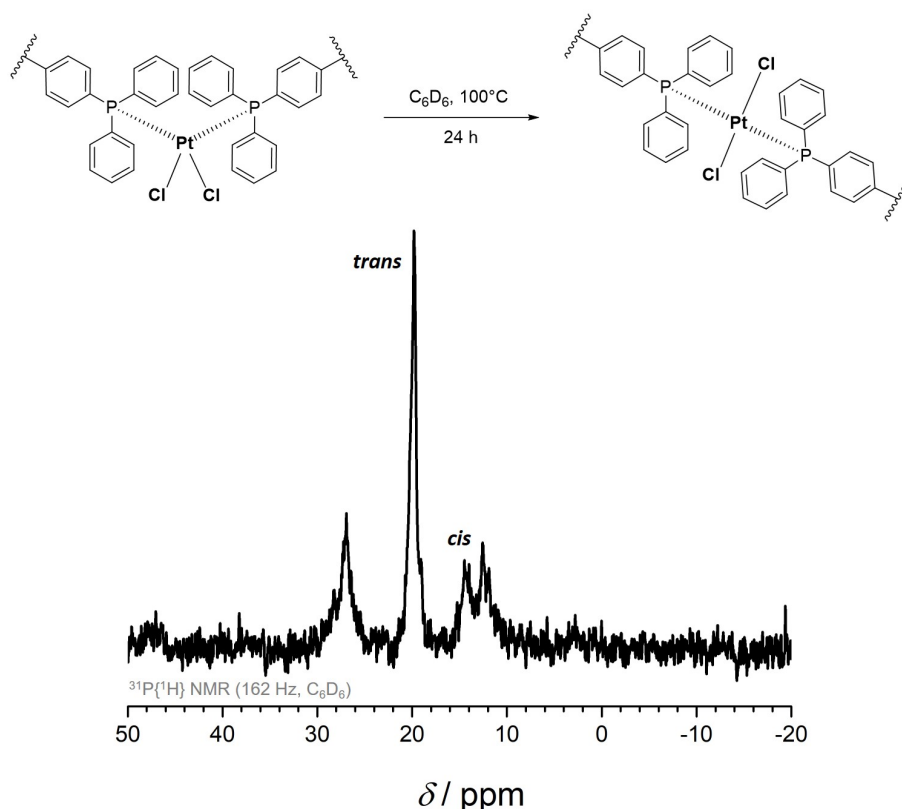


Figure 3.14: Pt(II)-SCNPs show a temperature-related change in conformation. Upon heating in C_6D_6 for 24 hours, the primarily *cis*-coordinated structures were converted into the *trans*-species. Adapted from [207] with permission from John Wiley and Sons.

After clarification of the origin of the different resonances in the $^{31}P\{^1H\}$ NMR spectrum, the Pt(II)-SCNPs were employed in a second catalytic cycle. This second cycle was performed to verify that not only the structure of the Pt(II)-SCNPs remained intact, yet also the particles were still catalytically active.

However, the amount of catalyst was less than for the first cycle, since small amounts of the first batch were needed for NMR, SEC and DLS measurements. Furthermore, $SnCl_2$ was not recovered after the first catalysis, yet washed out by methanol in the purification *via* dialysis. Thus, $SnCl_2$ had to be added again to the reaction mixture for the following catalytic cycle. To demonstrate the catalytic activity of the recycled Pt(II)-SCNPs, the reaction of aniline (1a) and propenol alcohol was repeated under the same reaction conditions as before ($SnCl_2$ (0.96 mol%), C_6D_6 , $100^\circ C$, 24 hours, 3 \AA molecular sieves), with 0.24 mol% the Pt(II)-SCNPs as catalyst. Depicted in Figure 3.15 are the corresponding proton NMR spectra at time zero and after 24 hours. In comparison to the first catalytic cycle, the recycled Pt(II)-SCNPs still accomplished a conversion of the allyl alcohol of approx. 70 %, proving that they are still catalytically active.

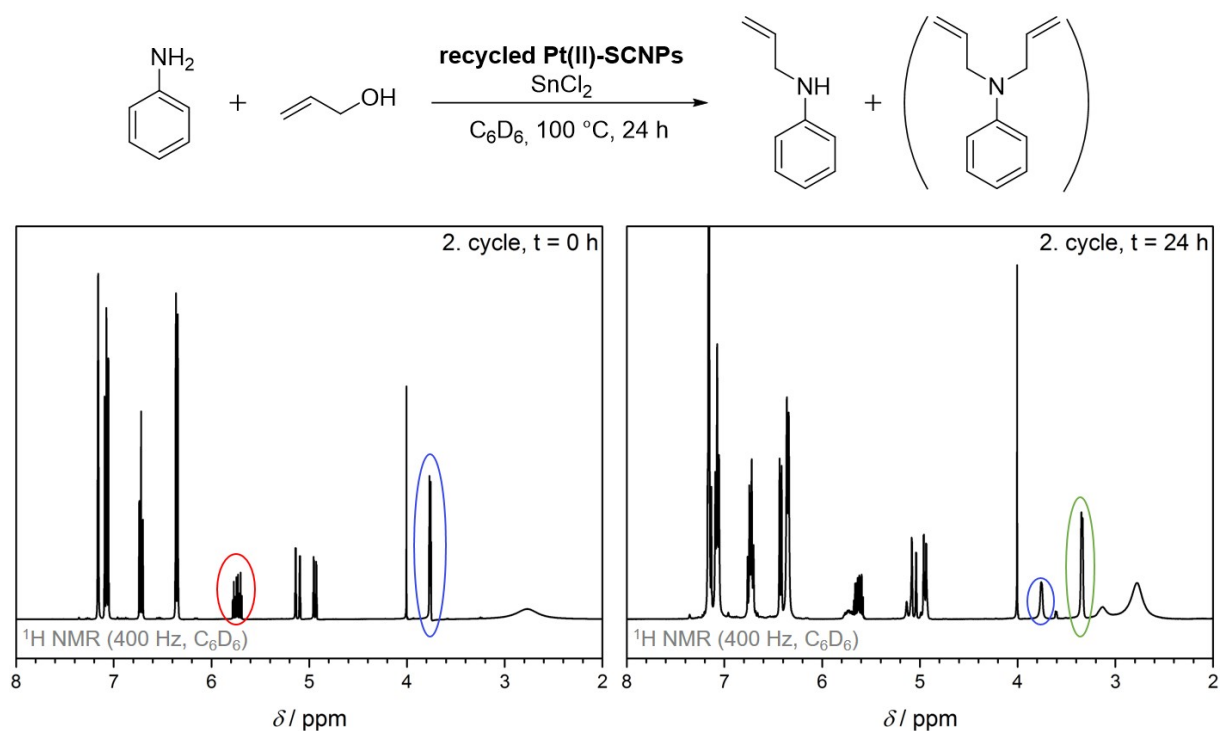


Figure 3.15: Recovered Pt(II)-SCNPs still show catalytic activity in a second cycle of amination of allyl alcohol. Presented are the ¹H NMR spectra of the catalytic reaction at time zero and after 24 hours. In comparison to the first catalytic cycle, the Pt(II)-SCNPs still accomplished a high conversion of the allyl alcohol of approx. 70 %, verifying their consistent activity. Adapted from [207] with permission from John Wiley and Sons.

In further experiments, the SCNPs were not separated after the first catalytic cycle (reaction of aniline with allyl alcohol), yet left in solution, thus avoiding the work up procedure. Addition of the starting material (2 equiv. aniline, 1 equiv. allyl alcohol) to the reaction mixture started the following cycles, performed under same reaction conditions. The corresponding ¹H NMR spectra showed an almost quantitative allyl alcohol conversion for the first catalytic cycle and still over 85 % conversion for the second and third cycle, proving the SCNPs to be reusable homogeneous catalysts.

3.5 Summary

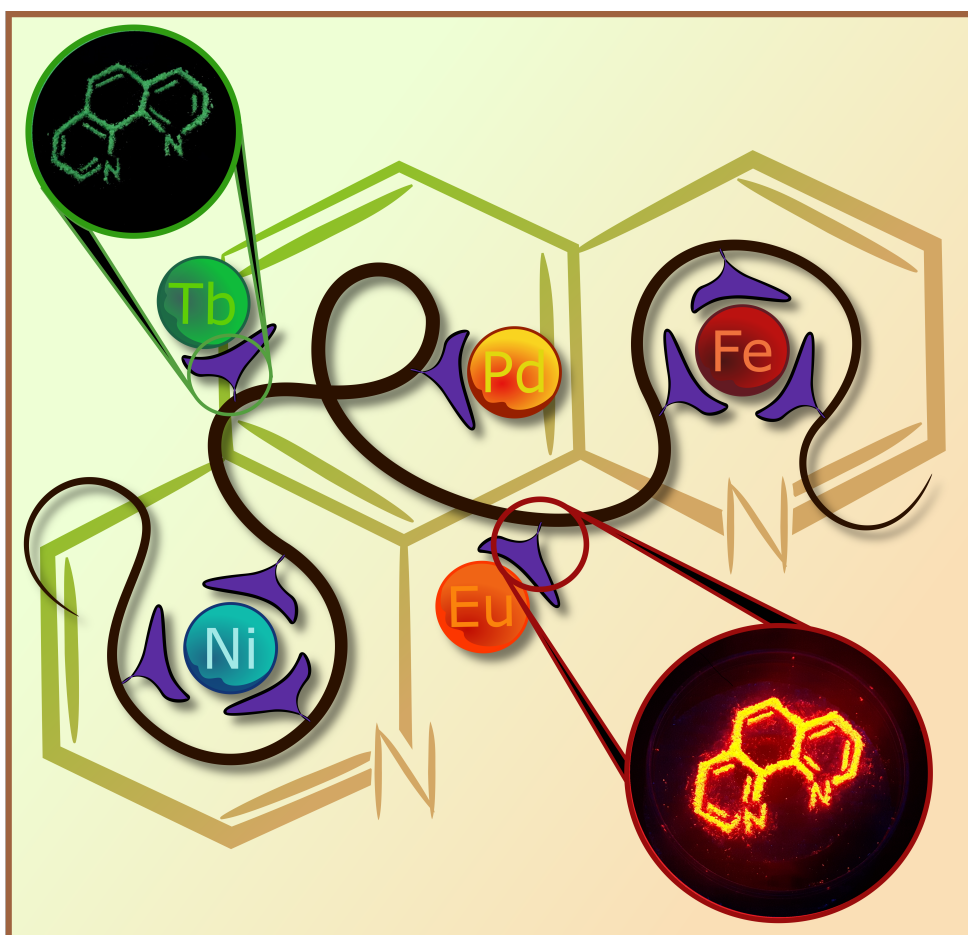
In summary, the current project introduced platinum(II) ions into a linear, phosphine functionalized polymer scaffold yielding Pt(II)-SCNPs. The collapse into compact nanoparticles, exhibiting a smaller hydrodynamic radius than the former polymer chains, was evidenced by SEC analysis, NMR (^1H , $^{31}\text{P}\{^1\text{H}\}$ and ^{195}Pt spectroscopy), DLS and DOSY measurements.

The generated Pt(II)-SCNPs demonstrated their activity as homogeneous catalysts in the amination of allyl alcohol. In contrast to many heterogenized molecular catalysts, which in comparison to the molecular system show a decrease in activity, the presented system was as active and as selective as the homogeneous reference catalyst. Advantageously, the polymer lattice of the nanoparticles did not negatively influence their catalytic activity, while allowing to heterogenize the system, which enabled facile isolation and purification of the Pt(II)-SCNPs.

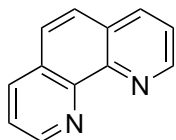
Hence, for the first time, a SCNP catalyst was recovered after the catalysis without being compromised in its collapsed structure, as confirmed by SEC and $^{31}\text{P}\{^1\text{H}\}$ NMR spectroscopy. In the subsequent analysis, small alterations in the structure of the recycled SCNPs were observed, for instance a change of the *cis/trans* ratio in the platinum(II)-phosphine geometry. Further investigations revealed a temperature-related ligand rearrangement in the system, which however did not affect the catalytic activity significantly. Finally, the recycled Pt(II)-SCNPs were applied in a second catalytic cycle demonstrating their constant catalytic activity.

In a separate experiment, in which the same catalytic reaction was performed without work up, high conversions employing the Pt(II)-SCNPs were achieved even after three catalytic cycles.

Phenanthroline as a Versatile Ligand for Polymeric Material



4.1 Motivation



1,10-Phenanthroline

Figure 4.1: The chemical structure of Phen.

1,10-Phenanthroline (Phen) is a versatile, nitrogen-based, commonly employed ligand in coordination chemistry (Chapter 2.5.3). Its strong appeal is based on its characteristic to form stable complexes with main group elements, transition, and f-block metals.^[174] The stability of Phen originates from its rigid, heteroaromatic structure, pre-organizing the nitrogens to efficiently chelate metal centers. In combination with transition metals, Phen has been established as a powerful supporting ligand, forming catalytically active metal complexes.^[216, 217] Moreover, upon coordination to several lanthanides, some

Phen–metal complexes exhibit unique photophysical properties.^[218] Thereby, the ligand Phen takes up the position as a triplet-state photosensitizer, enhancing the emission of poorly absorbing metals as a light harvesting antenna (refer to the Chapter about lanthanides 2.5.5 and 2.5.3).^[172, 199, 219]

As such a multi-faceted ligand, Phen and its derivatives have already been exploited in numerous macromolecular architectures or for surface functionalization.^[173, 220, 221] Particularly appealing seems the conversion of Phen into a building block for polymeric material, regarding the significant potential as a polymer framework for metal-complexed single-chain nanoparticles (SCNPs) or luminescent metallopolymers.

To date, two main synthetic procedures have been reported in the literature for implementing Phen moieties into polymeric structures. One approach describes the synthesis of a Phen-containing monomer, however, its subsequent copolymerization follows the technique of conventional free radical polymerization.^[222] Consequently, only slight control over the molecular weight and the dispersity of the polymer chains was achieved. In the other approach, at first Phen-free, narrowly distributed polymer chains were synthesized, followed by an implementation of Phen moieties into the polymeric structure *via* postmodification reactions. Thus, while the length and distribution of the chains were adjustable, there was limited control concerning the degree of functionalization.^[223, 224]

Therefore, the aim of the present project is the synthesis of a polymer, which contains a predictable and quantifiable amount of functional Phen groups, while simultaneously exhibiting a defined and uniform polymer distribution. This novel synthetic procedure shall be an effective method, opening avenues for the preparation of functional soft matter materials such as catalytically active SCNPs by encapsulation of transition metals or luminescent metallopolymers by lanthanide incorporation.

To cover the full range of possible applications, two polymer systems are developed with either a polar or non-polar polymer framework. With regard to the transition metal embedding, the solubility of the polar system in aqueous solutions is a critical aspect, when employing commercially available, cheap metal salts.

Prerequisite for both systems is a linear polymer chain of a minimum molecular weight of 25 000 g · mol⁻¹ and a dispersity below 1.5. As established in previous experiments, SCNPs originating from chains exhibiting a molecular weight below this size result in nanoparticles of a very small hydrodynamic radius, often close to the detection limit of various analysis methods. Hence, obtaining meaningful data is challenging. Furthermore, broadly distributed polymer chains vary widely in the amount of functional groups, limiting a controlled functionalization process and subsequent analysis. Consequently, the polymerization has to be mediated by a reversible-deactivation radical polymerization (RDRP) mechanism to control the molecular weight and distribution.

Another request concerns the amount of functional Phen groups in the polymers. Depending on the future applications of the polymer chains, different degrees of functionalization are required. In the polar system, which will be utilized to form metal complexed SCNPs, approx. 5 % of Phen-functionality is targeted to allow a successful crosslinking within the chains. Instead, for the decoration of the non-polar polymer chains with luminescent lanthanides, only approx. 2 % of Phen-functionalities are necessary.

At first, the synthesis of a Phen-monomer is targeted. To enable the prediction of functional groups in the polymers before their synthesis, a set relation between the monomer feed ratio and the polymer composition is essential. Furthermore, the presence of additional functionalities, which can coordinate to metal complexes, has to be excluded to enable the exclusive formation of Phen-to-metal bonds.

Furthermore, the stability and solubility of the polymer chains at high temperatures is an important factor with respect to possible future application as catalysts (not demonstrated in this project). Thus, metallopolymer architectures have to withstand a minimum temperature of 100 °C, while simultaneously exhibiting a low critical solution temperature at least above the same temperature.

The following sections introduce a synthesis route for Phen-containing polymer scaffolds and the subsequent systematic construction of Phen-functionalized polymer architectures.

Starting with the polar system, potential approaches to implement Phen by different methods into a polymer chain are described, followed by synthetic procedures for Phen-containing monomers. After presenting the polymerization of acrylate based Phen-monomers, their application scope in the creation

of single-chain nanoparticles by encapsulation of transition metals is demonstrated. The adjacent section addresses the synthesis of a styrene-based Phen-monomer, ready for implementation into a non-polar polymer system. The chapter closes with the generation of luminescent metallopolymers by embedding lanthanides into the polymer framework

The syntheses of the employed compounds were performed in a cooperation with N. Knöfel. The diffusion coefficients for the Fe(II)- and Ni(II)-SCNPs and the NOESY and TOCSY spectra of the lanthanide metallopolymers were measured by P. Tzvetkova. Steady State and Time Resolved Spectroscopy in Solution measurements were performed by N. Michenfelder. S. Baraban contributed to the project in his Vertieferarbeit. E. Blasco is thanked for fruitful discussions about polymerization techniques. C. Barner-Kowollik and P. W. Roesky supervised and motivated the project. Parts of this Chapter are reproduced from Rothfuss*, H.; Knöfel*, N. D.; Tzvetkova, P.; Michenfelder, N. C.; Baraban, S.; Unterreiner, A. N.; Roesky, P. W.; Barner-Kowollik, *C. Chem. Eur. J.* **2018**, *24*, 17475, with permission from John Wiley and Sons.

4.2 First Steps for a Polar Phen-Containing Polymer System

First considerations for a Phen-containing polymer are based on possible future applications. Aiming for a metal embedding into the polymer scaffold, the properties of the polymer chains have to match the reaction conditions for a transition metal complexation. Most of the transition metal salts bearing no additional organic ligands are only soluble in water or very polar solvents, for instance methanol. Consequently, the prerequisite for a Phen-containing polymer is a polar framework to enable dissolution in polar organic solvents or even in aqueous media.

However, not only the simple incorporation of transition metals in a 1:1 metal-to-ligand ratio is targeted, but also a metal-induced chain collapse yielding SCNPs is envisioned.

As observed in previous experiments and projects exploring SCNP formation, a precursor polymer is required which contains only a small percentage of functional units. On that account, the characteristics of the final polymer chains are determined by the comonomer. When selecting a suitable comonomer, *N,N*-dimethylacrylamide (DMAA) appeared promising, having already demonstrated its suitability in various reversible-deactivation radical polymerization (RDRP) procedures.^[225, 226] Furthermore, the non-toxic and non-ionic homoDMAA polymer provides excellent solubility behavior in aqueous solvents, a stability over wide pH intervals (3–11) and a lower critical solution temperature (LCST) of above 200 °C, as required for future applications (refer to Chapter 4.1).

Besides the general structure of the polar polymer framework, the polymerization method has to be selected. Among the potential three RDRP techniques dealing with monomers containing a vinyl unit, nitroxide mediated polymerization (NMP), atom transfer radical polymerization (ATRP) and reversible addition-fragmentation radical polymerization (RAFT), ATRP was excluded. In a similar mechanism as NMP, ATRP minimizes possible termination reactions, reducing the overall radical concentration by reversibly trapping the propagating radicals. However, the equilibrium between dormant and active species in ATRP is maintained *via* a transition metal complex in two oxidation states. Typically, a copper complex is employed, establishing an equilibrium between $\text{Cu(I)} \leftrightarrow \text{Cu(II)}$.^[227, 228] In this context, the application of Phen-containing substances harbors the high risk of a copper–Phen coordination, perturbing the polymerization mechanism. Moreover, the coordination sites in the Phen moieties have to remain unoccupied for the following envisioned reactions with metal complexes.

Comparing NMP and RAFT, there are only a few literature reports concerning a controlled polymerization of acrylamides by NMP. Instead, numerous synthetic protocols for a polymerization

via RAFT are described. Therefore, the RAFT technique was selected as the most suitable RDRP for the current project.

In summary, a polymer that is soluble in polar media for subsequent transition metal SCNP formation is provided when utilizing the acrylamide monomer DMAA, polymerized via RAFT, to form the basic copolymer structure.

4.2.1 Evaluation of Suitable Polymerization Conditions for DMAA

Initially, the reaction conditions for a homoDMAA polymerization via the RAFT mechanism were established. According to the literature,^[229–232] the RAFT agents 2,2'-(thiocarbonylbis(sulfaneyl))-bis(2-methylpropanoic acid) (TRITT), the pentafluorophenol ester derivative of TRITT, *S,S*-dibenzyl trithiocarbonat (DBTTC) and 2-(dodecylthiocarbonothioylthio)-2-methylpropionic acid (DDMAT) provide excellent control over the polymerization of acrylamides for high molecular weight polymers. Adopting literature known procedures,^[233, 234] the RAFT agents TRITT and DDMAT were synthesized. The TRITT-pentafluorophenol ester was kindly supplied by Thomas Gegenhuber (KIT) and the RAFT agent DBTTC was purchased.

In a screening experiment for optimum polyDMAA polymerization, all four RAFT agents were employed. The four structures of the RAFT agents along with the corresponding SEC traces (DMAc, RI) of the resulting polymer chains are depicted in Figure 4.2 (P_{RAFT_1-4}). The SEC trace of P_{RAFT_4}, stemming from the RAFT agent DDMAT, was analyzed on a different instrument and can therefore not be plotted in the same graph as the traces of the other three RAFT agents. Comparing the results of the polymerizations (refer to the Table in Figure 4.2) reveals that all RAFT agents, except TRITT, show a good accessibility towards polyDMAA, complying with the targeted minimum molecular weight of 25 000 g · mol⁻¹ with a dispersity of \mathcal{D} below 1.5. The best results are obtained utilizing DDMAT (P_{RAFT_4}), generating a polymer of adequate molecular weight of 32 700 g · mol⁻¹ with a narrow molecular weight distribution of $\mathcal{D} = 1.10$.

Having established appropriate conditions for a polymerization of DMAA, the next step comprised the incorporation of Phen units into the polymer chain.

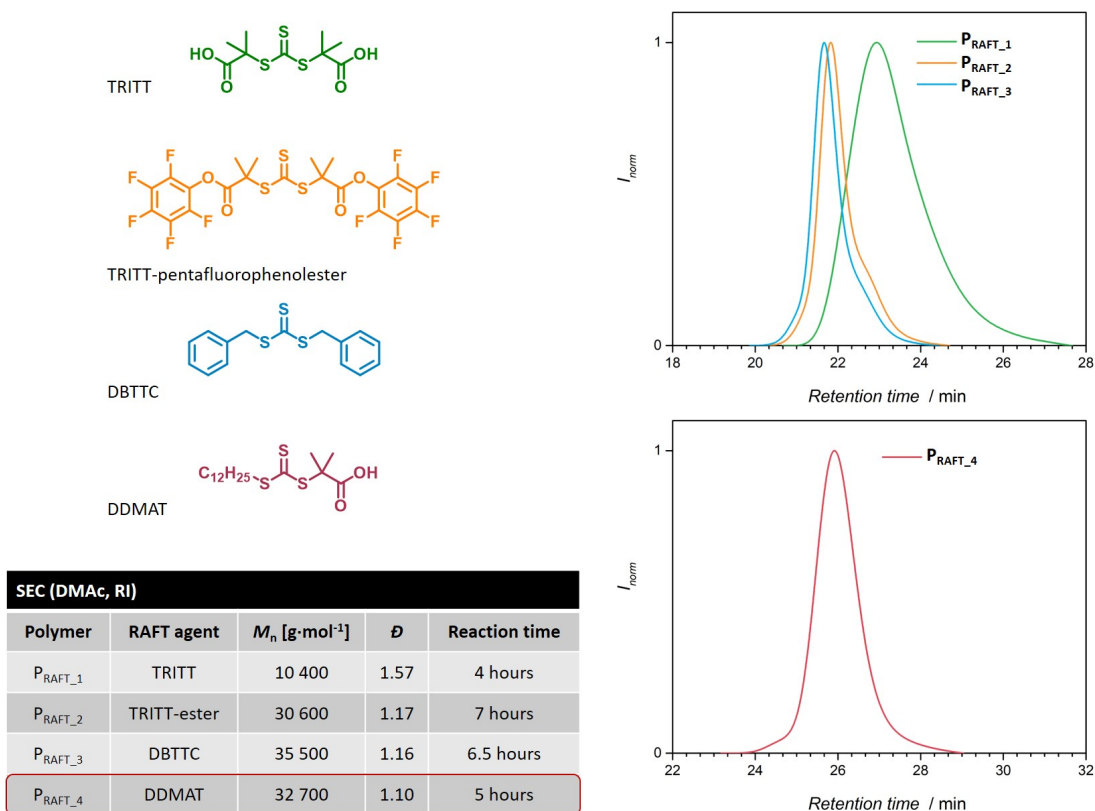
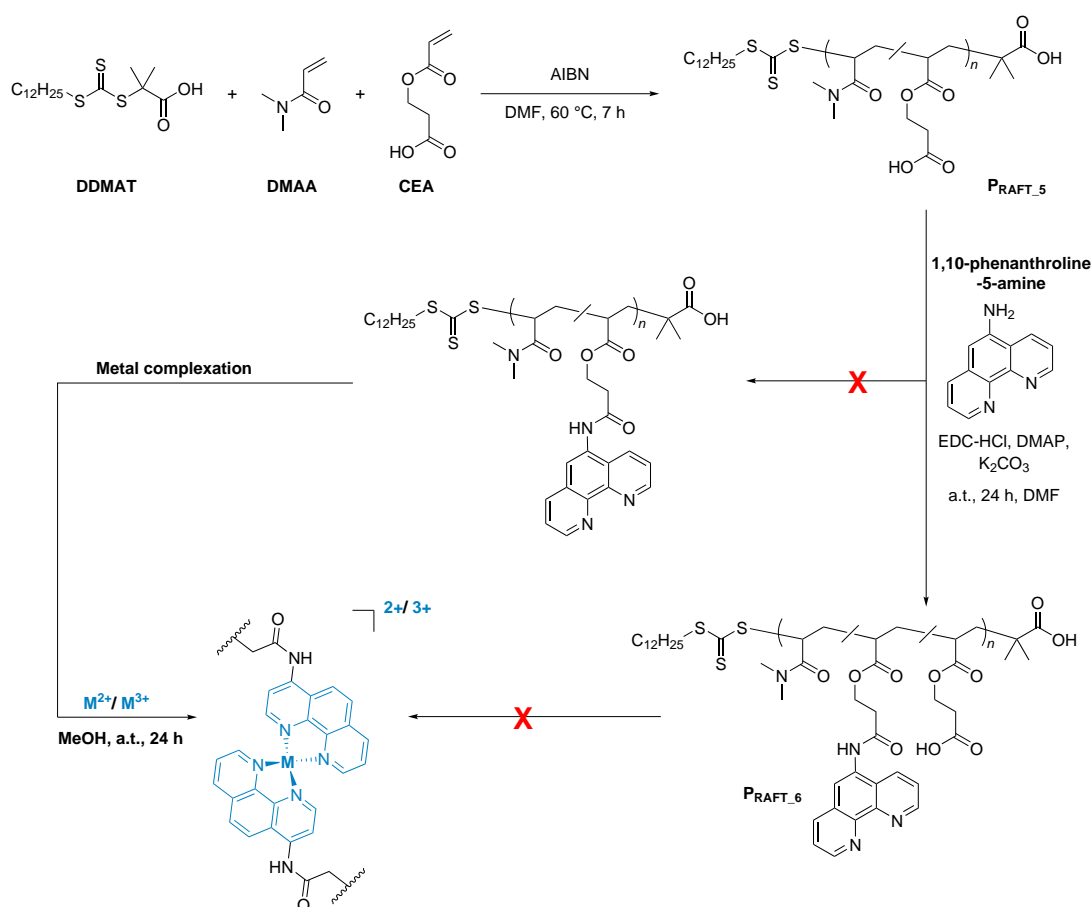


Figure 4.2: To establish the optimum conditions for a homo-polymerization of DMAA, the four RAFT agents TRITT, TRITT-pentafluorophenol ester, DBTTC and DDMAT were employed to mediate a DMAA polymerization. *Top, left:* Chemical structures of the four RAFT agents. *Right:* SEC traces (DMAc, RI) of the resulting polymers polyDMAA. *Bottom, left:* Important reaction conditions and the results of the analysis of the resulting polymers via SEC (DMAc, RI). The best results for a homo-polymerization of DMAA are obtained when employing DDMAT, reaching high molecular weight ($M_n = 32\,000\text{ g} \cdot \text{mol}^{-1}$) with a low dispersity ($\mathcal{D} = 1.10$).

4.2.2 Postfunctionalization

The first attempt included the implementation of Phen moieties into polymer chains *via* a postfunctionalization method. The concept comprises the synthesis of a copolymer *via* a RDRP mechanism, the functionalization with Phen and a further chain collapse. The detailed synthesis pathway is depicted in Scheme 4.1, entailing the copolymerization of DMAA with the monomer carboxyethyl acrylate (CEA), employing the RAFT agent DDMAT. After the determination of the monomer composition in the copolymer *via* ^1H NMR spectroscopy, the Phen-derivative 1,10-phenanthroline-5-amine is attached to the carboxylic acid moiety of CEA. In the last step, the Phen moieties coordinate to transition metal ions in the oxidation state +2 or +3 in a 2:1 ratio, thereby inducing the chain collapse.



Scheme 4.1: Pathway for the synthesis of a Phen-containing polymer and its subsequent collapse into a nanoparticle by the coordination of Phen moieties to transition metals in a 2:1 ligand-to-metal ratio. In the first step, a well-defined controlled copolymer is synthesized *via* the RAFT method, employing the monomers DMAA and CEA (P_{RAFT_5}). After purification of the copolymer, 1,10-phenanthroline-5-amine is attached to the carboxylic acid moiety of CEA *via* EDC coupling. Ideally, all carboxylic units of CEA are converted into amides with pendant Phen moieties to allow for further metal encapsulation. However, due to a non-quantitative EDC coupling reaction leaving free carboxylic acid groups and difficulties to determine the monomer composition in P_{RAFT_6}, this pathway was found unsuitable.

The copolymerization of DMAA with CEA as a comonomer mediated by DDMAT resulted in the copolymer P_{RAFT_5}, revealing a sufficiently high molecular weight of $M_n = 28\,400\text{ g}\cdot\text{mol}^{-1}$ with a narrow dispersity of $D = 1.14$, determined by SEC measurements (DMAc, RI). The actual monomer composition in the copolymer was calculated employing ¹H NMR spectroscopy, comparing the resonances of the dimethyl groups of DMAA, at $\delta = 3.10\text{--}2.62$ ppm, with the resonances of the methylene groups of CEA at $\delta = 3.34$ ppm and 2.12 ppm. The integration and comparison of the resonances resulted in a monomer ratio of approx. 1:15 CEA to DMAA. This ratio is equivalent with ~6% of acidic side groups, thus sufficiently high for the desired future SCNP application.

Subsequently, the amine derivative (1,10-phenanthroline-5-amine) was attached to the carboxylic acid groups of the monomer CEA in a so-called EDC coupling reaction. In this reaction, the compound 1-ethyl-3-(3-dimethylaminopropyl)carbodiimide (EDC HCl) activates the carbonyl unit in CEA to facilitate a nucleophilic attack of the primary amine in the Phen compound, resulting in the formation of an amide.

The obtained polymer P_{RAFT_6} was analyzed *via* ¹H NMR spectroscopy to determine the amount of Phen units. However, even though resonances for aromatic protons appear in the ¹H NMR spectrum, no meaningful monomer composition could be derived due to discrepancies of the integrals of the monomer resonances. Additionally, the existence of slight amounts of carboxylic groups couldn't be excluded. This constitutes a critical obstacle, since carboxylic moieties are also a class of ligands coordinating metals (refer to the Chapter about carboxylate ligands **2.5.4**). Hence, their presence in the polymer hinders gathering evidence for an exclusive metal encapsulation by the Phen units.

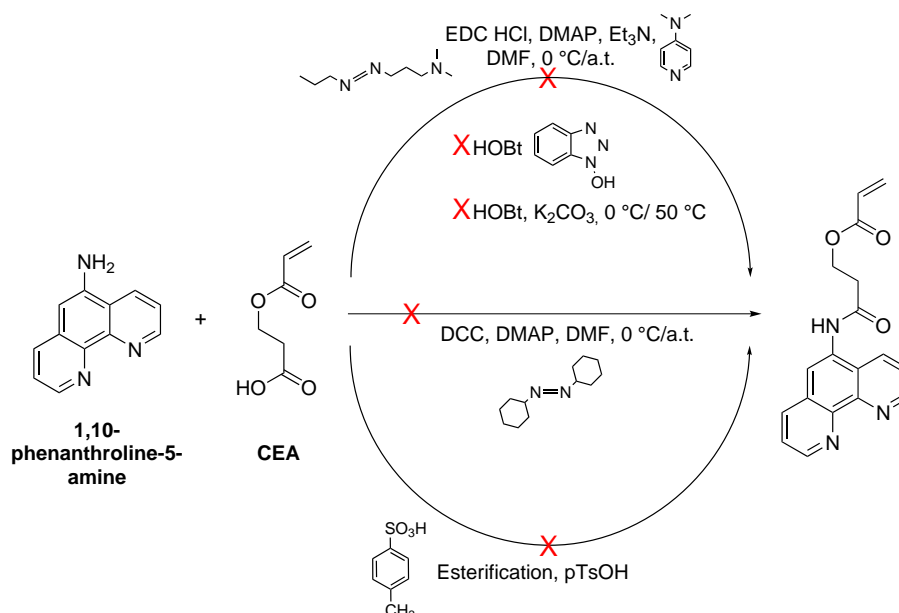
Further reactions under different conditions (different base and carboxyl activating agent) did also not lead to a quantitative coupling of the amine-Phen derivative to the carboxylic acids, therefore the pathway of postmodification was discarded.

Instead of a postfunctionalization of an already existing chain with Phen, the generation of a narrowly distributed polymer chain was targeted *via* the synthesis and polymerization of a Phen-monomer.

4.3 Polar System – Monomer Synthesis

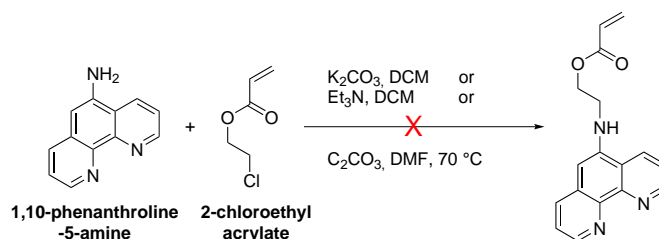
For the synthesis of a Phen-containing monomer, key conditions regarding the structure of the monomer have to be established. As required in ideal copolymerizations for the generation of a monomer composition in the polymer similar to the monomer feed ratio, analogous reactivities of both participating monomers are necessary (refer to Chapter 2.1.4). Having opted for DMAA as the comonomer, the Phen-monomer has to be designed to pertain to the class of acrylate or acrylamide monomers.^[57, 235] Due to the use of the Phen compound as a monomer, high amounts of material (approx. 500 mg) are required, hence reactions with a yield of at least 20 % are essential.

Access to an acrylate functionality offers the earlier employed EDC coupling between CEA and the amine-Phen derivative. Instead of a postfunctionalization, the reaction was performed with the molecular compounds. However, under the before reported conditions or in variations of the parameters, *i.e.* the temperature, the base (4-(dimethylamino)-pyridine (DMAP), 1-hydroxybenzotriazole (HOBt) or K_2CO_3) or the coupling agent (EDC, *N,N'*-dicyclohexylcarbodiimide (DCC), esterification *via* *para*-toluenesulfonic acid), the desired product was obtained only in low yields, below the minimum threshold. In turn, side reactions between the double bond of CEA or the carbonyl unit occurred. The corresponding reactions are depicted in Scheme 4.2.



Scheme 4.2: Various reaction conditions to form an amide bond between 1,10-phenanthroline-5-amine and CEA are presented. Unfortunately, even by varying the base, the temperature, or the coupling agent, the desired product was always obtained only in low yields.

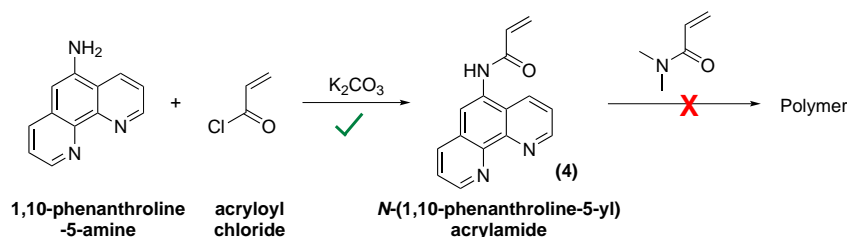
In the following reactions, the synthesis of a Phen-containing monomer was attempted *via* nucleophilic substitution (S_N) reactions between the amine-derivative of Phen and 2-chloroethyl acrylate (Scheme 4.3). As already observed in the coupling reactions before, the desired structure was not received in sufficiently high yields, even by changing the base, the solvent, or varying the temperature.



Scheme 4.3: Nucleophilic reactions conditions for a coupling between an amine-derivative of Phen and 2-chloroethyl acrylate. However, the usage of different bases, solvents and temperatures did not lead to the formation of the desired compound in appropriate yields.

In conclusion, it is assumed that the nucleophilicity of the amine functionality in the amine-Phen derivative is severely decimated, due to the electron poor heteroaromatic ring, to be sufficiently reactive to attack electrophilic reactants. Consequently, derivatives of carboxylic acids with a higher electrophilicity are utilized in the following reactions.

A higher electrophilicity and thus reactivity characterizes the group of acryl chlorides, for instance acryloyl chloride. This compound was employed by Su *et al.* in a nucleophilic reaction with the amine-derivative of Phen, forming *N*-(1,10-phenanthroline-5-yl)acrylamide (4).^[236] Indeed, after a slight modification of the reported procedure, high yields (approx. 90 %) of pure (4) without further purification were received (Scheme 4.4), as required for a Phen-monomer.

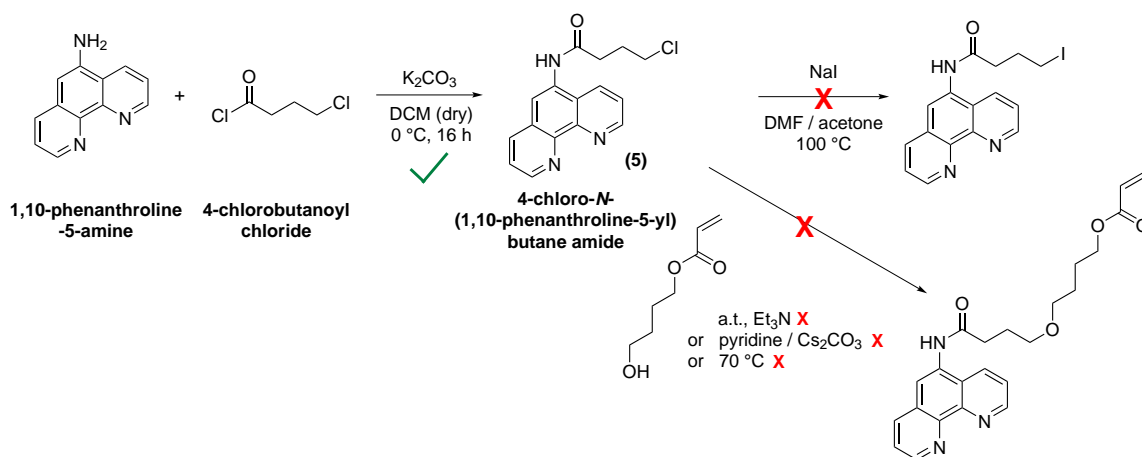


Scheme 4.4: Following the reaction procedure of Su *et al.*,^[236] the Phen-amine derivative reacted with acryloyl chloride to form *N*-(1,10-phenanthroline-5-yl)acrylamide (4) in high yields without elaborate purification. Yet, no polymer was obtained in a subsequently performed copolymerization with DMAA.

However, when employing (4) in subsequently performed homo- or copolymerizations with DMAA, by any of the hereinafter mentioned polymerization methods, *i.e.* conventional free radical or RAFT polymerization, no polymer was obtained.

Speculatively, a deactivation of the acrylic unit by the close proximity of the electron poor aromatic ring occurred, hence reducing its activity towards monomer addition. As a consequence, the necessity for a minimum spacer unit between the Phen moieties and the polymerizable unit was added to the prerequisites for the structure of a suitable Phen-monomer.

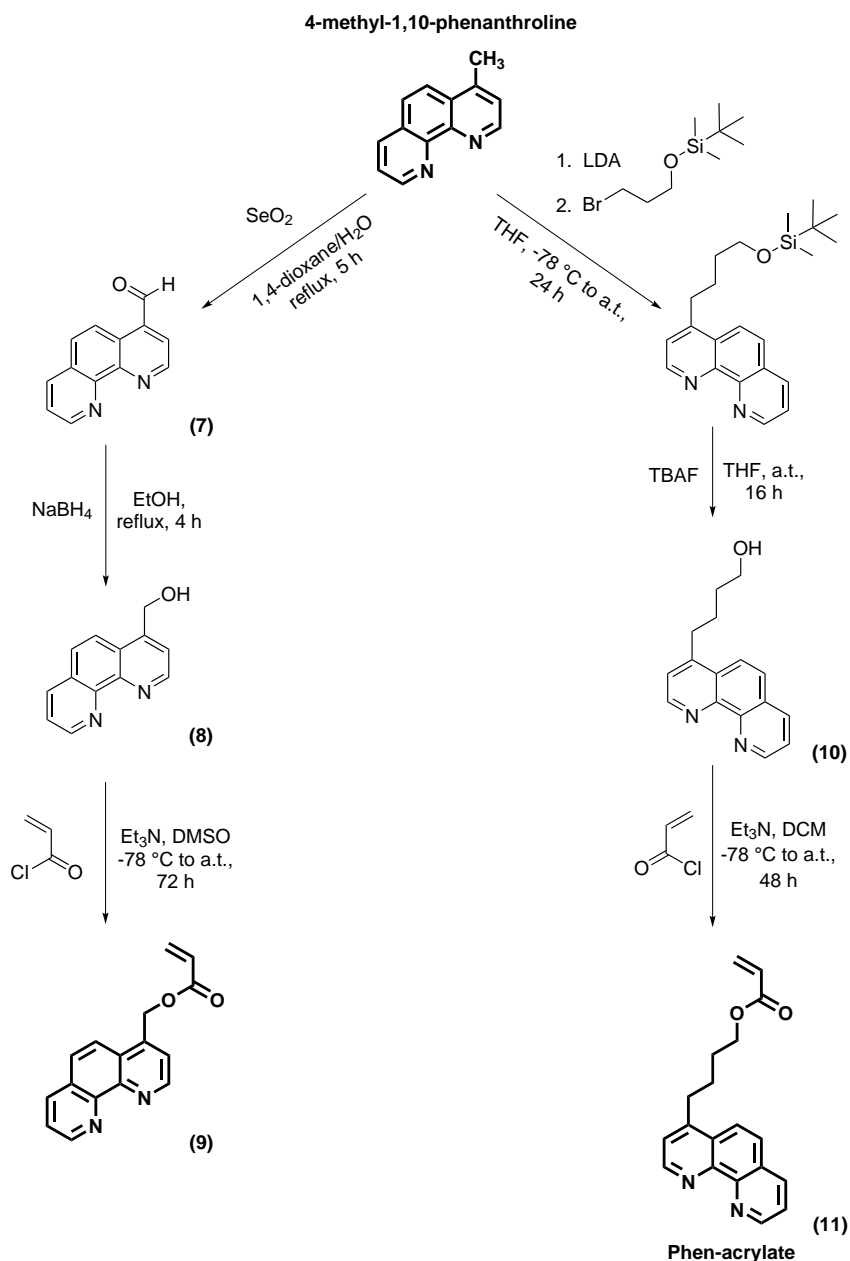
A pathway which combined the presence of a spacer unit with an active acryl chloride moiety, is the reaction between 1,10-phenanthroline-5-amine and the molecule 4-chlorobutanoyl chloride, which has three annexed methylene units (Scheme 4.5). While 4-chloro-*N*-(1,10-phenanthroline-5-yl) butane amide (5) was obtained in high yields and could be readily purified by simple washing, the subsequent modification of the chloride unit was unsuccessful. Neither a nucleophilic substitution between the chloride and an alcohol unit, nor the transformation of the chloride into the more active iodide was possible.



Scheme 4.5: The reaction between 1,10-phenanthroline-5-amine and 4-chlorobutanoyl chloride combined high reactivity at the acryloyl chloride unit with an alkyl spacer unit, resulting in 4-chloro-*N*-(1,10-phenanthroline-5-yl) butane amide (5). However, a further functionalization of (5) to implement an acrylate unit proved unsuccessful.

As an option to substitute acryl chlorides, another group of activated carbon acids, anhydrides, was employed in the following reactions. In a modified procedure reported in the literature,^[131] 1,10-phenanthroline-5-amine reacted with succinic anhydride, yielding 4-((1,10-phenanthroline-5-yl)amino)-4-oxobutanoic acid (6) (shown in Chapter 9.3.6). However, as already observed in previously performed reactions, a further functionalization by implementation of an acrylate unit did not result in the desired molecule.

In further experiments, the amine-Phen derivative was replaced by the starting material 4-methyl-1,10-phenanthroline. Performing reactions under harsh conditions, two synthesis procedures are developed to functionalize the Phen compound with a polymerizable unit. Both synthesis routes are depicted in Scheme 4.6.



Scheme 4.6: Synthetic procedure to design two Phen-containing monomers with an acrylate function, essential to allow further (co)polymerization with DMAA. Both synthetic routes employ the starting material 4-methyl-1,10-phenanthroline. In multi-step syntheses, a Phen-acrylate with either one methylene unit (9) or with four methylene units (11) is obtained. Adapted from [4] with permission from John Wiley and Sons.

For the synthesis of (1,10-phenanthroline-4-yl)methyl acrylate (9), the methyl group of 4-methyl-1,10-phenanthroline is oxidized to an aldehyde (7) by selenium(IV)oxide. Subsequently, the aldehyde is reduced to an alcohol, yielding (1,10-phenanthroline-4-yl)methanol (8). The last step entails an esterification reaction between the hydroxy group of (8) and acryloyl chloride, resulting in (1,10-phenanthroline-4-yl)methyl acrylate (9), a Phen-containing compound with acrylate function.

The initial step in the alternative pathway is the lithiation of the methyl group in 4-methyl-1,10-phenanthroline, immediately followed by a salt metathesis reaction with (3-bromopropoxy)-*tert*-butyldimethylsilane, forming a silyl ether protected alcohol. After deprotection, the esterification between the alcohol (10) and acryloyl chloride results in the acrylate-substituted Phen derivative 4-(1,10-phenanthroline-4-yl)butyl acrylate (11). The structure of both monomers is verified by ^1H NMR and $^{13}\text{C}\{^1\text{H}\}$ NMR spectroscopy, IR spectroscopy, mass spectrometry and elemental analysis. The proton spectra of both structures are depicted in Figure 4.3 and 4.4.

The three Phen-containing monomers, (4), (9), and (11), are all obtained in sufficiently high yields and complying with the required conditions of an acrylate functionality for further copolymerization with DMAA. However, the attachment of Phen in close proximity to the vinyl unit already demonstrated its non-suitability for polymerization reactions, therefore (4) was discarded. Instead, the monomers (9) and (11) exhibit one or four methylene spacer units, respectively, thus their suitability for polymerization reactions was investigated in the following sections.

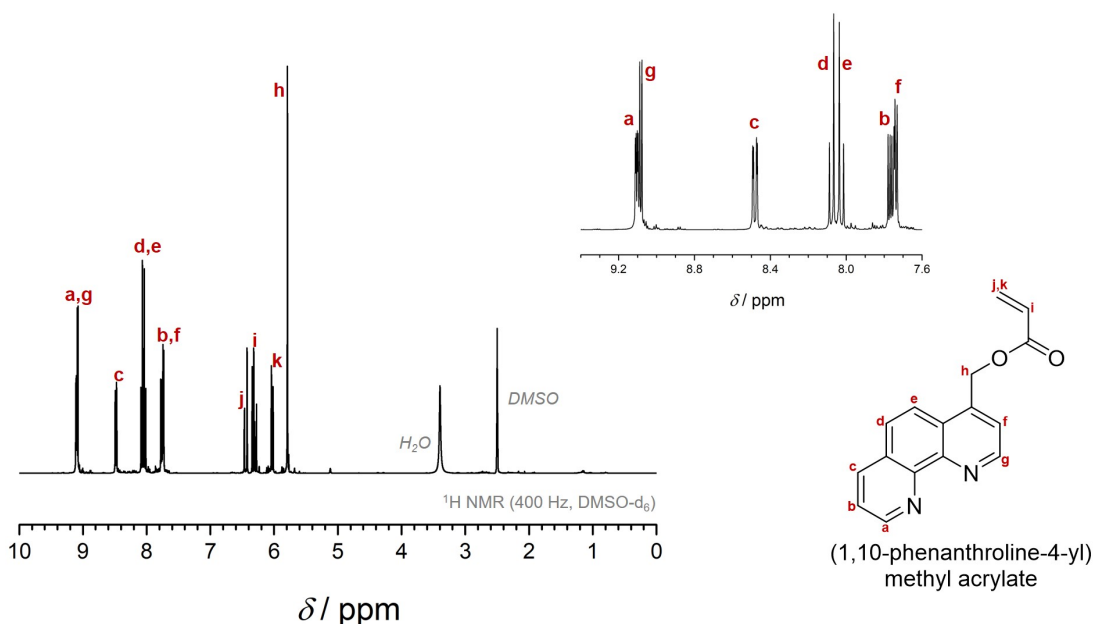


Figure 4.3: ^1H NMR spectrum and chemical structure of the acrylate-substituted Phen derivative (1,10-phenanthroline-4-yl)methyl acrylate (9). An enlargement of the region between $\delta = 7.6$ – 9.4 ppm enables better distinction of the resonances of the aromatic Phen protons. Additional analysis data of the compound can be found in the Experimental Section, Chapter 9.3.7. Adapted from [4] with permission from John Wiley and Sons.

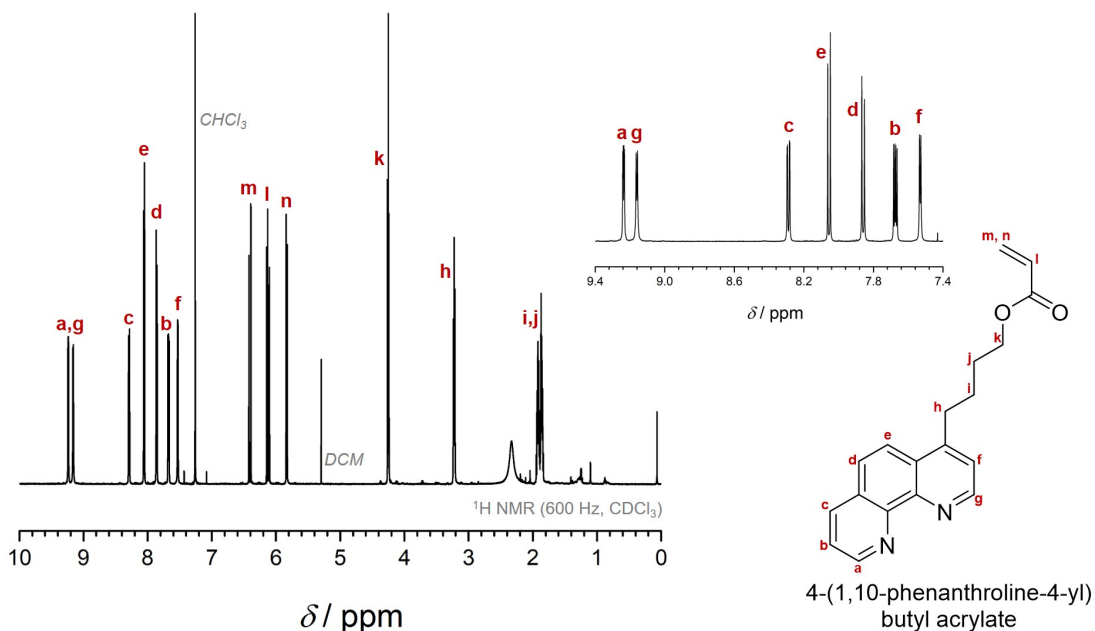
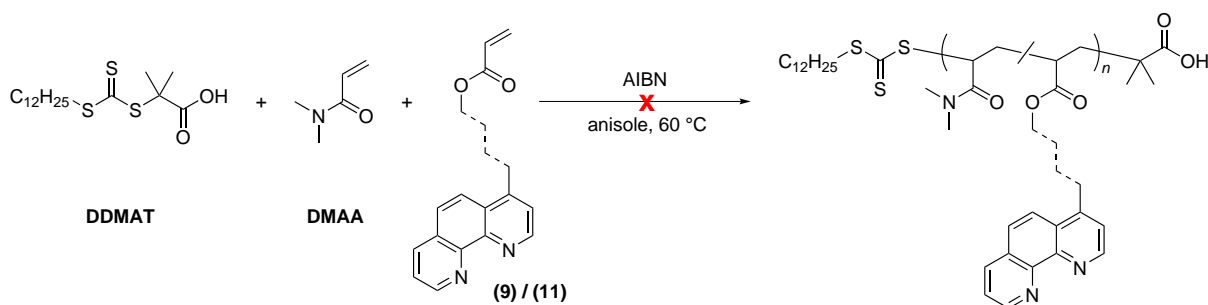


Figure 4.4: ^1H NMR spectrum and chemical structure of the acrylate-substituted Phen derivative 4-(1,10-phenanthroline-4-yl)butyl acrylate (11). An enlargement of the region between $\delta = 7.6$ – 9.4 ppm enables better distinction of the resonances of the aromatic Phen protons. Additional analysis data can be found in the Experimental Section, Chapter 9.3.8. Adapted from [4] with permission from John Wiley and Sons.

4.4 Polar System – Polymerization Techniques

4.4.1 Copolymerization of Phen-Monomers *via* RAFT

Having synthesized two acrylate-based Phen derivatives, the ability to copolymerize the monomers (9) and (11) with DMAA mediated by the RAFT agent DDMAT was investigated.



Scheme 4.7: Copolymerization of the Phen-containing monomers (9) and (11) with the comonomer DMAA mediated by the RAFT agent DDMAT. As indicated by the red cross, the expected copolymers were not obtained.

In the first reactions, the same conditions which were established for a homo DMAA polymerization were employed when adding small amounts of Phen-monomer (9) or (11) to the reaction mixture. The combined reaction scheme is depicted in Scheme 4.7. Subsequently, the polymers were analyzed *via* SEC (DMAc, RI) measurements. The SEC trace of the sample containing the Phen-species (9) indicates no formation of polymer, since only peaks for monomer compounds appear (Figure 4.5, *left*). In comparison, high molecular weight polymer in the copolymerization with the Phen-monomer (11) was already formed after a very short period of time, however with a broad distribution (Figure 4.5, *right*).

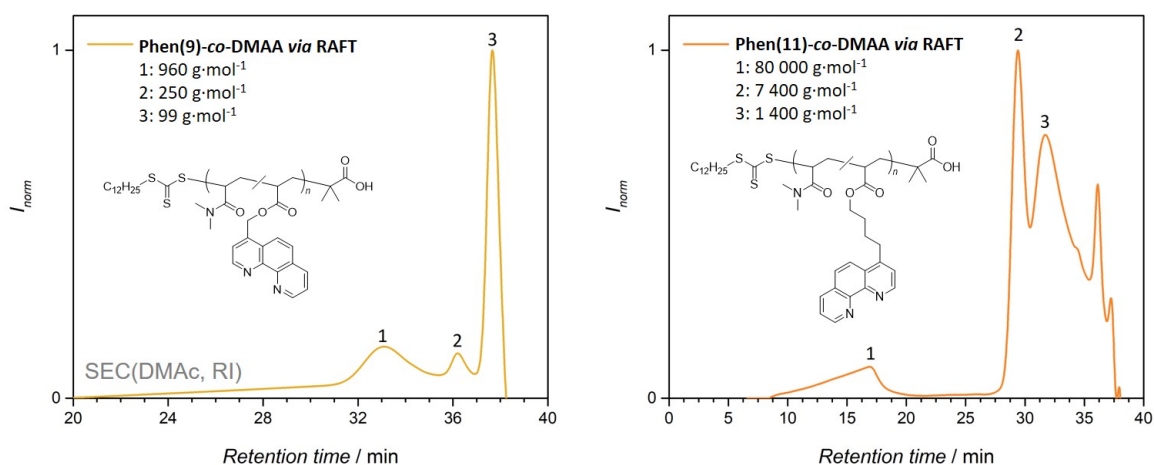


Figure 4.5: SEC traces (DMAc, RI) of the two copolymerizations of DMAA with either Phen-monomer (9) or (11). While in the reaction containing the Phen-monomer (9) no polymer was formed, *left*, the copolymerization employing Phen (11) showed characteristics of a conventional FRP, *right*.

In the further analysis of the copolymer chains containing (11) by ^1H NMR spectroscopy, the incorporation of Phen was evidenced. This was recognizable by resonances in the aromatic area, clearly related to the Phen-monomer (11). Although fulfilling the necessity of a Phen-containing polymer, the SEC analysis points towards conventional FRP polymerization behavior, yielding chains of a high dispersity in length.

The reason for the FRP polymerization behavior was assumed to be a side reaction between the Phen units and the RAFT agent, inhibiting its mediating function. Thus, the generation of high molecular weight polymer with a broad distribution after short time is plausible. To exclude the possibility of a side reaction with the initiator AIBN, a following reaction utilizing only DMAA, AIBN and small amounts of the Phen-monomer (11) was performed. As depicted in Figure 4.6 on the *right* hand side, a similar SEC trace is observed for the copolymer *via* conventional FRP as before in the intended RAFT mediated polymerization. Thus, a side reaction between the initiator AIBN and the Phen compounds was ruled out and an interaction with the RAFT agent DDMAT was further underpinned.

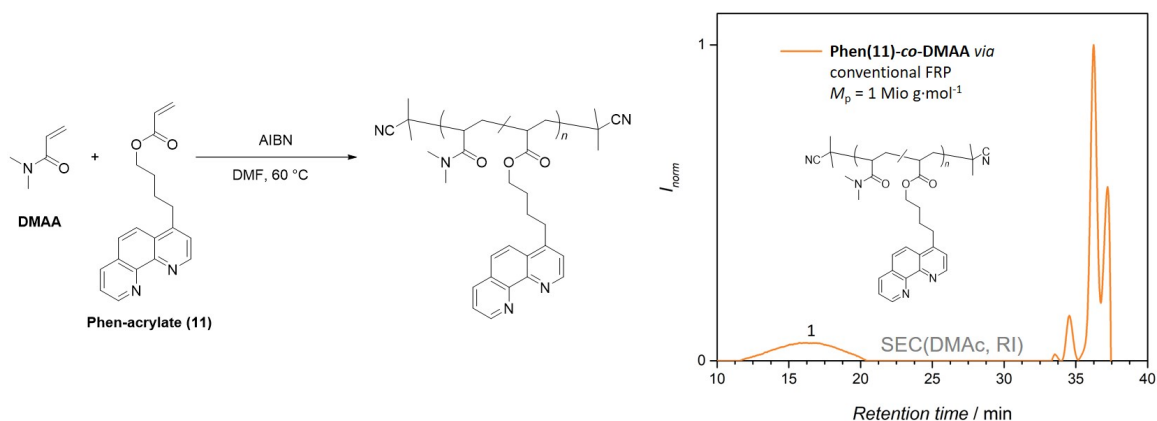


Figure 4.6: *Left:* Reaction scheme for a conventional FRP of DMAA and the Phen-monomer (11). *Right:* The resulting copolymer was analyzed *via* SEC measurement (DMAc, RI).

In a control experiment, interactions between Phen-containing compounds and DDMAT were investigated by preparing a homoDMAA polymerization in which molecular 1,10-phenanthroline was additionally added. Interestingly, no high molecular weight polymer was formed. This finding pointed towards a reaction between the RAFT agent and Phen, impeding the function of DDMAT for a controlled polymerization. However, permanent side reactions resulting in a change in chemical structures were not observed when analyzing a mixture of 1,10-phenanthroline and DDMAT *via* ^1H NMR spectroscopy.

Deducted from the two previous reactions, the interference between Phen and DDMAT presumable prohibits a controlled polymerization of Phen-containing compounds. Consequently, the tasks defined at the beginning are not completed and thus the present pathway is discarded.

Instead, additional three RAFT agents were screened for optimum reaction conditions in homo DMAA polymerization: 2-cyano-2-propyl dodecyl trithiocarbonate (CPDT), cyanomethyl dodecyl trithiocarbonate (CMDT) and methyl 2-(dodecylthiocarbonothioylthio)-2-methylpropionate (M-DDMAT).

The three resulting polymers P_{RAFT_8} , P_{RAFT_9} and $P_{\text{RAFT}_{10}}$, respectively, were analyzed *via* SEC measurements (DMAc, RI). Especially P_{RAFT_9} and $P_{\text{RAFT}_{10}}$ resulted in suitable high molecular weight above $25\,000\text{ g}\cdot\text{mol}^{-1}$ with a narrow dispersity below 1.5, as outlined in the table on the right of Figure 4.7. Due to promising results in mediating the polymerization of DMAA, the RAFT agent M-DDMAT was furthermore employed in the copolymerization of DMAA with small amounts of the Phen-monomer (11), yielding $P_{\text{RAFT}_{11}}$. In here, SEC (DMAc, RI) analysis returned a molecular weight of $16\,000\text{ g}\cdot\text{mol}^{-1}$ with $\mathcal{D} = 1.54$, not fulfilling the basic conditions for a Phen-containing copolymer.

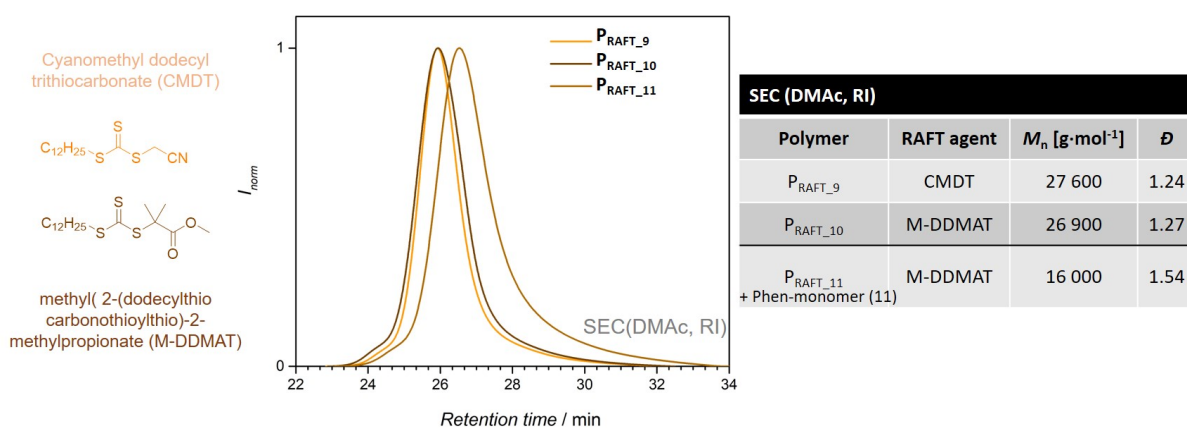


Figure 4.7: Left: Chemical structures and names of the two RAFT agents, cyanomethyl dodecyl trithiocarbonate (CMDT) and methyl 2-(dodecylthiocarbonothioylthio)-2-methylpropionate (M-DDMAT). Both revealed good control over the polymerization of homoDMAA, as indicated by the SEC traces (*center*) and the corresponding data in the table (*right*). The compatibility of M-DDMAT with the Phen-monomer (11) was further investigated in a copolymerization of Phen-acrylate with DMAA.

In a small side project, the monomer poly(ethylene glycol) methacrylate ($M_n = 500\text{ g}\cdot\text{mol}^{-1}$) was investigated regarding its polymerization *via* the RAFT technique. Although monodisperse polymers with a molecular weight of approx. $M_n = 28\,000\text{ g}\cdot\text{mol}^{-1}$ were obtained ($P_{\text{RAFT}_{12}}$), this approach was discarded. The long ethylene glycol units were expected to shield the Phen unit and thereby prohibit the access to metal ions.

To sum up the recent results, the RAFT agent DDMAT, which showed good compatibility with DMAA, yielding narrowly distributed, high molecular weight polymer, is not suitable for Phen-containing molecules. Instead, the RAFT agent M-DDMAT mediates well both a homoDMAA and its copolymerization with the Phen-monomer (11). However, neither the target of a minimum molecular weight of $\geq 25\,000\text{ g} \cdot \text{mol}^{-1}$ nor the required dispersity below 1.5 is achieved.

Therefore, another polymerization method for a copolymerization of DMAA and a Phen-monomer was explored.

4.4.2 Copolymerization of Phen-Monomers *via* NMP

Since under the aforementioned conditions the basic framework for a Phen-functionalized copolymer of $M_n \geq 25\,000\text{ g} \cdot \text{mol}^{-1}$ and $\mathcal{D} < 1.5$ were not fulfilled, in a parallel project, the copolymerization of DMAA *via* NMP was investigated. The substitution of a RAFT agent by nitroxides, e.g. alkoxyamines, is expected to result in a better controlled polymerization of the Phen-monomers with DMAA, yielding sufficiently high and narrowly distributed copolymers. The literature reports the mediation of a polymerization of acrylamides *via* the NMP method with several nitroxides.^[237–240] For more information about NMP refer to Chapter 2.1.2.

From a range of nitroxides, the most suitable appeared to be *N-tert*-butyl-*N*-[1-diethylphosphono-(2,2-dimethylpropyl) nitroxide] (SG1), either in combination with pure AIBN or with the alkoxyamine *N*-(2-methylpropyl)-*N*-(1-diethylphosphono-2,2-dimethylpropyl)-*O*-(2-carboxylprop-2-yl)-hydroxylamine (MAMA-SG1). At first, the homopolymerization of DMAA *via* both pathways was performed. Thereby several parameters were adjusted, regarding the ratio between the monomer DMAA to the alkoxyamine MAMA-SG1, the amount of additionally added SG1, the solvent volume and the reaction time. Kinetic studies of each variation were carried out. The best conditions revealed the need for a high monomer to initiator ratio with a low amount of solvent (DMF). Further results established the best reaction conditions for a DMAA polymerization *via* SG1 and MAMA-SG1. In addition, the compatibility of this specific NMP reaction with Phen compounds was investigated by adding either an amount of molecular 1,10-phenanthroline or the Phen-monomers (9) and (11) to the solution of starting material.

As depicted in Figure 4.8, the homo polymerization of DMAA was well mediated, as narrowly distributed, high molecular weight polymer was obtained. While the addition of molecular 1,10-phenanthroline did not influence the polymerization, the copolymerization with the Phen-monomer (9) resulted in shorter polymer chains with a molecular weight distribution > 2 . Thus, the current reaction conditions were rated unsuccessful.

4 Phenanthroline as a Versatile Ligand for Polymeric Material

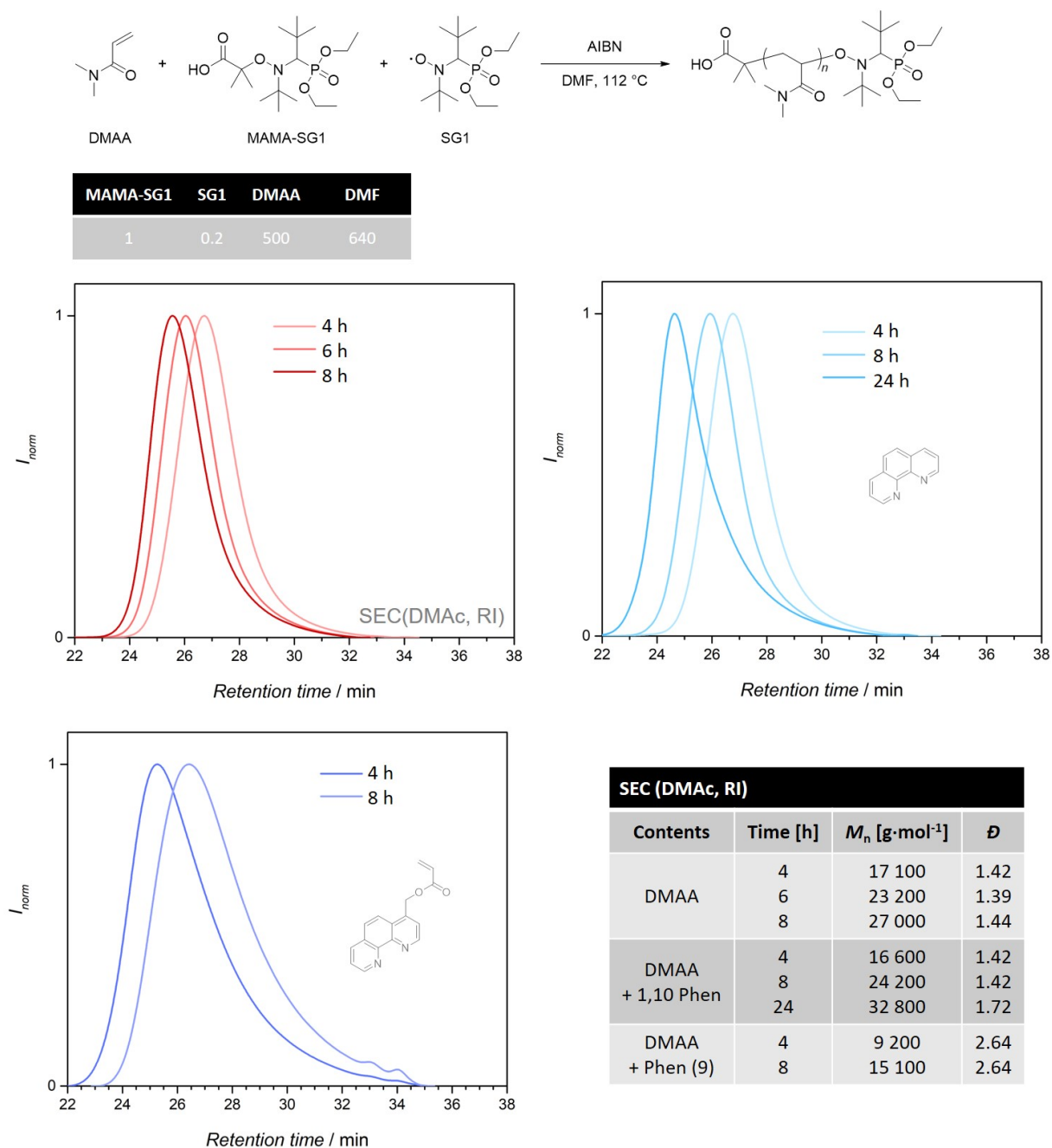


Figure 4.8: Investigation of the most suitable conditions for a polymerization of DMAA via NMP. *Top*: Reaction scheme for a polymerization of DMAA via the NMP method employing the nitroxide SG1 and the alkoxyamine MAMA-SG1. The table below contains the important reaction conditions. *Bottom, right*: Table with the parameters of the (co)polymerizations of DMAA, 1,10-Phen and the Phen-monomer (9) as well as the data of their SEC analysis. The corresponding SEC traces (DMAc, RI) are illustrated aside. As shown in the table, the addition of molecular Phen does not influence the polymerization, however the addition of the Phen-monomer (9) leads to lower molecular weight and higher molecular weight distribution.

Consequently, the reaction conditions were further adjusted, for instance by lowering the solvent amount, to improve the polyDMAA polymerization and obtain polymers of lower dispersity (Figure 4.9). Under identical conditions, the same reaction was performed by adding the Phen-monomer (11). Although the obtained polymer chains were again shorter ($M_n = 28\,300\text{ g}\cdot\text{mol}^{-1}$) and broader distributed ($\mathcal{D} = 1.83$) than in the polyDMAA approach, the resulting polymers almost fulfilled the requirements of a Phen-containing copolymer, only lacking a narrow distribution.

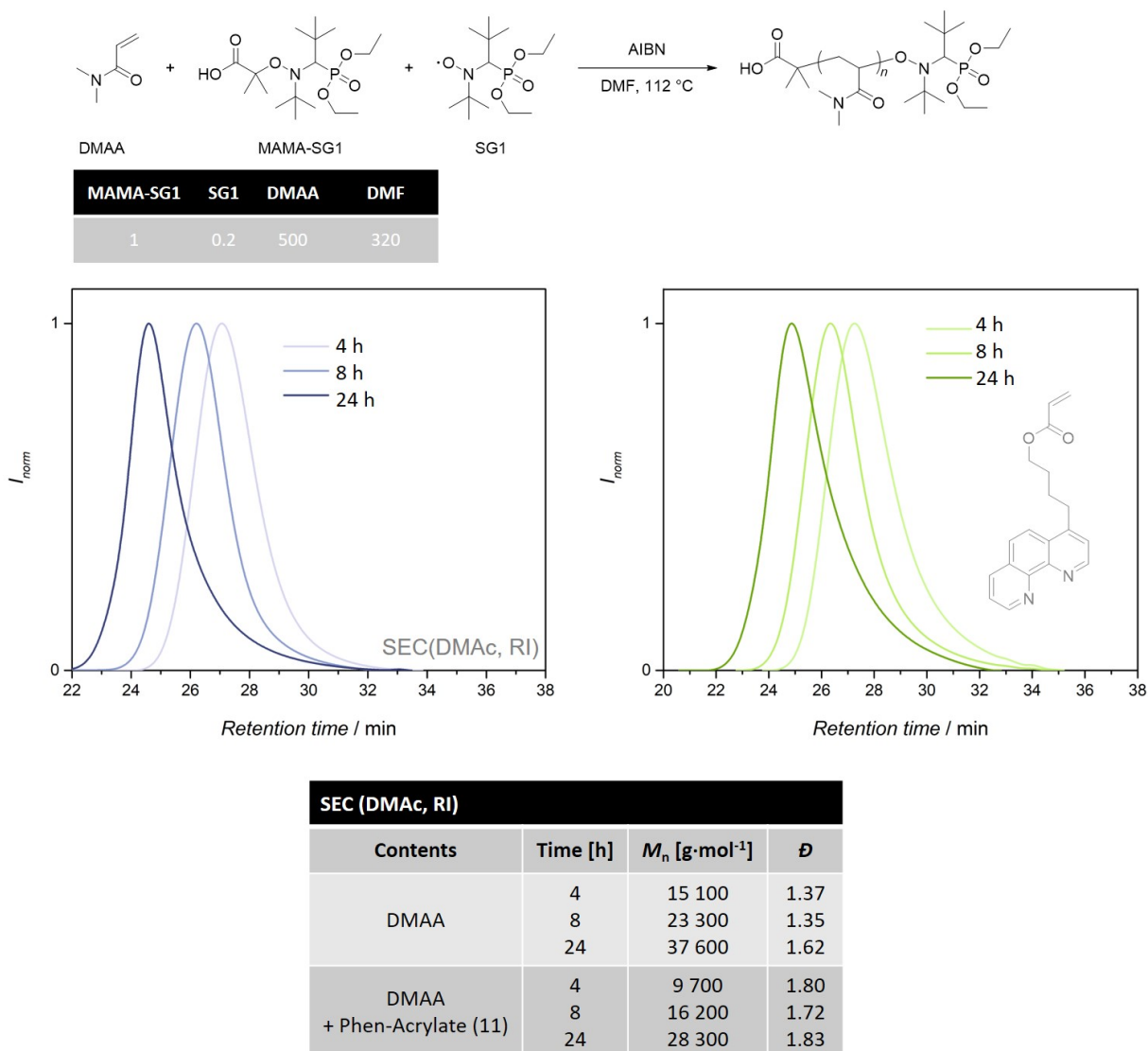


Figure 4.9: Further adaption of the reaction parameters for an optimized polymerization of DMAA and the copolymerization with Phen-monomer (11). *Top:* Reaction scheme for a polymerization of DMAA via the NMP method employing the alkoxyamine MAMA-SG1 and the nitroxide SG1. Corresponding ratios of the starting materials are given below in the table. *Middle:* SEC traces (DMAc, RI) of the copolymers. *Bottom:* Overview over the parameters employed in the (co)polymerizations and the data from the SEC analysis. The copolymerization with the Phen-monomer (11) leads to shorter and broader distributed polymer chains, however, the results are more promising than for previous reactions.

Summarizing the recent results, applying the nitroxide SG1 aligned with the alkoxyamine MAMA-SG1 for a copolymerization of DMAA and the Phen-monomer (11), the objective of a molecular weight of $25\,000\text{ g}\cdot\text{mol}^{-1}$ is reached ($M_n = 28\,300\text{ g}\cdot\text{mol}^{-1}$), yet the dispersity of the molecular weight is still too high ($\mathcal{D} = 1.83$).

Comparing the two Phen-containing monomers (9) and (11), clearly better results are obtained for (11), independently of the polymerization method, RAFT or NMP. A plausible reason is the longer spacer unit of four methylene groups of (11) in comparison to one methylene group in (9), thus less influencing the activity of the acrylate unit of (11). From hereon, only the Phen-monomer (11) is employed and termed Phen-acrylate.

4.4.3 Copolymerization Yielding P_{polar}

To determine the best conditions for a Phen-acrylate incorporation into a polymer chain, a direct comparison of the RAFT and NMP approach was carried out. Under the most suitable reaction conditions for each system, the identical monomer feed ratio is employed and an identical molecular weight and distribution is targeted (as defined before: $M_n = 25\,000\text{ g}\cdot\text{mol}^{-1}$, $\mathcal{D} < 1.5$). The resulting polymer chains are analyzed by SEC measurements (DMAc, RI) and ^1H NMR spectroscopy.

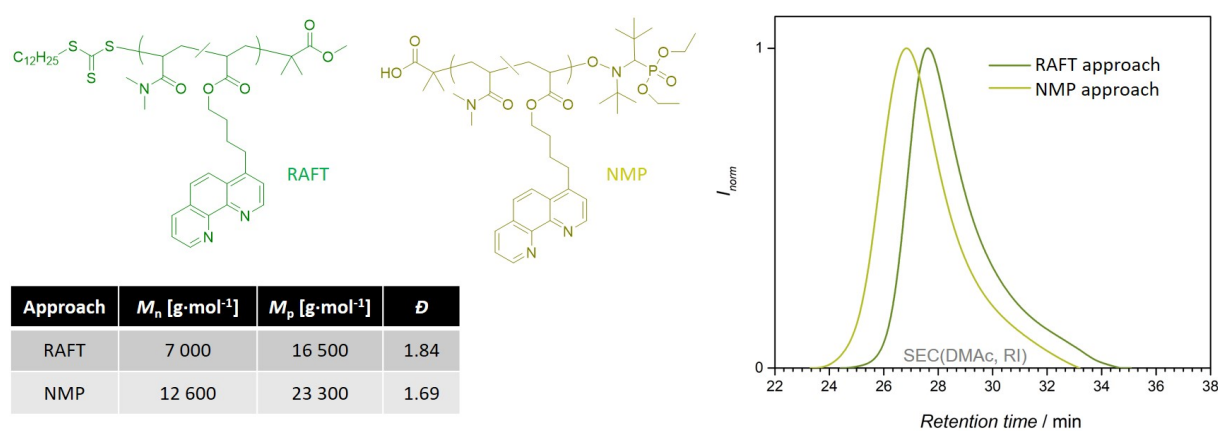


Figure 4.10: Direct comparison of a copolymerization of DMAA with Phen-acrylate either *via* the RAFT or NMP method. Both approaches were prepared with the same monomer feed ratio and performed under the respective optimum reaction conditions. *Top:* The respective structures of the copolymers. *Right:* SEC traces (DMAc, RI) of both copolymers. The corresponding data is given in the table, *bottom, left*.

The chemical structure of the copolymers, synthesized either *via* the RAFT or NMP technique, are depicted in Figure 4.10, along with their corresponding SEC traces (DMAc, RI). The results of the SEC analysis of both approaches are compared in the table, illustrating a preference for the NMP derived polymer, from now on labeled P_{polar} . In the NMP approach, polymer chains of higher molecular weight with a smaller dispersity are obtained than in the RAFT process. Although the number average

molar mass is low in comparison with the targeted molecular weight, $M_n = 12\,600\text{ g} \cdot \text{mol}^{-1}$, the value of the maximum peak M_p reached approx. $23\,000\text{ g} \cdot \text{mol}^{-1}$.

A feature of both SEC traces is a delayed elution time, low intensity signal, and a significant tailing towards small molecular weight polymer. It was therefore investigated if the broad distribution and the low number average molecular weight is the result of poor propagation control during the polymerization upon Phen-acrylate implementation or an analytical problem during SEC measurement. Although the SEC analysis was performed on an instrument with columns specifically prepared for polar material and the polar eluent DMAc was conducted at high temperatures ($60\text{ }^\circ\text{C}$), an interaction between the Phen units in P_{polar} and the porous column material is plausible and has already been reported previously in the literature.^[241]

To ensure that no interaction between the copolymer P_{polar} and the column material takes place, the Phen units were "protected". Therein, P_{polar} was reacted with palladium(II) ions, employing the precursor complex $[\text{PdCl}_2(\text{cod})]$. In an exchange reaction between the ligand 1,5-cyclooctadiene (COD) by the Phen moieties in P_{polar} , stable 1:1 complex formation of Phen–Pd(II) occurred, creating the metallopolymer $P_{polar}\text{--Pd(II)}$ as shown in Figure 4.11. The strong metal-to-ligand bonds allow SEC analysis of the Pd(II) protected polymer,^[242] resulting in a molecular weight of $M_n = 26\,400\text{ g} \cdot \text{mol}^{-1}$ with a dispersity of $\mathcal{D} = 1.46$. This experiment demonstrates that the employed NMP conditions lead to a controlled implementation of Phen-acrylate, resulting in a Phen-containing copolymer of the targeted molecular weight and dispersity. At this stage, the requirements of a Phen-functionalized polymer, regarding the molecular weight and dispersity, are achieved. In further analysis, the degree of polymerization and its predictability are evaluated.

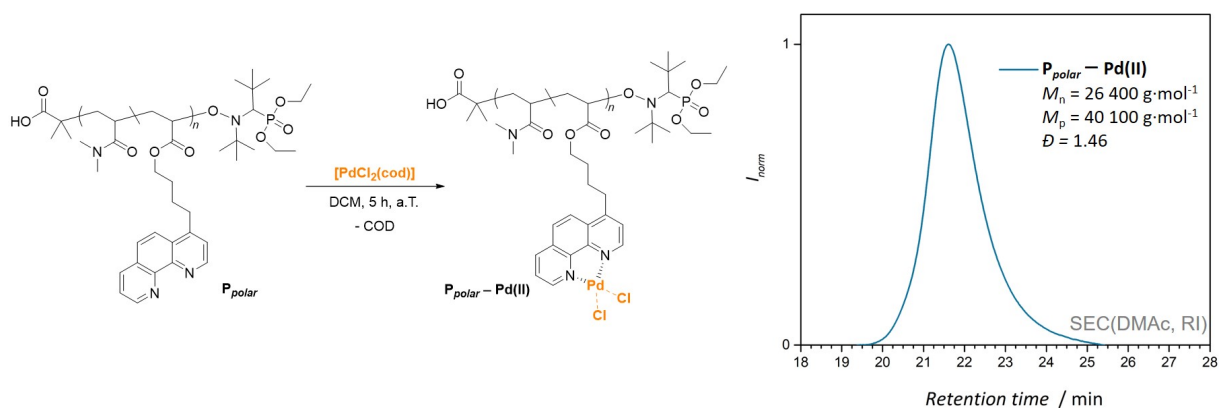


Figure 4.11: Left: Reaction scheme for a reaction between P_{polar} and $[\text{PdCl}_2(\text{cod})]$. Strong complex formation between palladium(II) ions and the Phen units in P_{polar} enable SEC measurements, excluding interactions between the Phen and the column material. Thus, the copolymer P_{polar} shows a high molecular weight and dispersity, which exceeded the requirements for a polar Phen-containing monomer ($M_n > 25\,000\text{ g} \cdot \text{mol}^{-1}$, $\mathcal{D} < 1.5$), as depicted in the SEC elugram, right. Adapted from [4] with permission from John Wiley and Sons.

Subsequently performed ^1H NMR spectroscopy of P_{polar} reveals distinct resonances for the Phen moieties, both in the aromatic and the aliphatic region (refer to the highlighted resonances in the ^1H NMR spectrum in Figure 4.12). Comparing the integrals of the resonances of the aromatic protons of Phen-acrylate units with the resonances of the methyl groups of DMAA, a monomer ratio of 1:20, Phen:DMAA, is calculated. This is synonymous to approx. 5 % Phen moieties and in good agreement with the monomer feed ratio, thus concluding another two important parameters of the desired polymer. As confirmed in additional experiments (not shown here), the polymer composition always correlates with the monomer feed ratio, allowing a facile prediction and control of the functionalization degree of the copolymers.

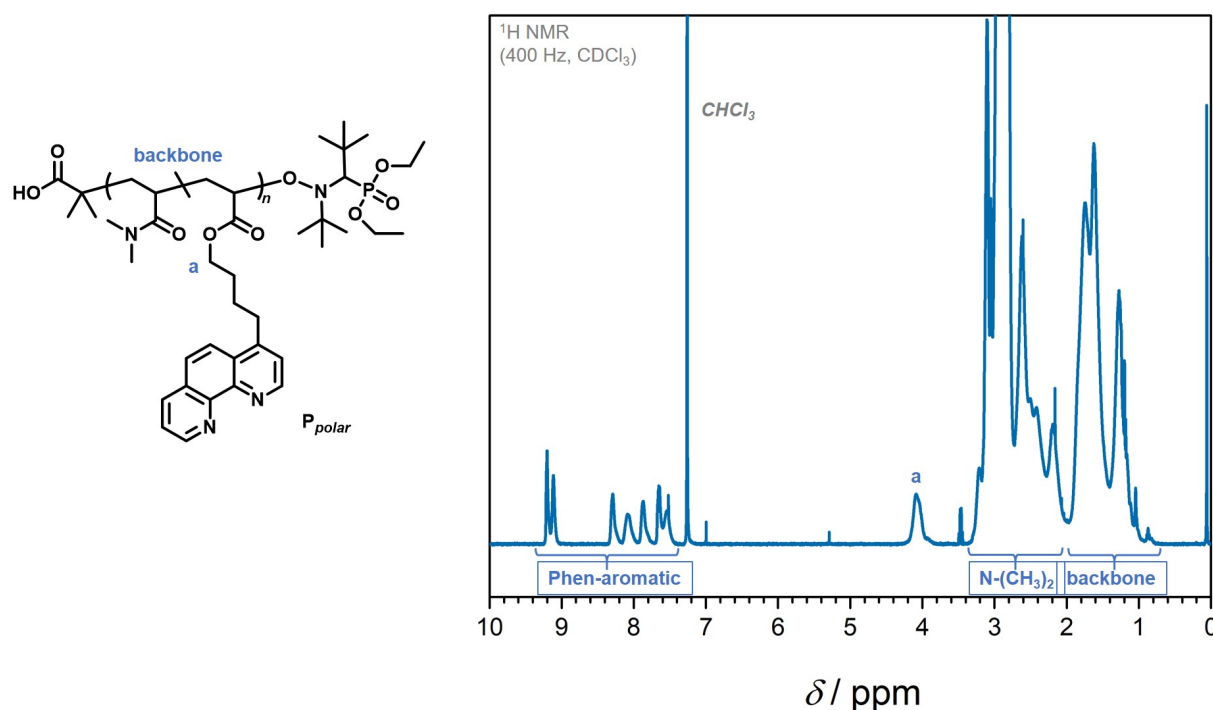


Figure 4.12: Chemical structure (left) and the corresponding ^1H NMR spectrum of P_{polar} (right). Integration allows the comparison of the resonances of the aromatic protons of Phen-acrylate at $\delta = 7.2\text{--}9.3$ ppm with the resonances of the methyl groups in $\text{N}(\text{CH}_3)_2$ at approx. $\delta = 2.0\text{--}3.3$ ppm resulting in a monomer composition of approx. 1:20, regarding the higher amount to DMAA. This ratio is in good agreement with the monomer feed ratio. Adapted from [4] with permission from John Wiley and Sons.

The successful incorporation of Phen-acrylate was further evidenced by UV/Vis and IR spectroscopy. Performed in methanol, in the UV/Vis spectrum of P_{polar} two maxima at $\delta = 224$ nm and 266 nm are detected, similar as for molecular 1,10-phenanthroline (confirmed by own measurements of Phen and shown in the application of P_{polar} and in the literature).^[243] Additionally, the characteristic $\text{C}=\text{O}$ mode for the acrylate functionality in comparison to the acrylamide functionality is detected in the

corresponding IR spectrum at $\tilde{\nu}(\text{C}=\text{O}, \text{acrylate}) = 1724 \text{ cm}^{-1}$ (refer to the Experimental Section, Chapter 9.4.9).

In summary, novel procedures for the synthesis of Phen-containing acrylate based monomers were developed. Thereby, especially Phen-acrylate demonstrates good compatibility in copolymerizations with DMAA *via* both the RAFT and NMP technique. Adapted reaction conditions and elaborated parameters allow the synthesis of polar Phen-copolymers with high molecular weight. The "protection" of the Phen units by Pd(II) ions enables facile SEC analysis, demonstrating the broader dispersity as a reason of undesired reaction with the instrument. UV/Vis and IR spectroscopy confirmed the implementation of Phen moieties into the copolymer. Interestingly, the analysis *via* ^1H NMR spectroscopy did not only verify the presence of Phen-acrylate in the polymer, it also enabled the determination of the polymer composition, which was in good agreement with the monomer feed ratio. As confirmed by further experiments, the monomer feed ratio is always consistent with the monomer composition in the polymer, thus the amount of functional groups in the polymer can be precisely planned and predicted.

After the successful synthesis of a polar Phen-containing polymer P_{polar} , the following section describes its application for SCNP formation, employing transition metals. Subsequently, the analogous synthesis of a non-polar Phen copolymer and its transformation into a luminescent metallopolymer is reported.

4.5 P_{polar} as a Polymer Scaffold for Transition Metal SCNP Formation

After the successful synthesis of a phenanthroline (Phen) functionalized polar system, yielding P_{polar} , this linear copolymer was employed to demonstrate its application possibilities in the formation of sophisticated metal coordinated 3D macromolecular architectures.

In addition to the 1:1 Pd(II)–Phen complex formation (P_{polar} –Pd(II)) described in Chapter 4.4.3, the synthesis of enhanced metallopolymer structures was targeted. Specifically, the collapse of P_{polar} into single-chain nanoparticles (SCNPs) upon metal ion coordination is appealing, resulting in soft matter material with the potential for application as catalysts. An advantage of the Phen moieties is their ability to coordinate in 2:1 or 3:1 ratios to various metal ions. Such a coordination of two or three Phen moieties to one metal center is essential to successfully fold the linear polymer P_{polar} into a collapsed nanoparticle.

Another prerequisite for metal-complexed SCNPs is the formation of stable metal–ligand linkages. The stability of complexes is expressed by the complex formation constant K_i .^[159] In multi-step complexes, the overall constant β is decisive, multiplying the stability constants of each step of the complex formation. For instance, in the complex of the type $[M(\text{Phen})_3]^{2+}$, the overall constant is dependent on the intermediate steps $[M(\text{Phen})]^{2+}$, $[M(\text{Phen})_2]^{2+}$ and $[M(\text{Phen})_3]^{2+}$, K_1 , K_2 , K_3 , respectively. Consequently, those constants are cumulated in β_3 . To be able to work with more convenient numbers, the overall constant β is stated logarithmic, $\log \beta$. A higher value of $\log \beta$ expresses a more favorable formation of the complex.

$$\log \beta_3 = \log K_1 K_2 K_3$$

Advantageously, P_{polar} is designed to be soluble in methanol allowing the application of common transition metal salts which require polar media to dissolve. Among the well-studied transition metal Phen complexes, especially Ni(II) and Fe(II) exhibit a high complex formation constant for a tris-Phen coordination ($\log \beta_3 ([\text{Ni}(\text{Phen})_3]\text{SO}_4) = 24.3$ and $\log \beta_3 ([\text{Fe}(\text{Phen})_3]\text{SO}_4) = 21.2$).^[244–247] Besides stable metal–ligand linkages, both complexes are readily formed at ambient temperature, another prerequisite for a convenient SCNP formation. Of particular interest is the intense red-colored iron(II) complex $[\text{Fe}(\sigma\text{-Phen})_3]\text{SO}_4$, also known as ferroin, which is often employed as a redox indicator in analytical chemistry.^[248]

This complex is extremely stable in a 3:1 Phen–Fe(II) ratio, due to a transformation of the high-spin complex $[\text{Fe}(\text{Phen})_2]^{2+}$ into a low-spin complex upon addition of the third Phen ligand. In such an octahedral arrangement, all six d-electrons of the iron(II) core occupy the three lower d-orbitals, wherefore the two empty d-orbitals can form along with the 4s and the three 4p orbitals the six free orbitals for ligand, e.g. Phen, coordination. For better understanding refer to Figure 4.13, in which the orbital splitting and orbital occupation is depicted. Since only paired electrons occur, the complex $[\text{Fe}(\text{Phen})_3]^{2+}$ is diamagnetic. The red color of iron(II) Phen complexes originates from metal-to-ligand charge-transfer processes, quantifiable by distinct UV/Vis traces.^[249]

In contrast to iron(II), in an octahedral arrangement of nickel(II), no free 3d orbitals exist, wherefore the six free orbitals for ligand coordination are formed by one 4s, three 4p and two 4d empty orbitals. Due to the two unpaired electrons in the complex, $[\text{Ni}(\text{Phen})_3]^{2+}$ exhibits a paramagnetic character.

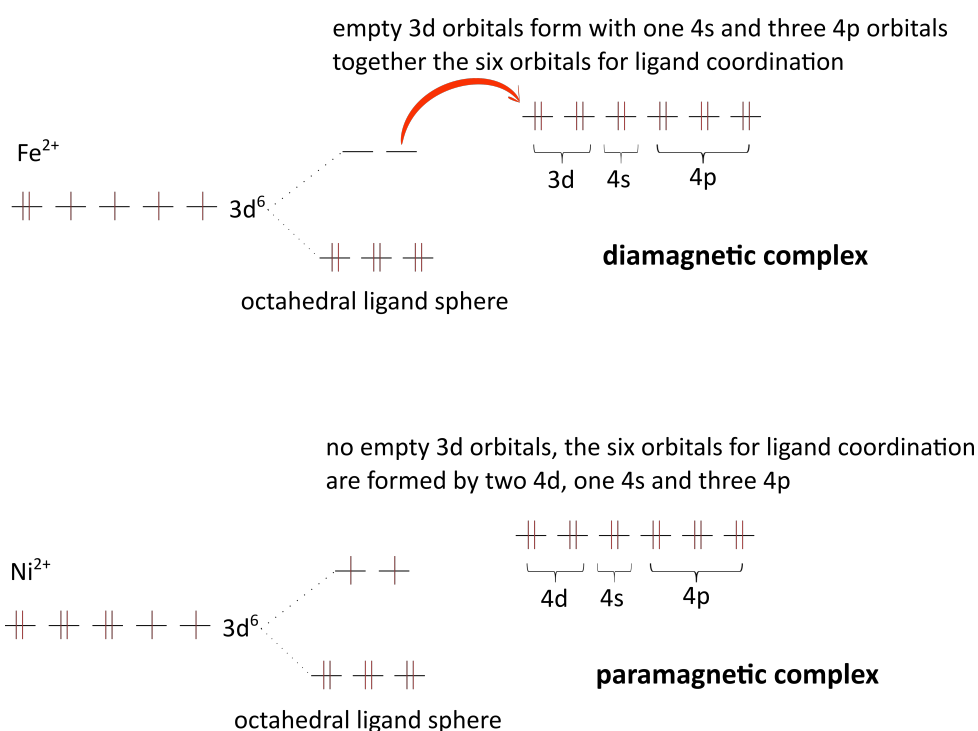


Figure 4.13: *Top:* Illustration of a theoretical arrangement of orbitals in an iron(II)–Phen complex. In an octahedral environment, caused by the Phen ligands, the formation of a low-spin complex in the iron(II) ion is enabled. Consequently, the spins are paired and the two empty d-orbitals are available for ligand coordination, along with one 4s and three 4p orbitals. *Bottom:* Theoretical arrangement of orbitals of a nickel(II) core in an octahedral environment with Phen. No empty 3d orbitals exist, wherefore the six orbitals coordinating to the ligand orbitals contain instead two 4d orbitals. The two unpaired electrons in nickel(II) cause the complex to be paramagnetic.

As a proof of principle for possible SCNP formation of P_{polar} with transition metals, the two precursor metal complexes $FeSO_4 \cdot 7 H_2O$ and $NiSO_4 \cdot 6 H_2O$ were employed. Due to the defined coordination of Fe(II) and Ni(II) to three Phen moieties, an incorporation into P_{polar} and thus a chain collapse is expected, resulting in metal-complexed SCNPs exhibiting $[M(Phen)_3]^{2+}$ folding units. A graphical overview and reaction scheme is given in Figure 4.14.

To employ the correct amount of metal salt for a 3:1 Phen–metal complex formation, the amount of Phen moieties per each chain has to be determined. Therefore, the data of the SEC analysis of P_{polar} ($M_n = 26\,400\text{ g} \cdot \text{mol}^{-1}$) was combined with the results of the 1H NMR spectrum, calculating on average an approximate number of twelve functional Phen units for each polymer chain.

The nanoparticle formation was performed as described in detail in the Experimental Section, Chapter 9.7. As for all SCNP formations, particular attention was paid to a sufficiently diluted system to prevent intermolecular linkages, which would otherwise lead to network formation instead of defined single-chain nanoparticles. For this purpose, P_{polar} was dissolved in methanol before the polymer solution was added to the highly diluted solutions of the respective metal salts $FeSO_4 \cdot 7 H_2O$ or $NiSO_4 \cdot 6 H_2O$. After isolation of the polymeric structures, the effective folding into a nanoparticle *via* generation of metal–Phen linker units was analyzed.

At first, the potential SCNP collapse was investigated *via* SEC (DMAc, RI) measurements. This is a conventional analytic method for polymeric SCNP formation in order to compare the hydrodynamic radius prior and after complexation (refer to Characterization of SCNPs *via* SEC, Chapter 2.4.1). However, the SEC traces of the polymeric structures after metal encapsulation exhibit chromatographic tailing (not shown). This occurrence is similar to SEC measurements of the pure polymer P_{polar} , thus indicating free Phen groups in the SCNPs (refer to Chapter 4.4.3). A possible explanation is a sterical hindrance during nanoparticle formation, preventing the coordination of each Phen unit to a metal ion. Moreover, the number of twelve Phen units per polymer chains is only a calculation based on statistical information. Most likely, some polymer chains exhibit more or fewer Phen units ($\neq 12$), which not necessarily participate in the metal coordination. Another reason can be a dissociation of the Fe(II) and Ni(II) ions from the polymer scaffold during SEC analysis, which would generate free Phen units.

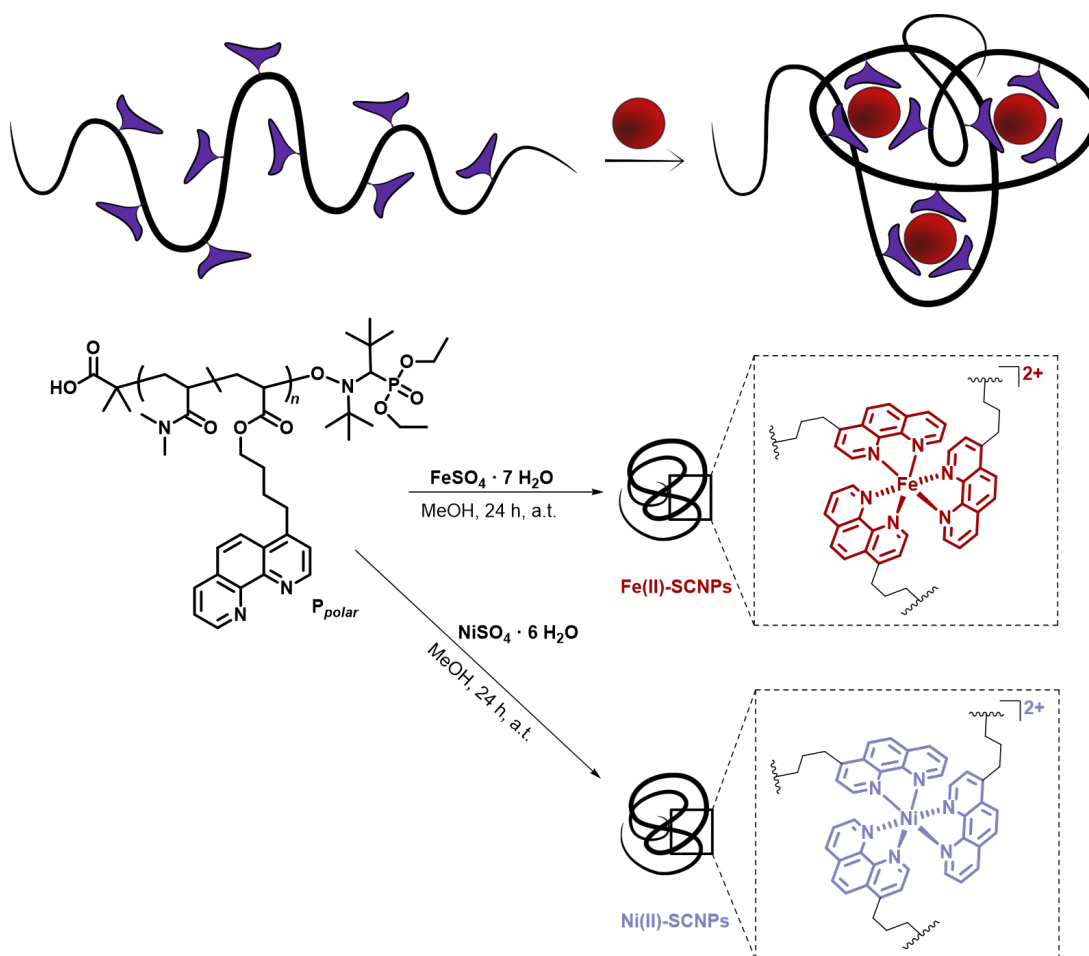

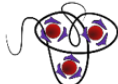
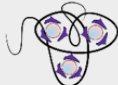


Figure 4.14: *Top:* Illustration of a single chain collapse into a particle. *Bottom:* Reaction scheme for the transformation of the linear precursor chain P_{polar} into Fe(II)- and Ni(II)-SCNPs, exhibiting metal–Phen linkages. As schematically depicted, a 3:1 Phen–Fe(II) complexation ratio is assumed. Adapted from [4] with permission from John Wiley and Sons.

In an alternative, established analysis method to confirm the chain compaction, the diffusion coefficients D of P_{polar} and the corresponding nanoparticles can be determined *via* diffusion ordered spectroscopy (DOSY). The diffusion coefficient of compounds is related to their size, specifically to their hydrodynamic radius (r_H). Therefore, this method enables to distinguish between polymer chains, SCNPs, and multi-chain aggregations, each exhibiting a different diffusion coefficient. The relation between radius and diffusion coefficient is described by the Stokes–Einstein Equation (Chapter 2.4.2). Employing the method and the equation, a $r_H = 2.8$ nm is calculated for P_{polar} . Upon metal incorporation, the radius of the polymer is reduced by approx. 50 %, revealed by the values of the nanoparticles $r_H = 1.3$ nm for the Fe(II)-SCNPs and $r_H = 1.4$ nm for the Ni(II)-SCNPs. The values for the diffusion coefficients D , their error and the corresponding r_H of P_{polar} and both nanoparticles

are collated in Table 4.1. Consequently, the analysis of the polymeric material *via* DOSY clearly reveals the formation of more compact structures.

Table 4.1: Diffusion coefficients and the respective error values of P_{polar} and the corresponding Fe(II)- and Ni(II)-SCNPs are determined by DOSY. Based on the diffusion coefficients, the hydrodynamic radii (r_H) of the compounds are calculated, applying the Stokes–Einstein Equation.

Substance		D [m^2s^{-1}]	Error	r_H [nm]
Copolymer P_{polar}		1.46×10^{-10}	3.05×10^{-13}	2.8
Fe(II)-SCNPs		3.08×10^{-10}	2.12×10^{-12}	1.3
Ni(II)-SCNPs		2.83×10^{-10}	2.19×10^{-12}	1.4

Next to evidencing the chain collapse, the anticipated folding motif $[M(\text{Phen})_3]^{2+}$ needs to be verified to ensure the metal encapsulation by the Phen moieties. Therefore, ^1H NMR measurements of the precursor polymer and the respective metal-SCNPs were performed (Figure 4.15).

The comparison of the ^1H NMR spectra of the Fe(II)-SCNPs and P_{polar} , merely reveal that aromatic proton resonances of Phen ($\delta = 6.5\text{--}9.8$ ppm, marked with a square) are broadened, yet remain distinguishable. This observation is an indication for the coordination of Phen moieties to the iron(II) cores. In the corresponding ^1H NMR spectrum of the Ni(II)-SCNPs the resonances of the aromatic protons of Phen moieties cannot be detected anymore (refer to the square in Figure 4.15), presumably a result of the strong paramagnetic character of the Ni(II) cores. Concluding, the change of resonances only regarding the Phen moieties in both spectra of the Fe(II)- and Ni(II)-SCNPs is a strong indication for their coordination to transition metals.

The incorporation of the metal cores by the Phen moieties was further investigated by performing UV/Vis measurements for additional insight into the folding motif. In first experiments the UV/Vis absorption spectrum of the molecular nickel(II) complex $[\text{Ni}(\text{Phen})_3]\text{SO}_4$ in methanol was recorded. This complex does not exhibit a pronounced color and thus high concentrations were necessary to detect a characteristic peak, which appeared in the area between 450–600 nm. However, such high concentrations could not be established for the Ni(II)-SCNPs.

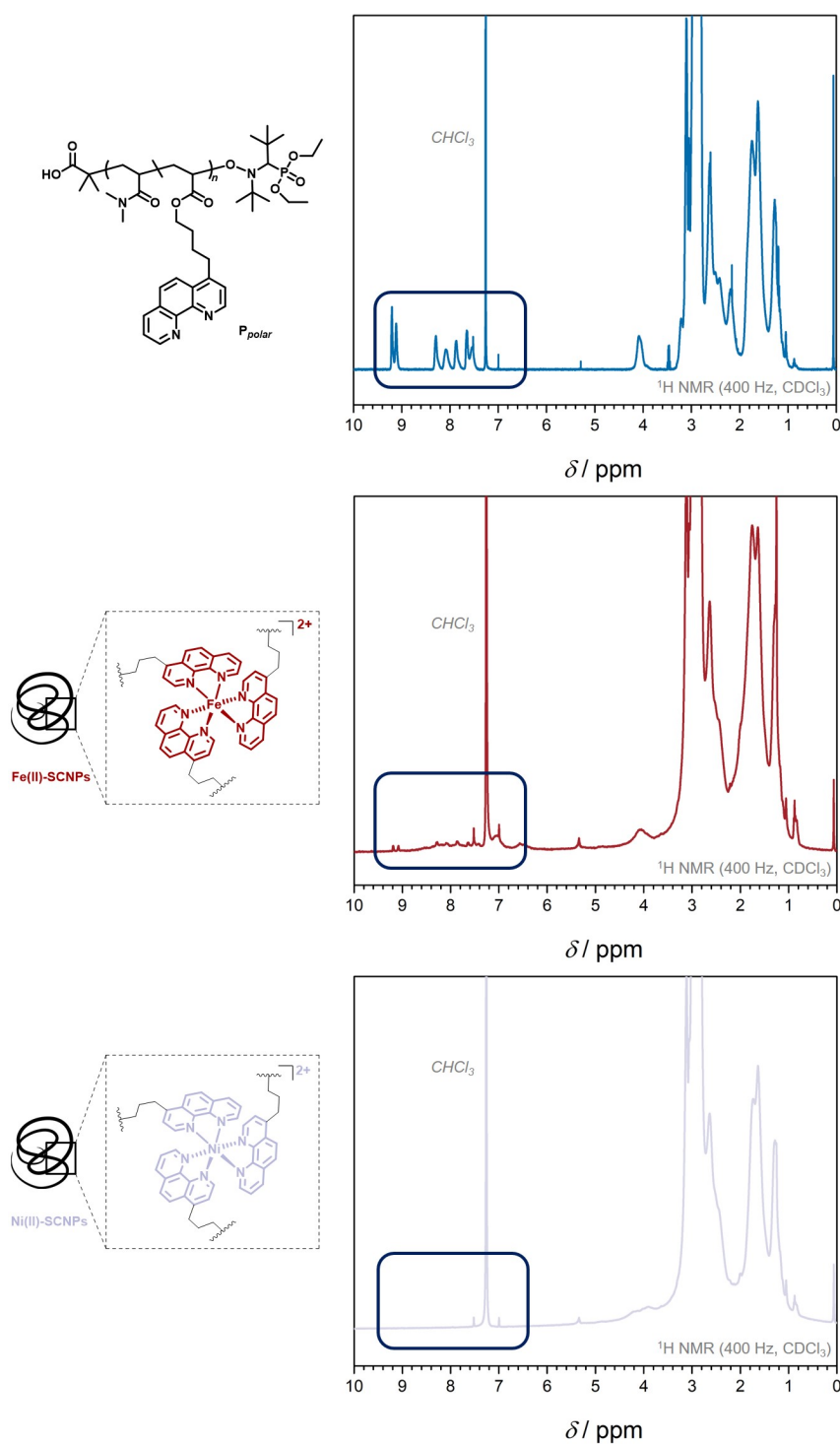


Figure 4.15: ^1H NMR of P_{polar} and the Fe(II) - and Ni(II) -SCNPs. The particularly interesting resonances in the spectra are marked with a square. In the spectrum of the Fe(II) -SCNPs the resonances for aromatic protons of Phen are broadened, caused by the Fe(II) cores. In the corresponding spectrum of the Ni(II) -SCNPs, the resonances of the Phen unit are not detected anymore, presumably a result of their coordination to the strong paramagnetic Ni(II) cores. Adapted from [4] with permission from John Wiley and Sons.

In comparison, already during the synthesis of the Fe(II)-SCNPs, the colorless solution of the dissolved polymer P_{polar} turned instantaneously bright red upon addition to the colorless Fe(II) solution. The reason are strong metal-to-ligand charge-transfer processes detectable in the visible and UV region.^[249]

To further validate $[\text{Fe}(\text{Phen})_3]^{2+}$ as the crosslinking motif in the SCNPs, likewise to nickel(II) the absorption spectrum of the molecular iron(II) complex $[\text{Fe}(\text{Phen})_3]\text{SO}_4$ in methanol was measured by UV/Vis spectroscopy. Thereby, a characteristic three shouldered trace with a maximum at 507 nm is obtained (refer to Figure 4.16). Afterwards, the Fe(II)-SCNPs were measured under identical conditions, exhibiting a similar trace shape with a maximum at 512 nm. The literature confirms such a trace shape in the presence of a 3:1 ligand-to-metal ratio,^[250, 251] thus validating the assumed folding unit in the Fe(II)-SCNPs.

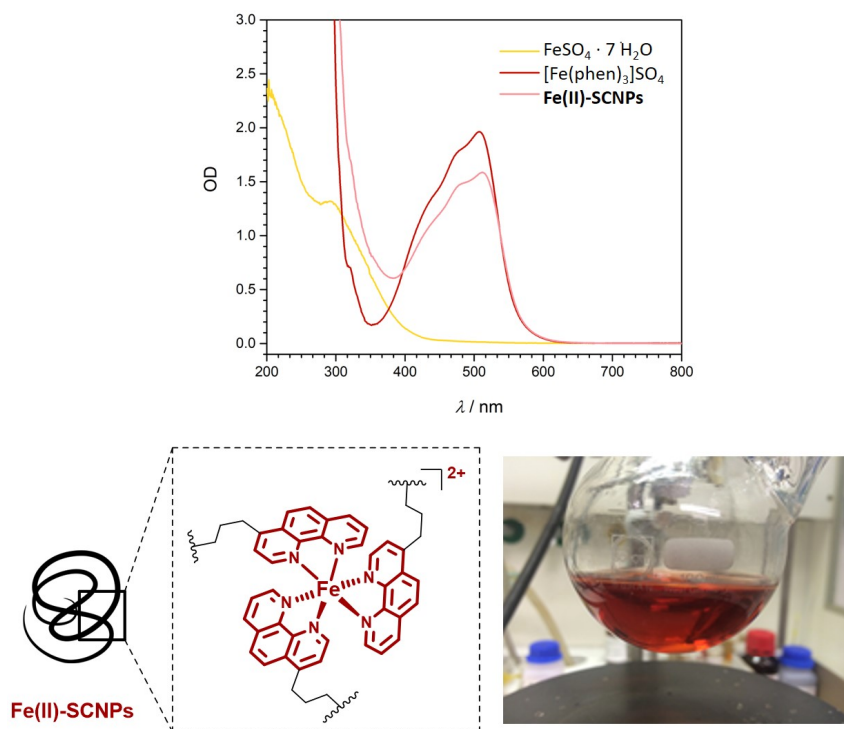


Figure 4.16: Top: UV/Vis traces of the precursor metal complex $\text{FeSO}_4 \cdot 7 \text{H}_2\text{O}$, the molecular model complex $[\text{Fe}(\text{Phen})_3]\text{SO}_4$ and the Fe(II)-SCNPs (in methanol). Similar shape of the UV/Vis traces of the model complex and the Fe(II)-SCNPs evidences a $[\text{Fe}(\text{Phen})_3]^{2+}$ folding motif in the SCNPs. Left: Simplified drawing of a $[\text{Fe}(\text{Phen})_3]^{2+}$ folding motif. Right: Upon addition of the precursor polymer P_{polar} to a solution of Fe(II) ions, the solution turned immediately bright red. Adapted from [4] with permission from John Wiley and Sons.

4.6 Polar System – Summary

The present section demonstrated various pathways to functionalize Phen derivatives. Of high interest was the synthesis of the two Phen monomers, of which especially Phen-acrylate showed good compatibility in a copolymerization with DMAA. Polymerization techniques based on NMP and RAFT methods have been established, yielding high molecular weight polymers with predictable, predetermined and quantifiable amounts of Phen functionalities (P_{polar}). The issue of interaction of Phen moieties with SEC column material was solved by protecting the Phen units by a coordination to Pd(II) ions. Consequently, access to SEC analysis was provided, allowing the determination of the length and distribution of the polymer chains of P_{polar} . Finally, the predicted possibility of P_{polar} for an application as polymer framework in the field of SCNPs was demonstrated. Employing iron(II) and nickel(II) precursor complexes, compact nanoparticles were obtained.

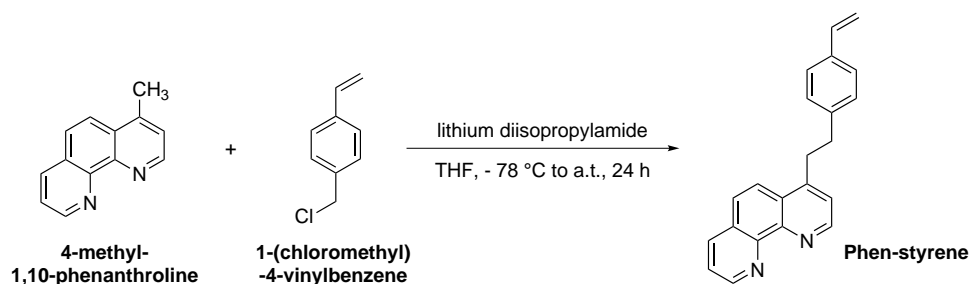
The size reduction of the linear polymer P_{polar} upon metal encapsulation was evidenced by DOSY analysis for the SCNPs structures of both metal complexes, Fe(II) and Ni(II). The incorporation of the metal ions by Phen moieties was confirmed, as in the corresponding ^1H NMR spectra exclusively the resonances of the Phen moieties were affected upon metal salt addition. Furthermore, the intense color of the Fe(II)-SCNPs allowed UV/Vis measurements, which revealed a similar trace shape in the spectrum of the Fe(II)-SCNPs and the corresponding molecular complex $[\text{Fe}(\text{Phen})_3]\text{SO}_4$, indicating the presence of such a unit within the polymeric structures. Although the less pronounced color of the Ni(II)-SCNPs complicated their comparison with molecular complexes, a similar procedure was assumed. Therefore, the crosslinking points in the SCNPs very likely consists of $[\text{M}(\text{Phen})_3]^{2+}$ units.

4.7 Non-Polar System – Monomer Synthesis

The polar system of phenanthroline (Phen) containing polymer chains was further extended to non-polar Phen-functionalized chains, ensuring adequate application possibilities in aqueous, yet also organic solvent media. Therefore, a non-polar Phen based monomer was designed to enable its copolymerization with another non-polar monomer. For the generation of a non-polar framework, styrene was selected as an appropriate comonomer. Beneficial for this purpose was the well-studied polymerization behavior of styrene and its derivatives, allowing facile polymer preparation and manifold monomer composition in the future polymer chains.^[252]

As achieved in the polar system, the establishment of a predictable, verifiable and defined inclusion of the non-polar Phen species into the copolymer is targeted. For this reason, similar reactivity ratios of styrene and the corresponding Phen species are required. This is achieved by creating a Phen monomer carrying a styrene functionality. Drawing upon the knowledge gained during the synthesis of the polar Phen monomer, a synthesis procedure including highly reactive species, is explored.

The reaction pathway to synthesize the non-polar Phen-monomer 4-(4-vinylphenethyl)-1,10-phenanthroline, labeled Phen-styrene, is depicted in Scheme 4.8. As starting material, the same compound employed in the synthesis of the polar monomers is utilized. Therefore, 4-methyl-1,10-phenanthroline is lithiated by lithium diisopropylamide (LDA) and subsequently reacts in a salt metathesis reaction with 1-(chloromethyl)-4-vinylbenzene, affording the monomer Phen-styrene.



Scheme 4.8: Reaction scheme of the synthesis of Phen-styrene. For the generation of a non-polar Phen-functionalized system, a Phen monomer, which contains similar reactivity as the comonomer styrene is designed. Therefore, at first 4-methyl-1,10-phenanthroline is lithiated by lithium diisopropylamide (LDA) and subsequently reacts in a salt metathesis reaction with 1-(chloromethyl)-4-vinylbenzene, yielding Phen-styrene. Adapted from [4] with permission from John Wiley and Sons.

The ^1H NMR spectrum of Phen-styrene is shown in Figure 4.17, in which the resonances are assigned to the corresponding protons in the structure. The proposed structure was furthermore confirmed by ^{13}C NMR and IR spectroscopy, mass spectrometry and elemental analysis (refer to the Experimental Section, Chapter 9.3.9).

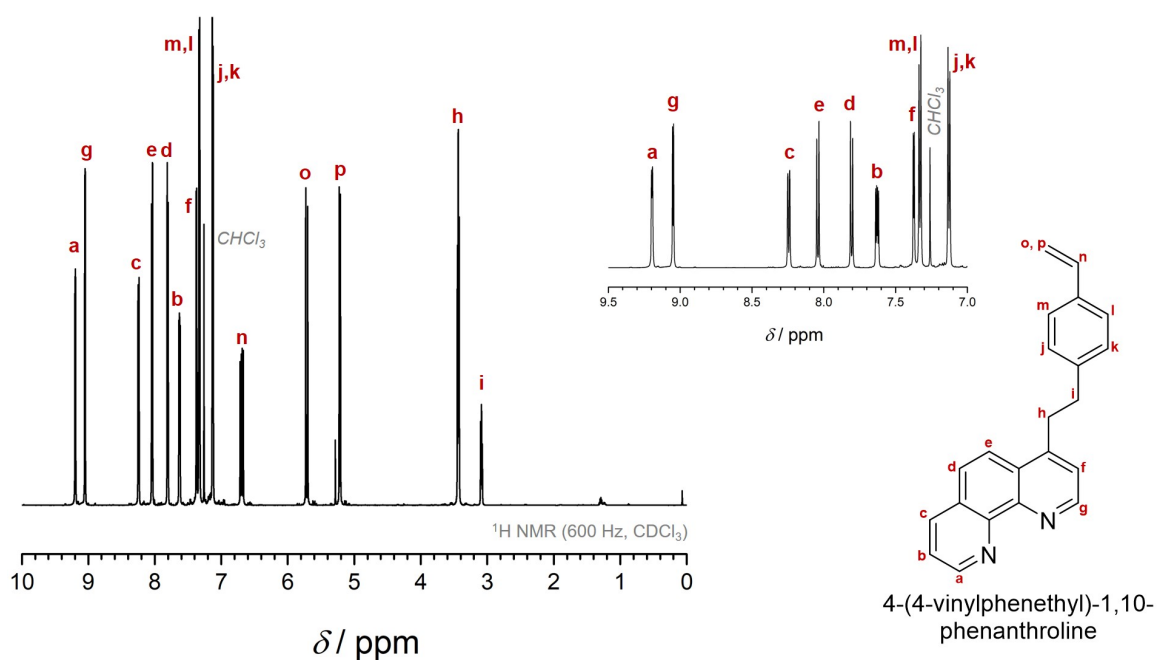
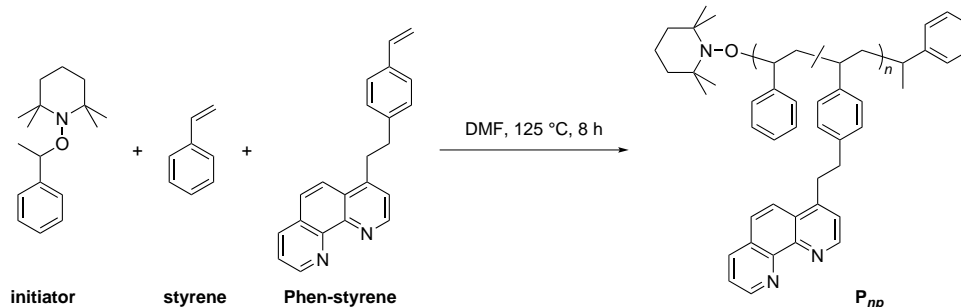


Figure 4.17: Left: ^1H NMR spectrum of the monomer Phen-styrene (chemical structure on the right), which is designed containing a styrene functionality to allow its facile copolymerization with styrene. Top: Zoom into the ^1H NMR spectrum depicting the resonances of the aromatic Phen protons. Adapted from [4] with permission from John Wiley and Sons.

4.8 Non-Polar System – Polymerization Techniques

Analogous to the polar system, described in Chapter 4.4.3, the copolymerization of styrene and Phen-styrene was carried out *via* nitroxide mediated polymerization (NMP). The use of styrene derivatives allows the utilization of the alkoxyamine 2,2,6,6-tetramethyl-1-(1-phenylethoxy)piperidine (refer to Chapter 2.1.2). The copolymerization yields the non-polar Phen-functionalized system P_{np} as depicted in Scheme 4.9.



Scheme 4.9: Reaction scheme for the NMP mediated copolymerization of Phen-styrene and styrene employing the alkoxyamine 2,2,6,6-tetramethyl-1-(1-phenylethoxy)piperidine, yielding the copolymer P_{np} .

As observed for the polar system, the analysis of the pure polymer *via* SEC measurements was negatively affected by the interaction of the Phen moieties with the column material, leading to broad SEC traces of low intensity. Therefore, the Phen groups in the copolymer P_{np} were "protected" by coordination to Pd(II) ions, analogous to the polar system. Subsequently performed SEC analysis (THF, MALLS) of P_{np} -Pd(II) revealed a number average molecular weight of $M_n = 31\,900\text{ g}\cdot\text{mol}^{-1}$ and a narrow dispersity of $\mathcal{D} = 1.14$ (refer to Figure 4.18).

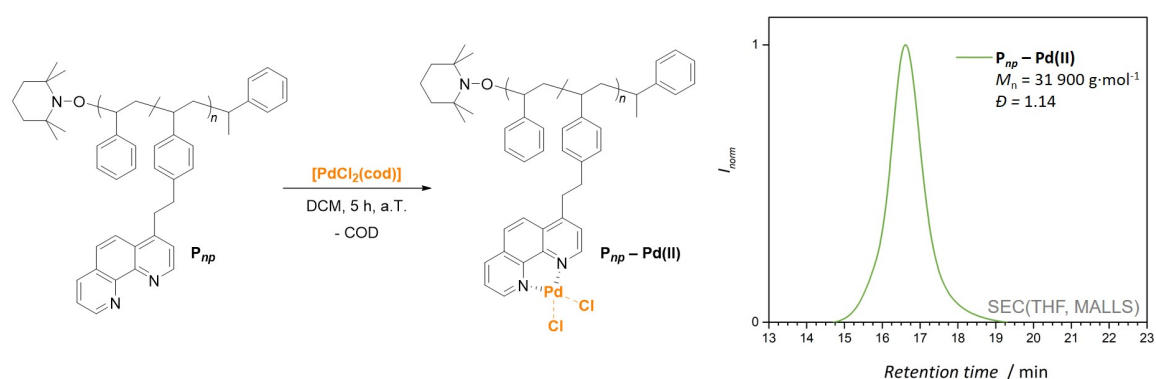


Figure 4.18: SEC trace (THF, MALLS) of $P_{np}\text{-Pd(II)}$. Upon addition of $[\text{PdCl}_2(\text{cod})]$ to the precursor polymer P_{np} , the Phen moieties substitute the former ligand 1,5-cyclootadiene (COD) and form stable complexes with the Pd(II) ions in a 1:1 ratio. The strong coordinative bonds between Pd(II) and the Phen moieties enable the SEC analysis of P_{np} . Adapted from [4] with permission from John Wiley and Sons.

The monomer composition in the copolymer P_{np} was determined via ^1H NMR spectroscopy, distinguishing the integrals of the resonances for each monomer (refer to Figure 4.19). In detail, the integral of the resonances of the methylene groups of the Phen-styrene monomer at $\delta = 3.4\text{--}3.0$ ppm (a and b) is compared to the integrals of the aromatic protons of all styrene units between $\delta = 9.5\text{--}6.1$ ppm, subtracting the aromatic styrene based protons of Phen-styrene. The amount of functional Phen groups in P_{np} is calculated, resulting in approx. 2 %, which is concomitant to the monomer feed ratio. This amount equals approx. six Phen moieties per chain. The small degree of functionality was selected with regard to further applications of P_{np} , as described in Chapter 4.9.

In any case, the monomer composition can readily be varied, depending on the desired degree of functionalization by adapting the monomer feed ratio.

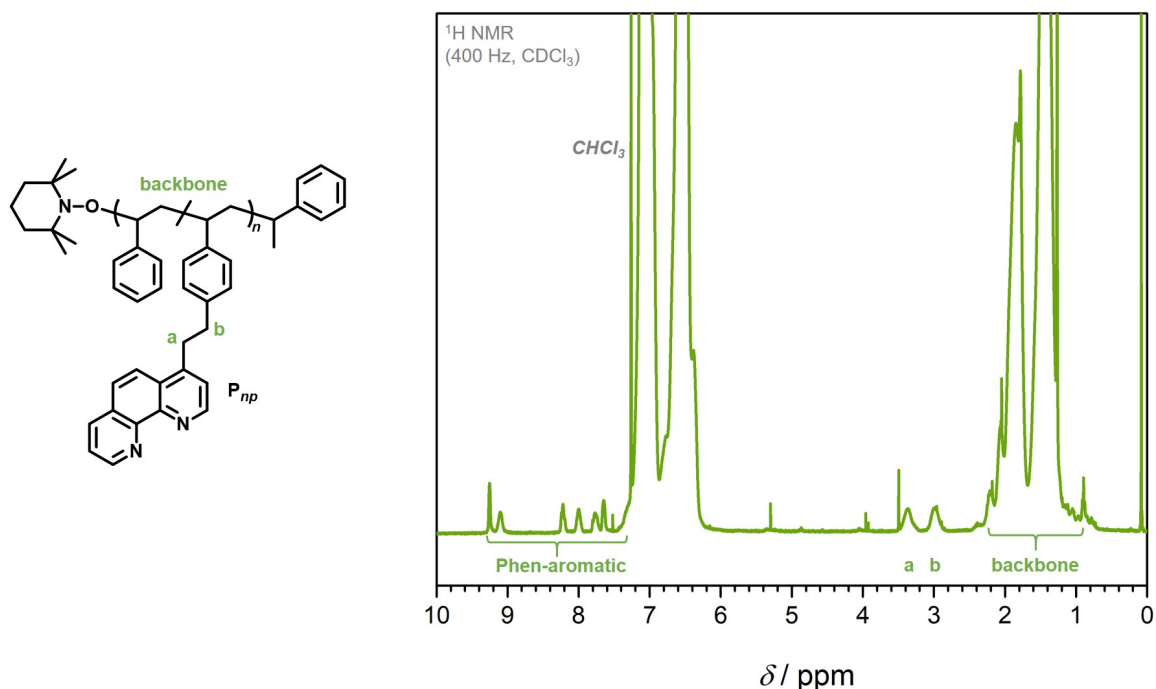


Figure 4.19: Left: Chemical structure of P_{np} . Right: ^1H NMR spectrum of the copolymer P_{np} , in which characteristic resonances of the protons of the comonomers are labeled. The comparison of the integrals of the resonances of the methylene units in Phen-styrene (a and b) with the resonances of all aromatic protons in the polymer allow the determination of the monomer composition in P_{np} , resulting in approx. 2 % Phen functionality. Adapted from [4] with permission from John Wiley and Sons.

4.9 P_{np} as a Polymer Framework for Lanthanide Metallopolymers

Appealing for the non-polar system P_{np} was the investigation of its optical properties when incorporating lanthanides into the polymer scaffold by coordinating them to the Phen moieties. As reported in the literature, Phen turns into a triplet state photosensitizer upon coordination to lanthanides, acting as an antenna ligand to enhance the luminescence of poorly absorbing metal ions, such as Eu(III) or Tb(III).^[199, 253, 254] Detailed information is given in Chapter 2.5.3 and 2.5.5.

Characteristic for such lanthanide complexes are sharp emission spectra, originating from shielded inner-shell 4f orbitals. As a consequence of the forbidden intramolecular 4f–4f transitions, their excited state has a long lifetime.^[255] The embedding of Eu(III) or Tb(III) into polymeric structures is therefore highly interesting for the formation of long-lived, luminescent material.^[256]

Due to the solubility of P_{np} in organic solvents, the non-polar system is restricted to precursor metal complexes containing organic ligands. Moreover, the energy level of the additional organic ligands, attached to the lanthanide centers has to be at least 1700 cm^{-1} higher than the excited state of the lanthanides. The difference in energy level between lanthanides and ligands is necessary to result in highly luminescent material, prohibiting backtransfer of the energy in the excited states of the lanthanides to the energy levels of the ligands. For more information on the excitation of lanthanides refer to Chapter 2.5.5 or Figure 4.24 in Chapter 4.10. Such suitable ligands are dibenzoyl methane (DBM) and acetylacetonate (ACAC), for an europium and terbium complex, respectively.^[197, 257] The corresponding precursor complexes are $[\text{Eu}(\text{dbm})_3(\text{H}_2\text{O})_2]$ and $[\text{Tb}(\text{acac})_3(\text{H}_2\text{O})_x]$ (Figure 4.20).

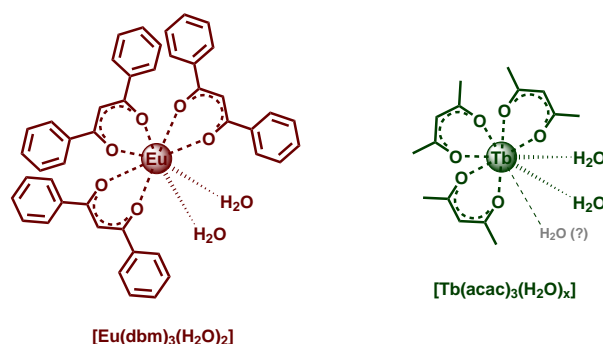


Figure 4.20: Chemical structure of the lanthanide precursor complexes $[\text{Eu}(\text{dbm})_3(\text{H}_2\text{O})_2]$ and $[\text{Tb}(\text{acac})_3(\text{H}_2\text{O})_x]$. The organic ligands dibenzoyl methane (DBM) and acetylacetonate (ACAC) are chosen due to their ability to support the luminescent character of the respective lanthanides. To saturate the coordination site, two water molecules coordinate to europium. The amount of water molecules in the terbium compound was not ambiguously determined, however a minimum of two molecules is assumed.

Both promote the luminescent properties of the lanthanides and shield the metal center from extensive coordination to water molecules, due to their space demanding character. For the europium complex, a coordination of two additional water molecules is indicated. The amount of coordinating water molecules is not determined for the terbium compound, indicated with a 'x' in the structural name, however, a minimum of two molecules is assumed. Both complexes offer exclusive 1:1 complex formation with one Phen unit, which substitutes two water molecules. The process for the europium complex is schematically depicted in Figure 4.21. A proposed mechanism for the enhancement of the luminescence by Phen in the complex $[\text{Eu}(\text{dbm})_3(\text{Phen})]$ reports an energy transfer of Phen to the DBM ligands, which subsequently populate the excited states of europium.^[258] A similar process is assumed for the terbium compound.

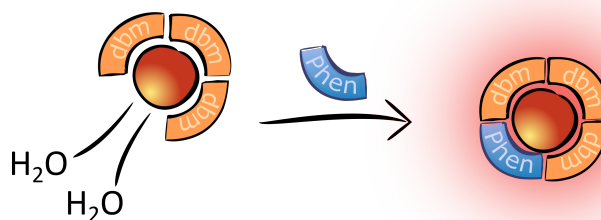


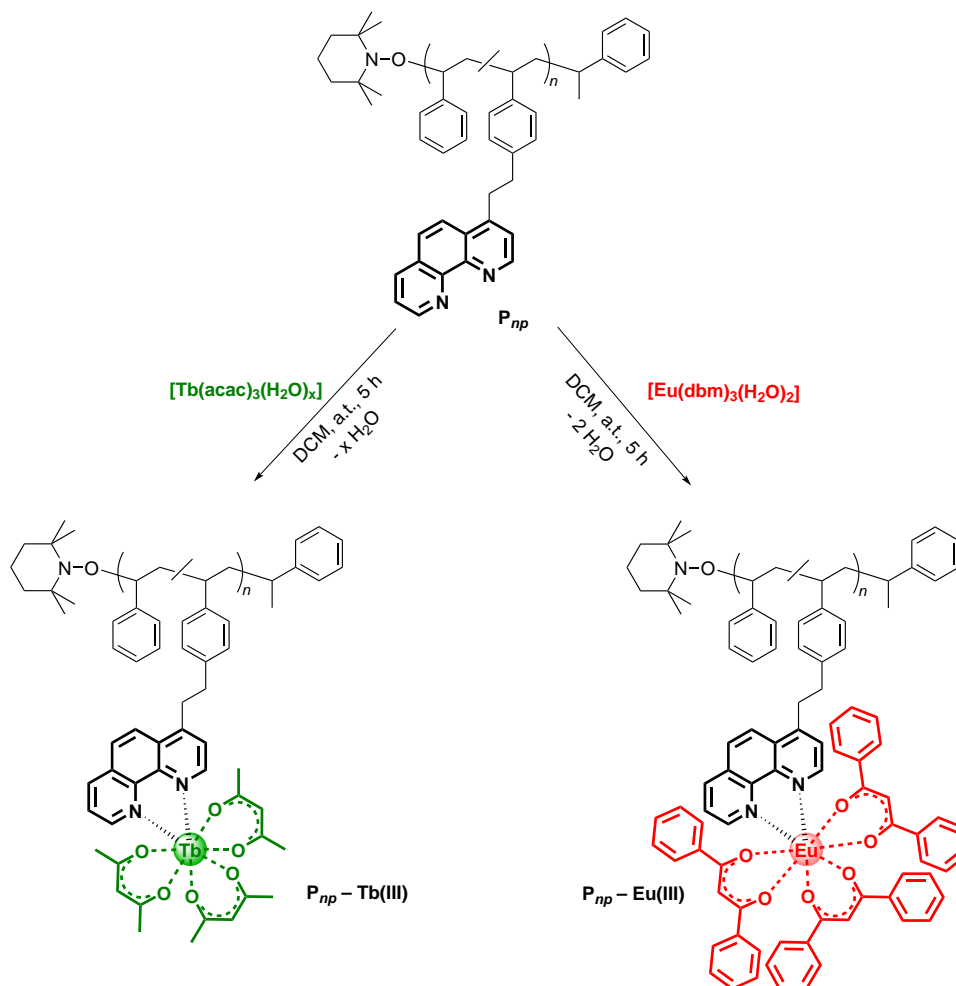
Figure 4.21: Schematic depiction of the enhancement of luminescence for a $[\text{Eu}(\text{dbm})_3(\text{H}_2\text{O})_2]$ complex upon Phen coordination, which substitutes the two luminescence quenching water molecules $\rightarrow [\text{Eu}(\text{dbm})_3(\text{Phen})]$. This replacement in combination with an enhanced aromatic structure results in luminescent material.

The europium and terbium containing metallopolymers are simply obtained by adding the respective lanthanide precursor complexes to the dissolved P_{np} in DCM. After stirring for several hours, the solutions were concentrated and precipitated into cold methanol. The subsequent filtering isolated the polymeric structures from the non-reacted molecular compounds (Scheme 4.10). After the complexation process, the successful encapsulation of the lanthanide complexes into the polymer matrix was investigated by multiple NMR techniques and absorption–emission spectroscopy.

At first, the metallopolymers were analyzed via ^1H NMR spectroscopy. In the ^1H NMR spectra of $P_{np}\text{--Eu(III)}$ and $P_{np}\text{--Tb(III)}$ new sets of resonances appear, which are assigned to the protons of the DBM or ACAC ligands, respectively (Chapter Appendix).

Comparing the ^1H NMR spectra of the precursor polymer P_{np} with the metallopolymer $P_{np}\text{--Eu(III)}$, a shift of the resonances of the aromatic protons and the methylene groups of the Phen groups is detected. In addition, exclusively the resonances of Phen-styrene are broadened, most likely caused by the paramagnetic character of the Eu(III) cores, which influence the NMR relaxation of close-by nuclei.

In the corresponding ^1H NMR of $\text{P}_{np}\text{-Tb(III)}$, the resonances for Phen-styrene are broadened to such an extent that they partially fuse with the baseline. The sole shift and broadening of the resonances of the implemented Phen-styrene monomer in both metallopolymer systems already suggest a successful lanthanide complexation.



Scheme 4.10: Reaction scheme for the synthesis of $\text{P}_{np}\text{-Ln(III)}$. The Phen moieties in copolymer P_{np} coordinate in a 1:1 ratio either to Tb(III) (*left*) or Eu(III) (*right*) precursor complexes. The enhancement of the aromatic system and the substitution of two water molecules from each precursor complex upon coordination to Phen result in luminescent material. Adapted from [4] with permission from John Wiley and Sons.

To further confirm an Eu(III) incorporation, in-depth 2D experiments were carried out with the support of Dr. Pavleta Tzvetkova (KIT). Suitable for this purpose was the Nuclear Overhauser Effect Spectroscopy (NOESY), a method in which peaks for cross relaxations between nuclear spins are visualized. For a NOESY spectrum, the spins of the nuclei need to be spatially close a typically in complexes or molecules.^[259]

The superimposed NOESY spectra of P_{np} (black) and P_{np} -Eu(III) (red) with the corresponding ^1H NMR spectra at the margin is depicted on top of Figure 4.22. As indicated with squares, additional cross peaks between the DBM ligand of the europium complex and the protons of the backbone in P_{np} and the methylene group of Phen-styrene appear. Only at a minimum distance between protons, such cross peaks are detected in NOESY measurements (through space), thus clearly indicating the complex formation of $[\text{Eu}(\text{dbm})_3(\text{Phen-styrene})]$ in P_{np} -Eu(III).

The coordination of Tb(III) to P_{np} proceeded analogous to the europium compound by a substitution of two water molecules by one Phen moiety. As shown in a superimposition of the NOESY spectra of P_{np} (black) and P_{np} -Tb(III) (green) in Figure 4.22, *bottom*, the resonances for the Phen-styrene moieties are completely vanished as indicated by squares. In comparison, the resonances for the backbone and further aromatic protons, originating from the other monomer styrene are still visible. Such a complete disappearance of resonances only takes place when in the near proximity a paramagnetic entity is present. Thus, the deletion only of the Phen moieties is explained by the proximity to paramagnetic terbium(III) cores, which can only be realized by coordination. This occurrence verifies the complexation of the Phen moieties of P_{np} to the terbium cores.

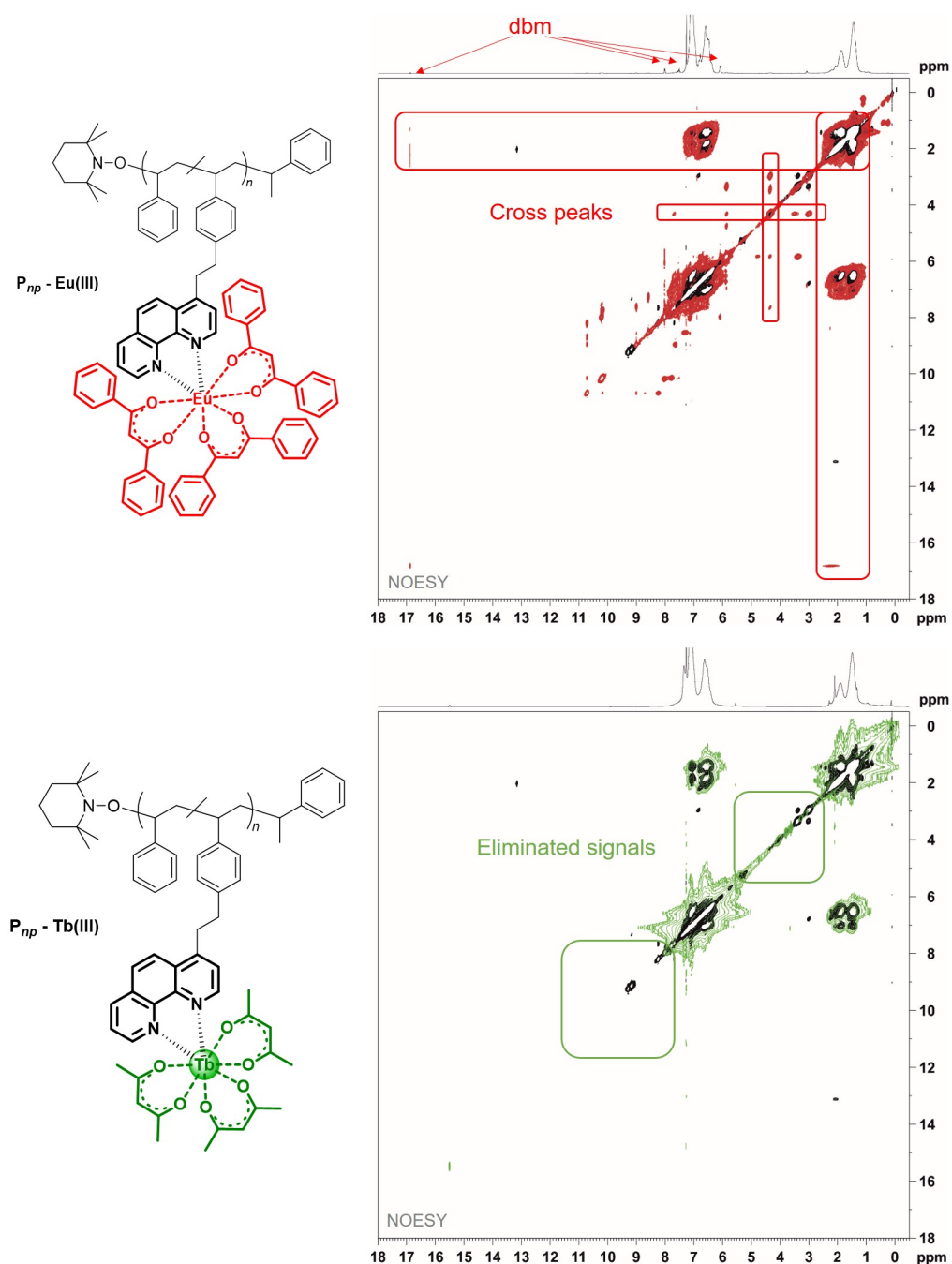


Figure 4.22: Superimposition of the NOESY spectra of the precursor polymer and the corresponding lanthanide metallopolymer to investigate the encapsulation of the metal complexes by the Phen moieties in P_{np} . *Top:* In an superimposition of the NOESY spectra of the precursor polymer P_{np} (black) and the metallopolymer P_{np} -Eu(III) (red), cross signals between the protons of the DBM ligand of the europium precursor complex and the protons of the copolymer indicate a successful encapsulation (marked in squares). *Bottom:* In the corresponding superimposition of the NOESY spectra of P_{np} (black) and the metallopolymer P_{np} -Tb(III) (green), the almost complete deletion of the resonances for the Phen-styrene monomer, caused by extensive broadening, point towards the embedding of the terbium center into the Phen moieties in the copolymer. Adapted from [4] with permission from John Wiley and Sons.

4.10 Non-Polar System – Photoexcitation in Solution

The synthesized metallopolymers P_{np} -Eu(III) and P_{np} -Tb(III), and the lanthanide precursor complexes are further employed for an in-depth investigation of the increase in luminescence upon coordination to Phen. Photographs of the two compounds P_{np} -Eu(III) and P_{np} -Tb(III) demonstrating the red and green luminescence are shown in Figure 4.23. The quantum yield and femto-second laser measurements were performed in cooperation with Nadine Michenfelder (KIT).

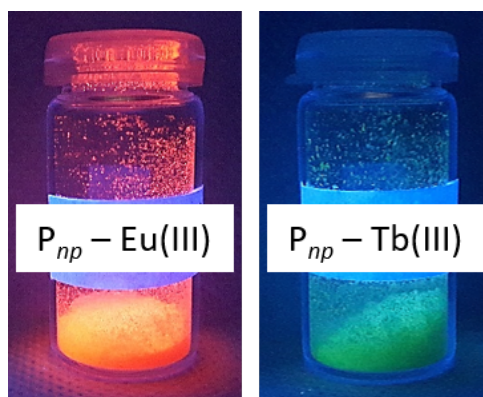


Figure 4.23: Photographs of the compounds P_{np} -Eu(III) and P_{np} -Tb(III), demonstrating the red and green luminescence, when being excited at $\delta = 366$ nm.

At first, the photophysical properties of the europium complexes were examined. To ensure a quantitative evaluation, the metallopolymer P_{np} -Eu(III) was compared to the analogous molecular complex $[\text{Eu}(\text{dbm})_3(\text{Phen})]$ and the precursor complex $[\text{Eu}(\text{dbm})_3(\text{H}_2\text{O})_2]$. Initially, the absorption spectra of all three compounds were recorded in DCM, shown on the *left* in Figure 4.24. In the spectra of all three species P_{np} -Eu(III) (red), $[\text{Eu}(\text{dbm})_3(\text{Phen})]$ (purple) and complex $[\text{Eu}(\text{dbm})_3(\text{H}_2\text{O})_2]$ (orange) the most intense band appears at approx. $\lambda = 350$ nm, corresponding to the DBM ligand.^[260] The two compounds containing Phen (purple and red) show an additional peak at $\lambda = 262$ nm, which is assigned to an absorption of Phen.^[260] Excitation of the absorption band at $\lambda = 350$ nm results in the associated emission spectrum, Figure 4.24, *right*.

The obtained emission traces in the emission spectra of the current experiment match the correspondent theoretically predicted 4f–4f transitions of Eu(III) compounds (Figure 4.24, *right*).^[258, 261–264] As described in the literature, after the population of the excited state $^5\text{D}_0$ of the europium core, transitions proceed to an $^7\text{F}_J$ level. The emission spectrum is dominated by the intense band at $\lambda = 612$ nm ($^5\text{D}_0$ – $^7\text{F}_2$), a hypersensitive transition, which is very strongly dependent on the environment,^[265] causing the red emitting luminescence of the three Eu-species.

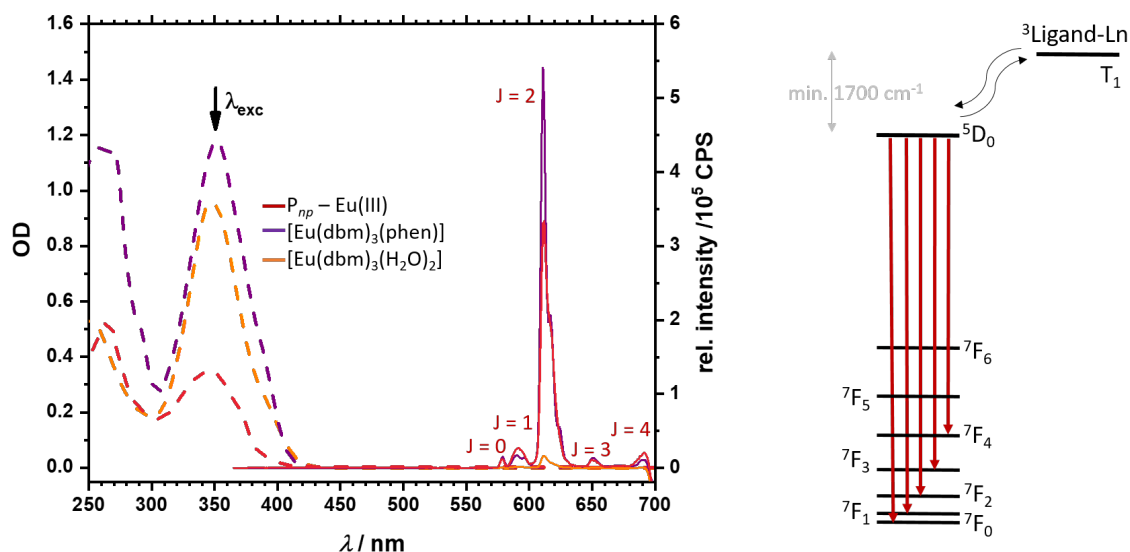


Figure 4.24: Left: Absorption and emission spectra of P_{np} -Eu(III) (red), $[\text{Eu}(\text{dbm})_3(\text{Phen})]$ (purple) and complex $[\text{Eu}(\text{dbm})_3(\text{H}_2\text{O})_2]$ (orange). The most intense band in the absorption spectra at approx. $\lambda = 350$ nm corresponds to the DBM ligands. The depicted emission spectra are obtained upon excitation at $\lambda = 350$ nm. Right: Energy diagram of the triplet state T_1 of the ligand and the excited state 5D_0 of europium. After population of the excited state of europium, transition into the 7F_J levels occurs. This theoretically predicted transitions into $J=0-4$ are observed for the current system, as marked for the bands in the emission spectra.^[258] The most intense band at $J=2$ caused the red emitting emission of the europium species. Adapted from [4] with permission from John Wiley and Sons.

The higher luminescence, observed for the europium species containing a Phen ligand, P_{np} -Eu(III) and $[\text{Eu}(\text{dbm})_3(\text{Phen})]$, was quantitatively determined by measuring the quantum yield (QY) of each species. The QY is thereby defined as the amount of emitted photons per absorbed photons.^[266]

Therefore, the QYs of the three europium compounds are determined by a comparison with the QY of a suitable dye (refer to the Instrumental Section, Chapter 9.2). The values for the three europium species are depicted in Table 4.2. As stated in the table, the QY of the molecular complex increases from 0.1 % to 2.4 % comparing $[\text{Eu}(\text{dbm})_3(\text{H}_2\text{O})_2]$ with $[\text{Eu}(\text{dbm})_3(\text{Phen})]$. Upon coordination of the precursor europium complex to P_{np} forming P_{np} -Eu(III), the QY increases to 1.0 %. The reason for a smaller QY of the europium complex in the polymer framework is inferred as an ultrafast energy dissipation into the polymer chain as a competing process to the europium luminescence.

Table 4.2: Optical density (OD) at the excitation wavelength $\lambda_{exc} = 350$ nm and QY resulting from steady-state absorption and emission spectra for $[\text{Eu}(\text{dbm})_3(\text{H}_2\text{O})_2]$, $[\text{Eu}(\text{dbm})_3(\text{Phen})]$ and $\text{P}_{np}\text{-Eu(III)}$. Adapted from [4] with permission from John Wiley and Sons.

Eu(III) species	λ_{exc} [nm]	OD 350 nm	QY [%]
$[\text{Eu}(\text{dbm})_3(\text{H}_2\text{O})_2]$	350	0.95	0.1
$[\text{Eu}(\text{dbm})_3(\text{phen})]$	350	1.17	2.4
$\text{P}_{np}\text{-Eu(III)}$	350	0.34	1.0

Analogous measurements of absorption and emission spectra were performed for the Tb(III) species, employing $\text{P}_{np}\text{-Tb(III)}$ (green) and the precursor complex $[\text{Tb}(\text{acac})_3(\text{H}_2\text{O})_3]$ (black). For simplification reasons, an amount of three coordinating water molecules in the terbium compound is assumed. At first, the absorption spectra of both compounds were measured (Figure 4.25, *left*). Thereby, the most intense peak appears at $\lambda = 280$ nm, corresponding to the ACAC ligands in the complexes. Upon excitation at $\lambda = 280$ nm, the emission spectrum in Figure 4.25, *right*, was obtained. The peaks in the emission spectra correspond well to the theoretically expected transitions (*right*). After populating the excited state $^5\text{D}_4$ of terbium(III), transitions into levels of $^7\text{F}_{3-6}$ occur, as marked in the emission spectrum.^[196] The dominant emission band for all terbium species is the band at $\lambda = 545$ nm (a transition into $^7\text{F}_5$), causing the compounds' green luminescence.

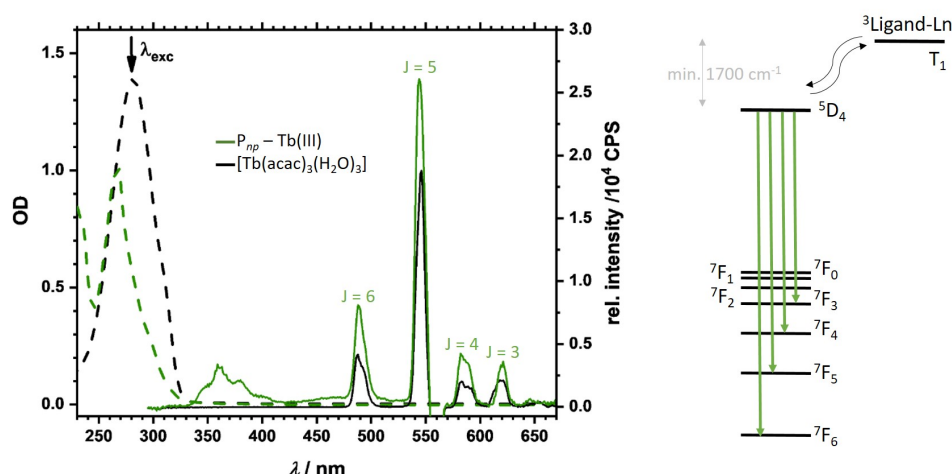


Figure 4.25: Left: Emission and absorption spectra of P_{np} -Tb(III) (green) and the precursor complex $[Tb(acac)_3(H_2O)_3]$ (black). Upon excitation into $\lambda = 280$ nm, the emission spectra of both terbium species were obtained. Right: Theoretical emissions in an excited terbium complex. After populating the excited state of terbium 5D_4 by a transfer from the triplet state of the ligands, transitions into the levels $^7F_{3-6}$ can occur. The corresponding emission bands for the analyzed compounds correspond well with the theoretical process.^[196] Adapted from [4] with permission from John Wiley and Sons.

As performed for the europium species, the QY of the two terbium compounds were determined and compared (Table 4.3). Analogous to the europium species, the QY of the precursor complex $[Tb(acac)_3(H_2O)_3]$ enhances upon replacement of two water molecules by one Phen unit in P_{np} from 0.1 to 0.3 for P_{np} -Tb(III).

Table 4.3: Optical density (OD) at the excitation wavelength $\lambda_{exc} = 280$ nm and QY resulting from steady-state absorption and emission spectra of $[Tb(acac)_3(H_2O)_3]$ and P_{np} -Tb(III). Adapted from [4] with permission from John Wiley and Sons.

Tb(III) species	λ_{exc} [nm]	OD 280 nm	QY [%]
$[Tb(acac)_3(H_2O)_3]$	280	1.38	0.1
P_{np} -Tb(III)	280	0.58	0.3

The enhanced fluorescent QY in both polymeric systems P_{np} -Eu(III) and P_{np} -Tb(III) additionally confirms the coordination of the europium and terbium precursor complexes to the Phen moieties of P_{np} .

The increase in QY of P_{np} -Eu(III) and P_{np} -Tb(III) originates to a large extent from the replacement of water molecules of the precursor complexes upon coordination to Phen. In the molecular complex, the electronically excited states of the rare-earth metals are deactivated by a rapid exchange of energy

with the surrounding water molecules. The vibrational frequency of the O–H bonds matches exactly the energy of the excited states of the lanthanides, resulting in a quenching of their luminescence (more details are presented in the Chapter about lanthanides **2.5.5**).^[267] Moreover, the Phen-styrene units enhance the aromatic system around europium and terbium, which leads to an additional increase in luminescence.^[268]

The ultrafast processes occurring after photoexcitation were further investigated to determine the origin of the QY increase. For this purpose, transient absorption (TA) experiments of the Eu(III) species were performed. For the exact performance of the experiments refer to the Instrumental Section, Chapter **9.2**. After excitation at the maximum absorption of the DBM ligands in [Eu(dbm)₃(Phen)] at $\lambda = 350$ nm, the following simplified deactivation process was observed, which is in line with the literature reported procedures:^[258] Upon excitation in the singlet state S_1 , intersystem crossing (ISC) into the triplet state T_1 of the DBM ligand is possible. This process is followed by a transfer into the excited state of europium, 5D_0 . Further relaxation into the 7F_J levels results in luminescence.^[260, 263, 269, 270]

Interestingly, a decrease of the lifetime of the triplet state (T_1) of the DBM ligands was noted only in the Phen containing compounds [Eu(dbm)₃(Phen)] and P_{np} -Eu(III). This shortening was an indication for a faster transition into the 5D_0 Eu(III) state, which probably is the reason for an increase of the QY.

4.11 Non-Polar System – Summary

The current chapter presented the synthesis of a non-polar, Phen-functionalized polymer system, which was able to transform into luminescent metallopolymers upon lanthanide incorporation, P_{np} -Eu(III) and P_{np} -Tb(III). 2D spectroscopy measurements and the investigation of the photoexcitation of the polymer–lanthanide systems pointed both towards a successful coordination of the lanthanide complexes to the Phen units in P_{np} . The origin of the red and green luminescence, caused by europium(III) and terbium(III), was determined by measuring the respective emission spectra, which were in good agreement with the literature reported traces and values. Similarly, the increase of luminescence upon coordination to Phen proceeded as described theoretically, confirming a promotion of the luminescent characteristics of lanthanides by Phen.

Carboxylate Paddlewheel Structures as Folding Motifs in SCNPs

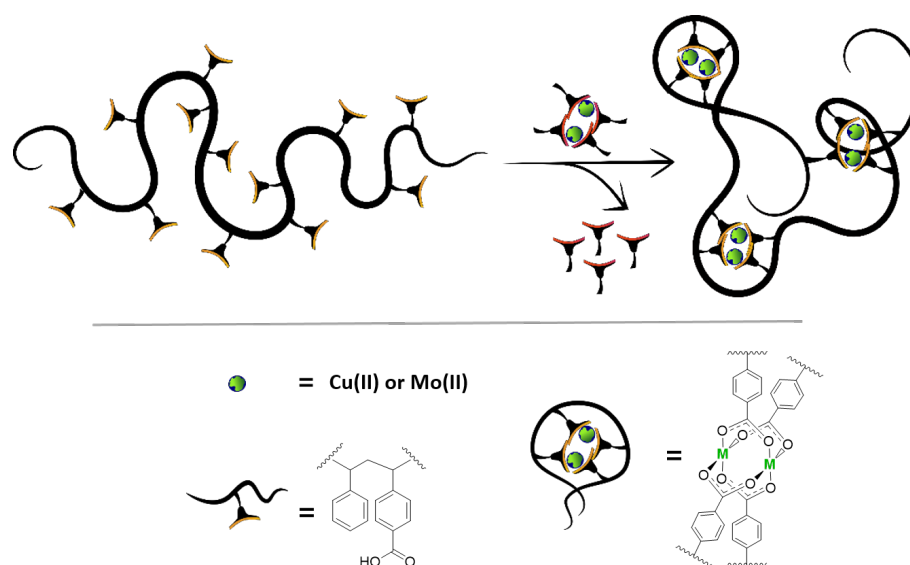


Figure 5.1: Schematic illustration of a collapse of a single-chain into a nanoparticle, exhibiting carboxylate paddlewheel structures as folding motifs. The dinuclear metal units M_2^{4+} consist either of copper(II) or molybdenum(II) cores. Depicted is the possible coordination of four benzoic acid moieties to the metal unit. Adapted from [271] with permission from The Royal Society of Chemistry.

5.1 Motivation

Having explored and created ligand environments for metal-induced single-chain nanoparticles based on phosphine and nitrogen ligands, the possibility to employ a polymeric framework containing linkers that coordinate *via* oxygen to metal ions was investigated. As discussed for oxygen ligand moieties

in Chapter 2.5.4, the class of carboxylates exhibit several binding motifs with metal centers. Of specific interest are the sophisticated architectures of carboxylate paddlewheel structures, since this arrangement offers the possibility to incorporate two metal centers into one folding unit (Figure 5.1). Thereby, the carboxylates act as bidentate bridging ligands between the metal centers, keeping them in close proximity.^[185, 272] This vicinity of two metals is potentially interesting for magnetic studies in NMR technology or, in the case of multiple dinuclear bond formation, for the generation of highly reactive material for catalytic applications.^[273, 274]

So far, mainly the use of monometallic complexes in the field of SCNPs was reported, employing single metal centers as crosslinkers and only three approaches using dimetallic species are demonstrated in the literature. One project was published by Berda and colleagues,^[110] in which a diiron cluster was attached to the end of a polymer chain. Subsequently, the chain collapsed into a nanoparticle, which was induced by a light triggered [4+4] cycloaddition of additional anthracene functionalities in the polymer. The arrangement of a polymeric scaffold around the diiron cluster created a synthetic [FeFe] enzymatic mimic. However, in this approach the metal cluster did not participate in the actual SCNP formation.

In another study, reported by the group of Lemcoff, the synthesized metal-SCNPs exhibited μ -chloro bridged dinuclear binding motifs of rhodium and iridium cores.^[105, 275] For this purpose, the ligands ethylene (C₂H₄) and cyclooctene (COE) in the precursor complexes [RhCl(C₂H₄)₂]₂ and [IrCl(coe)₂]₂, respectively, were exchanged by diene moieties in the polymer polycycloocta-1,5-diene (pCOD), causing an encapsulation of the dinuclear cores into the polymeric scaffold.

In a similar approach the formation of a μ -chloro bridged dinuclear nickel motif as crosslinking unit in pyridine-functionalized polymer chains was proposed by Freytag *et al.*^[276]

In the present chapter, the formation of crosslinks in the unique form of carboxylate bridged M₂⁴⁺ units is investigated. Thereby, not only two metal centers participated in the formation of intramolecular linkages, yet also rarely observed metal–metal bonds in SCNPs were generated (not participating in the crosslinking process).

The formation of such sophisticated paddlewheel structures is reported in the literature for a certain number of metal complexes.^[184] In the current project, the dinuclear species of chromium, copper, molybdenum and rhodium were investigated towards their ability to induce a single-chain collapse. However, no incorporation into the polymer chains was observed for the chromium and rhodium complexes and thus no nanoparticles were formed.

Therefore, herein the encapsulation of copper and molybdenum ions into a polymeric scaffold is reported, yielding $M_2(II)$ -SCNPs. Thereby, for the dinuclear copper species no metal–metal bond is formed. However, such compounds exhibit interesting properties in the field of paramagnetic materials, since upon ‘dimerization’ the former mono-nuclear paramagnetic substances can be converted into diamagnetic compounds, which is caused by a magnetic super-exchange interaction.^[277, 278] Moreover, the dinuclear copper species have already shown their characteristic to be successful crosslinking agents in polymeric architectures.^[279] Dinuclear molybdenum compounds instead, which exhibit quadruple Mo–Mo bonds, have already demonstrated their importance as catalysts.^[280, 281] Until now, the presence of multiple metal–metal bonds in the crosslinking moieties in SCNPs technology was not reported.

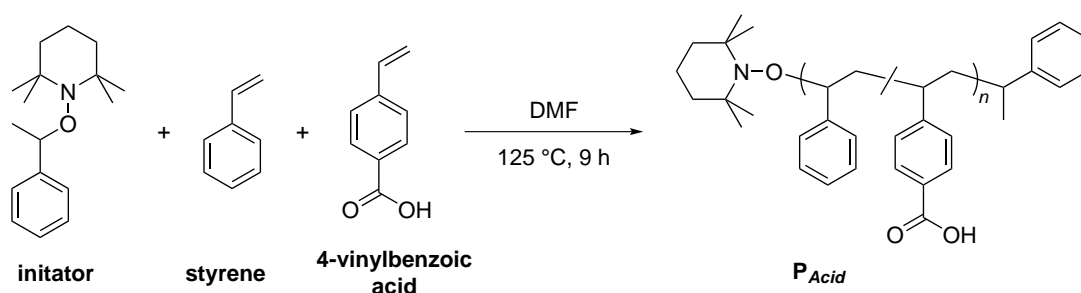
Initially, linear polymer chains were synthesized and subsequently collapsed into single-chain nanoparticles by incorporation of dinuclear metal complexes. The evidence for a chain compaction upon metal encapsulation and detailed insight into the folding unit were provided by size-exclusion chromatography (SEC), diffusion ordered spectroscopy (DOSY), $^1H/^2H$ NMR, IR, Raman and UV/Vis spectroscopy. To complete the analytic data, reference measurements were performed with comparative analogous molecular structures.

The synthesis of the polymeric structures was performed in cooperation with Nicolai Knöfel. Molecular structures and their analysis were provided by Nicolai Knöfel. C. Barner-Kowollik and P. W. Roesky supervised the project. Parts of this chapter are adapted or reproduced from Knöfel*, N. D.; Rothfuss*, H.; Barner-Kowollik, C.; Roesky, P. W. *Polym. Chem.* **2019**, 86-96 with permission from The Royal Society of Chemistry (RSC) on behalf of the Centre National de la Recherche Scientifique (CNRS) and the RSC.

5.2 Synthesis of a Benzoic Acid Functionalized Copolymer and SCNP Formation

Prerequisite to generate paddlewheel structures in SCNPs are suitable precursor complexes that allow their further incorporation into a polymeric scaffold. Appealing were the dimeric tetracarboxylates $[M(OAc)_2]_2$, since these complexes occur already in a paddlewheel structure, in which the acetates act as bidentate bridging ligands. Moreover, the acetate ligands can readily be substituted by benzoic acids, which benefit from a stronger acidity.^[282–284] This replacement is known to proceed at ambient temperature, essential for a straightforward SCNPs formation.

Consequently, by the exchange of at least two acidic side groups per each dimetal center in the precursor complex, a single-chain collapse was anticipated. Therefore, benzoic acid functionalities were required in the precursor polymer chains. For this purpose, the readily accessible monomers 4-vinylbenzoic acid and styrene were statistically copolymerized *via* nitroxide mediated polymerization (NMP), enabling direct implementation of carboxylate units into the chains (Scheme 5.1).



Scheme 5.1: Reaction scheme for the nitroxide mediated polymerization of 4-vinylbenzoic acid and styrene, resulting in P_{Acid}, allowing the direct implementation of benzoic acid moieties into the polymers, ready for a further encapsulation of metal cores by arrangement into a paddlewheel structure. Adapted from [271] with permission from The Royal Society of Chemistry.

The resulting copolymer P_{Acid} was analyzed *via* ¹H NMR spectroscopy (THF-d₈) to determine the monomer composition (Figure 5.2). Comparing the integrals of the resonances of the two aromatic protons in 4-vinylbenzoic acid at the distinct position at $\delta = 7.9–7.5$ ppm (b) with the remaining aromatic protons of both monomers ($\delta = 7.2–6.0$ ppm), a ratio of approx. 1:14, regarding the higher amount to styrene was found. This equaled 7 % of carboxylic units, hence approx. 20 functional groups per chain. The ratio of the monomer composition was in good agreement with the monomer feed ratio. The acidic proton was detected at $\delta = 11.2$ ppm (a).

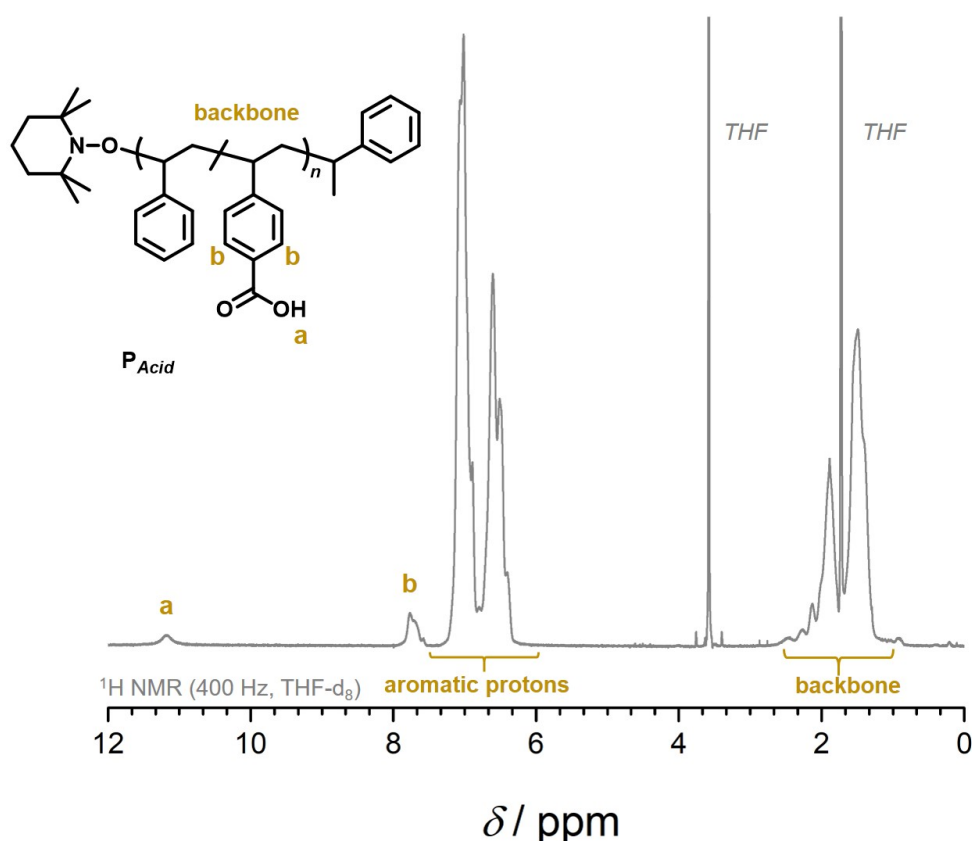


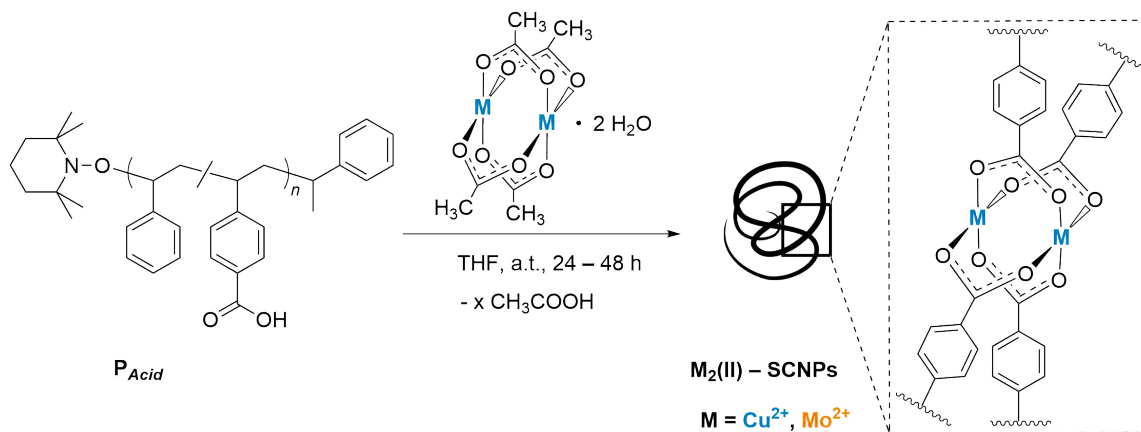
Figure 5.2: ^1H NMR spectrum of P_{Acid} , in which the relevant resonances are highlighted and assigned to the chemical structure. The monomer composition in the copolymer was determined by comparing the integrals of the resonances (b) of 4-vinyl benzoic acid with the overall amount of aromatic protons of both monomers. Calculation revealed a monomer ratio of approx. 1:14, regarding the higher amount to styrene. The acidic proton (a) is detected at $\delta = 11.2$ ppm. Adapted from [271] with permission from The Royal Society of Chemistry.

Concluding the analysis of P_{Acid} , the number average molecular weight (M_n) of $32\,200\text{ g} \cdot \text{mol}^{-1}$ and a dispersity of $\mathcal{D} = 1.22$ was determined *via* SEC measurements (DMAc, RI).

In the following SCNP formation, the choice for suitable precursor complexes was made for $[\text{Cu}(\text{OAc})_2]_2 \cdot 2\text{H}_2\text{O}$ and $[\text{Mo}(\text{OAc})_2]_2$. Both complexes contain acetate ligands, which can be exchanged by the benzoic acid moieties of P_{Acid} . Thereby, the M_2^{4+} unit in the molecular complexes is created in the polymer scaffold. In addition, the high crosslinking level of four carboxylate units to one metal core was expected to result in a significant compaction of the polymer chains (Scheme 5.2).

The SCNP formation, employing the copper(II) and molybdenum(II) precursor complexes, was performed as described in the Experimental Section (Chapter 9.7.3 and 9.7.4). As typical for SCNP formation, the fundamental condition was the preparation of a high dilution during the crosslinking reaction to prohibit interchain linkage formation (networks). In addition, multiple-bonded molybdenum compounds can be highly sensitive towards oxygen and moisture, therefore the respective SCNPs had

to be prepared under strict inert atmosphere.^[285] Upon encapsulation of the transition metals into P_{Acid} , the soft material exhibited blue (copper) and orange (molybdenum) color.



Scheme 5.2: The addition of either $[Cu(OAc)_2]_2 \cdot 2H_2O$ or $[Mo(OAc)_2]_2$ to P_{Acid} in highly diluted solutions, leads to a chain collapse *via* metal encapsulation. Thereby, the benzoic acid groups in P_{Acid} substituted, due to their higher acidic strength, the weaker acetate units of the precursor complexes. In each folding motif, the carboxylates act as bidentate bridging units, creating a paddlewheel structure containing two metal cores in close proximity. Whereas for copper(II) no metal–metal bond was generated, in the case of molybdenum cores quadruple bonded Mo–Mo moieties were formed. The folding unit is depicted for the copper moiety, assuming a replacement of all four acetate ligands and neglecting axial coordination of additional donor molecules. Adapted from [271] with permission from The Royal Society of Chemistry.

After isolation and purification of the colorful polymeric structures, the collapse into compact nanoparticles was investigated and the actual folding motif, expected to arrange in a paddlewheel structure, was analyzed.

The reduction of the hydrodynamic radius was initially evidenced *via* SEC analysis (THF, RI) by measuring the samples of P_{Acid} and the $Cu_2(II)$ -SCNPs in a row. As depicted in the elution diagram in Figure 5.3, a clear shift towards higher retention times of the trace of the SCNPs compared to the trace of P_{Acid} was obtained. Such an observation suggests a smaller hydrodynamic radius, indicating a size reduction upon metal encapsulation.

Unfortunately, multiple molybdenum bonds are air and moisture sensitive, hence no SEC analysis of the $Mo_2(II)$ polymer structures was feasible.

As a second verification for the collapse of exclusively single-chains into nanoparticles was realized by diffusion ordered NMR spectroscopy (DOSY) (refer to Chapter 2.4.2). The dependency of the hydrodynamic radius on the diffusion coefficient makes this technique appropriate for comparing the sizes of precursor polymers and nanoparticles. Furthermore, the inclusion of the $Mo_2(II)$ -SCNPs into sealed NMR tubes allowed their analysis. The relation between the diffusion coefficient of a compound and its hydrodynamic radius (r_H) is described by the Stokes–Einstein Equation. Analyzing

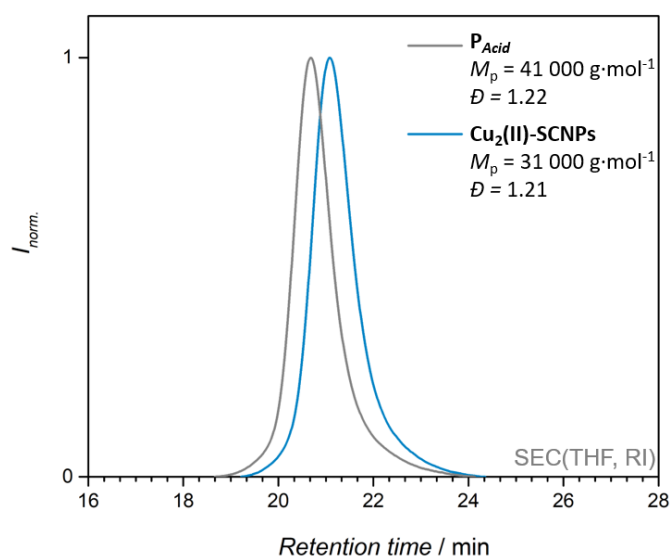

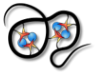
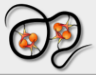


Figure 5.3: SEC (THF, RI) traces of P_{Acid} and $Cu_2(II)$ -SCNPs. The shift of the trace of the $Cu_2(II)$ -SCNPs towards higher retention times in comparison to the trace of P_{Acid} , indicates a decrease of the hydrodynamic radius. Adapted from [271] with permission from The Royal Society of Chemistry.

the precursor polymer P_{Acid} and the nanoparticles $Cu_2(II)$ - and $Mo_2(II)$ -SCNPs, the corresponding hydrodynamic radii were calculated and summarized in Table 5.1. A hydrodynamic radius of 3.9 nm was calculated for P_{Acid} . In comparison, values of $r_H = 2.3$ nm for the $Cu_2(II)$ -SCNPs and $r_H = 2.6$ nm for the $Mo_2(II)$ -SCNPs were obtained. This values corresponds to a reduction of the hydrodynamic radius of the copolymer of approx. 35–40 %, evidencing the successful formation of SCNPs for both structures.

Table 5.1: Diffusion coefficients and the corresponding hydrodynamic radii were acquired for the linear copolymer P_{Acid} and the $Cu_2(II)$ - and $Mo_2(II)$ -SCNPs via DOSY analysis. Measuring the diffusion coefficients, the hydrodynamic radii r_H of the compounds were calculated from the measured diffusion coefficients, employing the Stokes–Einstein Equation.

Substance		D [m^2s^{-1}]	Error	r_H [nm]
Copolymer P_{Acid}		1.03×10^{-10}	5.4×10^{-12}	3.9
$Cu_2(II)$ -SCNPs		1.77×10^{-10}	1.5×10^{-11}	2.3
$Mo_2(II)$ -SCNPs		1.57×10^{-10}	0.9×10^{-11}	2.6

The structure of the folding motif in both SCNP structures was further analyzed by ^1H NMR spectroscopy. The ^1H NMR spectra (THF- d_8) of the $\text{Cu}_2(\text{II})$ - and $\text{Mo}_2(\text{II})$ -SCNPs are depicted in Figure 5.4. In the ^1H NMR spectrum of the copper species (*top*), a resonance at $\delta = 11.2$ ppm was detected. This resonance is associated with the R-COOH acidic protons of P_{Acid} (refer to Figure 5.2, resonance a). Comparing the integral of this resonance with the integral of the same resonance of P_{Acid} , it becomes apparent that approx. 30 % of the non-reacted acidic proton did still appear for the copper species. A probable explanation for its existence could be an axial coordination of acidic functionalities to the $\text{Cu}_2(\text{II})$ moieties during SCNP formation. During the formation of the paddlewheel structure, four acid moieties coordinate as bridging ligands between the two copper centers. However, the coordination sphere of the copper ions is thereby not saturated and two additional ligands can coordinate in axial position to the copper centers. While this can be simply solvent molecules, it can also be additional acidic protonated moieties. Thus, such moieties would not participate in further copper complexation reactions and remain protonated. This hypothesis was further investigated for the molecular structure in the following chapter. Eventually, such acidic moieties were identified as the remaining acidic protons detected in the ^1H NMR spectrum of the copper SCNPs.

In contrast to the copper moieties, no resonance for acidic protons in the ^1H NMR spectrum of the $\text{Mo}_2(\text{II})$ -SCNPs appeared (marked in a square in Figure 5.4, *bottom*), indicating a complete substitution of all acetate ligands of the precursor complex by the benzoic acid groups in the copolymer.

To confirm the quantitative replacement of the former acetate ligands in the precursor complexes by the benzoic acid moieties of P_{Acid} ^2H NMR spectroscopy was performed. At first the molybdenum species were investigated. Therefore, a molybdenum complex was synthesized, containing deuterated, instead of protonated, acetate ligands, yielding the complex $[\text{Mo}(\text{OAc})_2]_2\text{-}d_{12}$. Under the same conditions as before, $\text{Mo}_2(\text{II})$ -SCNPs were prepared. Subsequently, the molybdenum SCNPs were analyzed *via* ^2H NMR spectroscopy. Here, no remaining deuterium resonances of the former $\text{CD}_3\text{COO}^{-1}$ were detected, pointing towards a replacement of all deuterated acetate ligands by the benzoic acid moieties in P_{Acid} . Consequently, the results of the deuterium NMR supported the hypothesis that all benzoic acids of P_{Acid} were deprotonated and coordinated to molybdenum cores.

In an analogous procedure to quantify the actual number of substituted acetate ligands, the deuterated copper complex $[\text{Cu}(\text{OAc})_2]_2\text{-}d_{12}$ was synthesized and reacted with P_{Acid} . However, in the following ^2H NMR analysis of the respective precursor and SCNPs, no meaningful data was collected, probably due to the paramagnetic nuclei of the copper cores.

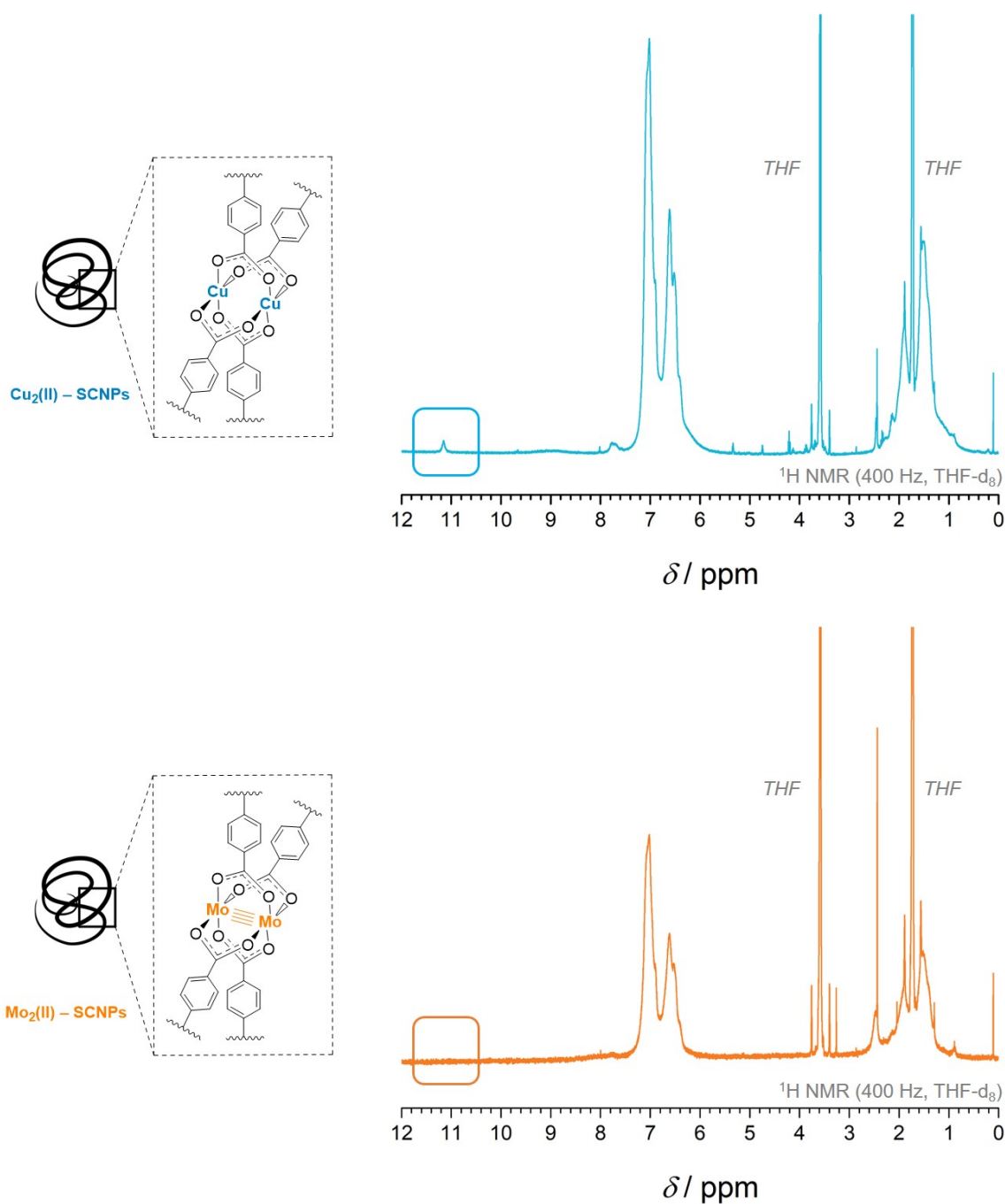


Figure 5.4: ^1H NMR spectra (THF-d_8) of the $\text{Cu}_2(\text{II})$ - (top) and $\text{Mo}_2(\text{II})$ -SCNPs (bottom). Marked in a square is the residual resonance of the acidic protons of the $\text{Cu}_2(\text{II})$ -SCNPs (top). Possible is the coordination of additional benzoic acid units of P_{Acid} in axial position to the dinuclear copper moieties during the folding process, thus non-participating in the folding process and staying protonated. In comparison to the ^1H NMR spectrum of P_{Acid} , approx. 30 % of the former resonance is still detected for the $\text{Cu}_2(\text{II})$ -SCNPs. On the contrary, no resonance for the acidic protons shows up in the ^1H NMR spectrum of the $\text{Mo}_2(\text{II})$ -SCNPs (bottom). Adapted from [271] with permission from The Royal Society of Chemistry.

For a detailed insight into the folding unit, the corresponding molecular complexes, containing benzoic acid ligands, of the copper and molybdenum species were synthesized, analyzed and compared with the SCNP structures.

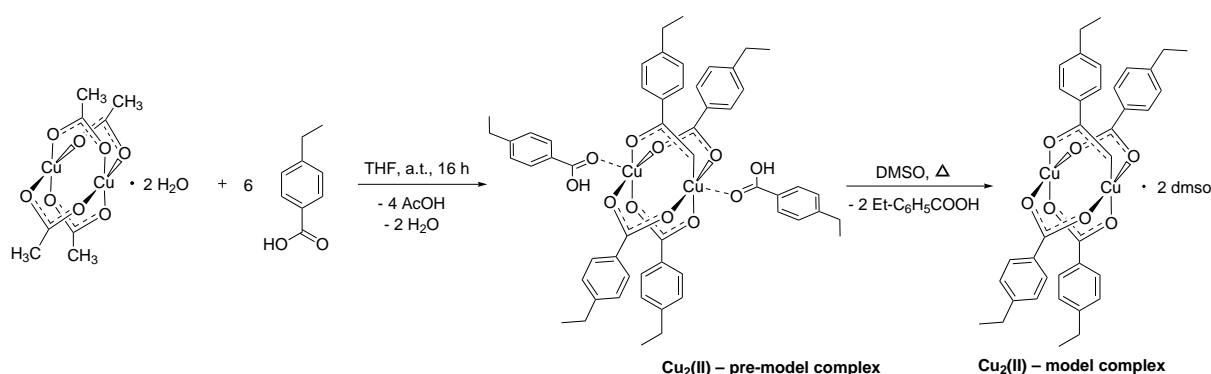
5.3 Model Complexes of Cu₂(II) and Mo₂(II) Structures

The chain compaction of P_{Acid} upon encapsulating either copper or molybdenum units was confirmed by DOSY and SEC measurements. Although first hints towards the nature of the single-chain folding process were obtained by ¹H NMR spectroscopy, no further information about the crosslinking was established.

In order to gain closer insight into the actual folding moiety in the Cu₂(II)- and Mo₂(II)-SCNPs, the two corresponding molecular, dinuclear complexes were synthesized. Here, the performance of the reaction under the same reaction conditions as the M₂(II)-SCNPs was essential to create the analogous crosslinking structure in the model complexes, expected to be a paddlewheel structure.

To imitate the structure of the polymeric framework, the ligand 4-ethylbenzoic acid was chosen. However, in contrast to the disperse polymeric structures, the highly pure model complexes were able to crystallize. Hence, the arrangement of the ligands around the metal center could be determined *via* X-ray crystallography (synthesis and analysis was carried out by Nicolai Knöfel (KIT)).

Analogous to the SCNP synthesis, the precursor metal complexes [Cu(OAc)₂]₂ · 2 H₂O and [Mo(OAc)₂]₂ were employed, in which subsequently the acetates were replaced by the 4-ethylbenzoic acid moieties. The complete reaction scheme for the synthesis of the copper species is depicted in Scheme 5.3. Interestingly, when performing the reaction in THF, X-ray crystallography indicates that not only four, yet six carboxylate ligands bind in different coordination modes to the dinuclear copper unit (Cu₂(II)–pre-model complex). Thereby, four of the carboxylate units coordinated as bridging ligands between the dicopper cores, while two additional carboxylate acids attached to the axial position of the Cu₂⁴⁺ centers.



Scheme 5.3: Synthesis of the model complex of the copper species performed in THF *via* a carboxylic exchange reaction. In addition to the four carboxylates bridging the metal cores, two carboxylic acids coordinated axially to the Cu₂⁴⁺ unit. The subsequent crystallization from DMSO caused a replacement of the two axial ligands by DMSO, resulting in Cu₂(II)–model complex. Adapted from [271] with permission from The Royal Society of Chemistry.

The solid state structure of the $\text{Cu}_2(\text{II})$ pre-model complex is shown in Figure 5.5, *left*. The observation of a possible coordination of protonated carboxylates in axial position to the transition metal in the molecular complexes confirmed the probability of a similar process in the reaction of the $\text{Cu}_2(\text{II})$ -SCNPs. If such an axial coordination occurred as well for the polymeric system, this would explain the residual acidic protons in their ^1H NMR spectrum.

Surprisingly, in a subsequent recrystallization of the copper pre-model complex in DMSO, the two axially coordinated acids were substituted by two DMSO solvent molecules ($\text{Cu}_2(\text{II})$ -model complex).

In the structure of the pre-model and the model complex, a Cu–Cu distance of 2.602 Å was determined. In the literature, similar distances were found for dicopper complexes, exhibiting no direct bond between the two copper atoms. Consequently, the herein synthesized copper model complexes as well as the $\text{Cu}_2(\text{II})$ -SCNPs are expected to be established without a Cu–Cu bond.^[286]

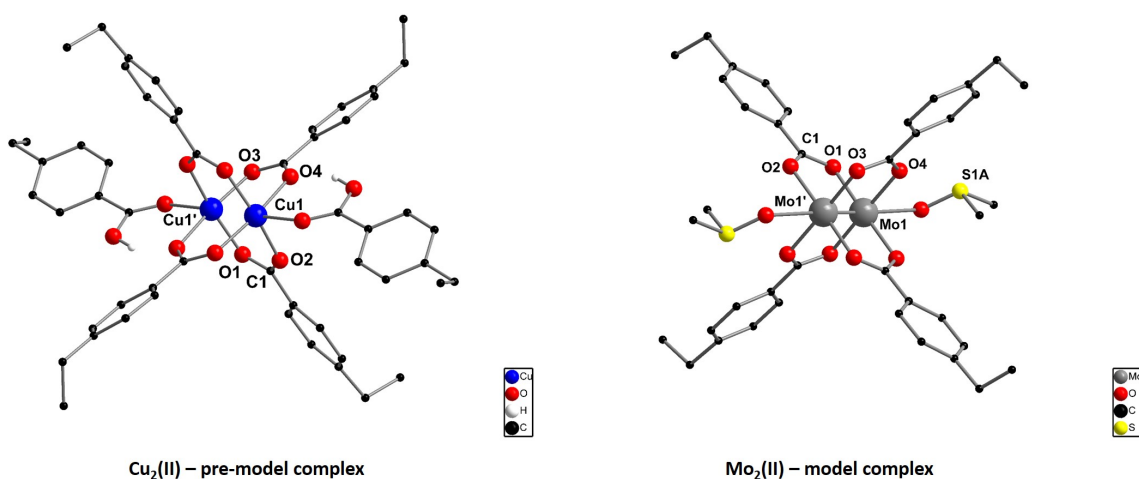
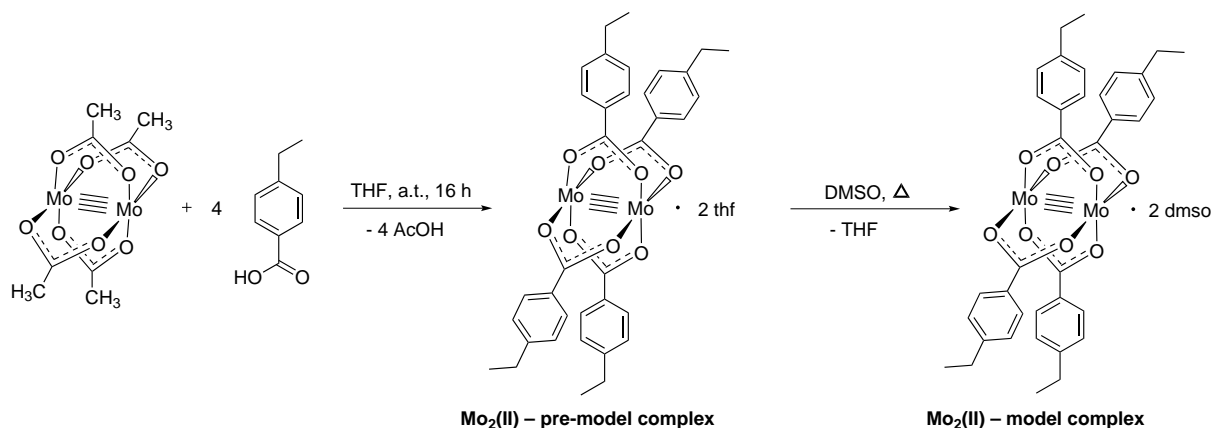


Figure 5.5: Solid state structures of the copper (*left*) and molybdenum model complexes (*right*). For the copper species, the pre-model complex is depicted, in which two additional carboxylate acids coordinated axially to the copper centers. Thereof independent, the structures of the model complexes illustrate the assumed folding motif of bidentate carboxylate units in the $\text{Cu}_2(\text{II})$ - and $\text{Mo}_2(\text{II})$ -SCNPs. For clarity, most of the hydrogen atoms and non-coordinating solvent molecules are omitted. Adapted from [271] with permission from The Royal Society of Chemistry.

In an analogous reaction, the model complex of the molybdenum species was synthesized, refer to Scheme 5.4. In contrast to the copper complex, in the molybdenum species no coordination of axial carboxylic acids was observed and instead THF solvent molecules saturated the axial coordination sites. Specifically, upon recrystallization in DMSO, the axial THF molecules were replaced by DMSO moieties. The final molecular structure of the $\text{Mo}_2(\text{II})$ -model complex in its solid state is depicted on the *right* side in Figure 5.5. As expected, a highly symmetric, tetra-carboxylato-bridged paddlewheel structure was obtained. Between the two molybdenum atoms, a nuclei distance of 2.12 Å was acquired,

which is in good agreement with typical values for a quadruple Mo–Mo bond in such bidentate bridged coordination geometries. Values between 2.06–2.13 Å are reported in the literature.^[285]



Scheme 5.4: Synthesis of the $\text{Mo}_2(\text{II})$ –model complex via a carboxylic exchange reaction in THF. In addition to the four carboxylate ligands bridging the two metal cores, two THF molecules coordinated axially to the Mo_2^{4+} unit. The subsequent crystallization from DMSO caused a replacement of the two axial THF ligands by DMSO, resulting in $\text{Mo}_2(\text{II})$ –model complex. Adapted from [271] with permission from The Royal Society of Chemistry.

As for the SCNP structures, the synthesis of both model complexes proceeded at ambient temperature. Both approaches resulted in the exclusive formation of homoleptic paddlewheel structures, neglecting axial solvent coordination, in high yields. The analogous reaction procedure for SCNPs and model complexes enabled to infer a similar arrangement of the folding units in the nanoparticles as determined for the model complexes. However, the complete substitution of all acetate ligands of the precursor complexes by benzoic acid moieties in the SCNPs might have been impeded by steric hindrance after a certain folding degree. Thus, structures of a mixture of substituted and non-substituted acetate ligands were likely to be present in the nanoparticles.

Further spectroscopy analysis was performed for the SCNPs and model complexes to gain more information about the folding moiety.

5.4 Spectroscopic Studies of the SCNPs and Model Complexes

In order to compare changes in the vibrational modes of P_{Acid} upon metal encapsulation, the precursor polymer and the resulting SCNPs were analyzed by vibrational spectroscopy.

A characteristic band to investigate structural changes in compounds with a R-COOH structure is the C=O stretching mode. In the infra red (IR) spectrum of P_{Acid} this stretching mode was detected at $\tilde{\nu} = 1690 \text{ cm}^{-1}$, as depicted in Figure 5.6 in black. After the transformation of such a free R-COOH group into a bridged bidentate carboxylate unit RCO_2^{-1} , the two C–O bonds are equivalent. The related frequencies of the symmetric and asymmetric stretching modes of a RCO_2^{-1} appear as strong bands in the region between $1400\text{--}1600 \text{ cm}^{-1}$, dependent on the nature of ligand and metal core.^[286–288]

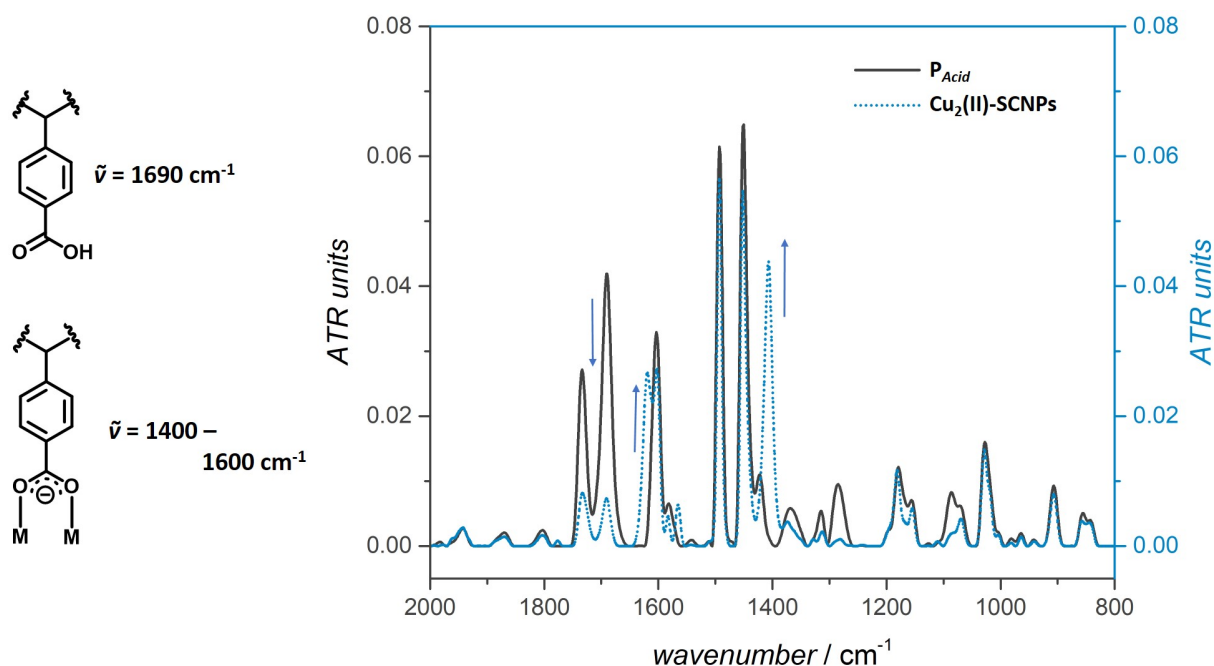


Figure 5.6: Superimposed IR spectra of P_{Acid} (black) and $\text{Cu}_2(\text{II})\text{-SCNPs}$ (blue, dotted). Marked with arrows are changes in the spectrum of the precursor polymer upon encapsulation of the metal cores: The band for the C=O stretching mode in the precursor polymer at $\tilde{\nu} = 1690 \text{ cm}^{-1}$ was significantly reduced, while novel bands for asymmetric and symmetric C–O stretching modes at $\tilde{\nu}_a = 1619 \text{ cm}^{-1}$ and $\tilde{\nu}_s = 1407 \text{ cm}^{-1}$ appeared in the spectrum of the $\text{Cu}_2(\text{II})\text{-SCNPs}$. Adapted from [271] with permission from The Royal Society of Chemistry.

Comparing the IR spectra of P_{Acid} and the $\text{Cu}_2(\text{II})\text{-SCNPs}$, the stretching mode of P=O of P_{Acid} decreased significantly upon coordinating to copper ions, yet did not disappear completely (Figure 5.6). This existence of approx. 30 % of R-COOH remaining groups in the $\text{Cu}_2(\text{II})\text{-SCNPs}$ was in good accordance with the results of the ^1H NMR spectrum, in which also a resonance for the acidic proton

was detected. Additionally, two new bands appeared in the IR spectrum of the $\text{Cu}_2(\text{II})$ -SCNPs at $\tilde{\nu}_a = 1619 \text{ cm}^{-1}$ and at $\tilde{\nu}_s = 1407 \text{ cm}^{-1}$. Those bands correspond to the asymmetric and symmetric C–O stretching modes (blue) in a RCO_2^{-1} unit.

When analyzing the $\text{Cu}_2(\text{II})$ model complex *via* IR spectroscopy, similar bands appeared for the RCO_2^{-1} unit with bands at $\tilde{\nu}_a = 1619 \text{ cm}^{-1}$ and $\tilde{\nu}_s = 1398 \text{ cm}^{-1}$.

In contrast to the copper species, in the IR spectrum of the $\text{Mo}_2(\text{II})$ -SCNPs, the band for the C=O stretching mode of free carboxylate units R-COOH almost completely vanished, indicating the participation of all carboxylates in the coordinating process. This was in accordance with the results of the ^1H NMR spectrum of the $\text{Mo}_2(\text{II})$ -SCNPs. In the IR spectrum, an additional intense band at $\tilde{\nu}_s = 1401 \text{ cm}^{-1}$ appeared, associated with the symmetric C–O stretching mode of a bridged carboxylate unit. However, due to overlapping bands, the band for asymmetric stretching could not be distinguished.

Instead, Raman spectroscopy was employed as a complementary vibrational spectroscopy method to analyze the folding unit in the $\text{Mo}_2(\text{II})$ -SCNPs. Figure 5.7 shows the superimposition of the Raman spectra of P_{Acid} (black) and $\text{Mo}_2(\text{II})$ -SCNPs (orange). The two bands at $\tilde{\nu}_a = 1513 \text{ cm}^{-1}$ and $\tilde{\nu}_s = 1411/1401 \text{ cm}^{-1}$, which originate from the asymmetric and symmetric C–O stretching modes, were only detected for the $\text{Mo}_2(\text{II})$ -SCNPs, indicating bridged carboxylate units. The relatively small distance of approx. 100 cm^{-1} between those two bands is typical for a dimolybdenum species.^[286] Interestingly, a further significant band appeared in the Raman spectrum at $\tilde{\nu}_{\text{Mo–Mo}} = 408 \text{ cm}^{-1}$, which is literature known for a quadruple bonded Mo–Mo stretching mode.^[289] This evidenced an intact Mo–Mo quadruple bond within the SCNP structure (Figure 5.7).

For direct comparison, the $\text{Mo}_2(\text{II})$ – model complex was analyzed as well *via* Raman spectroscopy. In its Raman spectrum, similar bands as for the SCNPs were obtained. The bands for the asymmetric and symmetric C–O stretching modes were detected at $\tilde{\nu}_a = 1515 \text{ cm}^{-1}$ and $\tilde{\nu}_s = 1415/1398 \text{ cm}^{-1}$, as well as the band for the Mo–Mo stretching mode at $\tilde{\nu}_{\text{Mo–Mo}} = 403 \text{ cm}^{-1}$ (not shown here).

As a means to explore the origin of the blue and orange color of the $\text{Cu}_2(\text{II})$ - and $\text{Mo}_2(\text{II})$ -SCNPs, the absorption spectra of the nanoparticles were measured. In the UV/Vis spectrum of the $\text{Cu}_2(\text{II})$ -SCNPs a broad absorption band between 550–800 nm, as also reported for similar complexes in the literature.^[290] UV/Vis measurements of the $\text{Cu}_2(\text{II})$ model complex and the copper precursor complex exhibited a similar trace shape and absorption maxima (Figure 5.8). This validated the assumption of a successful copper center implementation into the polymeric structure.

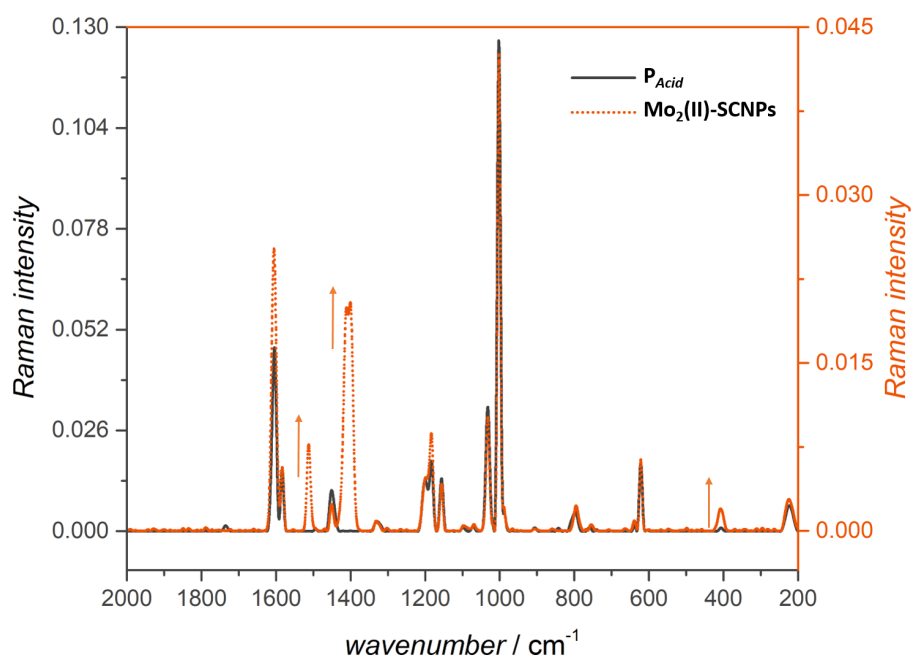


Figure 5.7: Superimposed Raman spectra of P_{Acid} (black) and $Mo_2(II)$ -SCNPs (orange, dotted). Marked with arrows are changes in the spectrum of the precursor polymer upon encapsulation of metal cores: The band for the C=O stretching mode in the precursor polymer at $\tilde{\nu} = 1690\text{ cm}^{-1}$ almost completely vanished, while novel bands for asymmetric and symmetric C–O stretching modes at $\tilde{\nu}_a = 1513\text{ cm}^{-1}$ and $\tilde{\nu}_s = 1401\text{ cm}^{-1}$ appeared in the spectrum of the $Mo_2(II)$ -SCNPs. In addition, the novel band at $\tilde{\nu}_{Mo-Mo} = 408\text{ cm}^{-1}$ was ascribed to a Mo–Mo stretching mode of a quadruple bond. (*The intensity of the spectra is referenced to the band at $\tilde{\nu} = 1028\text{ cm}^{-1}$.*) Adapted from [271] with permission from The Royal Society of Chemistry.

Analogous measurements were performed for the $Mo_2(II)$ -SCNPs, which exhibited a characteristic absorption band between 350–500 nm with a maximum at approx. 430 nm (Figure 5.9). The intense color of this absorption originates from a fully-allowed electronic transition between the δ orbitals of the Mo_2^{4+} unit and the π^* orbitals of the aromatic ligands.^[291–293] Comparing the UV/Vis spectrum of the $Mo_2(II)$ -SCNPs with the spectrum of the precursor complex $[Mo(OAc)_2]_2$, no absorption in this area was detected, as no π acceptor ligand moieties were present. Only by coordination to the benzoic moieties of P_{Acid} such $\delta-\pi^*$ transitions were enabled. Consequently, the existence of this band, also detected in the spectrum of the molybdenum model complexes, confirmed the encapsulation of the molybdenum species into the polymeric scaffold.

Since similar reactivities for dinuclear metal complexes were reported in the literature for the complexes of dinuclear rhodium and chromium complexes,^[184] their usage in SCNPs formation was investigated. However, their encapsulation by the benzoic acid moieties of P_{Acid} did not result in the formation of SCNPs.

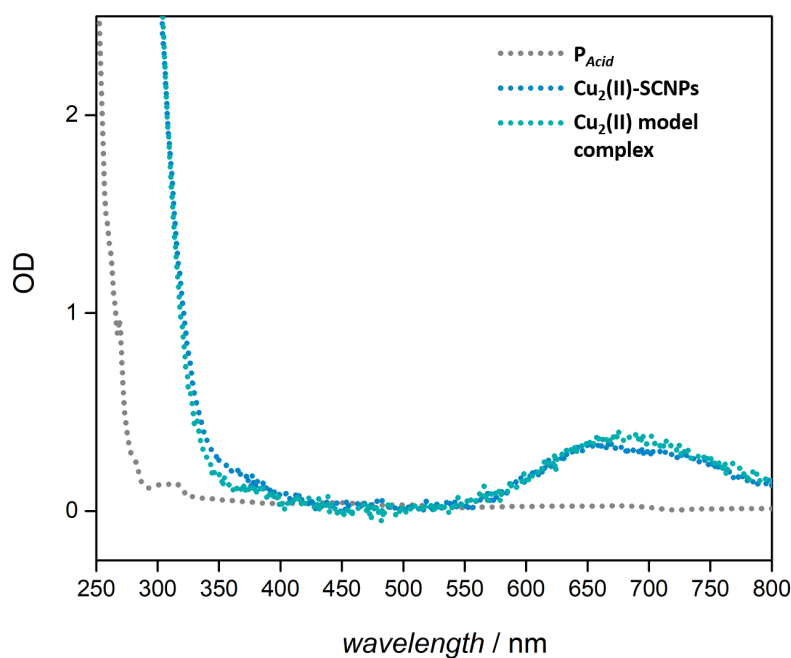


Figure 5.8: UV/Vis spectra of P_{Acid} , the $Cu_2(II)$ -SCNPs and the copper model complex. The broad absorption band between 550–800 nm originated from d–d interactions in the copper species, confirming the incorporation of copper(II) ions into the polymer lattice. Adapted from [271] with permission from The Royal Society of Chemistry.

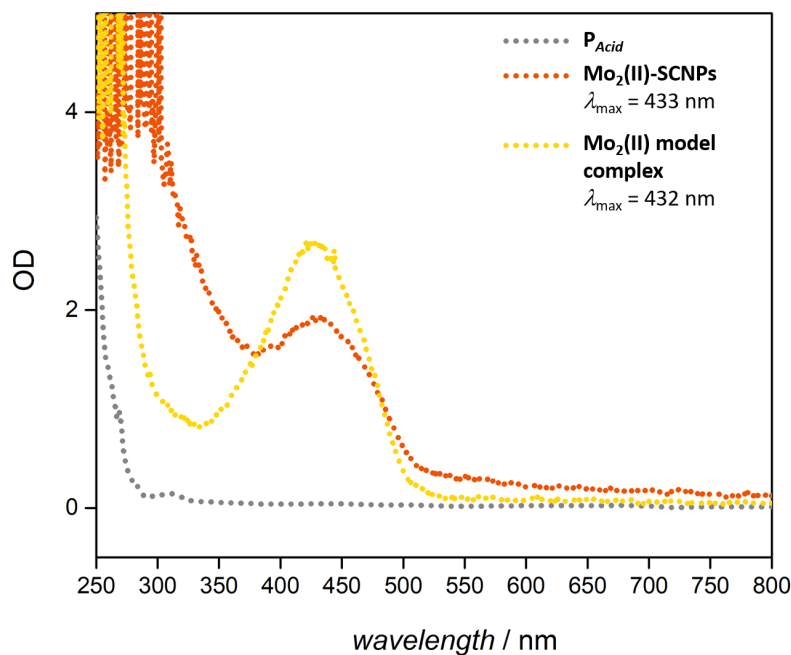
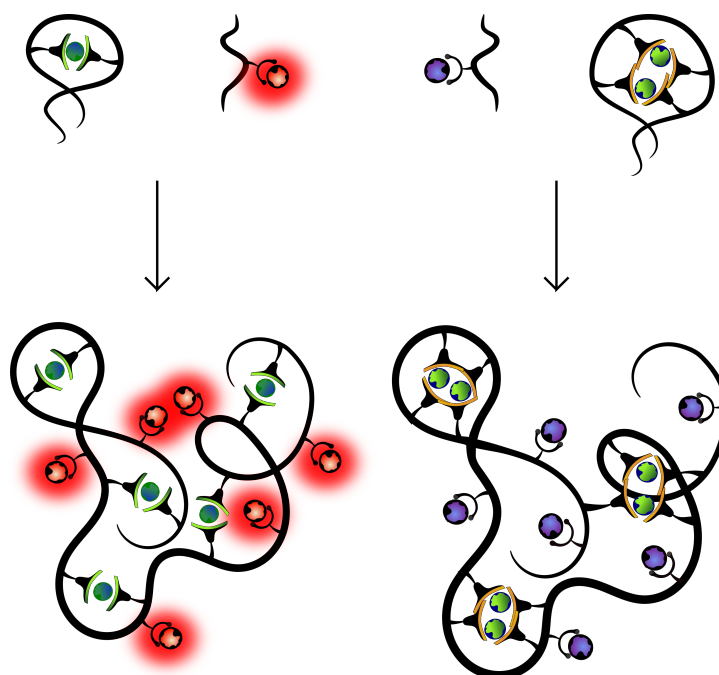


Figure 5.9: UV/Vis spectra of P_{Acid} , the $Mo_2(II)$ -SCNPs and the molybdenum model complex. The local absorption band at 430–435 nm originates from a transition between the δ orbitals of molybdenum and π^* orbitals of aromatic ligands in P_{Acid} , confirming the incorporation of molybdenum(II) ions into the polymer framework. Adapted from [271] with permission from The Royal Society of Chemistry.

5.5 Summary

Commonly, metal-induced crosslinking in SCNPs relies on a 2:1 ligand-to-metal ratio, sufficiently efficient to ensure a chain collapse. In the present example, a high ratio of 4:1 was achieved (neglecting axial coordination). A size reduction of the linear precursor polymer P_{Acid} into a more compact structure upon metal incorporation of approx. 40 % was determined by SEC and DOSY measurements. The arrangement of the benzoic ligand moieties and the exact structure of the folding units were analyzed *via* IR, Raman and UV/Vis spectroscopy. All methods suggest a successful encapsulation of the dinuclear metal units into the polymeric scaffold. When synthesizing model complexes under the same reaction conditions as employed for the SCNPs, crystal structures were obtained, which allowed analysis *via* single X-ray diffraction. Thereby, the formation of a paddlewheel structure in the model complexes was determined and hence proposed as dimetallic folding moiety in the SCNPs. As observed for the model complexes, the stoichiometry is not trivial. In the presence of an excess of carboxylic acids, two protonated moieties can additionally attach to the metal centers.

Orthogonal Coordinated Heterometallic SCNPs



6.1 Motivation

The present chapter addresses an unprecedented concept in the realm of single-chain nanoparticles (SCNPs), describing orthogonal heterometallic nanoparticle formation.

Introducing various metal centers within one chain is highly appealing, enabling materials with versatile functionalities. Dependent on the implemented metal ions, the polymer framework can be equipped with different properties, such as luminescence or magnetism. Moreover, the encapsulation

of two catalytically active metal ions, at best in predefined areas, is highly attractive for multi-step or cascade reactions (Figure 6.1).

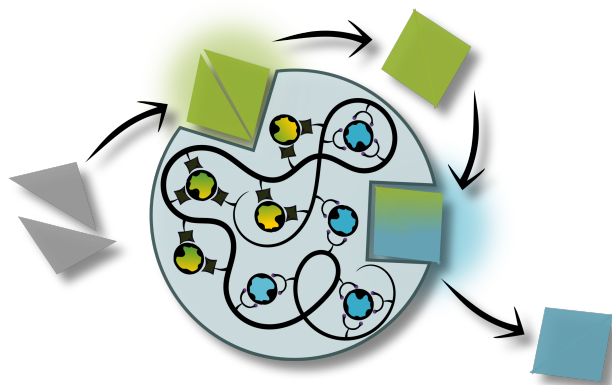


Figure 6.1: A single-chain nanoparticle, which is compartmentalized in areas containing metal ions of different functionalities, permits access to advanced catalytic reactions, such as multi-step or cascade reactions. Adapted from [8] with permission of the American Chemical Society.

An effective method to provide structural control within the polymer framework is by equipping the precursor polymer chain with ligand moieties that are divergent in their preferences for metal ion coordination. Consequently, the addition of selected metal complexes allows directed metal incorporation, affording soft matter materials of well-defined compartmentalization. Supportive for such an orthogonal metal encapsulation is the Pearson classification, dividing metal ions and ligands into hard and soft acids and bases (HSAB principle).^[160]

In the current project, ligand moieties and metal complexes, developed in former projects (Chapter 3 and 5), are adopted and appropriately combined. Thereby, two divergent polymer systems are established, each equipped with a set of two orthogonal ligand moieties, ready to coordinate to selected metal salts. In the process, one metal ion induces the functionalization of the chain, coordinating to ligand moieties in a metal-to-ligand ratio of 1:1. The other metal forms crosslinks within the chain, hence inducing the chain collapse of the linear metallopolymers into compact heterometallic nanoparticles.

In the first system, the selected ligand moieties are phosphines and carboxylic acids, coordinating to the metal ions gold(I) and copper(II), respectively. The divergent coordination behavior of the two pairs allows to dovetail only gold(I) with phosphine moieties and the already explored 4:1 coordination of carboxylates to a dinuclear copper species, leading to chain collapse.

In the second system, again phosphines are employed, yet this time combined with phosphine oxides as their counterpart. As noted in the Theoretical Section, Chapter 2.5.2, the coordination

behavior of phosphines changes rapidly upon oxidation, performing afterwards as hard bases, suitable for coordination to lanthanides.^[294] The functionalization in the current system is performed by a coordination of europium(III) to the phosphine oxide moieties in a 1:1 ratio, while the chain collapse is induced by a 2:1 coordination ratio of phosphines to platinum(II).

Whereas in the first system presented, the metal addition to the coordination sites is crucial to avoid undesired side reactions, the ligand and metal pair formations in the second system are entirely independent of each other and can be performed arbitrarily, hence the functionalization and single-chain collapse are performed simultaneously.

The selective, orthogonal coordination of phosphines to gold(I) and carboxylates to copper(II), as well as phosphine oxides to europium(III) and phosphines to platinum(II), has already been proven in small molecule studies. In addition, a molecular complex imitating the gold–copper system was synthesized by Nicolai Knöfel (KIT), which contains both functional moieties in one ligand. Even in close proximity, an orthogonal coordination of the respective functional units to gold(I) and copper(II) is observed. Moreover, the crystallization and subsequent X-ray diffraction analysis of the complexes permits insight into the intricate structural folding motifs.

The synthesis and analysis of the current project was performed in collaboration with N. Knöfel from the Roesky group. Diffusion ordered spectroscopy and NOESY spectroscopy were carried out by P. Tzvetkova. The synthesis of the model complexes was performed by N. Knöfel. The project was supervised by C. Barner-Kowollik and P. Roesky. Additional contributions to the project were made during the Vertieferarbeit of B. Kulendran and the Master thesis of M. Reith (‘Single-Chain Nanoparticles *via* Metal Complex Induced Folding’, 2017, KIT).

6.2 A Gold and Copper Based System

The first presented project employs the divergent ligand moieties of carboxylic acids and phosphines. Whereas carboxylates belong to the class of hard donor ligands (hard Lewis bases), favoring hard Lewis acids, the soft donor phosphine ligands prefer the coordination to soft acids. Such antagonistic functionalities are highly suitable to permit the directed coordination to two types of metals ions.

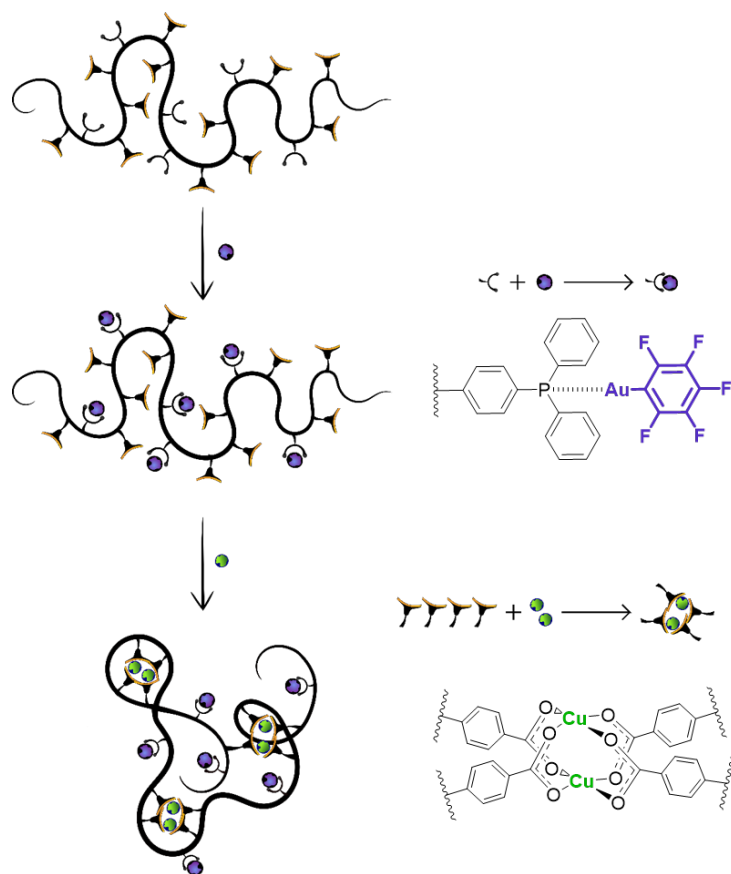


Figure 6.2: General overview for the generation of orthogonal, heterometallic SCNPs, achieved in a two step synthesis procedure. The polymer, consisting, in addition to styrene units, of phosphine and vinylbenzoic acid moieties is functionalized in a first step with gold(I) complexes, which coordinate exclusively to the phosphine moieties. The resulting metallo-polymer is subsequently collapsed into a nanoparticle, when implementing a dinuclear copper(II) species. Thereby, pendant carboxylate units create a bidentate, bridging paddlewheel structure.

As developed and demonstrated in the previous project focussing on carboxylate paddlewheel structures in SCNPs (Chapter 5), the incorporation of copper(II), as a Cu₂⁴⁺ unit, by bridging carboxylate units successfully induces single chain collapse. Besides the carboxylic acid moieties, phosphine ligands are chosen as a means to coordinate to catalytically active late transition metals (Chapter 3). Whereas in the project focusing on homogeneous, recyclable Pt(II)-SCNPs, the catalytic activity of platinum(II) was showcased, in the present case gold(I) compounds are investigated. In the last years, gold(I) complexes gained increased interest in synthetic chemistry performing as catalysts

at exceptionally mild reaction conditions with high turnover frequencies, for instance in the activation of C–H bonds in cross-coupling reactions.^[295–297]

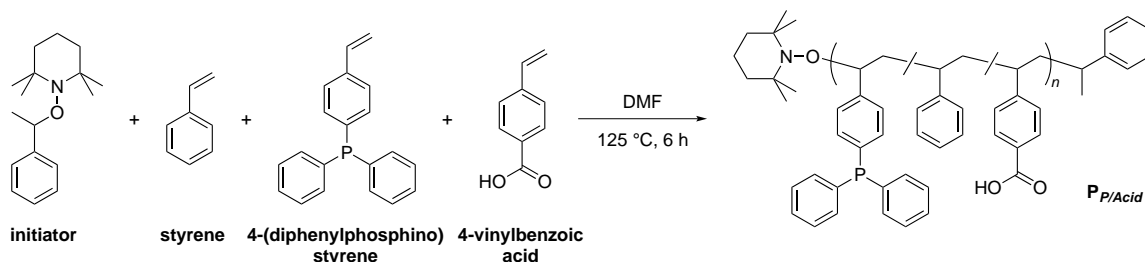
Concluding the scope of the current project, the intrinsic nature of phosphines and carboxylic acids coordinating towards distinct metal complexes, is harnessed to synthesize gold(I)–copper(II) functionalized SCNPs. However, while no interaction for gold(I) with carboxylic acids is expected, the facile oxidation of phosphines into phosphine oxides, catalyzed by copper(II) compounds is challenging.^[298, 299] Such an oxidation would prohibit further gold(I) coordination. This issue is circumvented in a two-step procedure, in which at first the gold(I) complexes occupy the phosphine moieties. Thereby, the gold–phosphine linkages are sufficiently strong to remain unaffected, when adding the copper salt in the second step.

6.2.1 Synthesis of a Terpolymer – Phosphines and Carboxylic Acids

In order to implement phosphine and carboxylic acid moieties into a polymer for further metal encapsulation, the synthesis of a terpolymer was targeted consisting of the previously employed monomers 4-(diphenylphosphino)styrene and 4-vinylbenzoic acid, separated by a non-functional monomer. Initially, the spacer monomer 2,3,4,5,6-pentafluorostyrene was chosen, due to its similar character to styrene, yet instead of aromatic protons, containing fluorides. The reason behind the introduction of pentafluorostyrene is a facilitated determination of the monomer composition in the final terpolymer.

To evaluate the polymerization behavior of the monomer 2,3,4,5,6-pentafluorostyrene, a kinetic investigation of the rate of polymerization of this monomer was carried out, investigating both a suitable ratio of monomer to initiator and the reaction period to reach high molecular weight with narrow distribution. As reported in previous projects (e.g. Chapter 4), a molecular weight of over 25 000 g · mol⁻¹ is targeted to facilitate the analysis of the subsequently performed SCNPs. When polymerizing pentafluorostyrene *via* nitroxide mediated polymerization (NMP) mediated by a TEMPO-based initiator, P_{Fluoro} was obtained (refer to Chapter 9.4.6 for P_{Fluoro}). Due to promising results regarding the molecular weight and chain length distribution of P_{Fluoro}, a polymerization of all three monomers 4-(diphenylphosphino)styrene, 4-vinylbenzoic acid and 2,3,4,5,6-pentafluorostyrene was performed. However, the subsequent ¹H NMR (400 Hz, THF-d₈) analysis of the purified polymer indicated that 4-vinylbenzoic acid has not been incorporated as no acidic proton resonances were detected (spectrum not shown here). Furthermore, the terpolymer exhibited a limited solubility behavior in several organic solvents and was only soluble in high amounts of THF. Consequently, this approach was discarded and 2,3,4,5,6-pentafluorostyrene was substituted by styrene.

The reaction scheme for the polymerization of the terpolymer *via* NMP is shown in Scheme 6.1, a procedure which allows the direct incorporation of phosphine and benzoic acid functional groups into a polymer. As developed in previous projects (refer to Chapter 3 and 5), a minimum of 5 % functional groups which participate in the chain collapse, *e.g.* acid moieties, is necessary for a successful chain folding. For a metal incorporation in a 1:1 ratio, less ligand moieties, *e.g.* phosphine groups, are required, thus a functionalization of approx. 3 % is targeted.



Scheme 6.1: Reaction scheme for the statistical polymerization of 4-(diphenylphosphino)styrene, 4-vinylbenzoic acid and styrene *via* the NMP technique, yielding P_{P/Acid}.

After purification of the obtained terpolymer P_{P/Acid}, the monomer composition was quantified by ¹H NMR analysis. Established before in the analysis of the ¹H NMR spectra of the copolymers in the compositions styrene–phosphine (P_{Phosphine}) and styrene–acid (P_{Acid}), the resonances associated with the protons of each monomer in a styrene copolymer are well-known and distinguishable, allowing for the estimation of the individual monomer incorporations. Selecting THF-d₈ as an appropriate solvent to detect acidic protons, the broad resonance of the acidic proton of 4-vinylbenzoic acid appears at $\delta = 11.1$ ppm. The amount of benzoic acid groups in the terpolymer was determined comparing the resonances of two of the protons of 4-vinylbenzoic acid (labeled with (a) in Figure 6.3) at $\delta = 8.0$ – 7.5 ppm and the styrene groups and remaining two aromatic protons of 4-vinylbenzoic acid at $\delta = 7.2$ – 6.1 ppm (b). The resonances between $\delta = 7.5$ – 7.2 ppm belong to the aromatic protons of 4-(diphenylphosphino)styrene. The analysis results for benzoic acids to styrene in a ratio of 1:15, equivalent to 6.7 % acidic functionality, and phosphine to styrene in a ratio of 1:35, equivalent to 2.8 %. These ratios are in good agreement with the required degree of functionalization (5 % acid groups, 3 % phosphine moieties).

In addition, the resonance at $\delta = -6.4$ ppm in the ³¹P{¹H} NMR spectrum of P_{P/Acid} indicated the incorporation of a triarylphosphine group in the polymer.

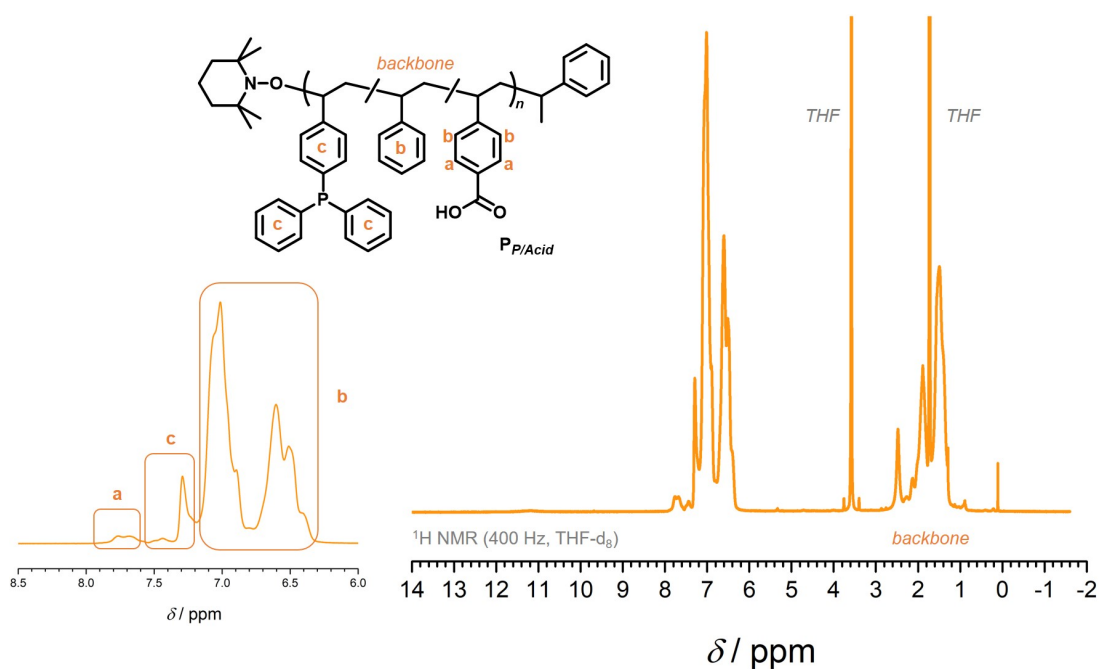


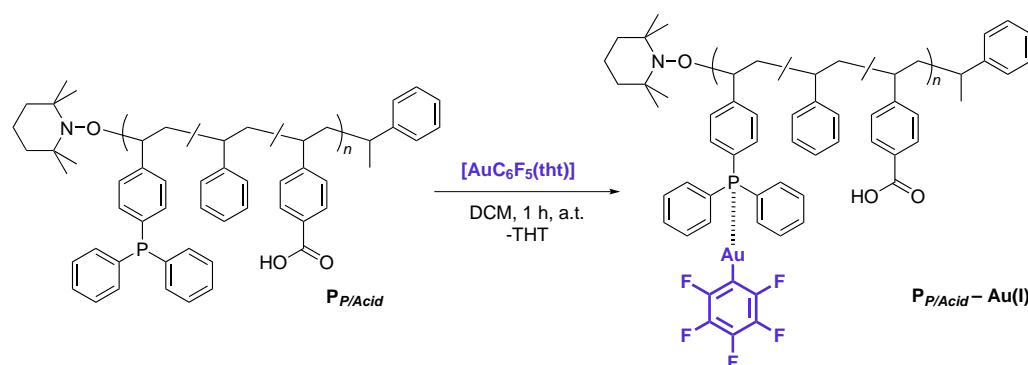
Figure 6.3: ^1H NMR spectrum of $P_{P/Acid}$, in which characteristic resonances for the two functional groups, 4-(diphenylphosphino)styrene and 4-vinylbenzoic acid, are detected. The comparison of the integrals allows the determination of the monomer composition in the polymer, resulting in 6.7 % acid and 2.8 % phosphine functionality.

The analysis of $P_{P/Acid}$ via SEC measurements (THF, RI) revealed a number average molecular weight of $M_n = 41\,300\text{ g} \cdot \text{mol}^{-1}$ and a monomodal distribution of $\mathcal{D} = 1.20$. Combined with the results of the ^1H NMR analysis, a value of 27 benzoic acid moieties and 11 phosphine groups in each chain was averaged.

6.2.2 Au(I) Functionalization

Subsequently, $P_{P/Acid}$ was transformed into a functional metallopolymer upon gold(I) incorporating by the phosphine moieties in the polymer chain.

For a proof of concept, revealing the ability to synthesize orthogonal heterometallic SCNPs, the gold(I) compound $[AuC_6F_5(tht)]$ was chosen as the precursor complex. Although not catalytically active, the complex contains a C_6F_5 group as a fluorine marker and the replaceable ligand tetrahydrothiophen (THT) as a good leaving group, facilitating the tracking of the complex and the incorporation into the polymer, respectively.^[300] As the coordination of gold(I) to phosphine proceeds in a metal-to-ligand ratio of 1:1, no crosslinking and therefore no high dilution during synthesis was necessary. In order to maintain the oxidation state of Au(I), which for some gold complexes is reported to be light sensitive,^[301] the reaction was performed in brown flasks to protect the metal salt solution from light exposure. On a molecular level, the phosphine moieties in $P_{P/Acid}$ replace the THT groups of the precursor complex and form phosphine–gold(I) coordinative linkages, yielding the metallopolymer $P_{P/Acid}-Au(I)$ (Scheme 6.2).



Scheme 6.2: Coordinative bonds in a 1:1 ratio are formed between the precursor complex $[AuC_6F_5(tht)]$ and the phosphine moieties in $P_{P/Acid}$, resulting in the gold-functionalized metallopolymer $P_{P/Acid}-Au(I)$. In the coordination process, the ligand tetrahydrothiophane (THT) is released from the precursor complex, when coordinating to triarylphosphine.

Crucial aspect when targeting orthogonal metal ion embedding was to proof the exclusive bond formation to the phosphine units in $P_{P/Acid}$ to gold(I), without affecting the benzoic acid moieties.

Analyzing $P_{P/Acid}-Au(I)$ via $^{31}P\{^1H\}$ NMR spectroscopy indicated a significant shift of the phosphine resonance in the spectrum upon coordination to the gold(I) units from $\delta = -6.4$ ppm to 41.1 ppm (Figure 6.4), similar to reports in the literature.^[302] As no residual resonance stemming from the free ligand is detected, a full complexation of the phosphine moieties by Au(I) is assumed.

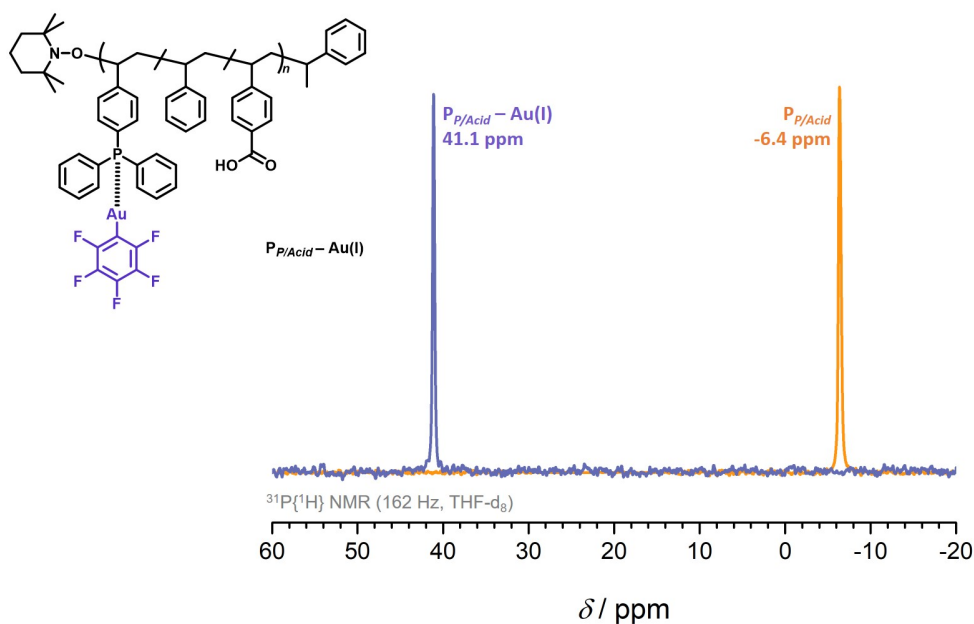


Figure 6.4: Superimposition of the $^{31}\text{P}\{^1\text{H}\}$ NMR spectra of $\text{P}_{P/Acid}$ and $\text{P}_{P/Acid}-\text{Au(I)}$. Upon coordination of the phosphine moieties to the gold(I) species, the resonance for former free triarylphosphine is shifted from $\delta = -6.4$ ppm to $\delta = 41.1$ ppm. No residual of the former resonance indicates a coordination of all phosphine moieties to the gold(I) complexes.

The first proof for an orthogonal embedding of gold(I) was demonstrated by analyzing $\text{P}_{P/Acid}-\text{Au(I)}$ via ^1H NMR spectroscopy in THF-d_8 . Comparing the spectra of $\text{P}_{P/Acid}$ and $\text{P}_{P/Acid}-\text{Au(I)}$, no amendment of the resonance of the acidic proton is shown at $\delta = 11.1$ ppm, pointing towards free benzoic acid groups. Moreover, exclusively the resonances of the protons of the phosphine species are shifted from $\delta = 7.5-7.2$ ppm to $7.6-7.4$ ppm. An overview of the shifts of the aromatic protons in the ^1H NMR spectrum is given for the final $\text{Au(I)}/\text{Cu}_2(\text{II})$ -SCNPs.

Due to the attached fluorine marker in the gold(I) complex, three resonances corresponding to the C_6F_5 unit were detected in the ^{19}F NMR spectrum (Figure 6.5).^[303] According to the abundance of fluorine, the resonances appear in a 2:1:2 ratio at $\delta = -116.3$ ppm (*ortho*), -160.4 ppm (*para*) and -163.9 ppm (*meta*).

In order to corroborate the embedding of Au(I) complexes into $\text{P}_{P/Acid}$, infra red (IR) spectroscopy was employed (Figure 6.6). In a direct comparison of the IR spectra of $\text{P}_{P/Acid}$ and $\text{P}_{P/Acid}-\text{Au(I)}$, additional bands appear for the metallopolymer at $\tilde{\nu} = 1061$ cm^{-1} and 954 cm^{-1} , attributed to the pentafluorophenyl group.^[303] Furthermore, the stretching vibration of $\text{C}=\text{O}$ of the benzoic acid moiety in the region of $\tilde{\nu} = 1680-1750$ cm^{-1} is detected in both spectra, confirming their continued presence, hence no interaction with the gold(I) complex.

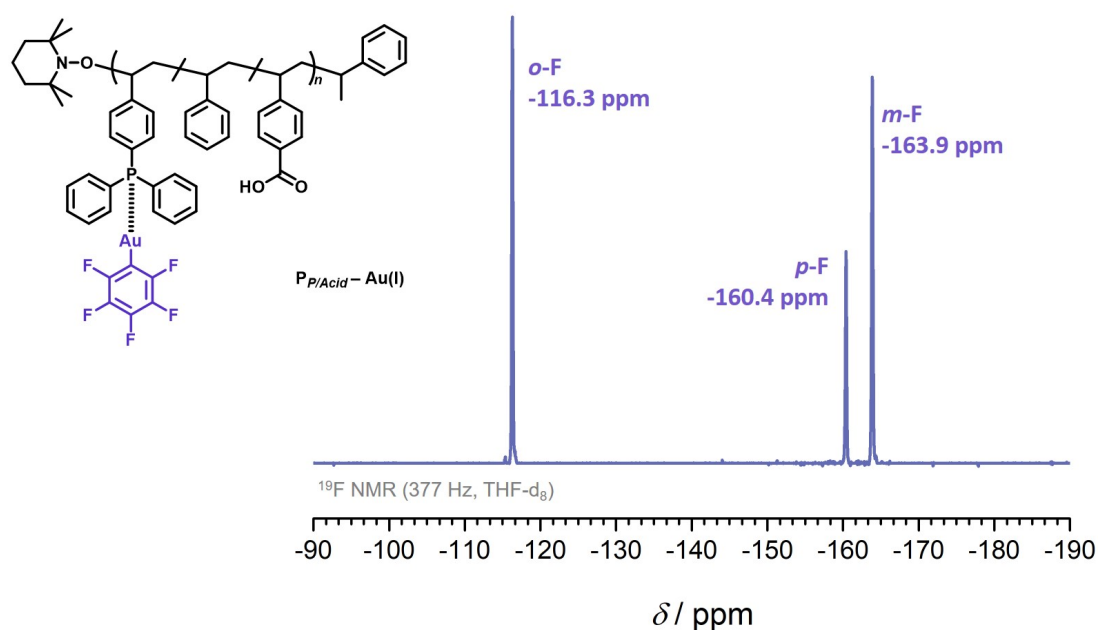


Figure 6.5: The presence of a C_6F_5 group in $P_{P/Acid}-Au(I)$ causes characteristic resonances in the ^{19}F NMR spectrum. Labeled are the *ortho*-, *para*- and *meta*-fluorine resonances.

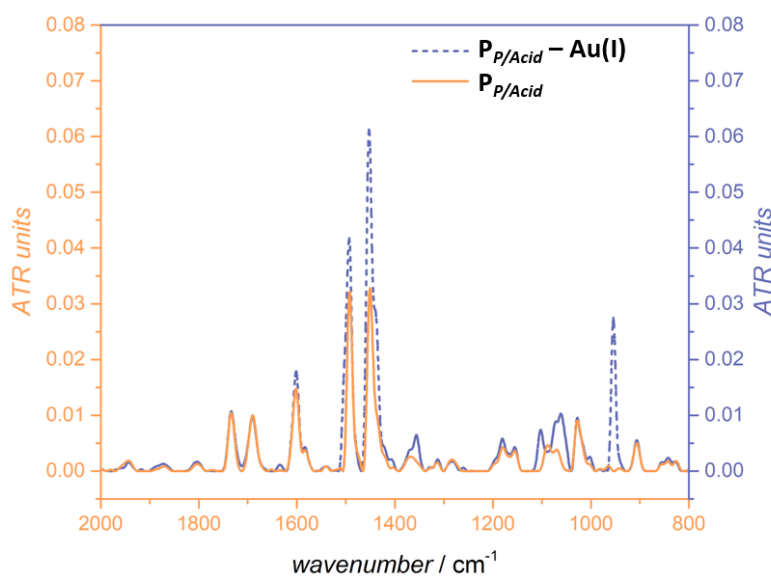


Figure 6.6: IR spectra of $P_{P/Acid}$ (yellow) and $P_{P/Acid}-Au(I)$ (blue). The new set of bands at $\tilde{\nu} = 1061$ cm^{-1} and 954 cm^{-1} in the spectrum of $P_{P/Acid}-Au(I)$ originates from the C_6F_5 group of the gold(I) complex, indicating its incorporation into the polymer. The band for the $C=O$ mode at $\tilde{\nu} = 1680-1750$ cm^{-1} , belonging to the benzoic acid moieties, appears in both spectra, thus confirms free benzoic acid groups.

The gold centers, situated on pendant groups along the chain effected significantly the molecular mass of the parent compound. In a rough calculation based on the number average molecular weight of $M_n = 41\,300 \text{ g} \cdot \text{mol}^{-1}$ of $P_{P/Acid}$ determined *via* SEC, hypothetically one polymer chain consists of 400 monomer units (molecular weight of styrene $104 \text{ g} \cdot \text{mol}^{-1}$). Assuming an amount of 2.8 % phosphine functionalities, this resulted in approximately 11 groups of phosphine units in each chain. Multiplied with the molecular weight of $[\text{Au(I)}\text{C}_6\text{F}_5]$ of $M = 364.0 \text{ g} \cdot \text{mol}^{-1}$, its incorporation contributed with approx. $4100 \text{ g} \cdot \text{mol}^{-1}$ to the former molecular mass. As a result, a molecular weight of $M_n = 41\,300 + 4100 = 45\,400 \text{ g} \cdot \text{mol}^{-1}$ was calculated for $P_{P/Acid}\text{-Au(I)}$. This value is in good agreement with the results of the SEC analysis (THF, RI) of $P_{P/Acid}\text{-Au(I)}$, $M_n = 45\,500 \text{ g} \cdot \text{mol}^{-1}$ (Figure 6.7). In addition, the change in the molecular weight distribution is marginal ($\mathcal{D} = 1.21$).

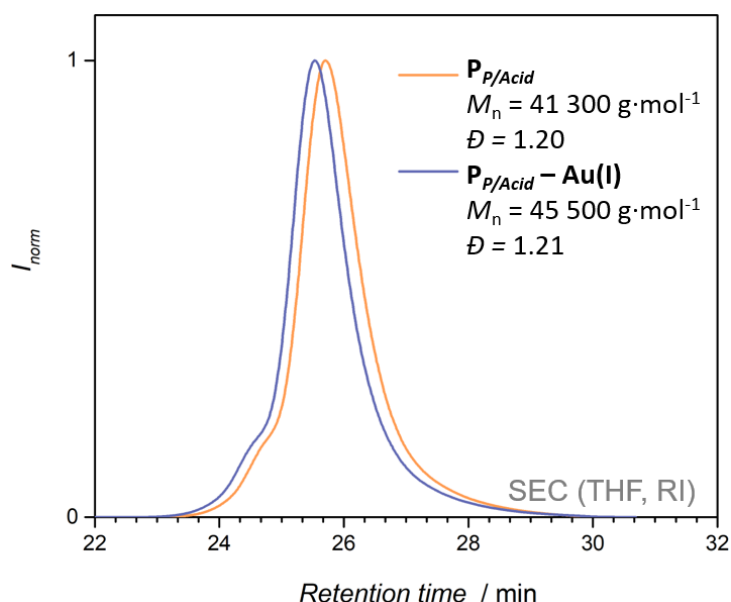


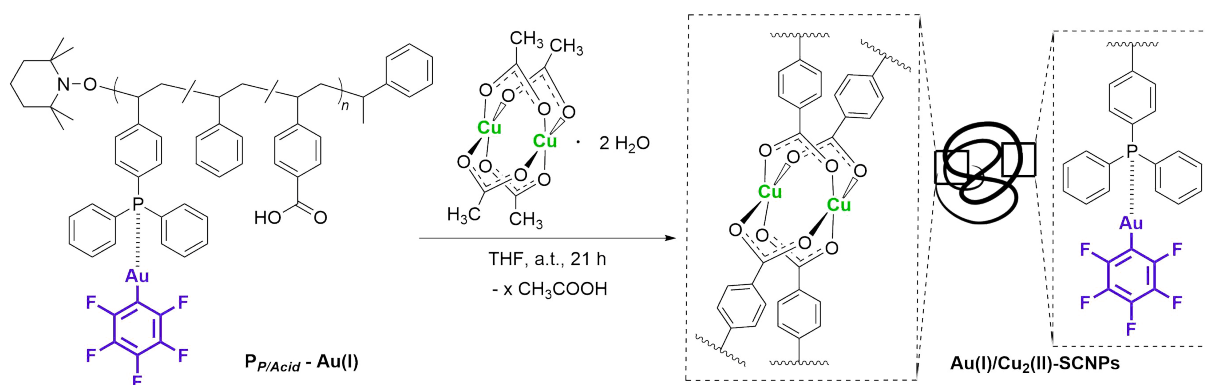
Figure 6.7: Superimposition of the SEC traces (THF, RI) of $P_{P/Acid}$ and $P_{P/Acid}\text{-Au(I)}$. The embedding of gold(I) centers into pendant phosphine groups in the polymer enhanced the molecular weight of the polymer.

Due to the results of the ^1H , ^{19}F , $^{31}\text{P}\{^1\text{H}\}$ NMR and IR spectroscopy, combined with SEC data, the successful incorporation of $\text{Au(I)}\text{C}_6\text{F}_5$ into the polymeric structure is established. The resonance for the acidic proton in the ^1H NMR spectrum in THF, as well as the bands for free $\text{C}=\text{O}$ modes in the IR spectrum, indicate an orthogonal coordination of Au(I) to the phosphine moieties, maintaining free benzoic acid groups in $P_{P/Acid}$.

6.2.3 Au(I)/Cu₂(II)-SCNP Formation

The following step entailed the reaction of the complex [Cu(OAc)₂]₂ with the linear metallopolymer P_{P/Acid}-Au(I). As already observed in the project describing the preparation of copper and molybdenum SCNPs (refer to Chapter 5), benzoic acid functionalities are stronger acids than the corresponding acetic acid ligands in the copper(II) precursor complex. Consequently, the ligand arrangement of bidentate bridging carboxylates in the molecular structure is maintained within the polymer frame.

As imperative in SCNP formation, high dilutions of polymer chains and metal ions are essential to form highly crosslinked, yet unimolecular nanoparticles. The performance of the ligand-exchange reaction under high dilution, in combination with a ligand-to-metal ratio of 4:1, causes a collapse of the chains, yielding in potential Au(I)/Cu₂(II)-SCNPs (Scheme 6.3).



Scheme 6.3: Reaction scheme for the synthesis of Au(I)/Cu₂(II)-SCNPs. The gold functionalized metallopolymer P_{P/Acid}-Au(I) collapses into a nanoparticle when replacing the acetate ligands of the precursor copper complexes by benzoic acids, which form bidentate bridging dinuclear paddlewheel structures.

After the synthesis and purification of the polymeric material, which turned blue after copper(II) addition, the potential nanoparticles were investigated regarding chain compaction and orthogonal implementation of copper(II) ions without disturbing the coordination sphere of the already coordinated gold(I) centers.

At first, the polymeric material was analyzed *via* SEC measurement (THF, RI) in comparison to the precursor P_{P/Acid} and metallopolymer P_{P/Acid}-Au(I). As seen before, the SEC trace for the gold(I) species is shifted towards shorter retention times, due to an increase in the hydrodynamic radius (Figure 6.8). After the encapsulation of the copper species, the trace is shifted towards higher retention times. Although in this reaction the overall molecular mass increased, the 4:1 ligand-to-metal ratio causes a chain collapse, visualized in a smaller hydrodynamic radius. These results are indicative for the formation of a more compact structure, *i.e.* the Au(I)/Cu₂(II)-SCNPs.

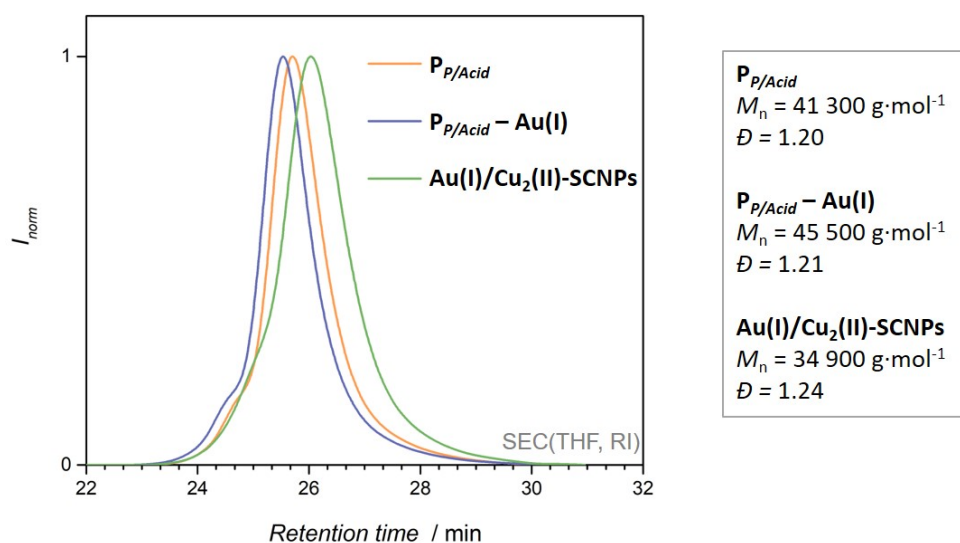
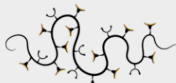



Figure 6.8: SEC traces (THF, RI) of the Au(I)/Cu₂(II)-SCNPs in comparison to the linear precursor polymer $P_{P/Acid}$ and the metallopolymer $P_{P/Acid}-\text{Au(I)}$ show the expected trend: Upon embedding gold(I) to the pendant phosphine groups of $P_{P/Acid}$, the complexes contributed to the overall mass, hence the respective SEC trace shifts towards shorter retention times. Although in the subsequent copper implementation the molecular mass is increased, the ligand-to-metal ratio of 4:1 causes a chain folding, indicated by the shift towards higher retention times for the Au(I)/Cu₂(II)-SCNPs. The corresponding data is summarized in the table aside.

The reduction of the hydrodynamic radius was additionally corroborated by diffusion ordered spectroscopy (DOSY) in THF (viscosity $\eta = 0.4730 \text{ mPa}\cdot\text{s}$, 298 K).^[304] Analogous to the DOSY measurements in former projects, the diffusion coefficients of the respective compounds were determined and, by applying the Stokes–Einstein Equation, converted into the corresponding hydrodynamic radii (Table 6.1). According to DOSY, $P_{P/Acid}$ possesses a hydrodynamic radius (r_H) of 4.0 nm. The subsequent copper encapsulation ensued a reduction of the radius of over 50 %, resulting in a $r_H = 1.9 \text{ nm}$ for the Au(I)/Cu₂(II)-SCNPs. Regrettably, the DOSY data of $P_{P/Acid}-\text{Au(I)}$ deviated from the expected trend. Repeated measurements did not result in constant values of the diffusion coefficient, although performed under the same conditions. A possible explanation entails the composition of a linear polymer chain, which contains intermittently gold(I) complexes in pendant polymer side chains, presumably not recognized as one connected compound by the instrument.

After verifying the chain compaction upon copper(II) encapsulation by the collocated data of SEC and DOSY measurements, the folding motif was investigated. Analogous to Chapter 5, a folding unit in form of a paddlewheel structure was assumed. In addition, intact Au(I)–phosphine bonds needed to be ensured, as they are the heart of the orthogonal heterometallic system.

Table 6.1: Diffusion coefficients and the corresponding hydrodynamic radii are acquired by DOSY measurements for the linear copolymer $P_{P/Acid}$ and the Au(I)/Cu₂(II)-SCNPs. Measuring the diffusion coefficients, the hydrodynamic radii r_H of the compounds are calculated, applying the Stokes–Einstein Equation.

Substance		D [m^2s^{-1}]	Error	r_H [nm]
Copolymer $P_{P/Acid}$		1.14×10^{-10}	1.3×10^{-12}	4.0
Au(I)/Cu ₂ (II)- SCNPs		2.50×10^{-10}	4.3×10^{-11}	1.9

Drawing a direct comparison between structural changes prior and after copper(II) implementation, Au(I)/Cu₂(II)-SCNPs were analyzed by IR spectroscopy (Figure 6.9). As described for the M₂(II)-SCNPs in Chapter 5, characteristic bands for asymmetric and symmetric C–O vibrational modes are detected normally between $\tilde{\nu} = 1400\text{--}1600\text{ cm}^{-1}$, depending on the respective ligands and metal ions.^[286–288] The band in the spectrum of P_{P/Acid} between $\tilde{\nu} = 1680\text{--}1750\text{ cm}^{-1}$, caused by the vibrations of free C=O bonds, is not detected anymore in the spectrum of the Au(I)/Cu₂(II)-SCNPs. This deletion is indicative of a quantitative coordination of the carboxylate ligands to Cu₂⁴⁺ units. Moreover, new bands at $\tilde{\nu}_a = 1617\text{ cm}^{-1}$ and $\tilde{\nu}_s = 1407\text{ cm}^{-1}$, corresponding to the asymmetric and symmetric C–O stretching vibration, appear.^[290] These IR data are consistent with previous observations in the single system of Cu₂(II)-SCNPs (Chapter 5) and support the assumption of paddlewheel structures in the Au(I)/Cu₂(II)-SCNPs.

In addition, the band for the pentafluorophenyl unit of the gold(I) compound is still detected in the spectrum of the SCNPs ($\tilde{\nu} = 1061\text{ cm}^{-1}$ and 954 cm^{-1}), inferring a selective coordination of copper to the benzoic acid moieties, without interaction with the phosphines.

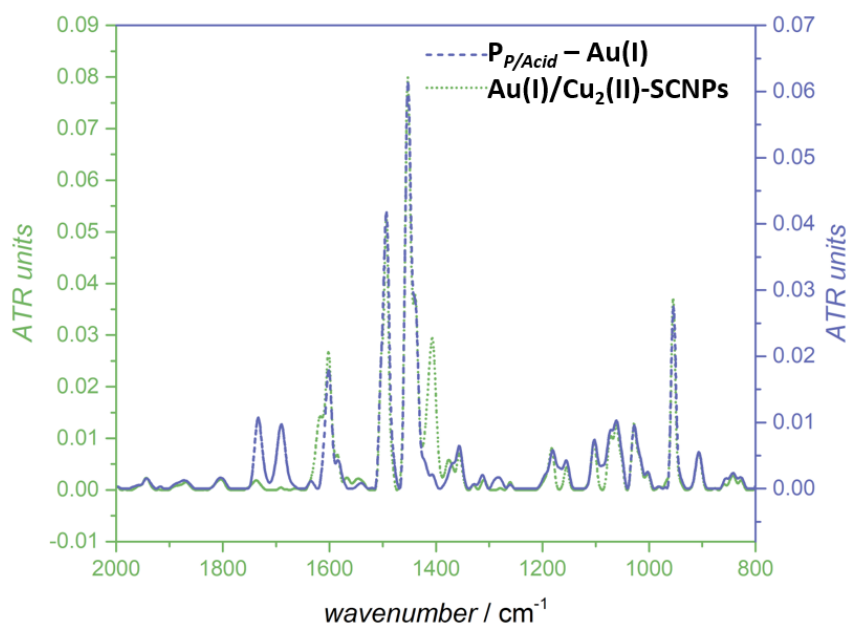


Figure 6.9: IR spectra of P_{P/Acid}–Au(I) (blue) and the Au(I)/Cu₂(II)-SCNPs (green). The disappearance of the band for the C=O modes in the spectrum of the nanoparticles, and instead novel sets of bands for the asymmetric and symmetric C–O vibrational modes point towards the generation of paddlewheel structures as crosslinking units in the SCNPs. The IR data of the Au(I)/Cu₂(II)-SCNPs is concomitant to the IR data of the single system of the Cu₂(II)-SCNPs. The unchanged bands of the C₆F₅ group of the gold(I) compound is indicative for intact bonds and thus no interaction of the phosphines with copper(II). (The spectra is referenced to the intensity of the band at $\tilde{\nu} = 1028\text{ cm}^{-1}$.)

The blue color of the Au(I)/Cu₂(II)-SCNPs is in-line with the results of the additionally performed UV/Vis spectroscopy, in which a broad absorption band between 550–800 nm is detected, typical for a Cu₂⁴⁺ unit in a carboxylate bridged environment.^[290, 305]

The Au(I)/Cu₂(II)-SCNPs were further analyzed by NMR spectroscopy. Superimposing the ¹H NMR (CDCl₃) spectra of P_{P/Acid}, P_{P/Acid}-Au(I) and Au(I)/Cu₂(II)-SCNPs, significant shifts for the resonances in the aromatic region were observed. After coordination of the phosphine units in P_{P/Acid} towards gold(I), the maximum of the resonance for the phosphine units at $\delta = 7.31$ ppm is shifted towards $\delta = 7.47$ ppm (1→2), and remains after coordination to copper. Instead, the broad resonance belonging to two of the aromatic protons of the monomer 4-vinylbenzoic acid (3) between $\delta = 8.1$ –7.6 broadens to such an extent that no differentiation to the base line is possible (Figure 6.10).

In the downfield region of the ¹H NMR spectrum (THF-d₈) of the Au(I)/Cu₂(II)-SCNPs, no resonance for an acidic proton is detected, which appeared for P_{P/Acid} and the gold(I) metallopolymer in their respective ¹H NMR spectra at $\delta = 11.1$ ppm. The deletion of the acidic protons in the present project points towards a participation of all benzoic acid moieties in the folding process.

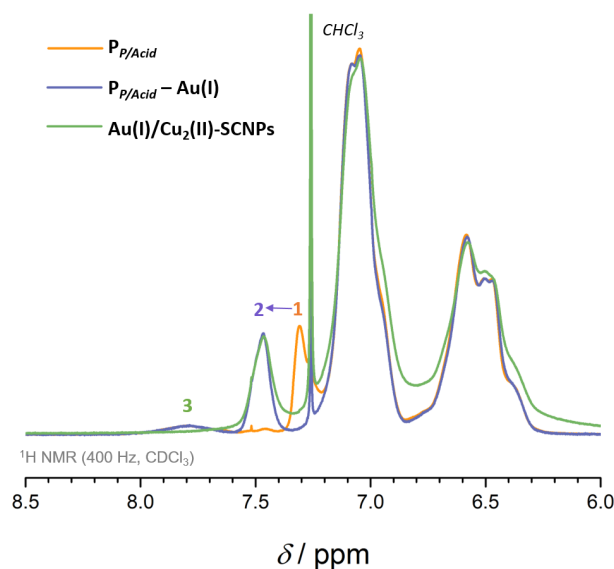


Figure 6.10: Superimposition of the ¹H NMR spectra (CDCl₃) of P_{P/Acid}, P_{P/Acid}-Au(I) and the Au(I)/Cu₂(II)-SCNPs to reveal changes in the aromatic region upon gold(I) and copper(II) encapsulation by the polymer framework. After coordination of the phosphine units in P_{P/Acid} towards gold(I), the maximum of the resonance for the phosphine units at $\delta = 7.31$ ppm is shifted towards $\delta = 7.47$ ppm (1→2) and remains unchanged after coordination to copper. Instead, the broad resonance belonging to two of the aromatic protons of the monomer 4-vinylbenzoic acid (3) between $\delta = 8.1$ –7.6 ppm broadens to such an extent that no differentiation to the base line can be detected.

The exclusive coordination of copper(II) to the carboxylic acid functionalities was demonstrated by verifying the continuous encapsulation of the gold(I) centers by the phosphine moieties. In the $^{31}\text{P}\{^1\text{H}\}$ NMR spectrum of the Au(I)/Cu₂(II)-SCNPs, the single resonance at $\delta = 41.1$ ppm remains unaffected, corroborating no disruption of the Au(I)–phosphine bonds by copper(II) (Figure 6.11). The same applied for the ^{19}F NMR spectrum, in which the three resonances for the aromatic fluorides are still detected (not shown).

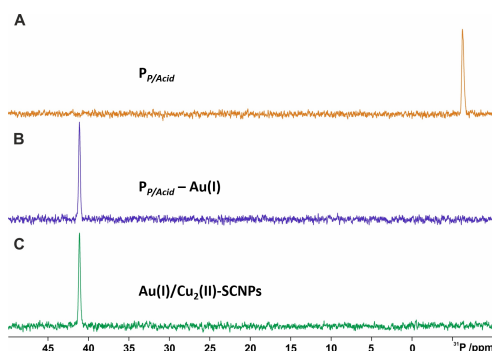
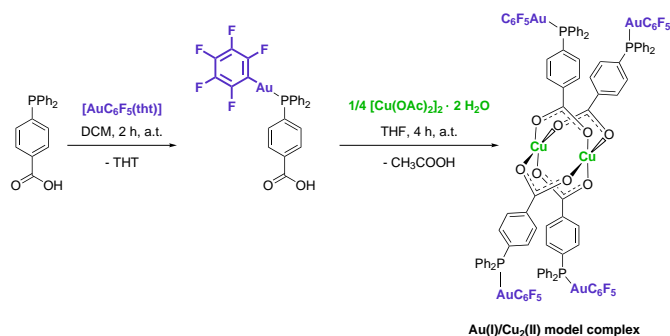


Figure 6.11: $^{31}\text{P}\{^1\text{H}\}$ NMR spectra of $\text{P}_{\text{P/Acid}}$ (A, yellow), $\text{P}_{\text{P/Acid}}-\text{Au(I)}$ (B, blue) and Au(I)/Cu₂(II)-SCNPs (C, green). Upon gold(I) implementation, the resonance of the triarylphosphine moieties is shifted from $\delta = -6.4$ ppm to $\delta = 41.1$ ppm and remains unchanged after the copper incorporation, inferring intact Au(I)–phosphine bonds in a copper(II) presence, thus indicating an orthogonal implementation.

Nicolai Knöfel (KIT) prepared a corresponding molecular complex, which contains bifunctional linker moieties of phosphine and benzoic acid (Scheme 6.4). As demonstrated for the polymeric system, an orthogonal incorporation of metal ions was observed, provided the addition of gold(I) first and the coordination to copper(II) second, yielding the Au(I)/Cu₂(II) model complex. Furthermore, the crystallization and subsequent X-ray analysis of the molecular structure revealed a 1:1 phosphine–gold coordination and the generation of a 4:1 carboxylate–copper paddlewheel structure.



Scheme 6.4: Synthesis of a molecular complex, employing a bifunctional 4-(diphenylphosphino)benzoic acid ligand, in which Au(I) and Cu₂(II) are incorporated in close proximity. Thus, the orthogonality of the previously described heterometallic functionalization in the polymeric framework is observed in a molecular structure and verified by X-ray analysis.

6.3 Summary

In conclusion, a styrene-based terpolymer ($P_{P/Acid}$) consisting of phosphine and benzoic acid functionalities was introduced and employed for a controlled, directed coordination of the two metal ions, gold(I) and copper(II). In a two step process, at first the gold(I) cores in a $[Au(I)C_6F_5]$ unit coordinated to the phosphine moieties, evidenced by characteristic resonances in the 1H , $^{31}P\{^1H\}$ and ^{19}F NMR and IR spectra. The orthogonal behavior of gold(I) exclusively to phosphine without interaction with the benzoic acid groups was indicated by the resonance of acidic protons in the 1H NMR spectrum and the detection of the bands of the $C=O$ modes of the benzoic acid groups in the IR spectrum. The increased molecular mass of the polymer framework after gold(I) incorporation ($P_{P/Acid}-Au(I)$) was verified by SEC measurements.

In the second step, copper(II) units were incorporated into $P_{P/Acid}-Au(I)$, inducing, due to a 4:1 ligand-to-metal ratio, a collapse into nanoparticles. Analogous to the project in Chapter 5, a paddlewheel structure of bidentate bridging carboxylates was formed. Evidence for a compact structure was obtained by SEC and DOSY analysis. The incorporation of copper(II) by the carboxylic acids was confirmed by IR spectroscopy, in which the bands for the $C=O$ modes were replaced by bands for $C-O$ symmetric and asymmetric vibration modes. In addition, a characteristic absorption band for copper(II) in a carboxylate environment in the range between 550–800 nm was detected in the UV/Vis spectrum. Before observed resonances in the $^{31}P\{^1H\}$ and ^{19}F NMR spectra, corresponding to a $[Au(I)C_6F_5]$ incorporation, remained unchanged after copper(II) addition, hence an orthogonal metal coordination for the $Au(I)/Cu_2(II)$ -SCNPs was verified.

The herein presented project showcased the ability to synthesize in a two step procedure heterometallic single-chain nanoparticles. The combination of the ligand–metal pairs of phosphines with gold(I) and carboxylates with copper(II) is a powerful tool to reach a controlled, orthogonal incorporation of two types of metal ions within one chain, establishing a potential system with divergent catalytic metal centers. The following chapter focuses on the approach of heterometallic, luminescent catalytic SCNP systems.

6.4 A Europium and Platinum Based System

Striving for a polymer system which exhibits luminescent and catalytic properties, an alternative strategy is developed to orthogonally implement two types of metal centers into one polymer chain.

A previous project (Chapter 3) demonstrated the dual role of platinum(II) to physically crosslinking the chain, due to a 2:1 ligand-to-metal ratio, whilst creating catalytic active centers. Thereby, the soft acid platinum(II) coordinated to the soft phosphine ligands. For the present project, this pair of ligand and metal ion is employed, completed by another pair of hard acids and bases. An ideal counterpart for the soft phosphine ligands are phosphine oxides. Upon straightforward oxidation of the triarylphosphine monomer to 4-(diphenylphosphine oxide)styrene, a divergent coordination behavior is generated. The quasi ionic trait of the P=O bond strongly favors the coordination to hard acids, forming a bond of high electrostatic character.^[171]

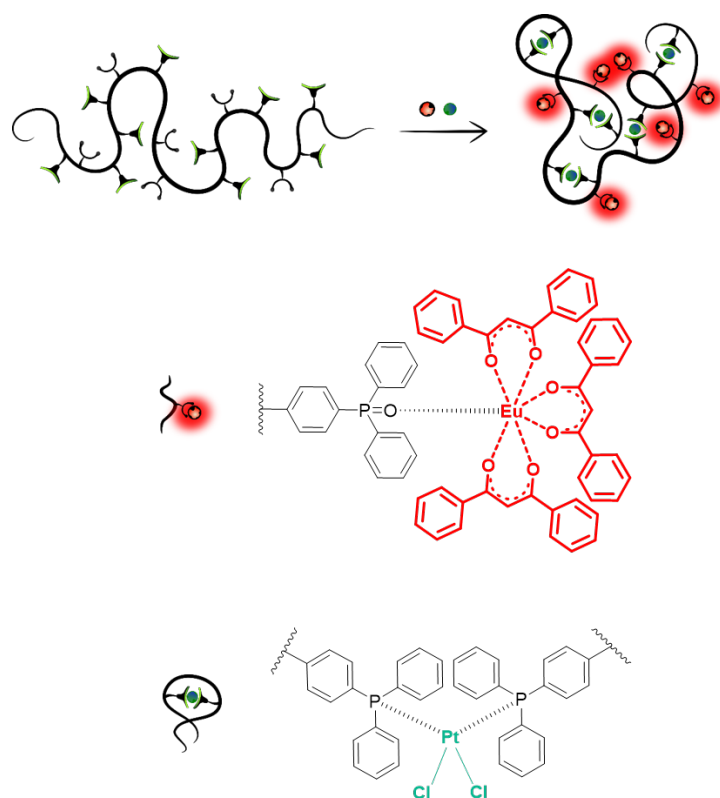


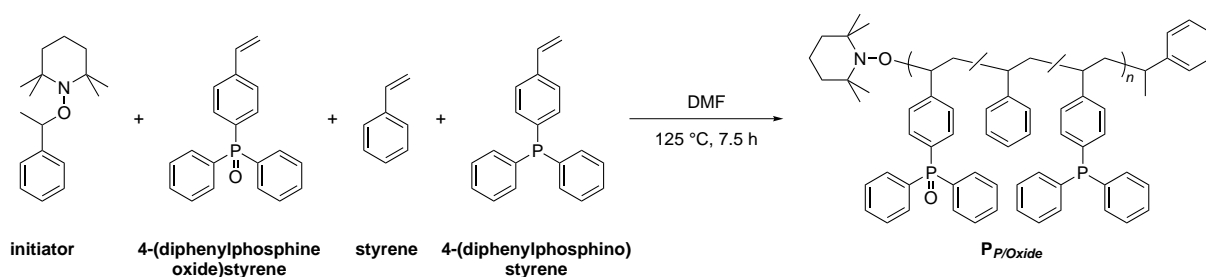
Figure 6.12: Two orthogonal linkage motifs, phosphine oxides and phosphines, coordinate selectively to europium(III) and platinum(II), thus enabling the formation of heterometallic single-chain nanoparticles (SCNPs). Whereas for europium(III) a coordination ratio of 1:1 to phosphine oxide moieties is assumed, thereby implanting luminescent properties, platinum(II) forms linkages to phosphine in a 1:2 ratio, causing the chain to collapse into a more compact particle.

Suitable metal ions, belonging to the group of hard acids and simultaneously featuring a luminescent character are lanthanides, especially europium(III). Similar as observed for the complexation of Eu(III) by phenanthroline (Phen) in Chapter 4, the coordination of phosphine oxides^[255, 306] to Eu(III)- β -diketonates is reported to enhance the quantum yield (QY).^[307, 308] The ligand Phen-styrene, which was utilized to encapsulate europium(III) in the aforementioned Chapter 4, is not suitable for the current project, due to the ability of Phen to coordinate to both platinum(II) and lanthanides(III).^[309] In other words, upon platinum(II) addition, coordinative linkages to both functionalities, phosphines and Phen, can be formed. A 'protection' of the Phen units by reacting them first with europium(III) has been considered. However, the strong propensity of platinum(II) to crosslink to Phen releases europium from the before tied Eu(III)–Phen linkages, rendering this approach unsuitable. In contrast, platinum(II) does not favor a coordination by phosphine oxides.

Consequently, a directed metal embedding is expected when employing the pairs of phosphine oxides with europium(III) and phosphines with platinum(II). The combination of the two metal types leads to the generation of a luminescent and catalytically active system (Figure 6.12). The exclusive bond formation between the two pairs without interaction enables the performance of the chain functionalization with both metal ions in a one-pot reaction, independent of the sequence of metal addition.

6.4.1 Synthesis of a Terpolymer – Phosphines and Phosphine Oxides

As for the gold–copper system (Chapter 6.2), a terpolymer containing the two functional units, phosphines and phosphine oxides, separated by styrene, was synthesized. Therefore, the monomers 4-(diphenylphosphino)styrene, 4-(diphenylphosphine oxide)styrene and the spacer monomer styrene, were copolymerized *via* nitroxide mediated polymerization (NMP), as depicted in Scheme 6.5. The compatibility of the three monomers allowed their direct polymerization yielding $P_{P/Oxide}$, in which phosphine and phosphine oxide functionalities are statistically distributed along the chain. Analogous to the gold–copper project (Chapter 6.2), a higher degree of functionalization regarding the phosphine units was targeted, approx. 4 %, while even less functional groups for a 1:1 coordination with phosphine oxides was required.



Scheme 6.5: Reaction scheme of the polymerization of 4-(diphenylphosphino)styrene, 4-(diphenylphosphine oxide)styrene and styrene *via* NMP, mediated by a TEMPO-based initiator, resulting in poly(styrene-*co*-4-(diphenylphosphino)styrene-*co*-4-(diphenylphosphine oxide)styrene) ($\text{P}_{\text{P/Oxide}}$).

After purification of $\text{P}_{\text{P/Oxide}}$, the monomer composition in the terpolymer was determined *via* ^1H NMR and $^{31}\text{P}\{^1\text{H}\}$ NMR spectroscopy. In the ^1H NMR spectrum (Figure 6.13), the integrals of the resonances between $\delta = 8.0\text{--}7.2$ ppm, belonging to both phosphine species, and $\delta = 7.2\text{--}6.1$ ppm appearing for the aromatic protons of styrene, are compared, excluding the solvent resonance. The analysis results in a ratio of 1:19, phosphine species to styrene.

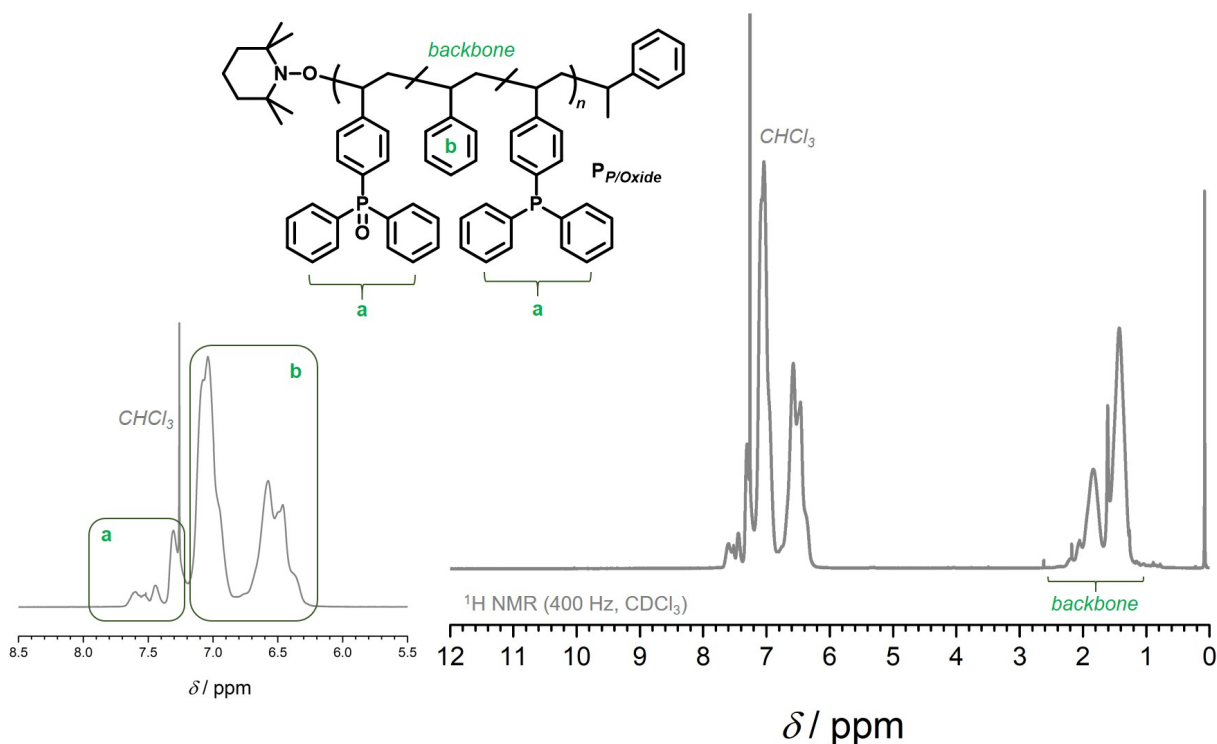


Figure 6.13: *Right:* ^1H NMR spectrum of $\text{P}_{\text{P/Oxide}}$ in CDCl_3 . *Left:* Zoom into the ^1H NMR spectrum of $\text{P}_{\text{P/Oxide}}$ focusing on the resonances of the aromatic protons to determine the ratio between phosphine and styrene units. Comparing the integrals between $\delta = 8.0\text{--}7.2$ ppm for the phosphine species and $\delta = 7.2\text{--}6.1$ ppm for the resonances of the aromatic styrene protons, results in a ratio of 1:19 (phosphine species : styrene).

The ratio between the phosphine species in $P_{P/Oxide}$ was revealed in the $^{31}\text{P}\{^1\text{H}\}$ NMR spectrum. By comparing the integrals of the resonances for triarylphosphine at $\delta = -6.2$ ppm with the resonance for phosphine oxide at $\delta = 29.2$ ppm (Figure 6.14), a ratio of 2:1 between phosphine and phosphine oxide is calculated.^[310] Transferred to the terpolymer, this results in a monomer ratio of 1:2:57 (phosphine oxide : phosphine : styrene) equivalent to 1.7 % phosphine oxide and 3.5 % phosphine functionality. The ratios match the desired degree of functionalization, hence $P_{P/Oxide}$ was employed for further metal embedding.

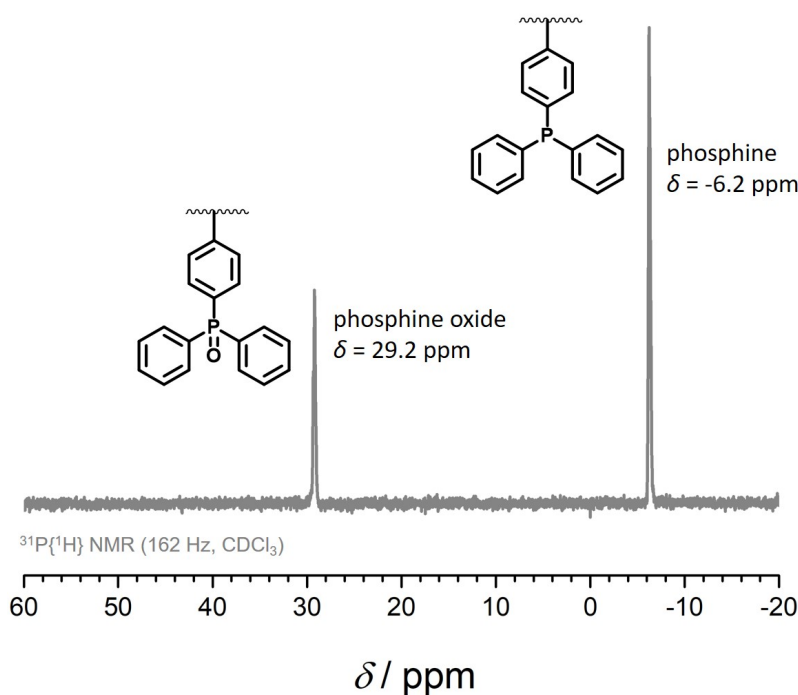


Figure 6.14: $^{31}\text{P}\{^1\text{H}\}$ NMR spectrum of $P_{P/Oxide}$, in which the resonances for triarylphosphine and the oxidized species are detected. Adequate measurements allow the integration of the resonances, revealing a ratio of approx. 1:2, phosphine oxide to phosphine.

In the characterization of $P_{P/Oxide}$ via SEC (THF, RI) the terpolymer exhibits a number average molecular weight (M_n) of $25\,300\text{ g} \cdot \text{mol}^{-1}$ with a dispersity of $\mathcal{D} = 1.41$. Combining the results of the SEC and ^1H NMR analysis, approx. 8–9 phosphine and 4 phosphine oxide functional groups are estimated per chain.

Analyzing $P_{P/Oxide}$ via IR spectroscopy, the significant band of the $\text{P}=\text{O}$ vibrational stretching mode has to be established. This is essential to allow further evaluation of the spectrum of the polymeric material after europium(III) embedding by the phosphine oxide moieties. Therefore, the IR spectrum of the terpolymer (grey) was compared to the IR spectrum of a copolymer, containing only styrene and 4-(diphenylphosphino)styrene, labeled $P_{Phosphine(2)}$ (yellow).

Identical bands in the IR spectra of $P_{P/Oxide}$ and $P_{Phosphine(2)}$ are detected, except for the two bands at $\tilde{\nu} = 1202 \text{ cm}^{-1}$ and $\tilde{\nu} = 1118 \text{ cm}^{-1}$, which consequently were attributed to the P=O stretching mode and C–H deformation mode of the triarylphosphine oxide unit, respectively.^[294, 311, 312] Both bands are additionally detected in the IR spectrum of the corresponding monomer 4-(diphenylphosphine oxide)styrene ($\tilde{\nu} = 1188 \text{ cm}^{-1}$ and $\tilde{\nu} = 1112 \text{ cm}^{-1}$), confirming the aforementioned assignment.

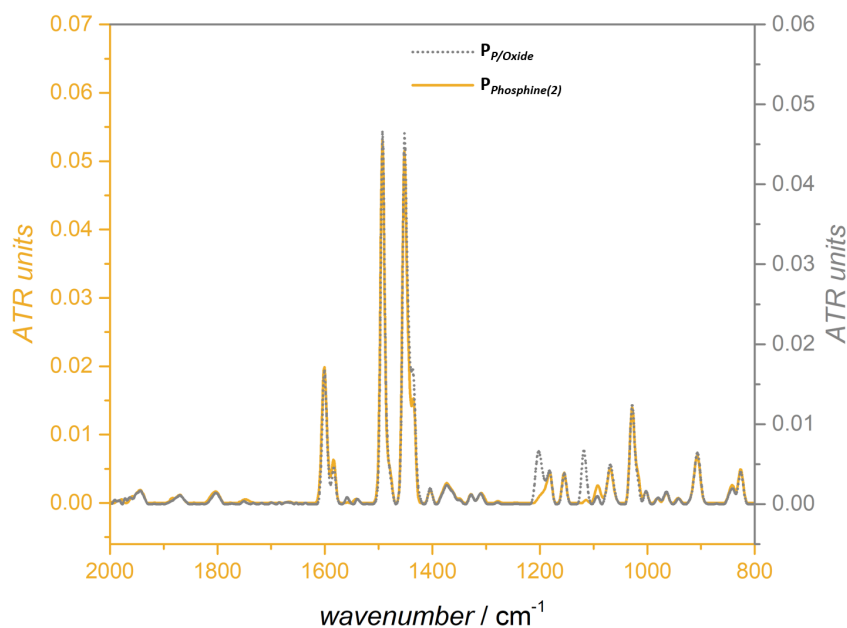
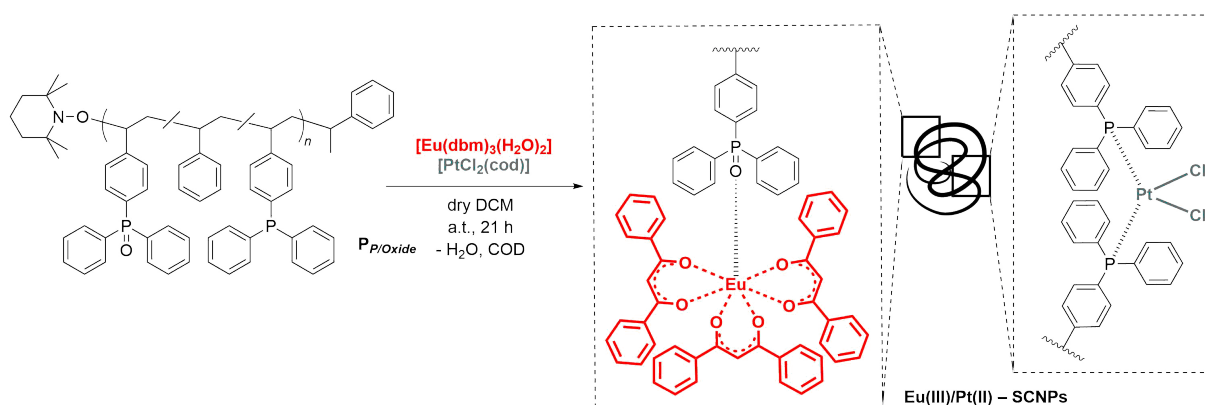


Figure 6.15: Superimposition of the IR spectra of the terpolymer $P_{P/Oxide}$ (grey) and the copolymer $P_{Phosphine(2)}$ (yellow), which is structurally similar to $P_{Phosphine}$ of the project in Chapter 3. Characteristic bands at $\tilde{\nu} = 1202 \text{ cm}^{-1}$ and $\tilde{\nu} = 1118 \text{ cm}^{-1}$ correspond to a P=O stretching mode and C–H deformation mode, respectively. (The spectra are referenced to the intensity of the band at $\tilde{\nu} = 1028 \text{ cm}^{-1}$.)

6.4.2 Eu(III)/Pt(II)-SCNP Formation

As precursor metal complexes, the already established platinum complex $[\text{PtCl}_2(\text{cod})]$ and the europium compound $[\text{Eu}(\text{dbm})_3(\text{H}_2\text{O})_2]$ are employed, where additional ligands, COD and DBM are abbreviations for 1,5-cyclooctadiene and dibenzoylmethanid, respectively. The favored linkage formation of platinum(II) with phosphines and europium(III) with phosphine oxides without interaction allows for the complexation to be a one-pot reaction. In order to ensure an intramolecular platinum–phosphine crosslinking, the reaction needs to be performed at high dilution. Therefore, the metal salts and the terpolymer were dissolved separately and mixed dropwise over a time period of 21 hours (Scheme 6.6). To avoid the oxidation of the phosphine moieties, working under inert atmosphere was essential.



Scheme 6.6: Reaction scheme for the synthesis of Eu(III)/Pt(II)-SCNPs. The orthogonal linkage preference of both metal centers to the two functional moieties, phosphine oxides and phosphines, allows a simultaneous coordinative linkage formation. Whereas a coordination of two phosphine moieties to one platinum(II) core is certain, the coordination behavior of europium(III) to phosphine oxides is not completely determined. In the scheme, a 1:1 ligand-to-metal ratio is depicted, however, conceivable is also a 2:1 ligand-to-metal ratio. Additional potentially coordinated water molecules are neglected.

Analogous to the synthesis of Pt(II)-SCNPs (Chapter 3), the phosphine units replaced the COD ligands of the platinum precursor complex and formed stable 2:1 ligand-to-metal coordination bonds. Simultaneously, the phosphine oxide moieties substitute coordinated water molecules of the europium precursor complex, allowing the formation of coordinative bonds to europium(III). In the literature, the attachment of either one or two phosphine oxides to one europium complex is reported.^[171, 294] At present, no meaningful statement about the amount of phosphine oxides per each europium(III) core can be made and the topic is under investigation. However, the occurrence of a 2:1 ratio of phosphine oxides to europium(III), observed for molecular compounds, is not necessarily confirmed in the current system. The low amount of approx. four functional phosphine oxides per chain, combined with possible steric hindrance by additional side groups in the polymer or the rigid backbone suggest a mixture of 2:1 and 1:1 coordination ratios.



Figure 6.16: Photograph of the potential Eu(III)/Pt(II)-SCNPs, exhibiting luminescent character, pointing towards an incorporation of europium(III).

After performing the coordination reaction, the polymeric material was irradiated at $\lambda = 365$ nm, showing a bright red luminescence as typical for a europium(III) compound (Figure 6.16).^[258]

To confirm the assumption of orthogonal metal coordination and probe the chain compaction, the potential Eu(III)/Pt(II)-SCNPs were thoroughly investigated.

The expected collapse into a more compact structure upon platinum(II) incorporation was verified by SEC (THF, RI) analysis (Figure 6.17). Indeed, the peak maximum of the trace of $P_{P/Oxide}$ at $M_p = 41\,400\text{ g}\cdot\text{mol}^{-1}$ was reduced to $M_p = 30\,800\text{ g}\cdot\text{mol}^{-1}$ for the Eu(III)/Pt(II)-SCNPs, indicated by a shift of the trace towards longer retention times. Hence, the coordination of the phosphine units in the precursor polymer towards the platinum(II) centers ensures a decrease of the hydrodynamic radius, resulting in the formation of single-chain nanoparticles. Important to mention is the detection of a signal at very high retention times in the detection limit (not shown here). Likely this signal originates from free europium complexes, which were released from former Eu–phosphine oxide bonds, which are not sufficiently strong to withstand the conditions of SEC measurements. Consequently, the depicted SEC trace represents the trace of Pt(II)-SCNPs.

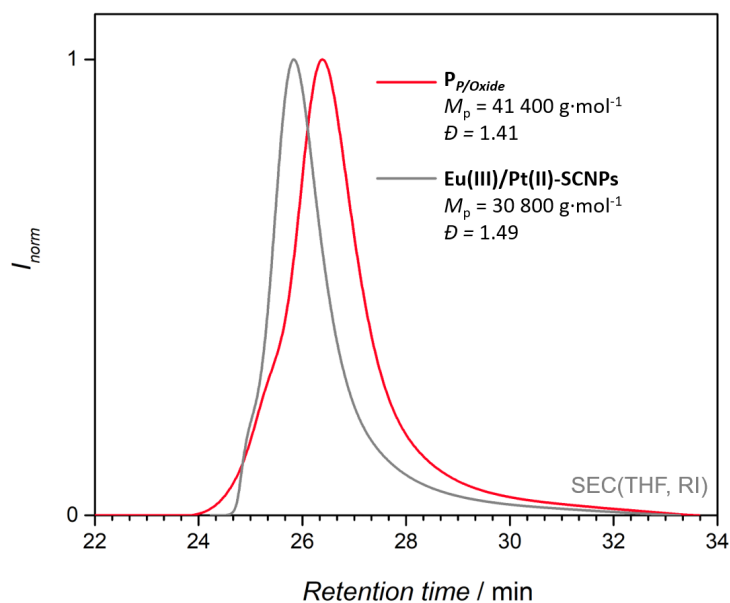


Figure 6.17: SEC traces (THF, RI) of $P_{P/Oxide}$ and the Eu(III)/Pt(II)-SCNPs. The trace of the nanoparticles is shifted towards higher retention time, synonymous with a smaller hydrodynamic radius in comparison to the precursor polymer. Hence, the SEC data indicates a collapse of the polymer chain into a more compact structure upon metal encapsulation.

To further confirm the collapse into a more compact particle, the terpolymer and the SCNPs were characterized by diffusion ordered spectroscopy (DOSY), measured in CDCl_3 . Based on the obtained diffusion coefficients, the hydrodynamic radii of the precursor polymer and the nanoparticle were calculated, applying the Stokes–Einstein Equation. First results indicate a hydrodynamic radius (r_H) of 3.6 ppm for $\text{P}_{\text{P}/\text{Oxide}}$, reduced to $r_H = 1.9$ ppm for the $\text{Eu(III)}/\text{Pt(II)}$ -SCNPs, verifying a chain compaction of over 40 %.

Additionally, the folding unit in the $\text{Eu(III)}/\text{Pt(II)}$ -SCNPs was characterized by various NMR experiments. In the $^{31}\text{P}\{^1\text{H}\}$ NMR spectrum (CDCl_3), characteristic resonances for a phosphine–platinum species were observed (Figure 6.18) analogous to the Pt(II) -SCNPs in Chapter 3. Thereby, the former resonance of the triarylphosphine species at $\delta = -6.2$ ppm is not detected. Instead, an intense resonance at $\delta = 13.5$ ppm appears, accompanied by platinum(II) satellites ($d, {}^1J_{\text{P,Pt}} = 3661$ Hz) and attributed to a *cis* phosphine–platinum(II) species. Another less intense resonance at $\delta = 19.5$ ppm is assigned to the *trans*-species. Both chemical shifts are in agreement with the data of the former Pt(II) -SCNPs and literature reported values.^[214] Comparing the integrals of the resonances for the *cis*- and *trans*-complexes, a ratio of approx. 30:1 *cis:trans* is calculated. The high preference for a *cis*-geometry in the $\text{Eu(III)}/\text{Pt(II)}$ -SCNPs was rationalized by the predetermined coordination of the precursor complex *cis*- $[\text{PtCl}_2(\text{cod})]$.

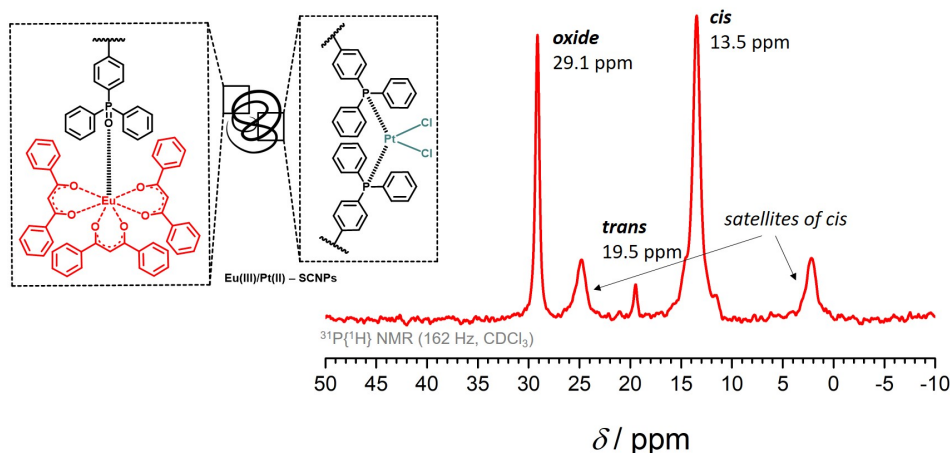


Figure 6.18: $^{31}\text{P}\{^1\text{H}\}$ NMR spectrum of the $\text{Eu(III)}/\text{Pt(II)}$ -SCNPs, depicting characteristic resonances for a *cis*- and *trans*-coordination of phosphine to platinum(II) at $\delta = 13.5$ ppm and $\delta = 19.5$ ppm, respectively. A comparison of their corresponding integrals reveals a *cis:trans* ratio of approx. 30:1. The preference for a *cis*-coordination is most likely based on the predetermined coordination of the precursor complex *cis*- $[\text{PtCl}_2(\text{cod})]$. In addition, the resonance at $\delta = 29.1$ ppm is attributed to phosphine oxide. Its slight broadening is presumably caused by its coordination to the paramagnetic europium(III) cores, pointing towards a successful complexation. A phosphine oxide:europium(III) ratio of 1:1 is depicted in the chemical structure.

Furthermore, the resonance at $\delta = 29.1$ ppm, corresponding to the phosphine oxide moiety, is still present. However, in comparison with the former resonance of the terpolymer, the peak shape changed and is now broader, hence partially blends with the baseline. The thus resulting decrease in integral value is presumably caused by the coordination of the triarylphosphine oxide to the paramagnetic europium cores.

In the corresponding ^{195}Pt NMR spectrum, a triplet resonance for a platinum–phosphine coordination is detected at $\delta = -4420$ ppm ($t, {}^1J_{\text{Pt,P}} = 3715$ ppm) (Figure 6.19). The chemical shift and the coupling constant are in high agreement with former reported values for the Pt(II)-SCNPs (Chapter 3). Based on literature reported values, the resonance is referenced to a *cis* Pt–phosphine species.^[205] Due to the low amount of complexes exhibiting *trans*-geometry, no resonance for this species is detected.

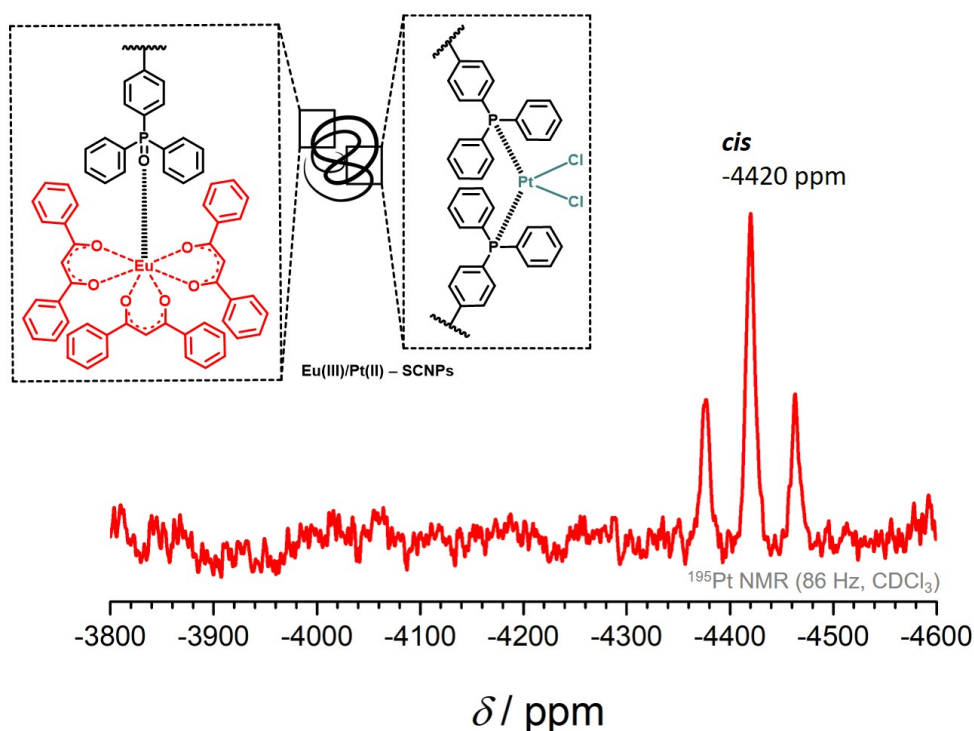


Figure 6.19: ^{195}Pt NMR spectrum of the Eu(III)/Pt(II)-SCNPs, depicting a characteristic resonance for a *cis*-coordination of platinum to phosphine at $\delta = -4420$ ppm. The low amount of *trans*-species prevents the detection of a corresponding resonance.

The coordination of $[\text{Eu}(\text{dbm})_3(\text{H}_2\text{O})_2]$ to the phosphine oxide moieties in $\text{P}_{\text{P/Oxide}}$ is additionally evidenced in the ^1H NMR spectrum (Figure 6.20). The resonance at $\delta = 16.9$ ppm is attributed to the $-\text{CH}-$ group of the DBM ligands. Additionally obtained new sets of resonances in the region between $\delta = 8.1-7.5$ ppm are assigned to the aromatic protons of the DBM ligands. Besides the first indications for a successful europium(III) incorporation, further on-going 2D NMR studies performed by Pavleta Tzvetkova (KIT), investigate possible crosspeaks between DBM and the polymer framework. As demonstrated in the project of phenanthroline–europium coordination (Chapter 4.9), the 2D NMR experiments can evidence successful lanthanide incorporation by cross-signals between the DBM ligand and the protons of the polymer backbone, only occurring for metal complexes coordinated to the polymer framework.

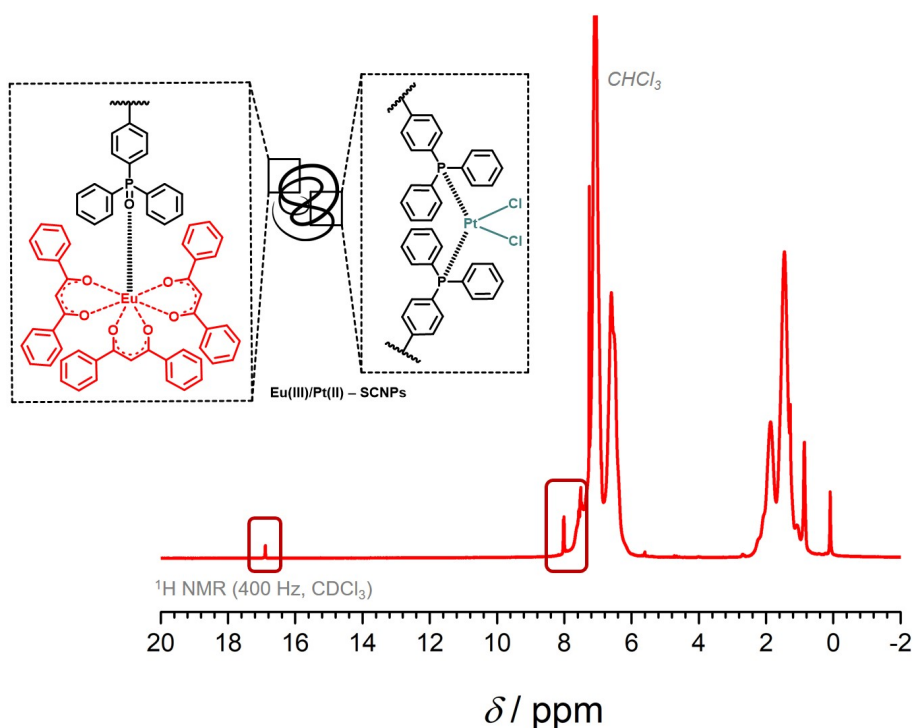


Figure 6.20: ^1H NMR spectrum of the $\text{Eu}(\text{III})/\text{Pt}(\text{II})\text{-SCNPs}$. New resonances at $\delta = 16.9$ ppm and in the region between $\delta = 8.1-7.5$ ppm are assigned to protons of the DBM ligand in the europium complex. Their detection points towards a successful encapsulation of europium by $\text{P}_{\text{P/Oxide}}$.

Further confirmation for the incorporation of the europium complex was provided by IR spectroscopy. Characteristic bands for the DBM ligand are detected at $\tilde{\nu} = 1519 \text{ cm}^{-1}$, 1549 cm^{-1} and 1600 cm^{-1} . Analogous bands are obtained in the IR spectrum of the precursor complex $[\text{Eu}(\text{dbm})_3(\text{H}_2\text{O})_2]$ pointing towards its encapsulation by $\text{P}_{\text{P/Oxide}}$. For the $\text{Eu}(\text{III})/\text{Pt}(\text{II})$ -SCNPs, the intensity of the bands belonging to the triarylphosphine oxide moieties at $\tilde{\nu} = 1202 \text{ cm}^{-1}$ and 1118 cm^{-1} decreased upon $\text{Eu}(\text{III})$ coordination. However, an exact assignment of the bands was complicated under the current conditions and not possible. Nonetheless, the IR analysis confirms the results of the ^1H NMR and $^{31}\text{P}\{^1\text{H}\}$ spectroscopy, indicating a $[\text{Eu}(\text{dbm})_3]$ implementation.

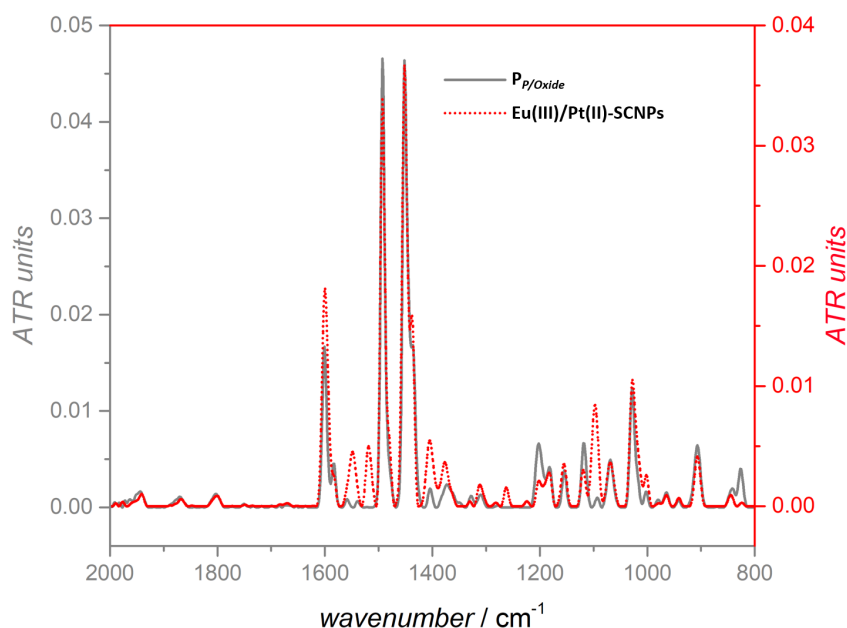


Figure 6.21: Superimposition of the IR spectra of $\text{P}_{\text{P/Oxide}}$ and the $\text{Eu}(\text{III})/\text{Pt}(\text{II})$ -SCNPs. New bands at $\tilde{\nu} = 1519 \text{ cm}^{-1}$ and 1549 cm^{-1} are attributed to the DBM ligand of the europium complex, indicating its incorporation into the polymeric framework. In addition, the band at $\tilde{\nu} = 1600 \text{ cm}^{-1}$ increased, speculatively by the vibrational stretching mode of the C=O bonds in the DBM ligands. (The spectra are referenced to the intensity of the band at $\tilde{\nu} = 1028 \text{ cm}^{-1}$.)

6.5 Summary

Similar to the first system, herein a terpolymer consisting of two divergent ligand moieties phosphines and phosphine oxides was synthesized. Employing the precursor complexes [PtCl₂(cod)] and [Eu(dbm)₃(H₂O)₂], an orthogonal linkage formation between platinum(II) with phosphines and europium(III) with phosphine oxides was ensured. Due to the orthogonal behavior of both precursor complexes, the coordination reaction was performed in one single step. Thereby, platinum(II) coordinated in a 1:2 ratio to the phosphine units, inducing a chain collapse. The coordination ratio of europium to phosphine oxide was yet not completely determined, however a mixture of 1:1 and 1:2 metal-to-ligand ratios was assumed.

Subsequently, the potential Eu(III)/Pt(II)-SCNPs were analyzed with regard to the formation of a more compact structure and orthogonal linkage formation. The collapse into a nanoparticle induced by metal coordination was revealed by SEC and DOSY measurements. In addition, characteristic resonances in the ¹H, ³¹P{¹H} and ¹⁹⁵Pt NMR spectra, combined with IR analysis verified a platinum(II) and europium(III) incorporation into the polymeric framework.

The current project is still in progress. Open questions regard for instance the ratio of coordinated phosphine oxide species with europium(III) cores. In addition, further evidence for an europium(III) incorporation by 2D NMR experiments will be gathered. Finally, the luminescence of the Eu(III)/Pt(II)-SCNPs in comparison to the molecular complexes has to be recorded, since a quantum yield enhancement for the current system is reported for similar molecular complexes in the literature.^[307, 308]

Conclusion

The present thesis demonstrated the synthesis of several metallopolymers and metal-complexed single-chain nanoparticles (SCNPs), employing four ligand moieties and various transition metals and lanthanides. In conclusion, phosphine, nitrogen and oxygen based ligand moieties were implemented into well-defined polymer chains, ready to coordinate to metal cores. Depending on the type of ligand and metal ion, different metal-to-ligand ratios occurred, resulting in either a metal decoration of the polymer chain, in the case of a 1:1 ratio, or in a metal-induced chain collapse, if more than one ligand coordinated to one metal center. In each system, the structural arrangement of the polymeric framework and the metal-complexed unit was investigated *via* several analytic methods such as NMR, IR and Raman spectroscopy, SEC and mass spectrometry.

Chapter 3 addressed the synthesis of phosphine containing copolymers, collapsing into nanoparticles upon coordination to platinum(II) cores in a 2:1 ligand-to-metal ratio. Here, catalytically active Pt(II)-SCNPs were obtained. Their application as homogeneous catalysts was demonstrated in the amination of allyl alcohol. In a direct comparison with the molecular catalyst, no reduction in catalytic activity was observed. Hence, although the metal centers were surrounded by a polymer framework, good access for the starting material was provided. Utilizing the characteristics of polymers to dissolve or precipitate depending on the solvent polarity, appropriate selection of reaction conditions allowed facile isolation and purification of the Pt(II)-SCNPs after their application as a catalyst. In a subsequently performed second catalytic cycle, the reused SCNPs remained catalytically active. Thus, in this project a homogeneous, recyclable SCNPs catalyst was generated, switching on demand between catalytic activity and heterogeneous recyclability.

The challenging and ambitious topic of synthesizing phenanthroline (Phen) functionalized polymer systems, hence nitrogen-based moieties, was reported in Chapter 4, aiming to showcase the ability of Phen as a versatile complexing ligand in polymeric architectures. To be able to predict and determine the degree of functionalization in the polymers, Phen-containing monomers for a polar and a non-polar polymer system were established. Followed by their copolymerization *via* NMP with appropriate

comonomers, the acrylamide DMAA and styrene, respectively, yielded the polar copolymer P_{polar} and the non-polar system P_{np} .

The suitability of P_{polar} for SCNP formation was demonstrated, utilizing the transition metals iron(II) and nickel(II) for the generation of Fe(II)- and Ni(II)-SCNP, respectively. Beyond those two examples, the versatility of Phen, coordinating to almost every transition metal, allows this copolymer system to be a future platform for further metal-complexed SCNPs resulting in functional soft matter material with numerous application possibilities.

On the basis of the second system P_{np} , the tuning of optical properties of the polymer was investigated when coordinating the Phen moieties in a 1:1 metal-to-ligand ratio to lanthanides, e.g. europium(III) and terbium(III). Upon irradiation at $\lambda = 350$ nm, luminescent material was obtained, exhibiting higher quantum yields than the simple molecular lanthanide complexes. One-step monomer synthesis, facile copolymer generation in arbitrary monomer ratios and feasible metal complexation makes the present system a perfect opportunity for further applications, such as potential lanthanide shift reagents (LSR) in enhanced NMR studies.^[313]

The project in Chapter 5 demonstrated a facile pathway to encapsulate dinuclear metal cores of copper(II) and molybdenum(II) in one folding unit, employing polymers containing benzoic acid moieties in a styrene-based backbone. In the complexation step, the benzoic acid groups turned into carboxylates and replaced acetate ligands from the dinuclear metal precursor complexes, taking advantage of a facile ligand exchange reaction. Thereby, the carboxylate ligands acted as bidentate bridging moieties between two metal cores, creating the ambitious structure of a paddlewheel inside the polymer framework. Following the described reaction procedure, single-chain nanoparticles containing dimetallic folding units of M_2^{4+} were obtained. This exceptional folding mechanism yielded high levels of crosslinking with 4–6 ligand moieties per each folding unit. In addition, the synthetic strategy allowed the encapsulation of two metal cores in close proximity, thereby, depending on the type of metal, creating metal–metal bonds inside SCNP structures. The parallel synthesis of molecular model complexes facilitated the analysis and confirmation of the structural arrangement.

This project is one of the few examples employing more than one metal core per crosslinking unit. Moreover, the incorporated metal ions were located in such a close proximity that they could interact with each other. In the case of copper, each core separately exhibits paramagnetic behavior, however due to their constrained vicinity they can turn into diamagnetic species, making them interesting for NMR studies.^[277] For molybdenum, reactive quadruple metal–metal bonds were formed, readily applicable for the activation of C–H bonds in cross-coupling reactions.^[281]

A topic of high future potential was introduced in Chapter 6. Based on the knowledge of the aforementioned projects, the possibility to incorporate more than one type of metal into one polymer chain was carefully investigated. Therefore, the behavior of metal ions towards different types of ligand moieties, previously established, was examined to combine suitable ligand–metal pairs in one system, allowing orthogonal coordination. Overall, two pathways towards heterometallic SCNPs were presented, combining the properties of each metal core in one polymer nanoparticle.

In the first system, carboxylic acids and phosphines coordinated to copper(II) and gold(I), respectively, resulting in Au(I)/Cu₂(II)-SCNPs. Thereby, two potentially catalytically active metal cores were employed. While the application of copper(II) as a catalyst in a paddlewheel carboxylate environment has been demonstrated in the literature,^[314] the next steps address the exchange of the currently employed precursor complex [AuC₆F₅(tbt)] by a more activated complex such as [AuCl(tbt)] to investigate its catalytic properties. Nevertheless, this system marks the first step towards multi-step catalysis, combining two catalytically active metal cores in one polymer framework.

Besides the synthesis of Au(I)/Cu₂(II)-SCNPs, in the second approach, the initially created Pt(II)-SCNP system was extended by phosphine oxide units which coordinated to europium(III). These linker units did not only behave contrarily to the phosphine moieties, favoring a coordination exclusively to europium(III) instead of platinum(II), they are also reported to enhance the quantum yield of the coordinated Eu(III)- β -diketonates. Consequently, a luminescent catalytically active Eu(III)/Pt(II)-SCNP system was generated, with the potential to track the presence of the polymeric systems by simple UV/Vis irradiation.

The logical extension of the herein presented projects envisions a two-step folding of the single-chains by encapsulating two types of metal cores, which both intramolecularly link the polymer chain into a nanoparticle. As performed for the heterometallic system in Chapter 6, an appropriate combination of metal ions and ligand moieties is expedient. The pathway for such an approach is depicted in Figure 7.1, showing a two-step folding process into a twice folded nanoparticle.

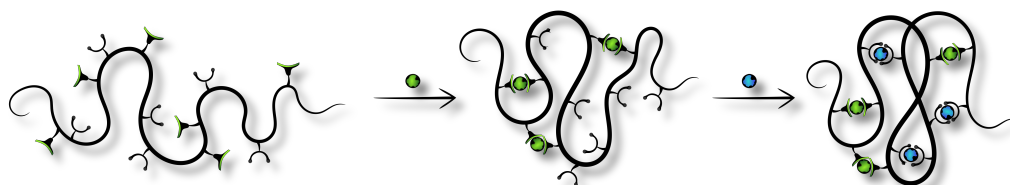


Figure 7.1: The current thesis envisions as a next step in SCNP chemistry, the utilization of two metal cores, both inducing a chain collapse by exhibiting a minimum ligand-to-metal ratio of 2:1, resulting in twice folded, metal-complexed SCNPs.

Herein, not only suitable pairs of orthogonal linker units and metal ions are essential to allow for a directed metal incorporation, also the appropriate amount of functional groups in each chain has to be established. Otherwise, the rigid backbone impedes the second folding step. Interesting studies can be performed by varying the amount of each functional unit and observe the consequences on the chain folding. Furthermore, the influence on the chain compaction, dependent on the order of metal core addition, can be investigated. First ideas for such a system employ phosphine moieties and carboxylic acid groups as in the Au(I)/Cu₂(II)-SCNPs, yet herein were completed by the metal cores platinum(II) and zirconium(IV). For molecular structures, stable complexes between acids and zirconium(IV) in a 2:1 ratio ligand-to-metal ratio are reported.^[315] Yet their application in polymer systems is still outstanding.

The Future of Catalytically Active SCNPs

To date, a series of metal crosslinked SCNP systems have been established and examined to some extent in initial catalytic studies, demonstrating promising results in terms of catalytic activity, product selectivity or substrate specificity.

However, despite high synthetic effort, the folded structure of today's SCNPs reflects only an intrinsically disordered protein structure. The reason is the inhomogeneity of the precursor polymer chains, regarding the size distribution, the degree of functionalization and the statistical placement of functional groups. These conditions cause an undirected chain collapse, yielding disperse nanoparticles of different shapes. However, when using SCNPs as catalytic systems, an influence of the shape of the nanoparticles on their activity, selectivity and specificity is highly probable. Moreover, different substrates require a different catalytic environment. The key term, therefore, is a 'catalytic pocket design' referring to the creation of a tailor-made polymer scaffold around the catalytic centers, adjusted to the desired reaction conditions. A proposed step towards a controlled chain collapse are orthogonal ligand moieties, restricting the amount of potential reaction partners.

In a further step towards obtaining nanoparticles of a similar shape, the synthesis of SCNPs could be performed in a two phase system, when creating block copolymers of different solubility within the same chain. Such environmental restrictions might support the directed metal encapsulation by simply reducing the amount of available functional groups in the polymer chain for each type of metal. This specific case

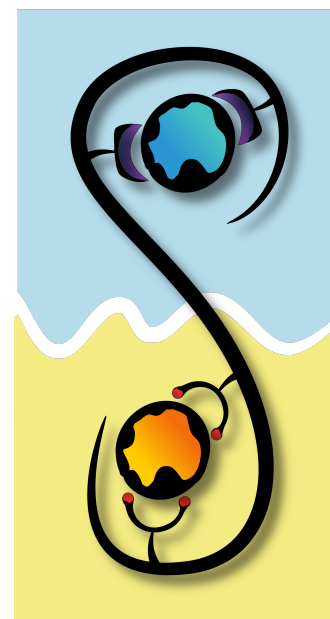


Figure 8.1: Block copolymers exhibiting different solubility behaviors, enable directed metal encapsulation combined with potential application as phase-transfer catalyst for reactions in solvent media of divergent polarity. Adapted from [8] with permission of the American Chemical Society.

is of potential interest for the catalysis of reactions in varying solvent media or cascade reactions, in which the starting material and the product exhibit different solubility behaviors. A conceivable structure of such heterometallic, amphiphilic SCNPs is graphically depicted in Figure 8.1, proposing the interesting application of SCNPs as a phase-transfer catalyst.

Besides influencing metal encapsulation and chain collapse by outer-sphere parameters, the ideal approach towards uniform SCNP formation lies in the synthesis of sequence-defined polymers containing the same amount of functional units at the same positions. In combination with the aforementioned options of orthogonal functional units, supported by divergent solvent environments, a directed metal incorporation into the chains, yielding uniform SCNPs, is enabled. For simplified reasons, first approaches can even employ oligomers with a reduced amount of functional groups to investigate subsequent nanoparticle formation. Finally, compartmentalized SCNPs equal in shape and function is a promising chemical approach for the high-throughput manufacturing of identical catalytic systems with protein-inspired bioprecision.

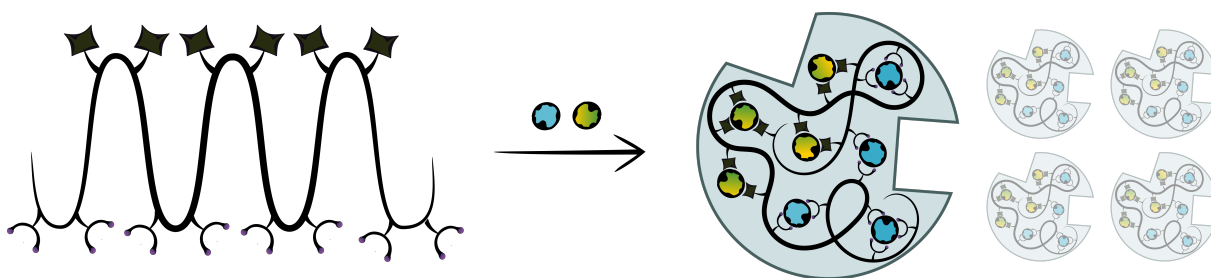


Figure 8.2: Future SCNPs: Unimolecular polymer chains, consisting of judiciously placed orthogonal functionalities, allow the generation of heterometallic SCNPs, which are equal in shape and thus function. This graphic is reproduced from Rothfuss*, H; Knoefel*, N. D.; Roesky, P. W.; Barner-Kowollik, C. *J. Am. Chem. Soc.* **2018**, *140*, 5875-5881. Copyright 2018 American Chemical Society.

Experimental Section

9.1 Materials

4-Methyl-1,10-phenanthroline (97 %, Sigma-Aldrich), lithium diisopropylamide (97 %, Sigma-Aldrich), (3-bromopropoxy)-tert-butyldimethylsilane (97 %, abcr), tetra-*n*-butylammonium fluoride (1.0 M in THF, Sigma-Aldrich), trimethylamine (for synthesis, 99.5 %, Roth), acryloyl chloride (Merck), dichloro(1,5-cyclooctadiene) palladium(II) (abcr), iron(II) sulfate heptahydrate (VWR Chemicals), nickel(II) sulfate hexahydrate (VWR Chemicals), terbium(III) acetylacetonate hydrate (99.9 %, abcr), europium(III) chloride hexahydrate (99.9 %, Sigma-Aldrich), 2,2'-azobis(2-methylpropionitril) (Merck), tris(dibenzoylmethane)mono(1,10-phenanthroline)europium(III) (95 %, Sigma-Aldrich), dibenzoylmethane (98 %, Acros Organics), 5-amino-1,10-phenanthroline (Toronto Research Chemicals), potassium carbonate (Alfa Aesar), selenium dioxide (99.99 %, Sigma Aldrich), TEMPO (98 %, Acros), sodium borohydride (> 98.0 %, Sigma-Aldrich), succinic anhydride (98 %, Sigma-Aldrich), pyridine (anhydrous, 99.8 %, Sigma-Aldrich), 4-chlorobutyl chloride (99 %, Sigma-Aldrich), magnesium sulfate (Roth), Celite (Hyflo Supercel, Merck, particle size < 0.1 mm), sodium bicarbonate (Roth), sodium chloride (Roth), N,N,N',N'',N''-pentamethyldiethylenetriamine (PMDETA) (for synthesis, 98 %, Merck), (1-bromoethyl)benzene (Merck), copper(I)bromide (99.9 %, Acros), TEMPO (98 %, Acros), 4-(diphenylphosphino)styrene (97 %, Sigma Aldrich), triphenylphosphine (for synthesis, Merck), dichloro(1,5-cyclooctadiene) platinum(II) (99 %, Alfa Aesar), *cis*-dichlorobis(triphenylphosphine)-platinum(II) (99 %, abcr), bis(triphenylphosphine)palladium(II)-dichloride (98 %, Sigma Aldrich), aniline (99 %, Alfa Aesar), 3-chloroaniline (99 %, Sigma Aldrich), 3-fluoroaniline (98 %, Acros), 4-chloroaniline (98 %, Acros), 2,6-dimethylaniline (99 %, abcr), tin(II)chloride (98 %, Acros), ferrocene (98 %, Sigma Aldrich), 4-vinylbenzoic acid (> 97 %, TCI), 4-ethylbenzoic acid (99 %, Alfa Aesar), copper(II) acetate monohydrate (99.9 %, Alfa Aesar), molybdenum hexacarbonyl (98 %, Sigma-Aldrich), acetic acid-d₃ (99.5 atom % D, Acros Organics), acetic anhydride-d₆ (99 atom % D, Sigma-Aldrich) and allyl alcohol (99 %, Sigma Aldrich) were used as received.

Chloroform-d₁ (CDCl₃, 99.8 %, Sigma-Aldrich), dimethylsulfoxide-d₆ (DMSO-d₆, 99.8 %, EURISO-TOP), benzene-d₆ (C₆D₆, 99.5 %, EURISO-TOP), tetrahydrofuran (THF), methanol (MeOH),

ethanol (EtOH), dimethylformamide (DMF), diethyl ether (Et₂O), anisole, chloroform (CHCl₃), dimethyl sulfoxide (DMSO), 1,4-dioxane and dichloromethane (DCM) were purchased as analytical grade and used as received.

Prior to use, dimethyl sulfoxide (DMSO) was distilled under nitrogen from CaH₂ and methanol (MeOH) was distilled under nitrogen from magnesium. Employed for NMR analysis of moisture and oxygen-sensitive substances, DMSO-d₆ was distilled from CaH₂ prior to use, and stored over molecular sieves (4 Å). CDCl₃ was distilled, degassed and stored over molecular sieves (4 Å). THF-d₈ was stored over a Na/K alloy. Styrene (Merck), *N,N*-dimethylacrylamide (99 %, Sigma Aldrich) and 1-(chloromethyl)-4-vinylbenzene (90.0 %, TCI) were passed through a column of basic alumina (Acros) and stored at -19 °C. Toluene (99.85 %, water < 30 ppm, extra dry, Acros Organics) was used as received. Tetrahydrofuran (THF) was dried using an MBraun solvent purification system (SPS-800) and additionally distilled under nitrogen from potassium before storage over 4 Å molecular sieves. Dichloromethane (DCM) (99.9 %, water < 30 ppm, stabilized with amylene, extra dry, Acros Organics) was additionally dried over calcium hydride and subsequently distilled.

For the laboratory dialysis “Standard Grade Regenerated Cellulose Dialysis Membranes (Spectra/Por6) Prewetted RC tubing” of spectrumbiol.com with a molecular weight cut off (MWCO) of 2 kD were applied.

Reactions and characterization methods of all molybdenum compounds were performed under exclusion of moisture and oxygen in flame-dried Schlenk-type glassware or in an argon-filled MBraun glovebox.

The Blockbuilder MAMA-SG1® (N-(2-methylpropyl)-N-(1-diethylphosphono-2,2-dimethylpropyl)-O-(2-carboxylprop-2-yl)hydroxylamine) and SG1 (N-tert-butyl-N-[1-diethylphosphono-(2,2-dimethylpropyl) nitroxide]) were kindly supplied by the group of Dr. Guillaume Delaittre.

9.1.1 Literature Known Molecular Structures

The following compounds, employed in the current thesis as precursor complexes or model complexes for polymeric structures, were synthesized by Nicolai Knöfel, following literature-known procedures: [Mo(OAc)₂]₄,^[287] [AuC₆F₆(tbt)],^[303] [Eu(dbm)₃(H₂O)₂]^[306] and 4-(diphenylphosphine oxide)styrene.^[316] The deuterated complex [Mo(OAc)₂]₂-d₁₂ was synthesized according to a procedure described for the non-deuterated complex, employing deuterated acetic acid and acetic anhydride.^[287]

9.2 Instrumentals

NMR spectroscopy

NMR spectra were recorded on a Bruker Avance II 300, 400 or 600 MHz NMR and Ascend 400 MHz Ft-NMR spectrometers. ^1H and $^{13}\text{C}\{^1\text{H}\}$ NMR chemical shifts were referenced to the residual solvent resonances of CHCl_3 ($\delta = 7.26$ ppm), DMSO ($\delta = 2.50$ ppm) or THF- d_8 ($\delta = 3.58$ ppm) and are reported relative to tetramethylsilane (TMS) (^1H), 85 % H_3PO_4 (^{31}P) or 1.2 M Na_2PtCl_6 in D_2O (^{195}Pt). ^2H NMR measurements were performed in non-deuterated THF. Abbreviations used in the description of the materials' syntheses include singlet (s), broad singlet (bs), doublet (d), triplet (t), quartet (q) and unresolved multiplet (m). Especially in polymers or upon coordination to metal ions, often the splitting of the resonances can not be determined and is therefore labeled as 'broad resonance' (br).

The diffusion coefficients of the Pt(II)-, Cu(II)- and Mo(II)-SCNPs and their corresponding precursor polymers were recorded in cooperation with Nicolai Knöfel, from the group of Prof. Dr. Peter Roesky, recorded on the Bruker Avance 400. The ^{195}Pt NMR spectra were recorded by Helga Berberich.

The diffusion coefficients for the compounds containing phenanthroline and the NOESY and TOCSY spectra of the lanthanide metallopolymers were recorded by Dr. Pavleta Tzvetkova, from the group of Prof. Dr. Burkhard Luy, using a Bruker 400 MHz Avance III HD spectrometer on a BBIF inversely detected $^1\text{H}/^{19}\text{F}$, BB double resonance room temperature probe head with actively shielded z-gradients. The temperature was controlled via a Bruker Smart VT unit and was calibrated to be exactly 300 K. The diffusion coefficients were measured with Diffusion Ordered NMR Spectroscopy (DOSY) experiments using bipolar gradient pulses and stimulated echo with or without longitudinal eddy current delay (STEBP or LEDBP).^[144]

Size-exclusion chromatography (SEC)

SEC traces for the non-polar copolymers and corresponding SCNPs containing Pt(II), Cu(II) and Eu(III)/Pt(II) metal complexes were recorded on a Polymer Laboratories PL-GPC 50 Plus Integrated System, including an autosampler, a PLgel 5 μm bead-size guard column (50 mm \times 7.5 mm) followed by one PLgel 5 μm Mixed E column (300 mm \times 7.5 mm), three PLgel 5 μm Mixed C columns (300 mm \times 7.5 mm) and a differential refractive index detector using THF as the eluent. The device was operated at 35 $^\circ\text{C}$ with a flow rate of 1 mL \cdot min $^{-1}$. For the calibration of the SEC system, linear polystyrene standards with molecular weights ranging from 160 g \cdot mol $^{-1}$ to 6 \times 10 6 g \cdot mol $^{-1}$ were employed. The molecular weight was calculated with the Mark-Houwink parameters for polystyrene ($K = 14.4 \times 10^{-5}$; $a = 0.70$).^[317] No baseline correction was performed. Consequently, M_n and \bar{D} values are estimates.

Additional SEC measurements for the non-polar compounds of the phenanthroline project were performed on an instrument equipped with multi angle laser light scattering (SEC-MALLS) from Polymer Standards Service, PSS, in Mainz, Germany. The SEC equipment is from the Agilent 1200 series, and the MALLS unit is the PSS SLD7000/BI-MwA, Brookhaven Instruments. The SEC measurements used THF as the solvent at 25 °C and a flow rate of 1 mL · min⁻¹. The SEC columns from PSS (SDV-Lux-1000 Å and 105 Å, 5 µm) were calibrated using linear PS standards ranging from 476 to 2.5 × 10⁶ g · mol⁻¹. Typically, 100 µL of a sample solution with a concentration between 0.7 and 3 mg · mL⁻¹ was injected onto the columns. The absolute weight-averaged molecular weight, M_w , was determined via the MALLS detector.

SEC traces for polar compounds were analyzed in N,N-dimethylacetamide (DMAc) containing 0.03 wt % LiBr as eluent at a flow rate of 1 mL · min⁻¹ with a sample concentration of 2 g · L⁻¹ on a Polymer Laboratories PL-GPC 50 Plus Integrated system comprising an autosampler, a PLgel 5.0 µm bead-size guard column (50 mm × 7.5 mm) followed by three PLgel 5 µm MixedC columns (300 mm × 7.5 mm) and a differential refractive index detector. The SEC system was calibrated against linear poly(methyl methacrylate) standards with molar masses ranging from 700 to 2 × 10⁶ Da. The samples were filtered through PTFE membranes with a pore size of 0.2 µm prior to injection. To obtain M_n and \bar{D} values, the integration of the polymer peak was carried out from low elution times to approx. 33 minutes due to overlap with an SEC system peak. No baseline correction was performed. Consequently, M_n and \bar{D} values are estimates.

Dynamic light scattering (DLS)

The DLS measurements were carried out on a Nicomp 380 DLS spectrometer from Particle Sizing Systems, Santa Barbara, USA (laser diode: 90 mW, 658 nm). The polymer solutions were prepared by dissolving the polymer samples in chloroform or THF at a concentration of 6 mg · mL⁻¹ for both, linear polymers and SCNPs. Before being analyzed, the solutions were filtered over a 0.2 µm filter. The measurements were performed in automatic mode at 25 °C and evaluated by a standard Gaussian and an advanced evaluation method, the latter using an inverse Laplace algorithm that allows to analyze multimodal distributions (NICOMP). Normally, the threshold is set to 3 %, if not otherwise indicated. Numbers given in text are the number weighted average values as calculated by the NICOMP evaluation. All measurements were determined at 90° to the incident beam.

Infra-red (IR) spectrometry

IR spectra were obtained on a Bruker Tensor 37 FTIR spectrometer, equipped with a room temperature DLaTGS detector and a diamond ATR (attenuated total reflection) unit in cooperation

with Nicolai Knöfel. Abbreviations used in the compounds' analysis include very strong (vs), strong (s), medium (m), weak (w) and very weak (vw).

Raman spectra were recorded by Nicolai Knöfel on a Bruker MultiRam spectrometer. Abbreviations used in the compounds' analysis include very strong (vs), strong (s), medium (m), weak (w) and very weak (vw).

Elemental analyses were carried out with an Elementar Micro Cube.

High resolution/orbitrap electrospray ionization mass spectrometry (ESI MS).

Mass spectra were recorded on a Q Exactive (Orbitrap) mass spectrometer (Thermo Fischer Scientific, San Jose, CA, USA) equipped with a HESI II probe. The spectrum was recorded in positive mode and the analyte was dissolved in a THF/MeOH or DCM/MeOH solution (3:2, doped with 100 μmol sodium trifluoroacetate, $c = 0.01 \text{ g} \cdot \text{mL}^{-1}$). The instrument was calibrated in the m/z range 74–1822 using premixed calibration solutions (Thermo Scientific). The Fourier-Transform resolution was set to 140 000. A constant spray voltage of 3.6 kV and a dimensionless sheath gas of 5 were applied. The capillary temperature and the S-lens RF level were set to 320 °C and 68.0, respectively. The flow rate was set to $5 \mu\text{L} \cdot \text{min}^{-1}$.

Ultraviolet/visible (UV/Vis) spectrometry

UV/Vis spectra of the compounds in the phenanthroline project were recorded on a Cary 100 UV-Visible Spectrophotometer (Agilent Technologies, USA) equipped with a tungsten halogen light source (190 to 900 nm, accuracy $\pm 2 \text{ nm}$) and a R928 PMT detector. Spectra were recorded in MeOH at 20 °C and collected between 200 and 800 nm. Samples were baseline corrected in respect to the pure solvent.

UV/Vis spectra of the project about paddlewheel structures and bimetallic compounds were recorded on a VARIAN Cary 50 Scan UV/Visible Spectrophotometer. Spectra were recorded in THF at room temperature and collected between 200 and 800 nm. Samples were baseline corrected with respect to the pure solvent. For the $\text{Cu}_2(\text{II})$ species a concentration of approx. $0.5 \text{ mg} \cdot \text{mL}^{-1}$ was applied and for the $\text{Mo}_2(\text{II})$ species a concentration of approx. $0.1 \text{ mg} \cdot \text{mL}^{-1}$.

Steady state spectroscopy in solution

The investigations of steady state absorption properties were performed by Nadine Michenfelder, from the group of Dr. Unterreiner, employing a Cary 500 UV/Vis-NIR spectrophotometer (Varian). Spectra were recorded in DCM (99.9 %, Roth) between 200 and 800 nm at ambient temperature in cuvettes made of fused silica (Suprasil, Hellma) with 10 mm optical path length, which were also used for fluorescence measurement. Concentrations lie between 0.01 and $0.06 \text{ mmol} \cdot \text{L}^{-1}$. Fluorescence

spectra were measured with a FluoroMax-4 spectrometer (Horiba Scientific) at 20 ± 0.1 °C with 3 nm slit widths for excitation as well as for detection from 365 nm for the Eu compound and 295 nm for the Tb compound to 800 nm. Fluorescence spectra were scaled to an optical density (OD) of 0.1 for better comparison. The concentration of absorber units was calculated based on the estimation of one phen moiety every 50th polymer unit in PB. To determine fluorescence quantum yields (QY), 4-(dicyanomethylene)-2-methyl-6-(4-dimethylaminostyryl)-4H-pyran (DCM) dye for the Eu complexes and coumarin 153 for the Tb complexes dissolved in EtOH (99.9 %, Merck) (QY: 40-50 %) were used as standards.^[318, 319] Due to the high Stokes shift in the complexes, standards are chosen with respect to the spectral range of the fluorescence of the complexes. The very low fluorescence QYs of the compounds compared to the dyes lead to an error of up to 30 % for the obtained values (especially for the lowest QYs on the order of 0.1 %).

Time resolved spectroscopy in solution

Transient absorption measurements with femtosecond (fs) time resolution were performed by Nadine Michenfelder, from the group of Dr. Unterreiner, with fundamental laser pulses from an Astrella laser system (Coherent) with a central wavelength of 800 nm (34 fs pulses, energies of 7 mJ, 1 kHz repetition rate). Using a non-collinear optical parametric amplifier followed by frequency doubling in a beta-barium-borate crystal, pulses of 350 nm wavelength could be generated from a small fraction of the fundamental beam, which were chopped at half of the repetition rate. These pulses served for excitation of the sample under magic angle conditions at various computer-controlled delay times. To probe at a spectral range between 350 and 700 nm a white light continuum was generated by focusing another part of the fundamental beam into a calcium fluoride crystal. After the sample, these pulses were detected by a CCD line scan camera (series 200, Entwicklungsbüro Stresing) and averaged over 1000 scans to optimize the signal to noise ratio. The pump-induced change of the optical absorbance, ΔA , was obtained by subtraction of spectra with and without pump pulse, before they were further analyzed by in-house written LabVIEW software. Samples were stirred with a micro fish in a quartz glass cuvette with 1 mm optical path length (Suprasil, Hellma) and an optical density, OD, between 1.2 and 1.5.

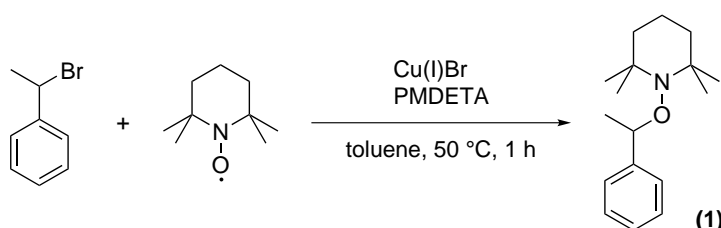
Single-crystal X-Ray diffraction (XRD)

For the analysis via XRD, a suitable crystal was covered in mineral oil (Aldrich) and mounted on a glass fiber. The crystal was transferred directly to the cold stream of a STOE IPDS 2 or a STOE StadiVari diffractometer. All structures were solved by using the program SHELXS/T^[320, 321] and Olex2.^[322] The remaining non-hydrogen atoms were located from successive difference Fourier map calculations. The refinements were carried out by using full-matrix least-squares techniques on F^2 by

using the program SHELXL. In each case, the locations of the largest peaks in the final difference Fourier map calculations, as well as the magnitude of the residual electron densities, were of no chemical significance. The XRD measurements were performed by Nicolai Knöfel.

9.3 Synthesis of Molecular Structures

9.3.1 Synthesis of 2,2,6,6-Tetramethyl-1-(1-phenylethoxy)-piperidine (1)



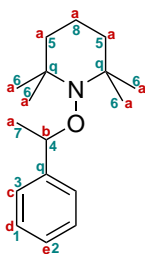
Scheme 9.1: Synthesis of the NMP initiator 2,2,6,6-tetramethyl-1-(1-phenylethoxy)-piperidine (1).

2,2,6,6-Tetramethyl-1-(1-phenylethoxy)-piperidine was synthesized in a procedure, similar described in the literature.^[207] Therefore, the starting material copper(I)bromide (0.84 g, 5.84 mmol, 1.20 equiv.) and N,N',N'',N''', N''''-pentamethyldiethylenetriamine (1.22 mL, 1.01 g, 5.84 mmol, 1.20 equiv.) were dissolved in 15 mL dry toluene in an evacuated round bottom flask. A second evacuated schlenk flask was equipped with TEMPO (0.84 g, 5.35 mmol, 1.10 equiv.), bromoethylbenzene (0.66 mL, 0.90 g, 4.86 mmol, 1.00 equiv.) and toluene (15 mL). The content of the second flask was added dropwise to the first flask. Subsequently, the reaction mixture was heated for 1 hour at 50 °C. After cooling to ambient temperature, the solution was filtered and concentrated under reduced pressure. The red supernatant was purified by column chromatography in toluene. The obtained oil was cooled over night at 5 °C, leading to the crystallization of the product. The resulting crystals were dried under high vacuum.

Table 9.1: Characterization of the NMP initiator 2,2,6,6-tetramethyl-1-(1-phenylethoxy)-piperidine (1).

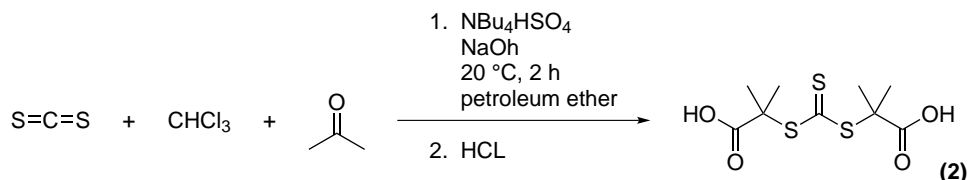
White crystals, obtained product: 0.91 g, yield: 75.6 %.

¹H NMR (400 MHz, CDCl₃): δ/ppm = 7.38–7.27 (m, 4H-c,d), 7.27–7.00 (m, 1H-e), 4.78 (q, ³J_{H,H} = 6.7 Hz, 1H-b), 1.66–0.60 (m, 21H-a).



¹³C{¹H} NMR (101 MHz, CDCl₃): δ/ppm = 145.8 (C-q), 128.0 (C-1), 126.8 (C-2), 126.6 (C-3), 83.1 (C-4), 59.7 (C-q), 40.4 (C-5), 34.5 (C-6), 34.1 (C-6), 23.6 (C-7), 20.3 (C-q), 17.24 (C-8).

9.3.2 Synthesis of 2,2'-(Thiocarbonylbis(sulfanediyl))bis(2-methylpropanoic acid) (TRITT, 2)

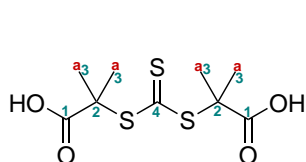


Scheme 9.2: Synthesis of 2,2'-(thiocarbonylbis(sulfanediyl))bis(2-methylpropanoic acid) (TRITT, 2).

In a procedure modified from the literature,^[233] a 500 mL two neck flask was equipped with acetone (17.2 g, 295 mmol, 2.50 equiv.), CHCl₃ (35.3 g, 295 mmol, 2.50 equiv.), NBu₄HSO₄ (0.80 g, 2.36 mmol, 0.02 equiv.) and 7.14 mL carbon disulfide (9.00 g, 118 mmol, 1.00 equiv.) in 50 mL petroleum ether. The solution was cooled down to <10 °C and stirred for 1 hour. While cooling, a 0.5 M solution of NaOH (67.0 mL) was added dropwise to the solution over a time period of 2–3 hours. The solution was stirred at ambient temperature overnight. Thereafter, 150 ml diluted HCl was added and the solution was purged with gaseous N₂ to remove non-reacted gaseous starting material. The yellow precipitate was filtered, washed with water and dried under high vacuum. The solid was purified *via* recrystallization in isopropanol/water 3:2 for four times.

Table 9.2: Characterization of 2,2'-(thiocarbonylbis(sulfanediyl))bis(2-methylpropanoic acid) (TRITT, 2).

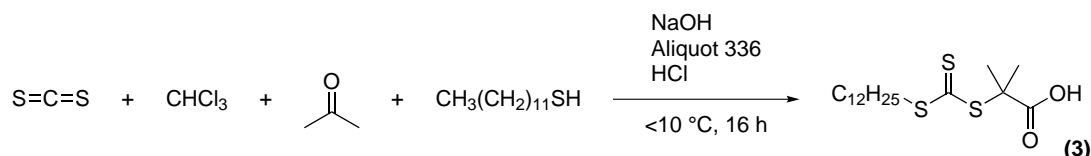
Yellow, crystalline powder, obtained product: 7.4 g, yield: 23 %.



¹H NMR (400 MHz, DMSO-d₆): δ/ppm = 12.91 (s, 1H, COOH), 1.59 (s, CH₃, 3H-a).

¹³C{¹H} NMR (101 MHz, DMSO-d₆): δ/ppm = 219.4 (C-4), 173.5 (C-1), 56.7 (C-2), 25.4 (C-3).

9.3.3 Synthesis of 2-(((Dodecylthio)carbonothioyl)thio)-2-methylpropanoic acid (DDMAT, 3)

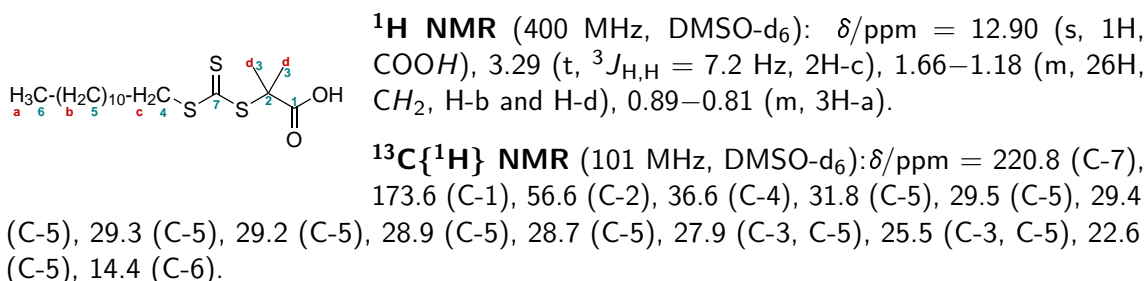


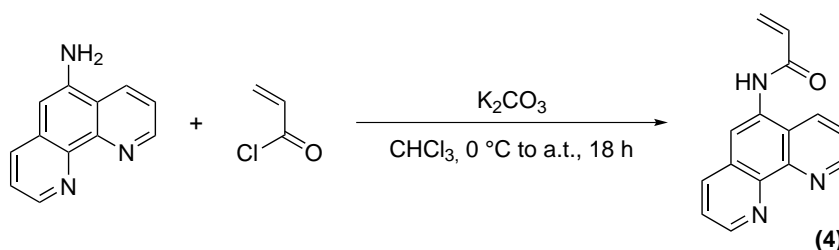
Scheme 9.3: Synthesis of 2-(((dodecylthio)carbonothioyl)thio)-2-methylpropanoic acid (DDMAT, 3).

According to the literature,^[234] dodecanthiol (8.70 g, 43.0 mmol, 1.00 equiv.) and Aliquot 336 (0.69 g, 786 mmol, 0.04 equiv.) were dissolved in 30 mL acetone (2.50 g, 43.0 mmol, 1.00 equiv.) in a 250 mL schlenk flask under the exclusion of oxygen. The flask was purged with gaseous N₂ and equipped with a dropping funnel, containing a 0.5 M solution of NaOH (1.89 g, 47.3 mmol, 1.10 equiv.). NaOH was added dropwise, while the solution was stirred. After 15 min, 2.60 mL carbon disulfide (3.27 g, 43.0 mmol, 1.00 equiv.) was dissolved in 5 mL acetone and added to the reaction mixture. The solution was stirred for 15 min. Thereafter, 5.20 mL CHCl₃ (7.70 g, 64.5 mmol, 1.50 equiv.) and 0.5 M NaOH (8.60 g, 215 mmol, 5.00 equiv) were added dropwise to the viscous mixture. After stirring over night, 65 mL distilled water and 10 mL concentrated HCl were added, until a pH level of 1 was reached. Remaining acetone was removed by flushing the solution with N₂. The brown solid was filtered off and dissolved in 100 mL isopropanol. Thereby, orange solid precipitated, which was filtered off and disposed. The red-colored solution was concentrated under reduced pressure, until yellow particles crystallized. The product was purified *via* recrystallization in cyclohexane.

Table 9.3: Characterization of 2-(((dodecylthio)carbonothioyl)thio)-2-methylpropanoic acid (DDMAT, 3).

Yellow crystals, obtained product: 3.00 g, yield: 19 %.



9.3.4 Synthesis of *N*-(1,10-phenanthroline-5-yl)acrylamide (4)Scheme 9.4: Synthesis of *N*-(1,10-phenanthroline-5-yl)acrylamide (4).

According to the literature,^[236] 5-amino-1,10-phenanthroline (1.50 g, 7.68 mmol, 1.00 equiv.) and K_2CO_3 (3.98 g, 28.8 mmol, 3.75 equiv.) were dissolved in 100 mL dry $CHCl_3$ in a 500 mL flask. The flask was equipped with a dropping funnel, containing 1.18 mL of acryloyl chloride (1.32 g, 14.6 mmol, 1.90 equiv.) in 100 mL dry $CHCl_3$. After stirring at 0 °C for 30 min, the acryloyl-chloride solution was added dropwise to the stirred solution within 2 hours. After complete addition, the reaction mixture was stirred for another 16 hours at ambient temperature. Thereafter, the red solution was washed three times with a 5 M $NaHCO_3$ solution, adjusting a pH level of 7 of the aqueous phase. The organic phase was dried over $MgSO_4$ and the solvent was removed under reduced pressure. The product was obtained as a orange, crystalline powder. If further purification was required, column chromatography (EtOH:DCM 4:6 + 1 % of Et_3N) was performed.

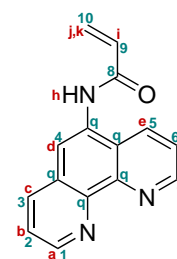
Table 9.4: Characterization of *N*-(1,10-phenanthroline-5-yl)acrylamide (4).

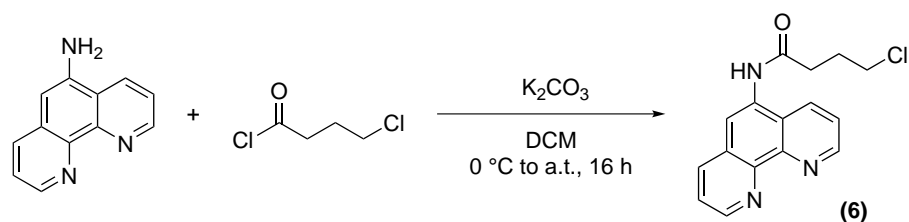
Orange, crystalline powder, obtained product: 2.11 g, yield: 95 %.

1H NMR (400 MHz, $DMSO-d_6$): $\delta/ppm = 10.37$ (s, 1H-h), 9.14 (dd, $^{3,4}J_{H,H} = 4.2, 1.6$ Hz, 1H-a), 9.04 (dd, $^{3,4}J_{H,H} = 4.3, 1.7$ Hz, 1H-g), 8.63 (dd, $^{3,4}J_{H,H} = 8.4, 1.6$ Hz, 1H-c), 8.46 (dd, $^{3,4}J_{H,H} = 8.2, 1.7$ Hz, 1H-e), 8.31 (s, 1H-d), 7.83 (dd, $^{3,3}J_{H,H} = 8.4, 4.2$ Hz, 1H-b), 7.75 (dd, $^{3,3}J_{H,H} = 8.1, 4.3$ Hz, 1H-f), 6.75 (dd, $^{3,4}J_{H,H} = 17.0, 10.2$ Hz, 1H-i), 6.37 (dd, $^{3,4}J_{H,H} = 17.0, 1.9$ Hz, 1H-j), 5.88 (dd, $^{3,4}J_{H,H} = 10.2, 1.9$ Hz, 1H-k).

$^{13}C\{^1H\}$ NMR (101 MHz, $DMSO-d_6$): $\delta/ppm = 164.8$ (C-8), 150.3 (C-1), 149.5 (C-7), 145.7 (C-q), 143.6 (C-q), 136.9 (C-5), 132.4 (C-3), 132.1 (C-9), 132.0 (C-q), 128.6 (C-q), 128.0 (C-10), 125.0 (C-q), 124.2 (C-6), 123.5 (C-2), 120.3 (C-4).

ESI-MS: $[M+H^+]/z_{exp.} = 250.0967$, $[M+H^+]/z_{theo.} = 250.0975$.

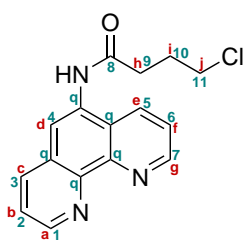


9.3.5 Synthesis of 4-Chloro-*N*-(1,10-phenanthroline-5-yl)butane amide (5)Scheme 9.5: Synthesis of 4-chloro-*N*-(1,10-phenanthroline-5-yl)butane amide (5).

5-Amine-1,10-phenanthroline (1.00 g, 5.12 mmol, 1.00 equiv.) and K_2CO_3 (5.66 g, 41.0 mmol, 8.00 equiv.) were dissolved in 30 mL dry DCM in a flame-dried round bottom flask and cooled to 0 °C. 4-Chlorobutyryl chloride (1.15 mL, 1.42 g, 41.0 mmol, 8.00 equiv.) was dissolved in 10 mL dry DCM and added dropwise to the reaction mixture *via* a dropping funnel. After complete addition, the reaction mixture was left to warm up to ambient temperature and stirred overnight. Thereafter, the reaction mixture was washed two times with saturated $NaHCO_3$ solution. The organic layer was dried with Na_2SO_4 , filtered and the solvent was removed under reduced pressure.

Table 9.5: Characterization of 4-chloro-*N*-(1,10-phenanthroline-5-yl)butane amide (5).

Ocher colored solid, obtained product: 1.19 g, yield: 77 %.



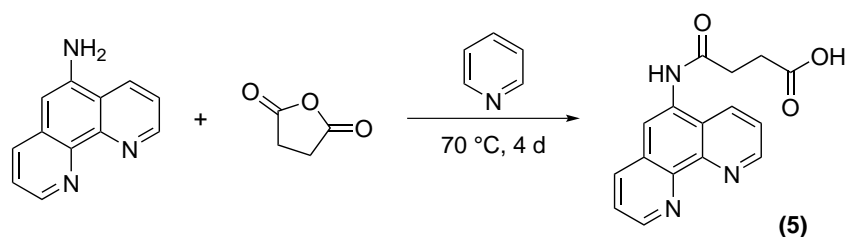
1H NMR (400 MHz, $DMSO-d_6$): $\delta/ppm = 10.92$ (s, 1H, NH), 9.30 (dd, $^3,4J_{H,H} = 4.6, 1.4$ Hz, 1H-a), 9.24 (dd, $^3,4J_{H,H} = 8.6, 1.4$ Hz, 1H-c), 9.19 (dd, $^3,4J_{H,H} = 5.1, 1.5$ Hz, 1H-g), 9.09 (dd, $^3,4J_{H,H} = 8.4, 1.4$ Hz, 1H-b), 8.58 (s, 1H-d), 8.23–8.14 (m, 2H-e,f), 3.78 (t, $^3J_{H,H} = 6.8$ Hz, 2H-j), 2.83 (t, $^3J_{H,H} = 7.2$ Hz, 2H-h), 2.18–2.11 (m, 2H-i).

$^{13}C\{^1H\}$ NMR (101 MHz, $DMSO-d_6$): $\delta/ppm = 172.4$ (C-8), 149.4 (C-1), 145.7 (C-7), 143.0 (C-2), 139.1 (C-q), 136.5 (C-3), 135.6 (C-q), 134.2 (C-q), 130.0 (C-q), 126.0 (C-5), 125.8 (C-q), 125.6 (C-6), 118.6 (C-4), 45.5 (C-11), 33.7 (C-10), 28.5 (C-9).

IR (ATR): $\tilde{\nu}$ [cm^{-1}] = 3200-2400 (br), 1687 (s), 1596 (m), 1535 (vs), 1493 (s), 1457 (m), 1415 (m), 1386 (m), 1365 (m), 1327 (m), 1316 (m), 1302 (w), 1231 (s), 1196 (m), 1184 (m), 1148 (w), 1109 (vw), 1060 (vw), 1044 (w), 1031 (w), 1002 (vw), 980 (w), 954 (vw), 895 (vw), 857 (s), 840 (m), 815 (m), 798 (m), 724 (s), 640 (m), 620 (m), 596 (m), 561 (w), 541 (w), 520 (vw), 473 (w), 436 (m).

ESI-MS: $[M+H^+]/z_{exp.} = 300.0892$, $[M+H^+]/z_{theo.} = 300.0898$.

9.3.6 Synthesis of 4-((1,10-Phenanthroline-5-yl)amino)-4-oxobutanoic acid (6)



Scheme 9.6: Synthesis of 4-((1,10-phenanthroline-5-yl)amino)-4-oxobutanoic acid (6).

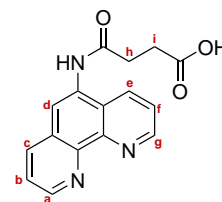
Taking basic information from a procedure described in the literature,^[131] 1,10-phenanthroline-5-amine (0.49 g, 2.51 mmol, 1.00 equiv.), succinic anhydride (302 mg, 3.01 mmol, 1.20 equiv.) and 30 mL dry pyridine were added to a flame-dried round bottom flask. The reaction mixture was stirred at 70 °C for 4 days. Thereafter, pyridine was removed under reduced pressure and the residue was dissolved in 25 mL MeOH and stored at 5 °C for 3 days. Formed crystals were separated from the supernatant solution, washed two times with MeOH and dried under vacuum.¹

Table 9.6: Characterization of 4-((1,10-phenanthroline-5-yl)amino)-4-oxobutanoic acid (6).

Off-white solid, obtained product: 1.71 g, yield: 68 %.

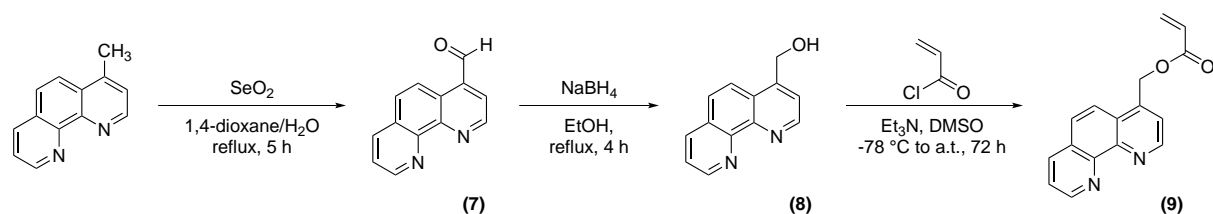
¹H NMR (400 MHz, DMSO-d₆): δ/ppm = 12.24 (bs, 1H, COOH), 10.20 (s, 1H, NH), 9.12 (dd, ^{3,4}J_{H,H} = 4.2, 1.6 Hz, 1H-a), 9.03 (dd, ^{3,4}J_{H,H} = 4.3, 1.8 Hz, 1H-g), 8.65 (dd, ^{3,4}J_{H,H} = 8.4, 1.7 Hz, 1H-e), 8.44 (dd, ^{3,4}J_{H,H} = 8.2, 1.8 Hz, 1H-c), 8.15 (s, 1H-d), 7.80 (dd, ^{3,3}J_{H,H} = 8.4, 4.3 Hz, 1H-f), 7.73 (dd, ^{3,3}J_{H,H} = 8.1, 4.3 Hz, 1H-b), 2.79 (t, ³J_{H,H} = 6.7 Hz, 2H-i), 2.62 (t, ³J_{H,H} = 6.7 Hz, 2H-h).

¹³C{¹H} NMR (101 MHz, DMSO-d₆): δ/ppm = 173.9, 171.4, 149.8, 149.2, 145.8, 143.8, 135.7, 131.8, 131.8, 128.1, 124.7, 123.5, 122.8, 120.0, 30.7, 29.0.



¹The synthesis was performed by Sergej Baraban.

9.3.7 Synthesis of (1,10-Phenanthroline-4-yl)methyl acrylate (9)



Scheme 9.7: Reaction pathway for (1,10-phenanthroline-4-yl)methyl acrylate (9) via a three step synthesis.

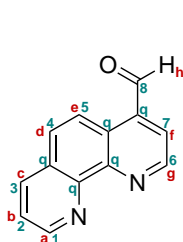
Step 1

Synthesis of 1,10-phenanthroline-4-carbaldehyde (7)

According to the literature,^[323] selenium dioxide (0.71 g, 6.37 mmol, 2.25 equiv.) was suspended in a mixture of 1,4-dioxane/water (10.0 mL/0.02 mL) in a 500 mL flask equipped with a reflux column and a dropping funnel on top. 4-Methyl-1,10-phenanthroline (0.55 g, 2.83 mmol, 1.00 equiv.) was dissolved in 1,4-dioxane/water (40.0 mL/2.00 mL) and added to the funnel. The suspension, containing selenium dioxide, was stirred and heated to reflux. Over 2 hours, the content of the dropping funnel was added dropwise to the solution. After complete addition, the reaction mixture was refluxed for additional 5 hours. Stirring overnight, the suspension was filtered through celite, resulting in a yellow solution. The organic phase was separated, dried and concentrated under reduced pressure. After a few hours, yellow crystals formed at ambient pressure.

Table 9.7: Characterization of 1,10-phenanthroline-4-carbaldehyde (7).

Yellow crystals, obtained product: 465 mg, yield: 92 %.



¹H NMR (400 MHz, DMSO-*d*₆): δ /ppm = 10.69 (s, 1H-h), 9.42 (d, ³*J*_{H,H} = 4.3 Hz, 1H-g), 9.16 (dd, ^{3,4}*J*_{H,H} = 4.3, 1.8 Hz, 1H-a), 8.98 (d, ³*J*_{H,H} = 9.2 Hz, 1H-d), 8.55 (dd, ^{3,4}*J*_{H,H} = 8.1, 1.7 Hz, 1H-c), 8.24 (d, ³*J*_{H,H} = 4.4 Hz, 1H-f), 8.20 (d, ³*J*_{H,H} = 9.2 Hz, 1H-e), 7.84 (dd, ^{3,4}*J*_{H,H} = 8.1, 4.3 Hz, 1H-b).

¹³C{¹H} NMR (101 MHz, DMSO-*d*₆): δ /ppm = 194.8 (C-8), 151.1 (C-1), 151.0 (C-6), 147.0 (C-q), 145.6 (C-q), 137.2 (C-q), 136.7 (C-3), 129.8 (C-4), 128.6 (C-q), 126.2 (C-7), 125.1 (C-q), 124.4 (C-2), 122.4 (C-5).

Step 2

Synthesis of (1,10-Phenanthroline-4-yl)methanol (8)

In a procedure similar described in the literature,^[324] 1,10-phenanthroline-4-carbaldehyde (7) (460 mg, 2.21 mmol, 1.00 equiv.) was dissolved in 200 mL absolute EtOH and degassed for 20 min with N₂. NaBH₄ (41.8 mg, 1.10 mmol, 0.50 equiv.) was dissolved in 100 mL absolute EtOH and added to the reaction mixture while stirring. After refluxing for 4 hours, the solution was cooled to ambient temperature and stirred overnight. The solution was concentrated under reduced pressure. Upon addition distilled water, a grey solid precipitated. The precipitate was washed with water and removed from the solvent mixture *via* centrifugation and filtering. The final product was recrystallized from MeOH.

Table 9.8: Characterization of (1,10-phenanthroline-4-yl)methanol (8).

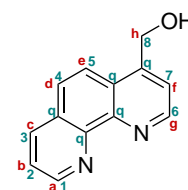
Gray solid, obtained product: 162 mg, yield: 34 %.

¹H NMR (400 MHz, DMSO-d₆): δ/ppm = 9.10 (dd, ^{3,4}J_{H,H} = 4.3, 1.8 Hz, 1H-a), 9.07 (d, ³J_{H,H} = 4.5 Hz, 1H-g), 8.50 (dd, ^{3,4}J_{H,H} = 8.1, 1.8 Hz, 1H-c), 8.09 (d, ³J_{H,H} = 9.1 Hz, 1H-d), 8.01 (d, ³J_{H,H} = 9.1 Hz, 1H-e), 7.82 (d, ³J_{H,H} = 4.5 Hz, 1H-f), 7.77 (dd, ^{3,4}J_{H,H} = 8.1, 4.3 Hz, 1H-b), 5.68 (t, ³J_{H,H} = 5.5 Hz, 1H-OH), 5.16–5.08 (d, ³J_{H,H} = 5.5 Hz, 2H-h).

¹³C{¹H} NMR (101 MHz, DMSO-d₆): δ/ppm = 150.5 (C-1), 150.2 (C-6), 148.3 (C-q), 146.3 (C-q), 145.6 (C-q), 136.5 (C-3), 128.5 (C-q), 126.9 (C-5), 126.2 (C-q), 123.7 (C-2), 122.7 (C-4), 120.7 (C-7), 60.4 (C-8).

IR (ATR): $\tilde{\nu}$ [cm⁻¹] = 3213 (br), 2898 (vw), 1615 (vw), 1585 (w), 1563 (vw), 1508 (m), 1415 (s), 1382 (m), 1362 (m), 1304 (vw), 1255 (vw), 1227 (w), 1158 (w), 1140 (vw), 1102 (s), 1076 (s), 1042 (w), 984 (m), 951 (vw), 889 (w), 849 (s), 831 (s), 787 (m), 737 (vs), 700 (s), 622 (m), 605 (m), 580 (m), 557 (w), 500 (m), 467 (m), 437 (m), 412 (w).

ESI-MS: [M+H⁺]/z_{exp.} = 211.0860, [M+H⁺]/z_{theo.} = 211.0866.



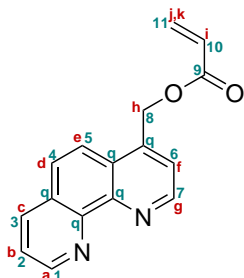
Step 3

Synthesis of (1,10-Phenanthroline-4-yl)methyl acrylate (9)

500 mg of (1,10-phenanthroline-4-yl)methanol (8) (2.38 mmol, 1.00 equiv.) was suspended in a mixture of 80.0 mL DCM and 4.0 mL DMSO. After cooling to $-78\text{ }^{\circ}\text{C}$, a solution of Et_3N (361 mg, 3.57 mmol, 1.50 equiv.) in 20 mL DCM was added. After 10 minutes, a solution of acryloyl chloride (332 mg, 3.57 mmol, 1.50 equiv.) in DCM was slowly added. The reaction was stirred for 6 hours at ambient temperature. Thereafter, the solution was again cooled to $-78\text{ }^{\circ}\text{C}$ and additional 0.50 equivalents of both Et_3N and acryloyl chloride, dissolved in DCM, were added. Subsequently, the mixture was stirred for 3 days at ambient temperature. Afterwards, the yellow solution was concentrated under reduced pressure and washed consecutively with 1 M NaOH solution, saturated NaHCO_3 solution, saturated brine and water. The organic phase was dried with MgSO_4 , filtered and dried under high vacuum. The obtained yellow solid was additionally washed three times with 10 mL n-pentane.

Table 9.9: Characterization of (1,10-phenanthroline-4-yl)methyl acrylate (9).

Yellow solid, obtained product: 480 mg, yield: 76 %.



^1H NMR (400 MHz, DMSO-d_6): δ/ppm = 9.12 (dd, $^3J_{\text{H,H}} = 4.2$, 1.8 Hz, 1H-a), 9.10 (d, $^3J_{\text{H,H}} = 4.4$ Hz, 1H-g), 8.52 (dd, $^3J_{\text{H,H}} = 7.8$, 1.8 Hz, 1H-c), 8.12 (d, $^3J_{\text{H,H}} = 9.1$ Hz, 1H-d), 8.07 (d, $^3J_{\text{H,H}} = 9.1$ Hz, 1H-e), 7.79 (dd, $^3J_{\text{H,H}} = 7.8$, 4.2 Hz, 1H-b), 7.77 (d, $^3J_{\text{H,H}} = 4.4$ Hz, 1H-f), 6.45 (dd, $^3J_{\text{H,H}} = 17.3$, 1.4 Hz, 1H-j), 6.33 (dd, $^3J_{\text{H,H}} = 17.3$, 10.4 Hz, 1H-i), 6.05 (dd, $^3J_{\text{H,H}} = 10.4$, 1.4 Hz, 1H-k), 5.82 (s, 2H-h).

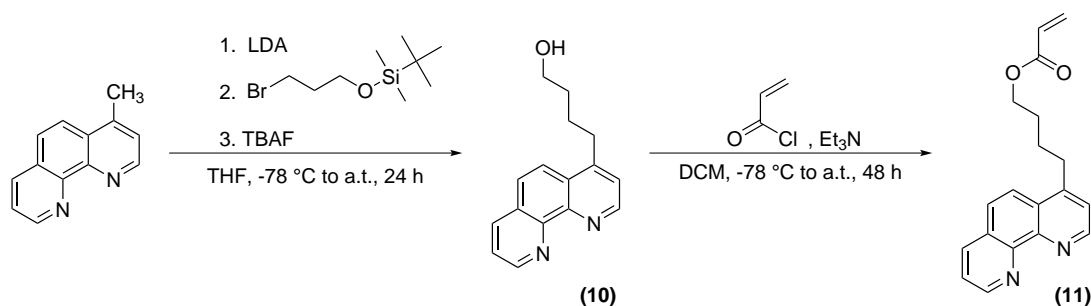
$^{13}\text{C}\{^1\text{H}\}$ NMR (101 MHz, DMSO-d_6): δ/ppm = 165.6 (C-9), 150.7 (C-1), 150.2 (C-7), 146.1 (C-q), 141.9 (C-q), 136.6 (C-3), 133.1 (C-11), 128.6 (C-q), 128.3 (C-10), 127.7 (C-5), 126.4 (C-q), 124.0 (C-2), 122.5 (C-4), 122.2 (C-6), 63.1 (C-8). – one quart. carbon atom is not visible, probably due to overlaying signals.

IR (ATR): $\tilde{\nu}$ [cm^{-1}] = 3028 (vw), 2988 (vw), 2920 (vw), 2852 (vw), 1726 (vs), 1637 (w), 1618 (m), 1585 (m), 1561 (m), 1511 (m), 1497 (m), 1445 (w), 1415 (m), 1401 (s), 1383 (m), 1295 (s), 1206 (vs), 1138 (m), 1098 (m), 1067 (m), 1016 (w), 985 (m), 951 (m), 922 (w), 892 (vw), 849 (s), 825 (s), 805 (s), 779 (m), 725 (s), 701 (m), 608 (m), 582 (w), 555 (vw), 531 (vw), 508 (w), 467 (vw), 422 (w).

ESI-MS: $[\text{M}+\text{H}^+]/z_{\text{exp.}} = 265.0964$, $[\text{M}+\text{H}^+]/z_{\text{theo.}} = 265.0972$.

Elemental analysis calcd. (%) for $[\text{C}_{16}\text{H}_{12}\text{N}_2\text{O}_2]$ ($264.28\text{ g}\cdot\text{mol}^{-1}$): C 72.72, H 4.58, N 10.60; found C 71.74, H 4.47, N 10.13.

9.3.8 Synthesis of 4-(1,10-Phenanthroline-4-yl)butyl acrylate (Phen-acrylate, 11)



Scheme 9.8: Two step synthesis for 4-(1,10-phenanthroline-4-yl)butyl acrylate (Phen-acrylate, 11).

Step 1

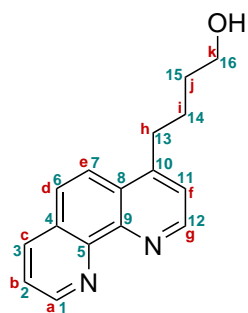
Synthesis of 4-(1,10-Phenanthroline-4-yl)butane-1-ol (10)

4-Methyl-1,10-phenanthroline (1.50 g, 7.72 mmol, 1.00 equiv.) was dissolved in 50 mL dry THF and cooled to $-78\text{ }^{\circ}\text{C}$. A solution of lithium diisopropylamide (0.99 g, 9.27 mmol, 1.20 equiv.) in 20 mL dry THF was added slowly to the reaction mixture, resulting in a red/purple colored solution. After stirring the mixture for 1 hour at $-78\text{ }^{\circ}\text{C}$, a solution of (3-bromopropoxy)-tert-butyldimethylsilane (2.25 g, 8.88 mmol, 1.15 equiv.) in 20 mL dry THF was added dropwise. The solution was stirred at ambient temperature for additional 24 hours. The reaction was quenched *via* addition of water, concentrated in vacuum and re-dissolved in DCM. After washing with water for 3 times, the organic phase was dried with MgSO_4 , filtered and concentrated in vacuum. A TBAF solution (1M in THF) (3.03 g, 11.6 mmol, 1.50 equiv.) was added and the mixture was stirred for 16 hours. Afterwards, the solvent was removed under reduced pressure and the remaining yellow oil was dissolved in DCM. The solution was washed with saturated NaHCO_3 solution, brine and water. The organic phase was dried with MgSO_4 , filtered and dried in vacuum. Finally, the yellow solid was additionally purified *via* flash column chromatography (DCM/MeOH 98:2).²

²The synthesis was performed by Nicolai Knöfel.

Table 9.10: Characterization of 4-(1,10-phenanthroline-4-yl)butane-1-ol (10).

Off-white solid, obtained product: 0.80 g, yield: 40 %.



^1H NMR (600 MHz, CDCl_3): $\delta/\text{ppm} = 9.19$ (dd, $^3,4J_{\text{H,H}} = 4.3, 1.5$ Hz, 1H-a), 9.07 (d, $^3J_{\text{H,H}} = 4.4$ Hz, 1H-g), 8.24 (dd, $^3,4J_{\text{H,H}} = 8.0, 1.6$ Hz, 1H-c), 8.05 (d, $^3J_{\text{H,H}} = 9.1$ Hz, 1H-e), 7.81 (d, $^3J_{\text{H,H}} = 9.1$ Hz, 1H-d), 7.63 (dd, $^3,3J_{\text{H,H}} = 8.0, 4.3$ Hz, 1H-b), 7.47 (d, $^3J_{\text{H,H}} = 4.5$ Hz, 1H-f), 3.74 (t, $^3J_{\text{H,H}} = 6.4$ Hz, 2H-k), 3.18 (t, $^3J_{\text{H,H}} = 7.8$ Hz, 2H-h), 1.96 – 1.85 (m, 2H-i), 1.79 – 1.70 (m, 2H-j).

$^{13}\text{C}\{^1\text{H}\}$ NMR (151 MHz, CDCl_3): $\delta/\text{ppm} = 150.3$ (C-12), 149.9 (C-1), 148.4 (C-10), 146.6 (C-5), 146.3 (C-9), 135.8 (C-3), 128.1 (C-4), 127.5 (C-8), 126.1 (C-6), 123.1 (C-11), 123.0 (C-2), 122.3 (C-7), 62.5 (C-16), 32.5 (C-13), 32.3 (C-15), 26.7 (C-14).

IR (ATR): $\tilde{\nu}$ [cm^{-1}] = 3314 (br), 3029 (w), 2930 (m), 2860 (m), 1617 (w), 1582 (m), 1561 (m), 1509 (s), 1499 (m), 1448 (w), 1417 (s), 1379 (m), 1342 (w), 1215 (vw), 1162 (vw), 1132 (vw), 1061 (s), 984 (w), 945 (vw), 835 (vs), 780 (m), 735 (s), 719 (s), 677 (m), 638 (s), 597 (m), 586 (m), 527 (w), 487 (m), 470 (w), 427 (w).

ESI-MS: $[\text{M}+\text{H}^+]/z_{\text{exp.}} = 253.1329$, $[\text{M}+\text{H}^+]/z_{\text{theo.}} = 253.1335$.

Elemental analysis calcd. (%) for $[\text{C}_{16}\text{H}_{16}\text{N}_2\text{O}]$ ($252.32 \text{ g} \cdot \text{mol}^{-1}$): C 76.16, H 6.39, N 11.10; found C 75.80, H 6.26, N 10.80.

Step 2

Synthesis of 4-(1,10-Phenanthroline-4-yl)butyl acrylate (Phen-acrylate, 11)

4-(1,10-Phenanthroline-4-yl)butane-1-ol (10) (0.45 g, 1.78 mmol, 1.00 equiv.) was dissolved in 50 mL DCM. The solution was cooled to $-78\text{ }^{\circ}\text{C}$ and a solution of Et_3N (0.27 g, 2.68 mmol, 1.50 equiv.) in 20 mL DCM was added. After 10 minutes, a solution of acryloyl chloride (0.24 g, 2.68 mmol, 1.50 equiv.) in DCM was added dropwise. Adjusting to ambient temperature, the reaction mixture was stirred for 48 hours. Then, the yellow solution was concentrated under reduced pressure and washed consecutively with 1 M NaOH solution, saturated NaHCO_3 solution, brine and water. The organic phase was dried with MgSO_4 , filtered and concentrated in vacuum. The remaining solution (in DCM) was poured into cold n-pentane. The solution was concentrated and the precipitate was subsequently filtered off. After drying in vacuum, a pale yellow solid was obtained.

Table 9.11: Characterization of 4-(1,10-phenanthroline-4-yl)butyl acrylate (Phen-acrylate, 11).

Off-white solid, obtained product: 415 mg, yield: 76 %.

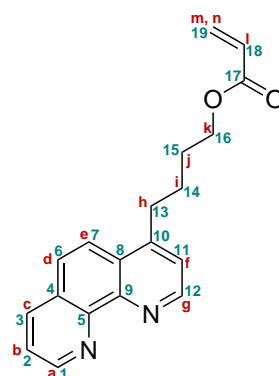
$^1\text{H NMR}$ (600 MHz, CDCl_3): $\delta/\text{ppm} = 9.24$ (dd, $^3,^4J_{\text{H,H}} = 4.3, 1.7$ Hz, 1H-a), 9.16 (d, $^3J_{\text{H,H}} = 4.6$ Hz, 1H-g), 8.29 (dd, $^3,^4J_{\text{H,H}} = 8.1, 1.7$ Hz, 1H-c), 8.06 (d, $^3J_{\text{H,H}} = 9.1$ Hz, 1H-e), 7.86 (d, $^3J_{\text{H,H}} = 9.1$ Hz, 1H-d), 7.67 (dd, $^3,^3J_{\text{H,H}} = 8.0, 4.3$ Hz, 1H-b), 7.53 (d, $^3J_{\text{H,H}} = 4.6$ Hz, 1H-f), 6.41 (dd, $^{2,^3}J_{\text{H,H}} = 17.3, 1.4$ Hz, 1H-m), 6.12 (dd, $^{3,^3}J_{\text{H,H}} = 17.3, 10.4$ Hz, 1H-l), 5.83 (dd, $^{2,^3}J_{\text{H,H}} = 10.4, 1.4$ Hz, 1H-n), 4.25 (t, $^3J_{\text{H,H}} = 6.3$ Hz, 2H-k), 3.23 (t, $^3J_{\text{H,H}} = 7.4$ Hz, 2H-h), $1.97\text{--}1.82$ (m, 4H-i,j).

$^{13}\text{C}\{^1\text{H}\}$ NMR (151 MHz, CDCl_3): $\delta/\text{ppm} = 166.3$ (C-17), 150.5 (C-1), 149.4 (C-12), 136.1 (C-3), 130.9 (C-19), 128.4 (C-18), 128.3 (C-9), 127.6 (C-8), 126.5 (C-6), 123.4 (C-2), 123.2 (C-11), 122.1 (C-7), 64.0 (C-16), 32.1 (C-13), 28.5 (C-15), 26.7 (C-14) - *three quart. carbon atoms (C-4, C-5, C-10) are not visible, due to overlaying signals.*

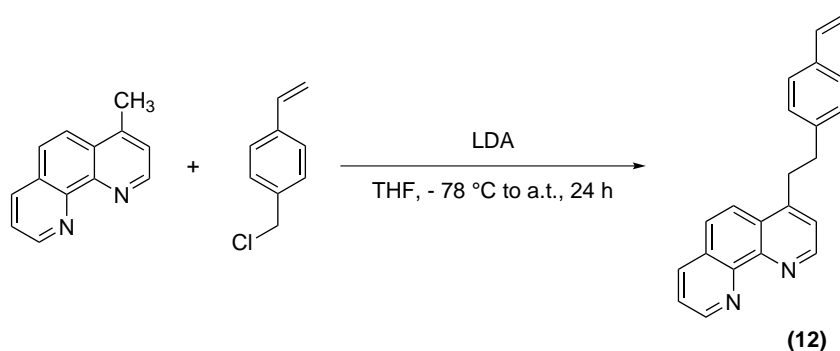
IR (ATR): $\tilde{\nu} [\text{cm}^{-1}] = 3061$ (vw), 3028 (vw), 2982 (vw), 2939 (w), 2900 (vw), 2867 (vw), 1710 (vs), 1616 (m), 1586 (m), 1564 (w), 1509 (m), 1464 (vw), 1429 (w), 1408 (s), 1326 (vw), 1284 (m), 1268 (m), 1213 (s), 1189 (s), 1161 (m), 1129 (m), 1101 (w), 1060 (m), 1042 (m), 994 (m), 982 (m), 960 (m), 936 (vw), 892 (vw), 843 (vs), 811 (s), 794 (m), 778 (m), 745 (m), 736 (s), 721 (m), 693 (w), 661 (vw), 618 (vw), 588 (m), 515 (vw), 491 (vw), 473 (vw), 433 (vw), 424 (vw).

ESI-MS: $[\text{M}+\text{Na}^+]/z_{\text{exp.}} = 329.1259$, $[\text{M}+\text{Na}^+]/z_{\text{theo.}} = 329.1260$.

Elemental analysis calcd. (%) for $[\text{C}_{19}\text{H}_{18}\text{N}_2\text{O}_2]$ ($306.37\text{ g}\cdot\text{mol}^{-1}$): C 74.49, H 5.92, N 9.14; found C 74.54, H 5.90, N 9.29.



9.3.9 Synthesis of 4-(4-Vinylphenethyl)-1,10-phenanthroline (Phen-styrene, 12)



Scheme 9.9: Synthesis of 4-(4-vinylphenethyl)-1,10-phenanthroline (Phen-styrene, 12).

Lithium diisopropylamide (0.40 g, 3.71 mmol, 1.20 equiv.) was dissolved in 20 mL dry THF and added slowly to a cooled solution ($-78\text{ }^{\circ}\text{C}$) of 4-methyl-1,10-phenanthroline (0.60 g, 3.09 mmol, 1.00 equiv.) in 50.0 mL THF. After stirring for 1 hour, 1-(chloromethyl)-4-vinylbenzene (0.54 g, 3.55 mmol, 1.15 mmol), dissolved in 10 mL dry THF, was added slowly to the dark red reaction mixture, while keeping the temperature at $-78\text{ }^{\circ}\text{C}$. The reaction mixture was stirred overnight at ambient temperature. Upon addition of 10.0 mL distilled water, the reaction was quenched. Remaining solid was removed *via* filtration. The yellow solution was concentrated and 30.0 mL DCM were added. The organic layer was subsequently washed with 20.0 mL of saturated NaHCO_3 solution and 20 mL water, dried with MgSO_4 , filtrated and concentrated to approx. 10 mL. The DCM solution was added dropwise into 200 mL cold n-pentane while stirring. The precipitate was removed *via* filtration and discarded. The filtrate was left at ambient pressure to slowly evaporate. After a few days, crystalline solid was obtained.³ A similar procedure is described in the literature.^[325]

³The synthesis was performed by Nicolai Knöfel.

Table 9.12: Characterization of 4-(4-vinylphenethyl)-1,10-phenanthroline (Phen-styrene, 12).

Yellow crystals, obtained product: 192 mg, yield: 20 %.

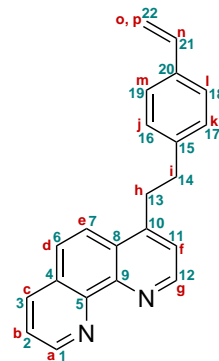
^1H NMR (600 MHz, CDCl_3): $\delta/\text{ppm} = 9.20$ (dd, $^3,4J_{\text{H,H}} = 4.3, 1.7$ Hz, 1H-a), 9.05 (d, $^3J_{\text{H,H}} = 4.5$ Hz, 1H-g), 8.24 (dd, $^3,4J_{\text{H,H}} = 8.0, 1.7$ Hz, 1H-c), 8.04 (d, $^3J_{\text{H,H}} = 9.1$ Hz, 1H-e), 7.81 (d, $^3J_{\text{H,H}} = 9.1$ Hz, 1H-d), 7.63 (dd, $^3,3J_{\text{H,H}} = 8.0, 4.3$ Hz, 1H-b), 7.37 (d, $^3J_{\text{H,H}} = 4.5$ Hz, 1H-f), 7.33 (d, $^3J_{\text{H,H}} = 8.0$ Hz, 2H-m,l), 7.13 (d, $^3J_{\text{H,H}} = 8.0$ Hz, 2H-j,k), 6.69 (dd, $^3,3J_{\text{H,H}} = 17.6, 10.9$ Hz, 1H-n), 5.72 (d, $^3J_{\text{H,H}} = 17.6$ Hz, 1H-p), 5.22 (d, $^3J_{\text{H,H}} = 10.9$ Hz, 1H-o), $3.49\text{--}3.30$ (m, 2H-h), $3.20\text{--}2.95$ (m, 2H-i).

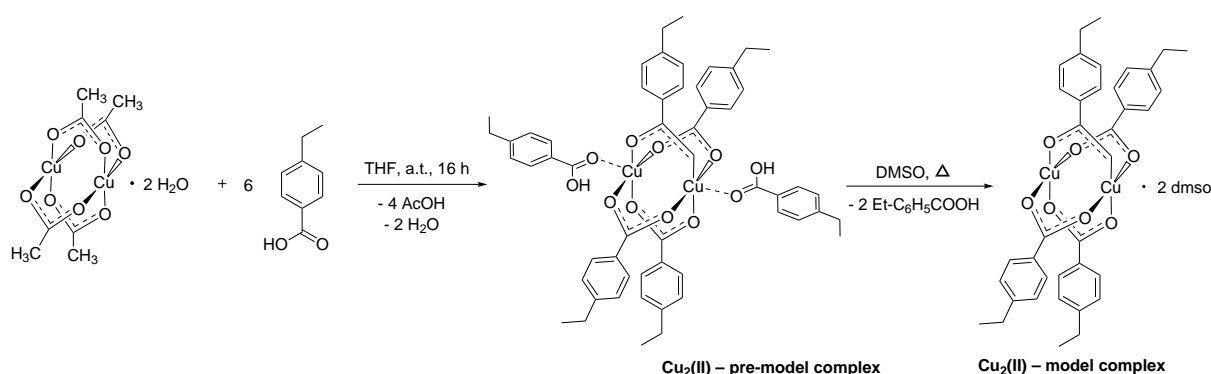
$^{13}\text{C}\{^1\text{H}\}$ NMR (151 MHz, CDCl_3): $\delta/\text{ppm} = 150.4$ (C-1), 149.9 (C-12), 147.4 (C-10), 146.7 (C-5), 146.3 (C-9), 140.3 (C-15), 136.5 (C-21), 135.8 (C-20), 135.8 (C-3), 128.6 (C-16,17), 128.1 (C-4), 127.4 (C-8), 126.4 (C-18,19), 126.2 (C-6), 123.2 (C-11), 123.0 (C-2), 122.1 (C-7), 113.4 (C-22), 36.2 (C-14), 34.4 (C-13).

IR (ATR): $\tilde{\nu} [\text{cm}^{-1}] = 3080$ (vw), 3020 (vw), 2998 (vw), 2946 (vw), 2925 (vw), 2898 (vw), 2862 (vw), 1615 (w), 1585 (m), 1561 (w), 1508 (m), 1451 (vw), 1407 (s), 1380 (w), 1285 (vw), 1259 (w), 1203 (vw), 1161 (w), 1128 (w), 1114 (w), 1097 (w), 1068 (vw), 1011 (w), 994 (m), 911 (s), 899 (m), 858 (m), 837 (vs), 784 (s), 731 (s), 682 (w), 654 (vw), 614 (w), 583 (m), 562 (vw), 538 (w), 520 (w), 484 (m), 426 (w).

ESI-MS: $[\text{M}+\text{Na}^+]/z_{\text{exp.}} = 333.1361$, $[\text{M}+\text{Na}^+]/z_{\text{theo.}} = 333.1362$.

Elemental analysis calcd. (%) for $[\text{C}_{22}\text{H}_{18}\text{N}_2]$ ($310.40 \text{ g} \cdot \text{mol}^{-1}$): C 85.13, H 5.85, N 9.03; found C 84.90, H 5.75, N 9.19.



9.3.10 Synthesis of the Cu₂(II) – model complex

Scheme 9.10: Reaction scheme for the synthesis of the Cu₂(II) – pre-model and model complex.

The synthesis of the pre-model and model complex in THF or DMSO leads to an axial solvent coordination to the M₂⁴⁺ unit, which cannot always be removed in vacuum. Thus, residues of THF and DMSO can be observed in the corresponding NMR-, IR- and Raman spectra and elemental analysis.

Following a procedure described in the literature,^[326] the dinuclear copper complex Cu₂(II) – model complex was synthesized by dissolving copper(II) acetate (300 mg, 0.75 mmol, 1.00 equiv.) and 4-ethylbenzoic acid (733 mg, 4.88 mmol, 6.50 equiv.) in THF. Subsequent crystallization from DMSO led to the substitution of both axially binding 4-ethyl benzoic acid moieties by two solvent molecules of DMSO.⁴

Table 9.13: Characterization of the Cu₂(II) – model complex.

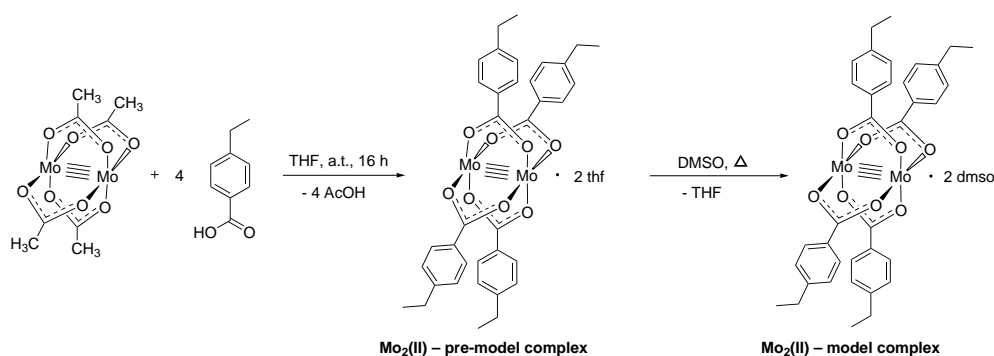
Blue crystals, obtained product: 500 mg, yield: 76 %.

¹H NMR analysis was not interpretable due to the paramagnetic core of Cu(II).

IR (ATR): $\tilde{\nu}$ [cm⁻¹] = 2962 (m), 2928 (vw), 2868 (vw), 1619 (s), 1564 (m), 1455 (vw), 1398 (vs), 1308 (w), 1177 (m), 1113 (vw), 1057 (m), 1019 (s), 956 (w), 933 (vw), 861 (w), 850 (w), 785 (m), 766 (m), 710 (m), 628 (m), 533 (vw), 457 (w).

Elemental analysis calcd. (%) for [C₃₆H₃₆Cu₂O₈ · 4 C₂H₆SO] (1036.28 g · mol⁻¹): C 51.00, H 5.84, S 12.37; found C 51.69, H 6.00, S 12.39.

⁴The synthesis and analysis was performed by Nicolai Knöfel.

9.3.11 Synthesis of the Mo₂(II) – model complex

Scheme 9.11: Reaction scheme for the synthesis of the Mo₂(II) – pre-model and model complex.

Under the complete exclusion of oxygen, molybdenum(II) acetate (300 mg, 0.70 mmol, 1.00 equiv.) and 4-ethylbenzoic acid (474 mg, 3.15 mmol, 4.50 equiv.) were dissolved in 20 mL THF and stirred at room temperature for 24 hours. Subsequently, the solution was concentrated under reduced pressure and 20 mL n-pentane were added. Thereby an orange solid precipitated, which was filtered off and dried under reduced pressure. Single crystals, suitable for X-ray analysis, were obtained after slow cooling in a hot DMSO solution, leading to an axial DMSO coordination.⁵

Table 9.14: Characterization of the Mo₂(II) – model complex.

Purple crystals, obtained product: 430 mg, yield: 78 %.

¹H NMR (400 MHz, DMSO-d₆): $\delta/\text{ppm} = 8.09$ (d, $^3J_{\text{H,H}} = 8.3$ Hz, 8H, Ph), 7.36 (d, $^3J_{\text{H,H}} = 8.3$ Hz, 8H, Ph), 2.67 (q, $^3J_{\text{H,H}} = 7.5$ Hz, 8H, CH₂), 1.17 (t, $^3J_{\text{H,H}} = 7.6$ Hz, 12H, CH₃). – An additional resonance for residual coordinated DMSO is observed at $\delta = 2.54$ ppm.

¹³C{¹H} NMR (101 MHz, DMSO-d₆): $\delta/\text{ppm} = 175.6$ (RCO₂), 148.1 (Ph, C-q), 129.8 (Ph), 128.5 (Ph, C-q), 128.1 (Ph), 28.1 (CH₂), 15.4 (CH₃).

IR (ATR): $\tilde{\nu} [\text{cm}^{-1}] = 2961$ (m), 2928 (w), 2867 (vw), 1606 (w), 1578 (w), 1488 (s), 1460 (s), 1394 (vs), 1304 (w), 1178 (m), 1139 (vw), 1110 (vw), 1060 (m), 1017 (s), 953 (vw), 849 (s), 765 (s), 707 (m), 624 (m), 527 (m), 457 (m), 412 (vw).

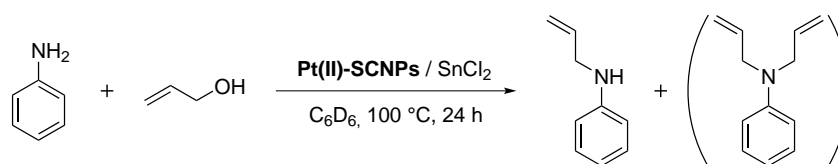
Raman (solid state): $\tilde{\nu} [\text{cm}^{-1}] = 1608$ (s), 1515 (s), 1414 (vs), 1398 (vs), 1205 (vw), 1182 (w), 1061 (vw), 1022 (vw), 864 (vw), 771 (w), 638 (m), 532 (vw), 465 (m), 453 (m), 403 (m), 372 (w), 157 (m).

Elemental analysis calcd. (%) for [C₃₆H₃₆Mo₂O₈ · C₂H₆SO] (866.73 g · mol⁻¹): C 52.66, H 4.88, S 3.70; found C 51.18, H 4.98, S 3.59.

UV-Vis : $\lambda_{\text{max.}}$ [nm] = 432.

⁵The synthesis and analysis was performed by Nicolai Knöfel.

9.3.12 Amination of Allyl Alcohol



Scheme 9.12: Amination of allyl alcohol catalyzed by Pt(II)-SCNPs.

For an amination of allyl alcohol, catalyzed *via* Pt(II)-SCNPs, a flame-dried schlenk flask was equipped with the starting materials aniline (0.76 g, 8.20 mmol, 2.00 equiv.) and the allyl alcohol 2-propen-1-ol (0.24 g, 4.10 mmol, 1.00 equiv.) under N₂ atmosphere. In addition, the Pt(II)-SCNPs (50.0 mg, 0.01 mmol, 0.0024 equiv.), anhydrous SnCl₂ (7.46 mg, 0.04 mmol, 0.0096 equiv.), ferrocene as an internal standard (38.1 mg, 0.21 mmol, 0.05 equiv.) and molecular sieves (3 Å) were added. The reaction mixture was dissolved in 1.00 mL C₆D₆ and stirred at 100 °C for 24 hours. The deuterated solvent was necessary to allow subsequent conversion and yield determination *via* ¹H NMR analysis.

The conversion and selectivity was determined via ¹H NMR spectroscopy with ferrocene as an internal standard. The ratio between ferrocene, the starting material allyl alcohol and the product(s) was calculated by comparing the integrals of the corresponding proton resonances (-CH₂ and respectively =CH) in the ¹H NMR spectrum.

Analogous catalytic reaction conditions and stoichiometries were employed for the aniline derivatives 3-chloroaniline, 3-fluoroaniline, 4-chloroaniline and 2,6-dimethylaniline (refer to the Appendix).

All reactions were additionally performed using the monomeric platinum complex *cis*-[PtCl₂(PPh₃)₂] (7.78 mg, 0.01 mmol, 0.0024 equiv.) as a molecular homogeneous catalyst.

In test reaction, the catalytic activity of the co-catalyst SnCl₂ was investigated. Results inferred slightly higher conversion rates when employing the co-catalyst. However, no product formation, hence conversion was observed for the sole application of SnCl₂ as a catalyst. Thus, the addition of SnCl₂ to the reaction had only a minor effect to the conversion of the amine, confirming a high catalytic activity of the pure Pt(II)-SCNPs.

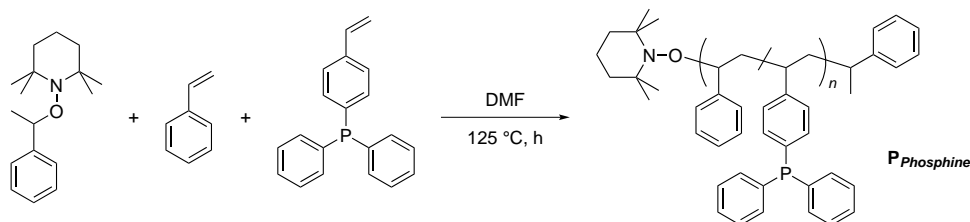
All catalytic reactions were performed minimum twice and the corresponding data was averaged.

For the second catalytic cycle, the same reaction conditions were employed as for the first cycle.

9.4 Polymerizations – NMP Technique

The chapter demonstrating the copolymerizations *via* the NMP technique is divided into two parts. The first one describes the polymerization of styrene and styrene-derivatives, mediated by a TEMPO-based initiator. The second part reports the polymerization of acrylates and acrylamides for which mainly SG1-based initiators were employed.

9.4.1 Synthesis of Poly(styrene-*co*-4-(diphenylphosphino)styrene) ($P_{Phosphine}$)



Scheme 9.13: Synthesis of poly(styrene-*co*-4-(diphenylphosphino)styrene) ($P_{Phosphine}$).

Styrene (11.9 mL, 5.65 g, 104 mmol, 750 equiv.), 4-(diphenylphosphino)styrene (1.20 g, 4.17 mmol, 30.0 equiv.) and 2,2,6,6-tetramethyl-1-(1-phenylethoxy)piperidine (36.0 mg, 0.14 mmol, 1.00 equiv.) were dissolved in 10.0 mL dry toluene in a flame-dried schlenk flask. To remove any remaining oxygen, 4 cycles of freeze-pump-thaw were performed. Thereafter, the reaction mixture was heated at 125 °C. After 10 hours reaction period, the polymerization was quenched by opening the flask to air and cooling to ambient temperature. Diluted with 5 mL THF, the colorless solution was precipitated three times into cold MeOH. The solid was filtered and dried under high vacuum.

Under similar conditions, the copolymer $P_{Phosphine(2)}$ was synthesized, employed as a reference substance for IR measurements in project about heterometallic SCNPs (Chapter 6). A ratio of initiator:styrene:4-(diphenylphosphino)styrene of 1:920:40 was employed. After 5 hours of polymerization, a number average molecular weight of $M_n = 36\,000\text{ g} \cdot \text{mol}^{-1}$, $\mathcal{D} = 1.23$ was obtained. The monomer composition was determined *via* ^1H NMR spectroscopy, revealing a ratio of approx. 1:19, regarding ^1H was detected in the $^{31}\text{P}\{^1\text{H}\}$ NMR spectrum.

Table 9.15: Characterization of poly(styrene-co-4-(diphenylphosphino)styrene) ($P_{\text{Phosphine}}$).

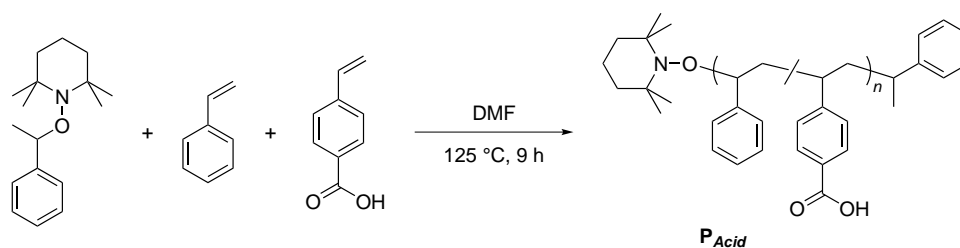
White powder, obtained product: 6.05 g.

SEC characterization (THF, RI): $M_n = 40\,600 \text{ g} \cdot \text{mol}^{-1}$, $D = 1.15$.

^1H NMR (400 MHz, CDCl_3): $\delta/\text{ppm} = 8.02\text{--}7.21$ (m, aromatic protons of 4-(diphenylphosphino)styrene (14H)), $7.21\text{--}6.11$ (m, aromatic protons of styrene (5H)), $2.73\text{--}0.54$ (m, aliphatic protons, backbone).

^1H NMR analysis revealed a monomer ratio of 1:21, regarding the higher amount to styrene. Thus, approx. 5 % of phosphine side-groups were implemented into the polymer chain \rightarrow 0.42 mmol phosphine species per 1 g of copolymer $P_{\text{Phosphine}}$.

$^{31}\text{P}\{^1\text{H}\}$ NMR (162 MHz, CDCl_3): $\delta/\text{ppm} = -6.22$ (s, PPh_2Ar).

9.4.2 Synthesis of Poly(styrene-co-4-vinylbenzoic acid) (P_{Acid})Scheme 9.14: Synthesis of poly(styrene-co-4-vinylbenzoic acid) (P_{Acid}).

A photovial was equipped with a solution of 2,2,6,6-tetramethyl-1-(1-phenylethoxy)piperidine (9.00 mg, 34.4 μmol , 1.00 equiv.), styrene (2.64 g, 25.3 mmol, 735 equiv.) and 4-vinylbenzoic acid (178 mg, 1.21 mmol, 35.0 equiv.) in 1.45 mL dry DMF. While stirring, the solution was degassed with argon for 30 min. Subsequently, the reaction mixture was heated at 125 $^{\circ}\text{C}$ for 9 hours. Cooling to ambient temperature and opening the flask to air, quenched the reaction. After diluting with DCM, the polymer (P_{Acid}) was precipitated twice into cold MeOH, resulting in a white powder.

Table 9.16: Characterization of poly(styrene-co-4-vinylbenzoic acid) (P_{Acid}).

White powder.

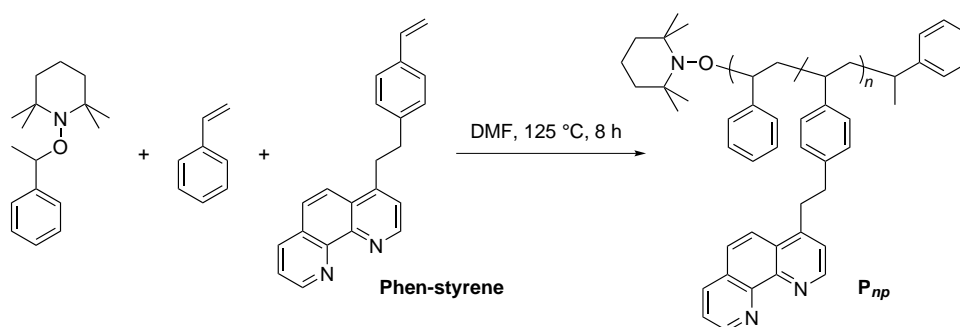
SEC characterization (THF, RI): $M_n = 32\,200\text{ g} \cdot \text{mol}^{-1}$, $M_p = 41\,000\text{ g} \cdot \text{mol}^{-1}$, $D = 1.22$.

$^1\text{H NMR}$ (400 MHz, THF- d_8): $\delta/\text{ppm} = 11.2$ (bs, COOH), 7.91–7.51 (m, aromatic protons of 4-vinylbenzoic acid (2H), *meta*-position), 7.25–6.27 (m, aromatic protons of styrene (5H) and 4-vinylbenzoic acid (3H)), 2.59–2.83 (m, aliphatic protons, backbone).

Characterization via $^1\text{H NMR}$ spectroscopy revealed a monomer ratio of approx. 1:14, regarding the higher amount to styrene \rightarrow 0.65 mmol of benzoic acid functionality in 1 g (P_{Acid}).

IR (ATR): $\tilde{\nu} [\text{cm}^{-1}] = 3082$ (vw), 3060 (w), 3026 (s), 3002 (vw), 2923 (s), 2849 (w), 1734 (m), 1690 (m), 1603 (m), 1582 (vw), 1493 (s), 1451 (s), 1423 (w), 1369 (vw), 1315 (vw), 1285 (w), 1179 (w), 1156 (vw), 1086 (vw), 1028 (w), 907 (vw), 856 (vw), 756 (s), 698 (vs), 540 (m).

Raman (solid state): $\tilde{\nu} [\text{cm}^{-1}] = 3055$ (s), 3002 (vw), 2978 (vw), 2903 (m), 2851 (w), 1604 (s), 1584 (m), 1451 (w), 1329 (vw), 1183 (m), 1156 (w), 1032 (m), 1002 (vs), 798 (w), 662 (m), 224 (w).

9.4.3 Synthesis of Poly(styrene-*co*-Phen-styrene) (P_{np})

Scheme 9.15: Reaction scheme of the polymerization of poly(styrene-*co*-Phen-styrene) (P_{np}).

2,2,6,6-Tetramethyl-1-(1-phenylethoxy)piperidine (7.00 mg, 26.8 μmol , 1.00 equiv.), styrene (2.07 g, 19.9 mmol, 742 equiv.) and Phen-styrene (108 mg, 0.35 mmol, 13.0 equiv.) were dissolved in 1.0 mL DMF in a vial. While stirring, the solution was degassed with N_2 for 30 min, before heated at 125 °C for 8 hours. Cooling to ambient temperature and opening the flask to air, quenched the reaction. After diluting with DCM, the polymer was precipitated twice into cold MeOH and filtered off.

Table 9.17: Characterization of poly(styrene-*co*-Phen-styrene) (P_{np}).

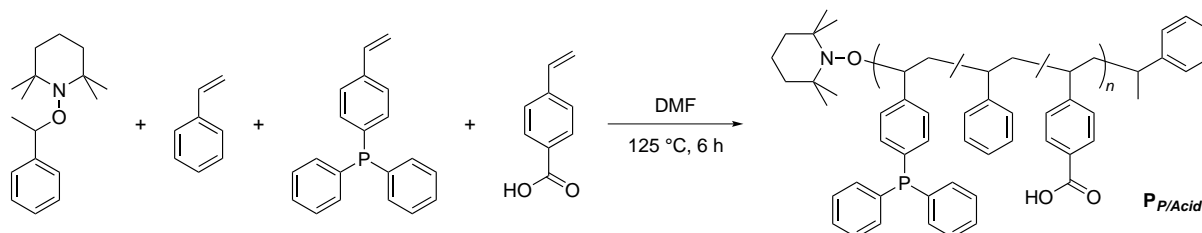
White powder, obtained product: 700 mg.

No **SEC characterization** was feasible, due to strong interactions of the Phen groups with the column material. To enable SEC characterization the Phen groups were "protected" by coordinating to Pd(II) ions, refer to Chapter 9.6.2.

$^1\text{H NMR}$ (400 MHz, CDCl_3): δ/ppm = 9.25 (br, Phen-aromatic), 9.10 (br, Phen-aromatic), 8.22 (br, Phen-aromatic), 8.00 (br, Phen-aromatic), 7.77 (br, Phen-aromatic), 7.65 (br, Phen-aromatic), 7.46–6.12 (m, aromatic protons), 3.36 (br, Phen-methylene), 2.99 (br, Phen-methylene), 2.61–0.94 (m, aliphatic protons, backbone).

$^1\text{H NMR}$ analysis revealed a monomer ratio between styrene and Phen-styrene of 60:1. Thus, approx. 1.7 % of Phen-styrene groups were implemented into the polymer chain \rightarrow 0.16 mmol Phen-styrene species per 1 g of copolymer P_{np} .

9.4.4 Synthesis of Poly(styrene-*co*-4-(diphenylphosphino)styrene-*co*-4-vinylbenzoic acid) ($P_{P/Acid}$)



Scheme 9.16: Synthesis of poly(styrene-*co*-4-(diphenylphosphino)styrene-*co*-4-vinylbenzoic acid) ($P_{P/Acid}$).

In a photovial, 2,2,6,6-tetramethyl-1-(1-phenylethoxy)-piperidine (14.0 mg, 0.05 mmol, 1.00 equiv.), styrene (4.66 mL, 4.23 g, 40.7 mmol, 760 equiv.), 4-vinylbenzoic acid (150 mg, 1.07 mmol, 20.0 equiv.) and 4-(diphenylphosphino)styrene (309 mg, 1.07 mmol, 20.0 equiv.) were dissolved in 1.5 mL dry DMF. Subsequently, the solution was degassed with argon for 1 hour and stirred for 6 hours at 125 °C. The polymerization was quenched by opening the vial to air and cooling to ambient temperature. After the addition of 10 mL DCM, the colorless solution was precipitated twice into cold MeOH. After filtration, the final product was obtained.

Table 9.18: Characterization of poly(styrene-*co*-4-(diphenylphosphino)styrene-*co*-4-vinylbenzoic acid) ($P_{P/Acid}$).

White powder, obtained product: 2.21 g.

SEC characterization (THF, RI): $M_n = 41\,300\text{ g} \cdot \text{mol}^{-1}$, $D = 1.20$.

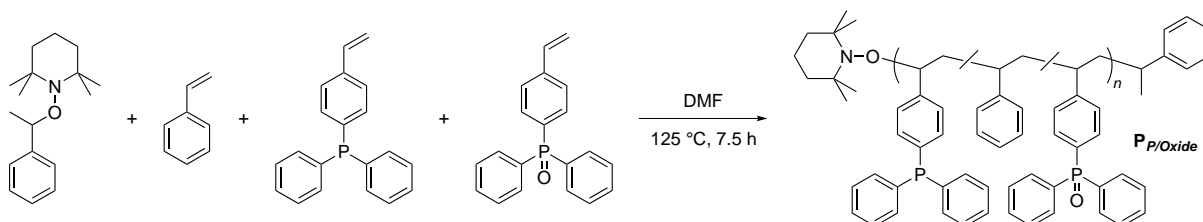
^1H NMR (400 MHz, THF- d_8): $\delta/\text{ppm} = 11.2$ (bs, COOH), 7.90–7.54 (m, aromatic protons of 4-vinylbenzoic acid (2H), *meta*-position), 7.51–7.17 (m, aromatic protons of 4-(diphenylphosphino)styrene (14H)), 7.17–6.27 (m, aromatic protons of styrene (5H) and 4-vinylbenzoic acid (2H)), 2.67–1.19 (m, aliphatic protons, backbone).

^1H NMR analysis revealed a monomer ratio between styrene and 4-(diphenylphosphino)styrene of 35:1, regarding the higher amount to styrene. Thus, approx. 2.8 % of phosphine side groups were implemented into the polymer chain \rightarrow 0.26 mmol phosphine species per 1 g of polymer. For 4-vinylbenzoic acid, a ratio of 15:1 was determined in comparison to styrene, hence approx. 7 % of acidic side groups were implemented into the polymer chain \rightarrow 0.65 mmol acidic side groups per 1 g of copolymer $P_{P/Acid}$.

$^{31}\text{P}\{^1\text{H}\}$ NMR (162 MHz, THF- d_8): $\delta/\text{ppm} = -6.36$ (s, PPh_2Ar).

IR (ATR): $\tilde{\nu} [\text{cm}^{-1}] = 3082$ (w), 3060 (m), 3025 (m), 3002 (vw), 2922 (s), 2848 (w), 1734 (m), 1690 (m), 1602 (m), 1583 (vw), 1492 (s), 1451 (s), 1368 (vw), 1313 (vw), 1283 (vw), 1180 (vw), 1155 (vw), 1088 (vw), 1070 (vw), 1027 (w), 907 (vw), 843 (vw), 826 (vw), 751 (s), 697 (vs), 540 (m).

9.4.5 Synthesis of

Poly(styrene-*co*-4-(diphenylphosphino)styrene-*co*-4-(diphenylphosphine oxide)styrene) ($P_{P/Oxide}$)

Scheme 9.17: Synthesis of poly(styrene-*co*-4-(diphenylphosphino)styrene-*co*-4-(diphenylphosphine oxide)styrene) ($P_{P/Oxide}$).

A photovial was equipped with styrene (4.36 g, 41.9 mmol, 735 equiv.), 4-(diphenylphosphino)styrene (460 mg, 1.60 mmol, 28.0 equiv.), 4-(diphenylphosphine oxide)styrene (121 mg, 0.40 mmol, 7.00 equiv) and 2,2,6,6-tetramethyl-1-(1-phenylethoxy)-piperidine (15.0 mg, 0.06 mmol, 1.00 equiv.). Dissolving the compounds in 1.45 mL dry DMF, the vial was purged with argon for 1 hour. Stirring the reaction mixture, the vial was heated at 125 °C for 7.5 hours. Afterwards, the reaction was quenched by cooling to ambient temperature and opening the vial to air. Repeated precipitation (three times) into cold MeOH resulted in the final polymer.

Table 9.19: Characterization of poly(styrene-*co*-4-(diphenylphosphino)styrene-*co*-4-(diphenylphosphine oxide)styrene) ($P_{P/Oxide}$).

White powder, obtained product: 2.10 g.

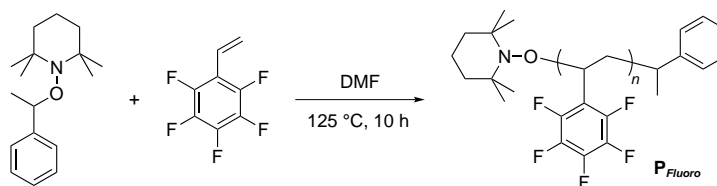
SEC characterization (THF, RI): $M_n = 25\,300\text{ g} \cdot \text{mol}^{-1}$, $D = 1.41$.

^1H NMR (400 MHz, CDCl_3): $\delta/\text{ppm} = 7.70\text{--}7.19$ (m, aromatic protons of 4-(diphenylphosphino)styrene and 4-(diphenylphosphine oxide)styrene), $7.19\text{--}6.20$ (m, aromatic protons of styrene), $2.41\text{--}0.90$ (m, aliphatic protons, backbone).

The combination of ^1H NMR and $^{31}\text{P}\{^1\text{H}\}$ NMR analyses revealed a monomer ratio between styrene, 4-(diphenylphosphino)styrene and 4-(diphenylphosphine oxide)styrene of 57:2:1. Thus, approx. 1.7 % of phosphine oxide side groups and approx. 3.5 % of phosphine side groups were implemented into the polymer chain \rightarrow 0.16 mmol phosphine oxide species and 0.32 mmol phosphine species per 1 g of copolymer $P_{P/Oxide}$.

$^{31}\text{P}\{^1\text{H}\}$ NMR (162 MHz, CDCl_3): $\delta/\text{ppm} = 29.2$ (br, $\text{O}=\text{PPh}_2\text{Ar}$), -6.23 (br, PPh_2Ar).

IR (ATR): $\tilde{\nu} [\text{cm}^{-1}] = 3082$ (w), 3059 (w), 3025 (m), 3001 (vw), 2922 (m), 2848 (w), 1601 (m), 1584 (vw), 1493 (s), 1452 (s), 1437 (m), 1373 (vw), 1202 (w), 1182 (vw), 1155 (vw), 1118 (w), 1069 (vw), 1028 (w), 907 (vw), 842 (vw), 826 (vw), 756 (s), 748 (s), 697 (vs), 541 (m), 506 (vw).

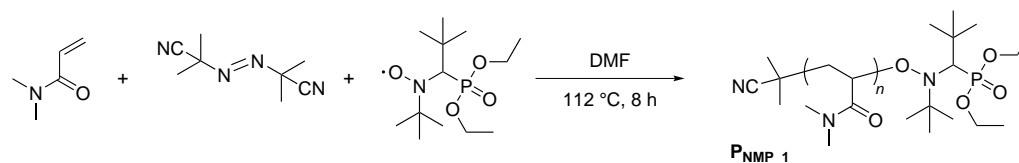
9.4.6 Kinetic Study of the Polymerization of Pentafluorostyrene (P_{Fluoro})

Scheme 9.18: Kinetic study of the homo-polymerization of P_{Fluoro} .

2,2,6,6-Tetramethyl-1-(1-phenylethoxy)-piperidine (5.00 mg, 0.02 mmol, 1.00 equiv.) and 2,3,4,5,6-pentafluorostyrene (2.82 g, 14.5 mmol, 760 equiv.) were dissolved in 1.0 mL dry DMF in a photovial. Thereafter, the solution was degassed with argon for 20 minutes and heated for 10 hours at 125 °C. Controlling the degree of polymerization by time, every two hours a sample was taken and analyzed via SEC measurement.

SEC characterization (THF, RI) after 10 hours: $M_n = 11\,200\text{ g} \cdot \text{mol}^{-1}$, $\mathcal{D} = 1.05$.

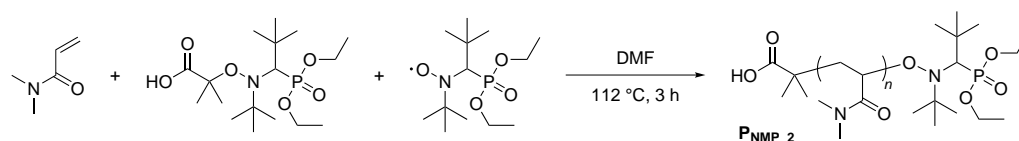
Further copolymerization reactions with 4-vinylbenzoic acid or 4-(diphenylphosphino)styrene did not result in the expected polymers, therefore the polymer P_{Fluoro} was not further analyzed.

9.4.7 Homo-Polymerization of DMAA via SG1 and AIBN (P_{NMP_1})

Scheme 9.19: Polymerization of poly(DMAA) via the NMP method, employing the nitroxide SG1 and AIBN (P_{NMP_1}).

In a test reaction, SG1 (10.0 mg, 34.0 μmol , 1.00 equiv.), 2,2'-azobis(2-methylpropanionitril) (2.79 mg, 17.0 μmol , 0.50 equiv.) and *N,N*-dimethylacrylamide (337 mg, 3.40 mmol, 100 equiv.) were dissolved in 0.35 mL degassed DMF. After purging with N_2 for 10 min, the vial was placed in a heating block for 8 hours at 112 °C. The reaction was quenched by opening to air and cooling to ambient temperature. A small amount of the viscous solution was applied for SEC analysis.

SEC characterization (DMAc, RI): $M_n = 12\,000\text{ g} \cdot \text{mol}^{-1}$, $D = 1.39$.

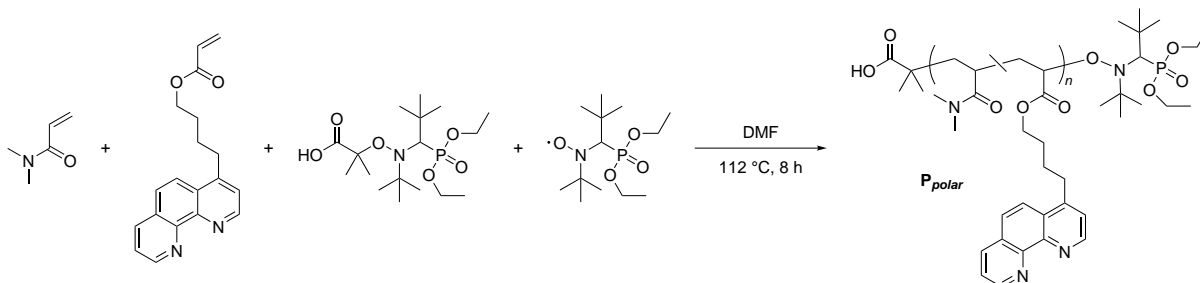
9.4.8 Homo-Polymerization of DMAA via MAMA-SG1 and SG1 (P_{NMP_2})

Scheme 9.20: Polymerization of poly(DMAA) via the NMP method, employing the alkoxyamine MAMA-SG1 and the nitroxide SG1 (P_{NMP_2}).

In a test reaction, MAMA-SG1 (1.50 mg, 3.93 μmol , 1.00 equiv.), SG1 (0.23 mg, 0.79 μmol , 0.20 equiv.) and *N,N*-dimethylacrylamide (585 mg, 5.90 mmol, 1500 equiv.) were dissolved in 0.02 mL degassed DMF (using a standard solution). After purging with N_2 for 10 min, the vial was placed in a heating block for 3 hours at 112 °C. The reaction was quenched by opening to air and cooling to ambient temperature. A small amount of the viscous solution was applied for SEC analysis.

SEC characterization (DMAc, RI): $M_n = 40\,100\text{ g} \cdot \text{mol}^{-1}$, $D = 1.44$.

9.4.9 Synthesis of Poly(DMAA-*co*-Phen-acrylate) (P_{polar}) via MAMA-SG1 and SG1



Scheme 9.21: Polymerization of poly(DMAA-*co*-Phen-acrylate) (P_{polar}) via the NMP method, mediated by MAMA-SG1 and SG1.

N,N-dimethylacrylamide (3.25 g, 32.8 mol, 500 equiv.), Phen-acrylate (0.50 g, 1.64 mol, 25.0 equiv.), MAMA-SG1 (25.0 mg, 65.5 mmol, 1.00 equiv.) and SG1 (3.68 mg, 11.1 μ mol, 0.20 equiv.) were dissolved in 1.6 mL dry DMF in a capped photovial. The solution was purged with N_2 for 45 min. Thereafter, the mixture was stirred at 112 °C for 8 hours. The reaction was quenched by cooling the reaction mixture to 0 °C and opening to air. After addition of DCM (approx. 10 mL), the solution was precipitated three times into cold Et_2O . After filtration, a yellow solid was obtained.

Table 9.20: Characterization of the copolymer P_{polar} .

Yellow powder, obtained product: 2.30 g.

1H NMR (400 MHz, $CDCl_3$): $\delta/ppm = 9.20$ (br, Phen-aromatic), 9.12 (br, Phen-aromatic), 8.29 (br, Phen-aromatic), 8.09 (br, Phen-aromatic), 7.87 (br, Phen-aromatic), 7.65 (br, Phen-aromatic), 7.55 (br, Phen-aromatic), 4.10 (br, Phen-methylene (2H)), 3.37–2.02 (m, Phen-methylene (2H) and $N-CH_3$), 1.98–0.72 (m, aliphatic proton, backbone).

Characterization via 1H NMR revealed a monomer ratio of 1:20, regarding the higher amount to DMAA \rightarrow 0.46 mmol of Phen-acrylate in 1 g P_{polar} .

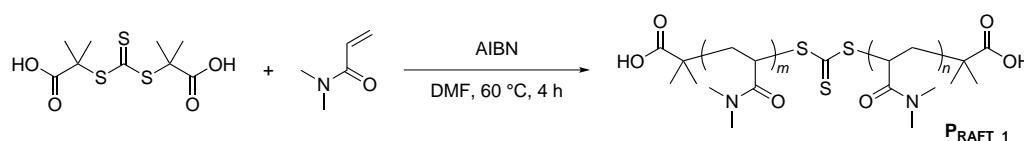
IR (ATR): $\tilde{\nu}$ [cm^{-1}] = 3463 (br), 2927 (w), 1724 (vw, (C=O Phen-acrylate), 1618 (vs, C=O DMAA), 1496 (s), 1455 (m), 1400 (s), 1355 (m), 1256 (m), 1140 (s), 1095 (m), 1055 (m), 1029 (w), 844 (vw), 741 (vw), 720 (vw), 624 (w), 486 (w).

9.5 Polymerizations – RAFT Technique

Aiming for optimal reaction conditions for a copolymerization of *N,N*-dimethylacrylamide (DMAA) with a Phen-containing monomer, in first approaches the homo-polymerization of DMAA *via* the RAFT technique was established. For this reason various RAFT agents were investigated and compared, regarding their ability to achieve high molecular weight polymers of approx. $M_n = 25\,000\text{ g} \cdot \text{mol}^{-1}$ and a distribution < 1.5 . The following sections demonstrate various reaction procedures for the synthesis of polyDMAA or related copolymerizations. Only if the (co)polymers were applied for further reactions, more than SEC data is provided. Some polymerizations were performed with different monomer-to-initiator ratios or at different reaction times, described in detail in Chapter 4.

The polymer polyDMAA was further analyzed *via* ^1H NMR and IR spectroscopy, described for P_RAFT4.

9.5.1 Synthesis of Poly(DMAA) *via* TRITT (P_RAFT_1)

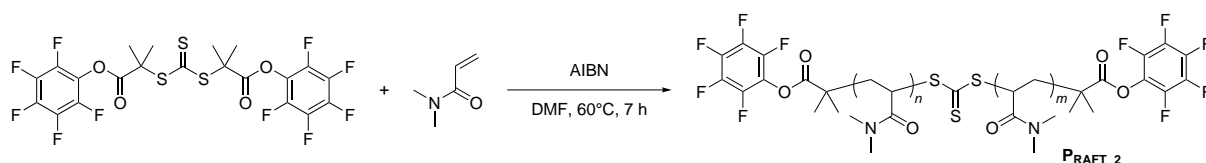


Scheme 9.22: Synthesis of poly(DMAA) (P_RAFT_1) *via* RAFT, employing the RAFT agent 2,2'-(thiocarbonylbis(sulfaneydiyl))bis(2-methylpropanoic acid) (TRITT).

N,N-dimethylacrylamide (0.21 g, 2.12 mmol, 300 equiv.), 2,2'-(thiocarbonylbis(sulfaneydiyl))bis(2-methylpropanoic acid) (2.00 mg, 7.08 μmol , 1.00 equiv.) and 2,2'-azobis(2-methylpropionitril) (116 μg , 0.71 μmol , 0.10 equiv.) were dissolved in 0.2 mL DMF in a photovial. After purging with N_2 for 10 min, the vial was heated at 60 °C for 4 hours. The polymerization was quenched by cooling the vial to ambient temperature. A small amount of the reaction mixture was precipitated into cold Et_2O , filtered and applied for SEC characterization.

SEC characterization (DMAc, RI): $M_n = 10\,400\text{ g} \cdot \text{mol}^{-1}$, $D = 1.57$.

9.5.2 Synthesis of Poly(DMAA) via TRITT-pentafluorophenol ester (P_{RAFT_2})

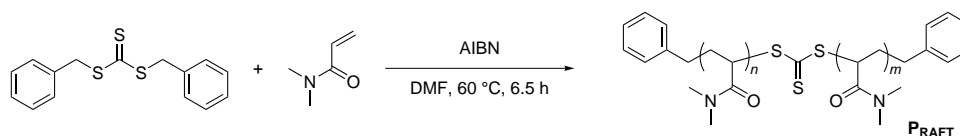


Scheme 9.23: Synthesis of poly(DMAA) (P_{RAFT_2}) via RAFT, employing the RAFT agent bis(perfluorophenyl) 2,2'-(thiocarbonyl-bis(sulfaneyl))-bis(2-methylpropanoate) (TRITT-pentafluorophenol ester).

N,N-dimethylacrylamide (1.94 g, 19.5 mmol, 300 equiv.), bis(perfluorophenyl) 2,2'-(thiocarbonyl-bis(sulfaneyl))-bis(2-methylpropanoate) (40.0 mg, 65.1 μmol , 1.00 equiv.) and 2,2'-azobis(2-methylpropionitril) (1.07 mg, 6.51 μmol , 0.10 equiv.) were dissolved in 1.5 mL DMF in a photovial. After purging with N_2 for 30 min, the vial was stirred in a heating block at 60 $^\circ\text{C}$ for 7 hours. Three times precipitation into cold Et_2O resulted in monomer-free yellow-powdered polymer.

SEC characterization (DMAc, RI): $M_n = 30\,600\text{ g}\cdot\text{mol}^{-1}$, $D = 1.17$.

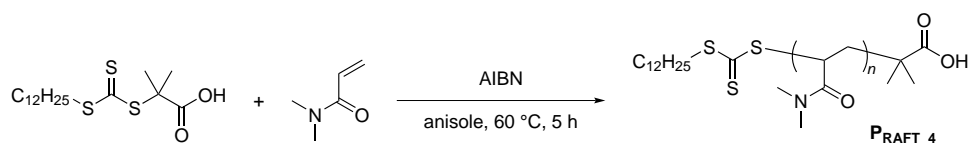
9.5.3 Synthesis of Poly(DMAA) via DBTTC (P_{RAFT_3})



Scheme 9.24: Synthesis of Poly(DMAA) (P_{RAFT_3}) via RAFT, employing the RAFT agent *S,S*-dibenzyl trithiocarbonat (DBTTC).

N,N-dimethylacrylamide (1.84 g, 18.6 mmol, 300 equiv.), *S,S*-dibenzyl trithiocarbonat (18.0 mg, 62.0 μmol , 1.00 equiv.) and 2,2'-azobis(2-methylpropionitril) (1.02 mg, 6.20 μmol , 0.10 equiv.) were dissolved in 1.5 mL DMF in a photovial. Oxygen was removed from the reaction mixture by flushing the vial with gaseous N_2 for 30 min. Afterwards, the vial was placed in a heating block at 60 $^\circ\text{C}$. After 6.5 hours the vial was cooled to ambient temperature and opened to air. The viscous liquid was diluted with 3 mL DCM and precipitated into cold Et_2O . After complete addition, the suspension was stirred for 1 hour to minimize the polymer droplets, allowing non-reacted monomer to be dissolved in Et_2O . The white powder was filtered off and dissolved in DCM. Repeating the precipitation process twice resulted in the final polymer.

SEC characterization (DMAc, RI): $M_n = 35\,500\text{ g}\cdot\text{mol}^{-1}$, $D = 1.16$.

9.5.4 Synthesis of Poly(DMAA) *via* DDMAT (P_{RAFT_4})

Scheme 9.25: Synthesis of poly(DMAA) (P_{RAFT_4}) *via* RAFT, employing the RAFT agent 2-(dodecylthiocarbonylthio)-2-methylpropionic acid (DDMAT).

N,N-dimethylacrylamide (2.45 g, 24.7 mmol, 300 equiv.), 2-(dodecylthiocarbonylthio)-2-methylpropionic acid (0.03 g, 0.83 mmol, 1.00 equiv.) and 2,2'-azobis(2-methylpropionitril) (1.35 mg, 8.23 μmol , 0.10 equiv.) were dissolved in 2.5 mL anisole. The flask was purged with N_2 for 30 min and subsequently stirred at 60 °C for 5 hours. Thereafter, the solution was dialyzed in EtOH for three days. At last, the yellow solution was precipitated in Et_2O and subsequently dried under reduced pressure.

Table 9.21: Characterization of poly(DMAA) (P_{RAFT_4}).

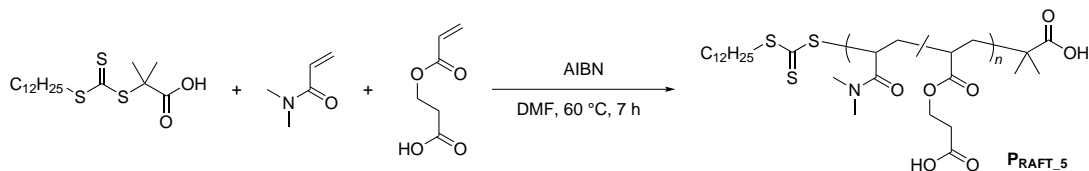
Yellow powder, obtained product: 1.50 g.

SEC characterization (THF, RI): $M_n = 31\,800 \text{ g} \cdot \text{mol}^{-1}$, $D = 1.10$.

^1H NMR (400 MHz, CDCl_3): $\delta/\text{ppm} = 3.35\text{--}2.20$ (m, $\text{N}(\text{CH}_3)_2$), 2.20–0.95 (m, aliphatic protons, backbone).

IR (ATR): $\tilde{\nu} [\text{cm}^{-1}] = 3468$ (br), 2927 (w), 1620 (vs, $\text{C}=\text{O}$ DMAA), 1496 (s), 1458 (m), 1431 (m), 1400 (s), 1355 (m), 1256 (m), 1140 (s), 1095 (m), 1056 (m), 720 (vw), 625 (w), 487 (w).

9.5.5 Synthesis of Poly(DMAA-co-3-(acryloyloxy)propanoic acid) via DDMAT (P_{RAFT_5})



Scheme 9.26: Copolymerization of the monomers DMAA and 3-(acryloyloxy)propanoic acid (P_{RAFT_5}) via RAFT, employing the RAFT agent 2-(dodecylthiocarbonothioylthio)-2-methylpropionic acid (DDMAT).

N,N-dimethylacrylamide (10.0 g, 101 mmol, 234 equiv.), 2-carboxyethyl acrylate (0.97 g, 6.72 mmol, 15.6 equiv.), 2-(dodecylthiocarbonothioylthio)-2-methylpropionic acid (0.16 g, 0.43 mmol, 1.00 equiv.) and 2,2'-azobis(2-methylpropionitril) (7.00 mg, 0.04 mmol, 0.10 equiv.) were dissolved in 10 mL DMF in a photovial. The reaction mixture was purged with N₂ for 30 min and subsequently heated at 60 °C. After 7 hours, the solution was cooled to ambient temperature and diluted with 10 mL DCM. Precipitating twice into cold Et₂O resulted in bright yellow powder, which was dried under high vacuum.

Table 9.22: Characterization of poly(DMAA-co-3-(acryloyloxy)propanoic acid) (P_{RAFT_5}).

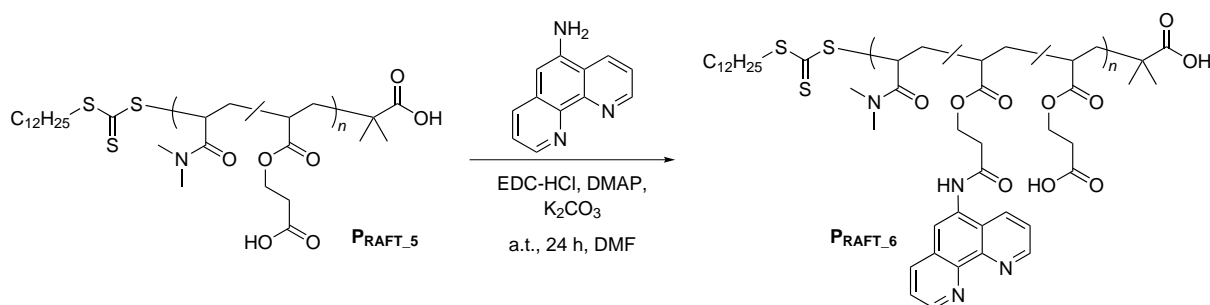
Yellow powder, obtained product: 8.80 g.

SEC characterization (DMAc, RI): $M_n = 28\,400\text{ g} \cdot \text{mol}^{-1}$, $D = 1.14$.

¹H NMR (400 MHz, CDCl₃): $\delta/\text{ppm} = 3.34$ (br, CH₂CH₂CO₂H protons of 2-carboxyethyl acrylate (2H)), 3.10–2.62 (m, N-(CH₃)₂, (6H)), 2.12 (br, CH₂CH₂CO₂H protons of 2-carboxyethyl acrylate (2H)), 1.75–0.76 (m, aliphatic protons, backbone).

¹H NMR analysis revealed a monomer ratio of 1:15, regarding the higher amount to DMAA → approx. 6 % of acidic side groups were implemented into the polymer chain.

9.5.6 Synthesis of Poly(DMAA-co-3-((1,10-phenanthroline-5-yl)amino)-3-oxopropyl acrylate) (P_{RAFT_6})



Scheme 9.27: Postfunctionalization of the acidic groups of P_{RAFT_5} with 1,10-phenanthroline-5-amine via an EDC coupling, resulting in poly(DMAA-co-3-((1,10-phenanthroline-5-yl)amino)-3 oxopropyl acrylate) (P_{RAFT_6}).

In a flame-dried schlenk flask, poly(DMMA-co-3-(acryloyloxy)-propanoic acid) (P_{RAFT_5}) (3.00 g, 1.77 mmol (referring to the amount of acidic side groups), 1.00 equiv.), 1,10-phenanthroline-5-amine (458 mg, 2.35 mmol, 1.33 equiv.), *N,N*-dimethylpyridin-4-amine (191 mg, 1.57 mmol, 0.89 equiv.) and potassium carbonate (406 mg, 2.94 mmol, 1.66 equiv.) were dissolved in 20 mL DMF. The reaction mixture was cooled to 0 °C and subsequently 3-(((ethylimino)methylene)amino)-*N,N*-dimethylpropan-1-amine hydrochloride (EDC · HCl) (750 mg, 3.91 mmol, 2.21 equiv.) was added. After stirring for 24 hours at ambient temperature, the reaction mixture was filtered and transferred into a dialysis tube to separate all non-reacted small molecules from the polymer. Dialysis was performed three times in H₂O and two times in MeOH with a dwell period of 4 to 16 hours. After dialysis, the content of the tube was dried in a flask *via* lyophilisation. The obtained yellow resin was dissolved in MeOH and precipitated in cold Et₂O.

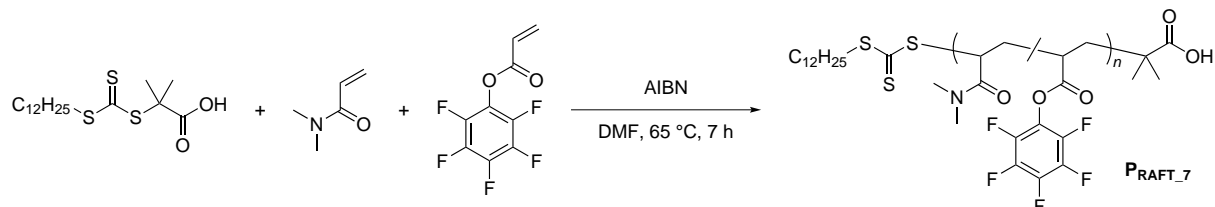
Table 9.23: Characterization of poly(DMAA-co-3-((1,10-phenanthroline-5-yl)amino)-3 oxopropyl acrylate) (P_{RAFT_6}).

Yellow powder, obtained product: 1.83 g.

SEC characterization (DMAc, RI): $M_n = 23\,000\text{ g} \cdot \text{mol}^{-1}$, $D = 1.20$.

¹H NMR (400 MHz, CDCl₃): $\delta/\text{ppm} = 9.31\text{--}7.97$ (m, aromatic Phen protons (7H)), 3.38 (br, CH₂CH₂CO₂H protons of 2-carboxyethyl acrylate (2H)), 3.10–2.65 (m, N(CH₃)₂ of DMAA (6H)), 2.13 (br, CH₂CH₂CO₂H protons of 2-carboxyethyl acrylate (2H)), 1.79–0.77 (m, aliphatic protons, backbone).

9.5.7 Synthesis of Poly(DMAA-*co*-pentafluorophenyl acrylate) via DDMAT (P_{RAFT_7})

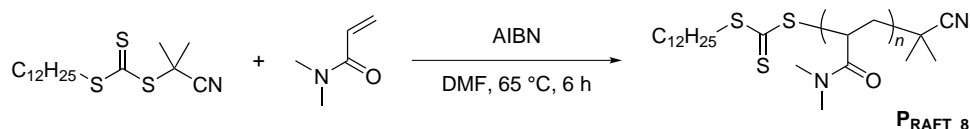


Scheme 9.28: Copolymerization of the monomers DMAA and pentafluorophenyl acrylate mediated by the RAFT agent DDMAT (P_{RAFT_7}).

N,N-dimethylacrylamide (1.20 g, 12.1 mmol, 220 equiv.), pentafluorophenyl acrylate (0.39 g, 1.65 mmol, 30.0 equiv.), 2-(dodecylthiocarbonylthio)-2-methylpropionic acid (20.0 mg, 54.9 μmol, 1.00 equiv.) and 2,2'-azobis(2-methylpropionitril) (0.90 mg, 5.49 μmol, 0.10 equiv.) were dissolved in 1.4 mL dry DMF in a photovial. After purging with N₂ for 30 min, the photovial was sealed and subsequently heated at 65 °C. After 7 hours, the solution was cooled to ambient temperature and diluted with 10 mL DCM. The mixture was precipitated twice into cold Et₂O, filtered and dried under high vacuum.

SEC characterization (DMAc, RI): $M_n = 29\,700\text{ g} \cdot \text{mol}^{-1}$, $D = 1.23$.

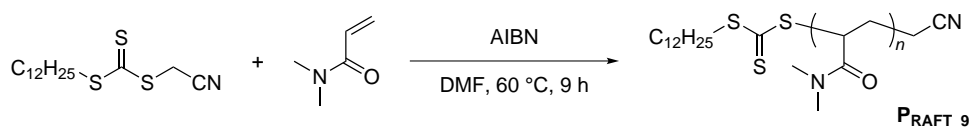
9.5.8 Synthesis of Poly(DMAA) via CPDT (P_{RAFT_8})



Scheme 9.29: Synthesis of poly(DMAA) via RAFT, employing the RAFT agent 2-cyano-2-propyl dodecyl trithiocarbonate (CPDT) (P_{RAFT_8}).

N,N-dimethylacrylamide (688 mg, 6.94 mmol, 300 equiv.), 2-cyano-2-propyl dodecyl trithiocarbonate (40.0 mg, 115 μmol, 5.00 equiv.) and 2,2'-azobis(2-methylpropionitril) (3.80 mg, 23.2 μmol, 1.00 equiv.) were dissolved in 0.7 mL dry DMF in a photovial. After purging with N₂ for 20 min, the photovial was sealed and subsequently heated at 65 °C. After 6 hours, the solution was cooled to ambient temperature. Small amounts of the reaction solution were diluted with DMAc and further applied for SEC characterization.

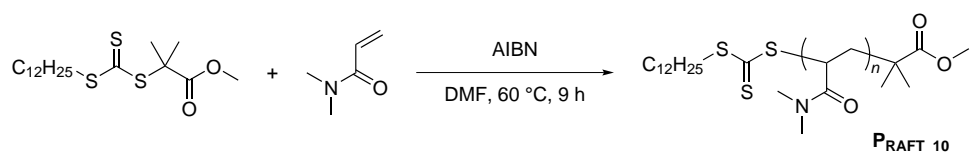
SEC characterization (DMAc, RI): $M_n = 6\,100\text{ g} \cdot \text{mol}^{-1}$, $D = 1.24$.

9.5.9 Synthesis of Poly(DMAA) *via* CMDT (P_{RAFT_9})

Scheme 9.30: Synthesis of poly(DMAA) (P_{RAFT_9}) *via* RAFT polymerization, employing the RAFT agent cyanomethyl dodecyl trithiocarbonate (CMDT).

A solution of *N,N*-dimethylacrylamide (1.40 g, 14.2 mmol, 300 equiv.), cyanomethyl dodecyl trithiocarbonate (15.0 mg, 47.2 μmol , 1.00 equiv.) and 2,2'-azobis(2-methylpropionitril) (0.78 mg, 4.72 μmol , 0.10 equiv.) in 1.4 mL dry DMF was added to a photovial. Purging with N_2 for 20 min removed remaining oxygen, and the vial was subsequently placed into a heating block at 60 °C. After 9 hours, the reaction was quenched by opening to air and cooling to ambient temperature. Small amounts of the reaction solution were diluted with DMAc and further applied for SEC characterization.

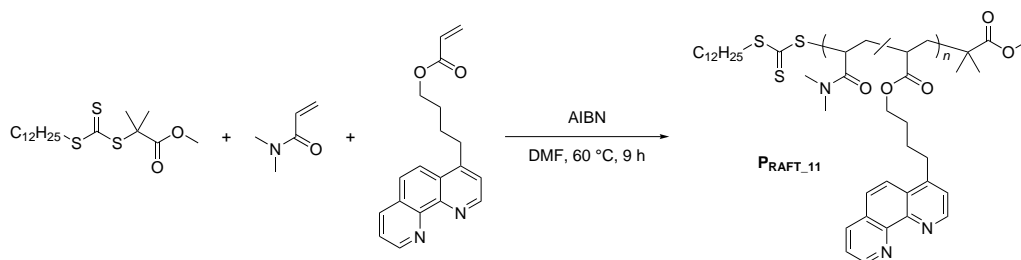
SEC characterization (DMAc, RI): $M_n = 27\,600 \text{ g} \cdot \text{mol}^{-1}$, $D = 1.24$.

9.5.10 Synthesis of Poly(DMAA) *via* M-DDMAT ($P_{\text{RAFT}_{10}}$)

Scheme 9.31: Synthesis of poly(DMAA) ($P_{\text{RAFT}_{10}}$) *via* RAFT polymerization, employing the RAFT agent methyl 2-(dodecylthiocarbonothioylthio)-2-methylpropionate (M-DDMAT).

A photovial was equipped with *N,N*-dimethylacrylamide (1.14 g, 14.3 mmol, 300 equiv.), methyl 2-(dodecylthiocarbonothioylthio)-2-methylpropionate (18.0 mg, 47.5 μmol , 1.00 equiv.) and 2,2'-azobis(2-methylpropionitril) (0.78 mg, 4.75 μmol , 0.10 equiv.). After the addition of 0.5 mL DMF, the vial was purged for 20 min with N_2 , sealed and heated for 9 hours at 60 °C. Opening the vial to air and cooling to ambient temperature quenched the reaction. The viscous solution was diluted with DMAc and a small amount was applied for SEC characterization.

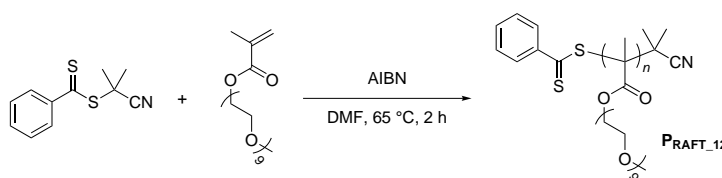
SEC characterization (DMAc, RI): $M_n = 26\,900 \text{ g} \cdot \text{mol}^{-1}$, $D = 1.27$.

9.5.11 Synthesis of Poly(DMAA-co-Phen-acrylate) via M-DDMAT (P_{RAFT_11})

Scheme 9.32: Synthesis of poly(DMAA) (P_{RAFT_11}) via RAFT polymerization, employing the RAFT agent methyl 2-(dodecylthiocarbonothioylthio)-2-methylpropionate (M-DDMAT).

The polymerization of P_{RAFT_11} equals the polymerization of P_{RAFT_10} , yet was performed with an additional amount of Phen-acrylate (11). Therefore, a photovial was equipped with *N,N*-dimethylacrylamide (1.14 g, 14.3 mmol, 300 equiv.), methyl 2-(dodecylthiocarbonothioylthio)-2-methylpropionate (18.0 mg, 47.5 μmol , 1.00 equiv.), Phen-acrylate (38.7 mg, 0.13 mmol, 2.65 equiv.) and 2,2'-azobis(2-methylpropionitril) (0.78 mg, 4.75 μmol , 0.10 equiv.). After the addition of 0.5 mL DMF, the vial was purged for 20 min with N_2 , sealed and heated for 9 hours at 60 °C. Opening the vial to air and cooling to ambient temperature quenched the reaction.

SEC characterization (DMAc, RI): $M_n = 16\,000\text{ g} \cdot \text{mol}^{-1}$, $D = 1.54$, $M_p = 27\,300\text{ g} \cdot \text{mol}^{-1}$.

9.5.12 Synthesis of Poly(PEGMA) via CPBD (P_{RAFT_12})

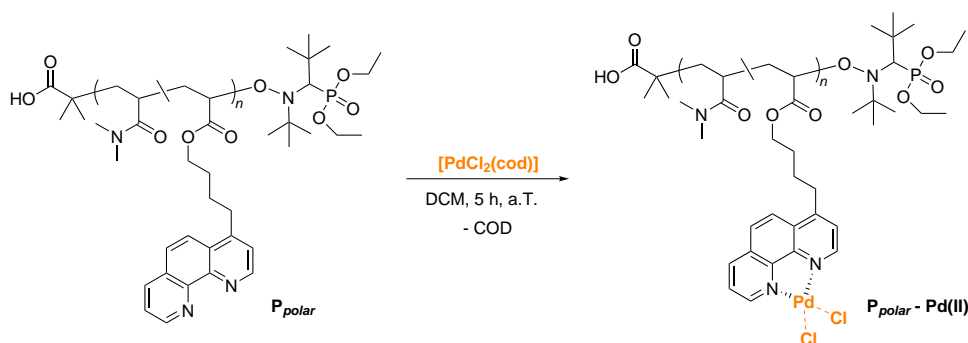
Scheme 9.33: Synthesis of poly(PEGMA) (P_{RAFT_12}) via RAFT polymerization, employing the RAFT agent 2-cyano-2-propyl benzodithioate (CPBD).

2-Cyano-2-propyl benzodithioate (15.0 mg, 67.8 μmol , 1.00 equiv.), the monomer poly(ethylene glycol) methyl ether methacrylate (PEGMA, $M_n = 500\text{ g} \cdot \text{mol}^{-1}$) (6.73 g, 13.6 mmol, 200 equiv.) and 2,2'-azobis(2-methylpropionitril) (2.78 mg, 16.9 μmol , 0.25 equiv.) were dissolved in 3.5 mL dry DMF and added to a photovial. After purging with N_2 for 20 min, the reaction was heated at 65 °C. Due to the reactive monomer, the reaction was already quenched after 2 hours.

SEC characterization (DMAc, RI): $M_n = 28\,000\text{ g} \cdot \text{mol}^{-1}$, $D = 1.27$.

9.6 Synthesis of Metallopolymers

9.6.1 Incorporation of Pd(II) Ions into P_{polar} ($P_{polar}-Pd(II)$)

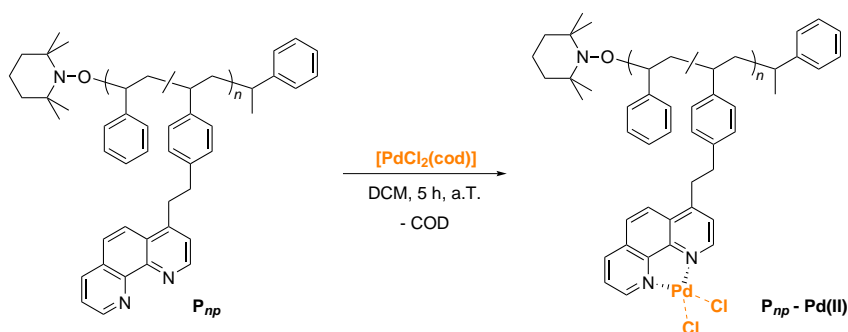


Scheme 9.34: The Phen units in P_{polar} coordinate in a 1:1 ratio to Pd(II) ions, yielding the metallopolymer $P_{polar}-Pd(II)$.

P_{polar} (60.0 mg, 0.03 mmol (referring to the amount of Phen functionality), 1.00 equiv.) was dissolved in 20 mL DCM and stirred. $[PdCl_2(cod)]$ (8.55 mg, 0.03 mmol, 1.00 equiv.) was dissolved in 10 mL DCM and added to the polymer solution. The reaction mixture was stirred for 5 hours at ambient temperature, concentrated and precipitated into cold Et_2O . Filtering of the solid, resulted in $P_{polar}-Pd(II)$.

Strong coordinative bonds allowed **SEC characterization** (DMAc, RI): $M_n = 26\,400\text{ g} \cdot \text{mol}^{-1}$, $D = 1.46$.

9.6.2 Incorporation of Pd(II) Ions into P_{np} ($P_{np}-Pd(II)$)



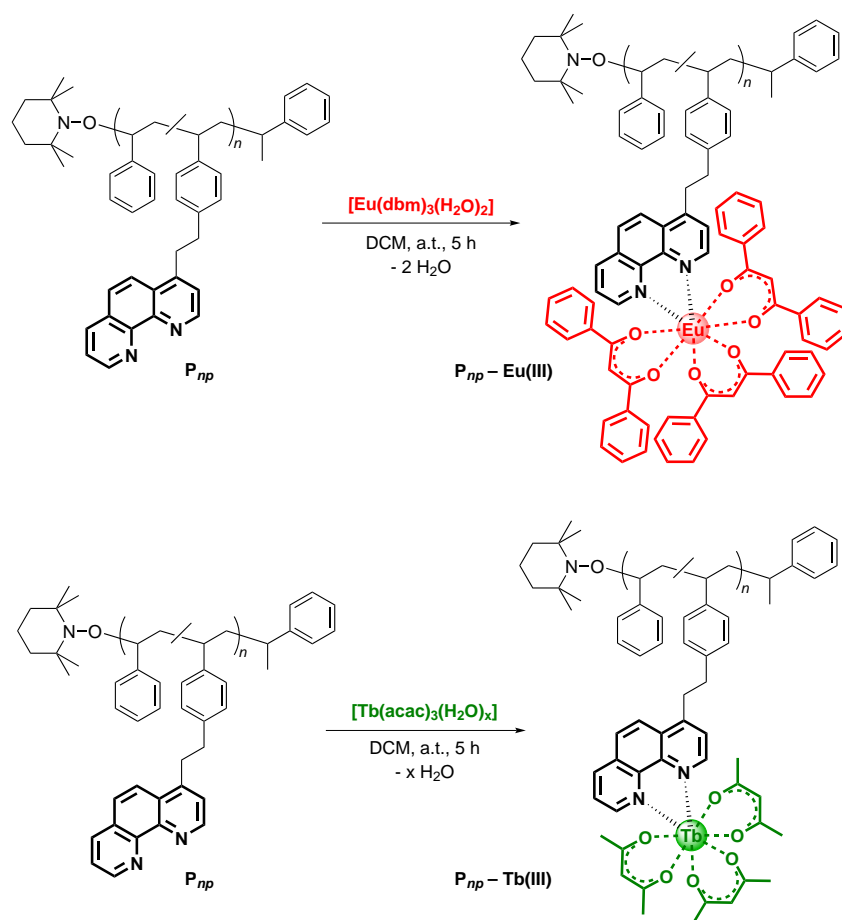
Scheme 9.35: The Phen units in P_{np} coordinate in a 1:1 ratio to Pd(II) ions, yielding the metallopolymer $P_{np}-Pd(II)$.

P_{np} (40.0 mg, 6.44 μmol (referring to the amount of Phen functionality), 1.00 equiv.) was dissolved in 20 mL DCM. In a second flask, $[PdCl_2(cod)]$ (1.84 mg, 6.44 μmol , 1.00 equiv.) was dissolved in

10 mL DCM and added *via* a glass pipette to the copolymer solution. The reaction mixture was stirred for 5 hours at ambient temperature, concentrated and precipitated into cold MeOH. The precipitate was subsequently filtered off, resulting in transition metal-complexed polymers.

Strong coordinative bonds allowed **SEC characterization** (THF, MALLS): $M_n = 31\,900 \text{ g} \cdot \text{mol}^{-1}$, $D = 1.14$.

9.6.3 Formation of Lanthanide Metallopolymers

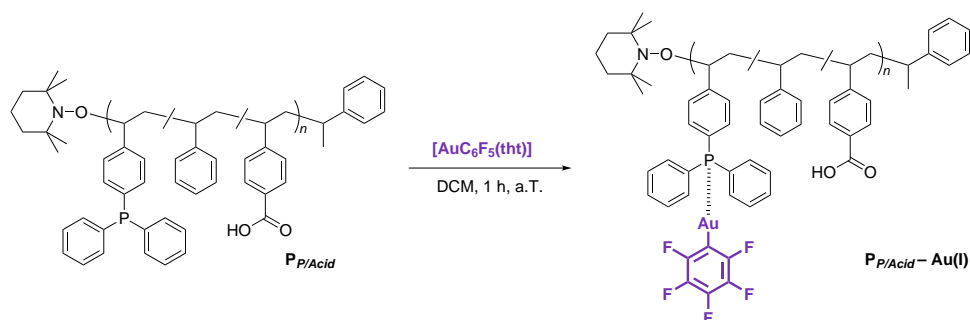


Scheme 9.36: Coordination of lanthanide(III) ions in a 1:1 ratio to the Phen units of copolymer P_{np} . Employing the precursor complex $[\text{Eu}(\text{dbm})_3(\text{H}_2\text{O})_2]$ (*top*), two water molecules are substituted by the Phen moieties. A similar reaction is assumed for the coordination of $[\text{Tb}(\text{acac})_3(\text{H}_2\text{O})_x]$ to P_{np} , in which as well two water molecules are replaced (*bottom*).

Poly(styrene-*co*-Phen-styrene) (40.0 mg, 6.44 μmol (referring to the amount of Phen functionality), 1.00 equiv.) was dissolved in 20 mL DCM. In a second flask, the lanthanide precursor complex (6.44 μmol , 1.00 equiv.) was dissolved in 10 mL DCM and added *via* a glass pipette to the copolymer solution. The reaction mixture was stirred for 5 hours at ambient temperature, concentrated and precipitated into cold MeOH. The precipitate was subsequently filtered off, resulting in transition metal-complexed polymers. To ensure a complete removal of non-reacted precursor complex, the solution can additionally be dialyzed in MeOH for 3 days.

Table 9.24: Lanthanide salts applied for the complexation of P_{np} .

$[\text{Eu}(\text{dbm})_3(\text{H}_2\text{O})_2]$	5.52 mg	857.74 $\text{g} \cdot \text{mol}^{-1}$
$[\text{Tb}(\text{acac})_3(\text{H}_2\text{O})_x]$	2.94 mg	456.25 $\text{g} \cdot \text{mol}^{-1}$ (anhydrous basis)

9.6.4 Functionalization of $P_{P/Acid}$ with $[AuC_6F_5]$ ($P_{P/Acid}-Au(I)$)

Scheme 9.37: The reaction between $[AuC_6F_5(tht)]$ and $P_{P/Acid}$ leads to a substitution of the tetrahydrothiophane (THT) ligand in the Au(I)-precursor complex by the phosphine moieties in the polymer, resulting in the gold-functionalized metallopolymer $P_{P/Acid}-Au(I)$.

Pentafluorophenyl(tetrahydrothiophene)gold(I) (40.0 mg, 0.09 mmol, 1.70 equiv. (in excess, in reference to the phosphine units in $P_{P/Acid}$)) was dissolved in 3.0 mL dry DCM in a 25 mL brown round bottom flask. Poly(styrene-*co*-4-(diphenylphosphino)styrene-*co*-4-vinylbenzoic acid) ($P_{P/Acid}$) (200 mg, 0.05 mmol, 1.00 equiv. (in reference to the phosphine units in the polymer)) was dissolved in 7.0 mL dry DCM and added to the flask containing the gold precursor *via* a pipette. The reaction mixture was stirred under the exclusion of light for 1 hour at ambient temperature. Subsequently, the mixture was concentrated under reduced pressure and the remaining solution was precipitated into cold MeOH. The final product was filtered off and dried under vacuum.

Table 9.25: Characterization of $P_{P/Acid}-Au(I)$.

White solid, obtained product: 198 mg.

SEC characterization (THF, RI): $M_n = 45\,500\text{ g}\cdot\text{mol}^{-1}$, $D = 1.21$.

1H NMR (400 MHz, THF- d_8): $\delta/\text{ppm} = 11.2$ (bs, COOH), 7.91–7.62 (m, aromatic protons of 4-vinylbenzoic acid (2H), *meta*), 7.62–7.38 (m, aromatic protons of 4-(diphenylphosphino)styrene (14H)), 7.36–6.21 (m, aromatic protons of styrene and 4-vinylbenzoic acid), 2.65–1.22 (m, aliphatic protons, backbone).

^{19}F NMR (377 MHz, THF- d_8): $\delta/\text{ppm} = -116.3$ (br, *ortho*-F), -160.4 (br, *para*-F), -163.9 (br, *meta*-F).

$^{31}P\{^1H\}$ NMR (162 MHz, THF- d_8): $\delta/\text{ppm} = 41.1$ (br, $PPh_2Ar-AuC_6F_5$).

IR (ATR): $\tilde{\nu} [\text{cm}^{-1}] = 3082$ (w), 3060 (m), 3026 (m), 3002 (vw), 2922 (s), 2849 (w), 1734 (w), 1690 (w), 1601 (m), 1584 (vw), 1493 (s), 1453 (s), 1356 (vw), 1313 (vw), 1283 (vw), 1181 (vw), 1155 (vw), 1103 (w), 1071 (w), 1061 (w), 1028 (w), 1002 (vw), 954 (m), 907 (vw), 842 (vw), 828 (vw), 792 (vw), 752 (m), 697 (vs), 538 (m).

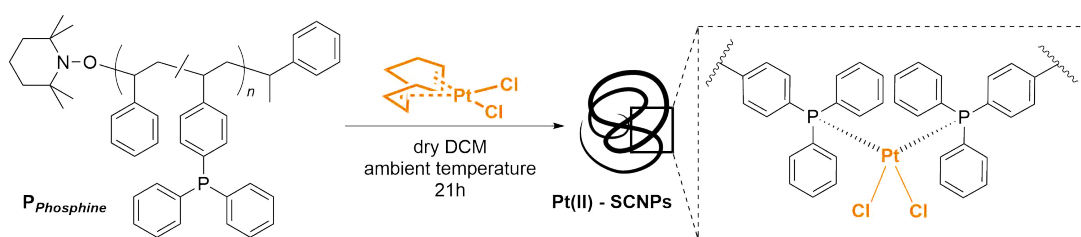
9.7 Formation of Single-Chain Nanoparticles

For a general procedure to collapse single-chains *via* coordination to metal complexes into nanoparticles, the polymer and the metal complex are dissolved separately in suitable solvents. Subsequently, the dissolved polymer chains are added to the solution containing the metal precursor complexes, in conditions appropriate for each system, *e.g.* type of crosslinking, amount of functional groups, reactivities, chain length. After complete addition, the combined solutions are concentrated under reduced pressure and the remaining oil is precipitated. The final SCNPs are obtained after filtering.

The main requirement for the preparation of metal-SCNPs is a high dilution during their formation to prohibit intermolecular linkages. Otherwise, the metal complexes crosslink between chains, resulting not in single, definable nanoparticles, yet in a disordered network. To avoid excessive use of solvent, a high dilution can be established employing a syringe pump, which adds the dissolved copolymer dropwise to the metal complex in solution. Depending on the percentage of functionality in the polymer, the dropping rate is adapted. In the current thesis a rate between 1.0 and 1.5 mL · hour⁻¹ was employed. The low dose rate ensures that the copolymer in every drop of the solution has already reacted, when the next drop of copolymer mixture is added to the solution of metal complexes.

Depending on the employed polymer or metal complex, additional precautions had to be taken. For instance in the present thesis, the oxidation of the phosphine side groups or of the molybdenum compounds had to be avoided. In both cases, the units would change their chemical properties and would no longer participate in the single-chain collapse.

9.7.1 Synthesis of Platinum(II)-complexed SCNPs



Scheme 9.38: Substitution of cyclooctadiene in the precursor complex $[\text{PtCl}_2(\text{cod})]$ by phosphine ligands in $\text{P}_{\text{phosphine}}$. The ligand-to-metal ratio of 1:2 causes the formation of Pt(II)-SCNPs.

Poly(styrene-*co*-4-(diphenylphosphino)styrene) ($\text{P}_{\text{Phosphine}}$) (0.05 g, 0.02 mmol (referring to the phosphine units), 1.00 equiv.) was dissolved in 20 mL dry DCM in a flame dried flask. In a separate flask, dichloro(1,5-cyclooctadiene)platinum(II) $[\text{PtCl}_2(\text{cod})]$ (5.61 mg, 0.01 mmol, 0.50 equiv.) was dissolved in 50 mL dry DCM, purged with argon and sealed with a septum. Applying a syringe pump, the polymer solution was added dropwise to the metal-salt solution (dropping-rate $1 \text{ mL} \cdot \text{hour}^{-1}$) at ambient temperature. After complete addition, the solution was stirred for another hour and subsequently concentrated to approx. 2 mL under reduced pressure. Precipitating into cold MeOH resulted in the final nanoparticles.

Table 9.26: Characterization of the Pt(II)-SCNPs.

White powder, obtained product: 50.2 mg.

SEC characterization (THF, RI): $M_n = 31\,000 \text{ g} \cdot \text{mol}^{-1}$, $D = 1.22$.

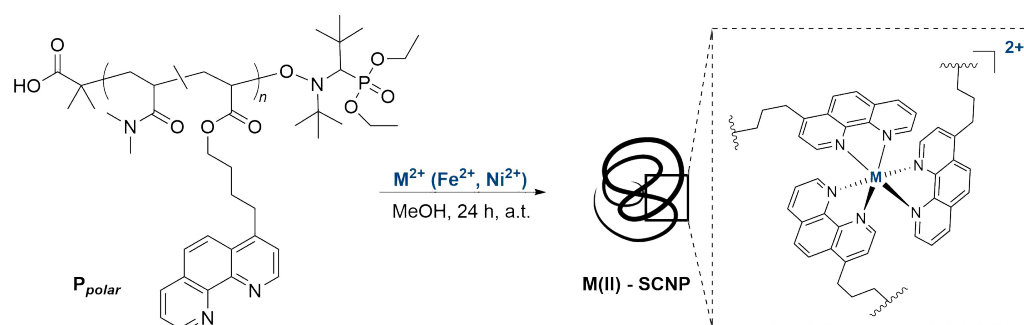
^1H NMR (400 MHz, CDCl_3): $\delta/\text{ppm} = 7.92\text{--}6.10$ (m, aromatic protons), $2.34\text{--}0.35$ (m, aliphatic protons, backbone).

$^{31}\text{P}\{^1\text{H}\}$ NMR (162 MHz, CDCl_3): $\delta/\text{ppm} = 19.5$ (d, $^1J_{\text{P,Pt}} = 2700 \text{ Hz}$, *trans*- $\text{PPh}_2\text{Ar-PtCl}_2\text{-PPh}_2\text{Ar}$), 13.4 (d, $^1J_{\text{P,Pt}} = 3706 \text{ Hz}$, *cis*- $\text{PPh}_2\text{Ar-PtCl}_2\text{-PPh}_2\text{Ar}$).

Ratio of *cis/trans* geometry approx. 9:1.

^{195}P NMR (86 MHz, CDCl_3): $\delta/\text{ppm} = -4033$ (t, $^1J_{\text{Pt,P}} = 2648 \text{ Hz}$, *trans*), -4413 (t, $^1J_{\text{Pt,P}} = 3694 \text{ Hz}$, *cis*).

9.7.2 Synthesis of Fe(II)- and Ni(II)-SCNPs

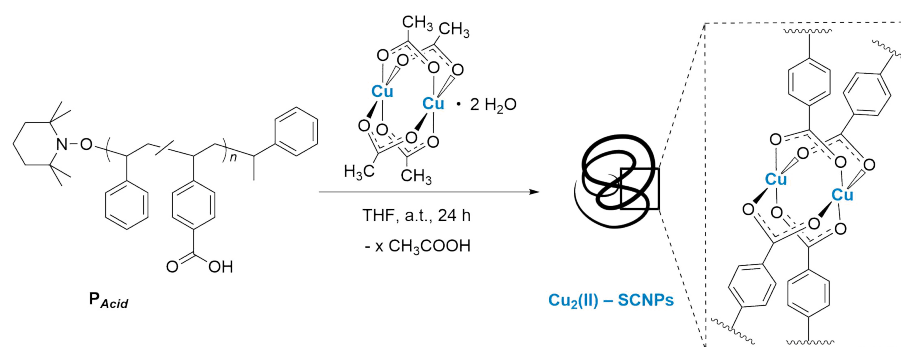


Scheme 9.39: A coordination of three Phen units in P_{polar} to one metal ion leads to a chain collapse. Performing the reaction under high dilution, thus preventing intermolecular bond formation, exclusively single-chain nanoparticles were formed. Employed were the transition metals iron(II) and nickel(II), resulting in Fe(II)- and Ni(II)-SCNPs.

In a flask, the corresponding metal salt (0.01 mmol, 0.33 equiv.) was dissolved at ambient temperature in 60.0 mL MeOH and the flask was sealed with a septum. P_{polar} (60.0 mg, 0.03 mmol (referring to the amount of Phen functionality), 1.00 equiv.) was dissolved in 20 mL MeOH. While stirring the first flask, the polymer solution was added dropwise to the stirred metal salt solution *via* a syringe pump with a dropping rate of $1 \text{ mL} \cdot \text{h}^{-1}$. After complete addition (20 hours), the solution was stirred for additional 4 hours. The solvent was removed under reduced pressure and the remaining solid was dissolved in a small amount of DCM ($\sim 1 \text{ mL}$). After precipitating into cold Et_2O , the solid was filtered off and dried, resulting in the desired Fe(II)-SCNPs and Ni(II)-SCNPs, respectively.

Table 9.27: Applied metal-salts for SCNP formation of P_{polar} .

$\text{FeSO}_4 \cdot 7 \text{H}_2\text{O}$	2.56 mg	$278.02 \text{ g} \cdot \text{mol}^{-1}$
$\text{NiSO}_4 \cdot 6 \text{H}_2\text{O}$	2.58 mg	$280.86 \text{ g} \cdot \text{mol}^{-1}$

9.7.3 Synthesis of Cu₂(II)-SCNPs

Scheme 9.40: The replacement of the acetic acid ligands in the precursor complex $[\text{Cu}(\text{OAc})_2]_2$ by the benzoic acid moieties of P_{Acid} results, provided a high dilution, in single-chain collapsed $\text{Cu}_2(\text{II})$ -SCNPs. The geometrical arrangement of the copper(II) precursor complex is transferred to the polymer chain, thus the linkage in the SCNPs exhibits paddlewheel $\text{Cu}_2(\text{II})$ motifs.

Copper(II) acetate $[\text{Cu}(\text{OAc})_2]_2$ (4.60 mg, 11.5 μmol , 0.25 equiv.) was dissolved in 25.0 mL THF ($c = 4.6 \cdot 10^{-4} \text{ mol} \cdot \text{L}^{-1}$) in a 250 mL flask, equipped with a dropping funnel. Copolymer P_{Acid} (70.0 mg, 45.5 μmol (referring to the benzoic acid functionality), 1.00 equiv.) was dissolved in 100 mL THF in the funnel. While stirring the metal salt solution, the polymer solution was added dropwise with a dropping rate of approx. $5 \text{ mL} \cdot \text{h}^{-1}$. After complete addition (20 hours), the blue solution was stirred for additional 4 hours, until concentrated under reduced pressure. Precipitation in cold MeOH and subsequent filtration resulted in blue solid, which was dried under high vacuum.

Table 9.28: Characterization of the $\text{Cu}_2(\text{II})$ -SCNPs.

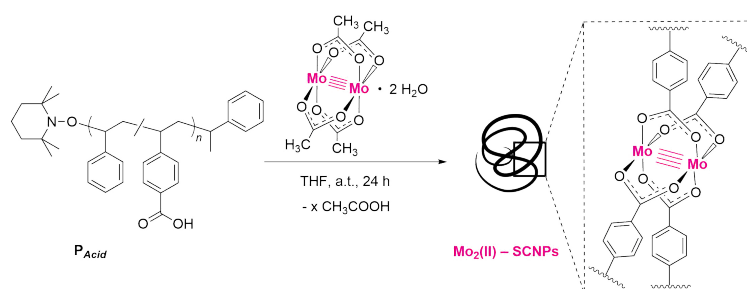
Blue powder.

SEC characterization (THF, RI): $M_n = 24\,500 \text{ g} \cdot \text{mol}^{-1}$, $M_p = 31\,000 \text{ g} \cdot \text{mol}^{-1}$, $D = 1.21$.

¹H NMR (400 MHz, THF-*d*₈): $\delta/\text{ppm} = 7.95\text{--}7.51$ (m, aromatic protons of 4-vinylbenzoic acid, *meta*-position (2H)), $7.59\text{--}5.82$ (m, aromatic protons), $2.36\text{--}0.62$ (m, aliphatic protons, backbone) – *The multiplet resonance at $\delta = 7.95\text{--}7.51 \text{ ppm}$ (CH-benzoic acid) is significantly broadened, compared to P_{Acid} , due to the coordination of paramagnetic Cu(II) ions. At $\delta = 11.2 \text{ ppm}$ a singlet resonance is detected for R-COOH, indicating free carboxylic acid moieties, most likely due to an axial coordination of the acidic functionalities to the Cu_2^{4+} moieties.*

IR (ATR): $\tilde{\nu} [\text{cm}^{-1}] = 3083$ (vw), 3060 (w), 3026 (s), 3001 (vw), 2923 (s), 2849 (w), 1733 (w), 1691 (w), 1619 (m), 1603 (m), 1583 (vw), 1565 (vw), 1493 (s), 1452 (s), 1407 (s), 1374 (vw), 1181 (w), 1155 (vw), 1070 (vw), 1028 (w), 907 (w), 857 (vw), 757 (s), 698 (vs), 540 (m).

UV-Vis: $\lambda_{\text{max}} [\text{nm}] = 433$.

9.7.4 Synthesis of Mo₂(II)-SCNPs

Scheme 9.41: The replacement of the acetic acid ligands in the precursor complex [Mo(OAc)₂]₂ by the benzoic acid moieties of P_{Acid} results, provided a high dilution, in single-chain collapsed Mo₂(II)-SCNPs. The geometrical arrangement of the molybdenum(II) precursor complex is maintained in the polymer chain, thus exhibiting paddlewheel Mo₂(II) motifs.

For the synthesis of Mo₂(II)-SCNPs the exclusion of water and oxygen is essential. Therefore, schlenk techniques were applied and only dry and degassed solvents (THF, MeOH) were utilized. Molybdenum(II) acetate [Mo(OAc)₂]₂ (7.00 mg, 16.3 μmol, 0.25 equiv.) was dissolved in 50.0 mL THF ($c = 3.3 \cdot 10^{-4} \text{ mol} \cdot \text{L}^{-1}$). 100 mg of copolymer P_{Acid} (65.0 μmol, referring to the amount of benzoic acid functionality, 1.00 equiv.) was dissolved in 120 mL THF. While stirring the metal salt solution, the polymer solution was added dropwise with a dropping rate of $\sim 3 \text{ mL} \cdot \text{h}^{-1}$. After complete addition (40 hours), the yellow solution was stirred for additional 8 hours. The solution was concentrated under reduced pressure and subsequently precipitated into cold MeOH. The solid was filtered off and dried under vacuum. The characterization of Mo₂(II)-SCNPs *via* SEC measurement was not feasible, due to their high sensitivity towards air and moisture.

Table 9.29: Characterization of the Mo₂(II)-SCNPs.

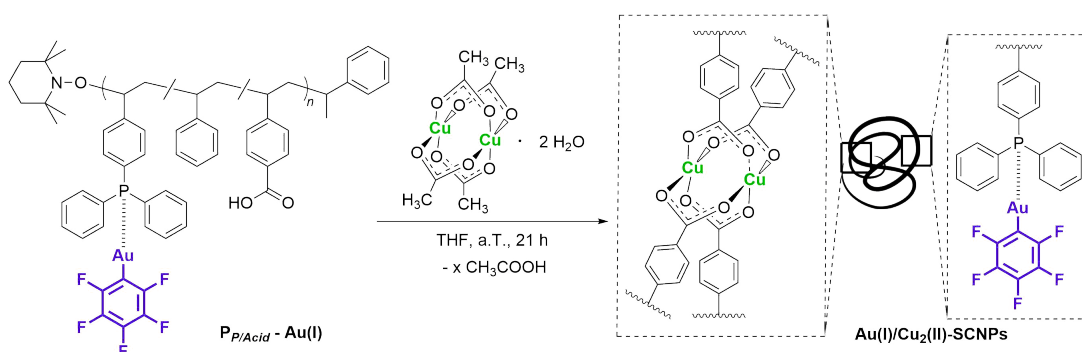
Orange/red powder.

¹H NMR (400 MHz, CDCl₃): $\delta/\text{ppm} = 8.16\text{--}7.54$ (m, aromatic protons of 4-vinylbenzoic acid, *meta*-position (2H)), 7.37–6.13 (m, aromatic protons), 2.55–0.89 (m, aliphatic protons, backbone). – *Additional NMR measurements in THF-*d*₈ revealed no free carboxylic acid proton resonances.*

IR (ATR): $\tilde{\nu} [\text{cm}^{-1}] = 3082$ (vw), 3060 (w), 3026 (s), 3001 (vw), 2922 (s), 2849 (w), 1602 (m), 1556 (w), 1493 (s), 1451 (s), 1401 (m), 1181 (w), 1154 (vw), 1068 (vw), 1028 (w), 907 (w), 845 (vw), 756 (s), 698 (vs), 540 (m).

Raman (solid state): $\tilde{\nu} [\text{cm}^{-1}] = 3055$ (s), 3000 (vw), 2977 (vw), 2910 (m), 2851 (w), 1606 (s), 1583 (m), 1513 (m), 1451 (w), 1411 (s), 1401 (s), 1332 (vw), 1184 (m), 1156 (w), 1032 (m), 1002 (vs), 795 (w), 622 (m), 408 (w), 225 (w).

UV-Vis: $\lambda_{\text{max.}} [\text{nm}] = 433$.

9.7.5 Synthesis of Heterometallic Au(I)/Cu₂(II)-SCNPs

Scheme 9.42: The benzoic acid moieties in P_{P/Acid} substitute the acetate units in the precursor complex [Cu(OAc)₂]₂(H₂O)₂, causing an incorporation of Cu₂(II) ions into the polymer scaffold and thus a collapse of the polymer into Au(I)/Cu₂(II)-SCNPs.

The precursor complex [Cu(OAc)₂]₂(H₂O)₂ (7.57 mg, 0.02 mmol, 0.50 equiv. (in reference to the benzoic acid units in the polymer)) was dissolved in 150 mL THF in a 250 mL flask. The polymer P_{P/Acid}-Au(I) (60.0 mg, 0.04 mmol, 1.00 equiv. (in reference to its benzoic acid units)) was dissolved in 24 mL THF and transferred into a syringe, which was covered in aluminum foil. The polymer solution was added dropwise to the copper-solution, applying a syringe pump (dropping rate 1.5 mL · h⁻¹), at ambient temperature. After complete addition, the mixture was stirred for an additional hour. Following, the solvent was removed under reduced pressure until a blue oil was obtained. Upon dropwise addition into cold MeOH, the polymeric material precipitated and was filtered off.

Table 9.30: Characterization of the Au(I)/Cu₂(II)-SCNPs.

Blue solid, obtained product: 40.2 mg.

SEC characterization (THF, RI): $M_n = 34\,900\text{ g} \cdot \text{mol}^{-1}$, $D = 1.24$.

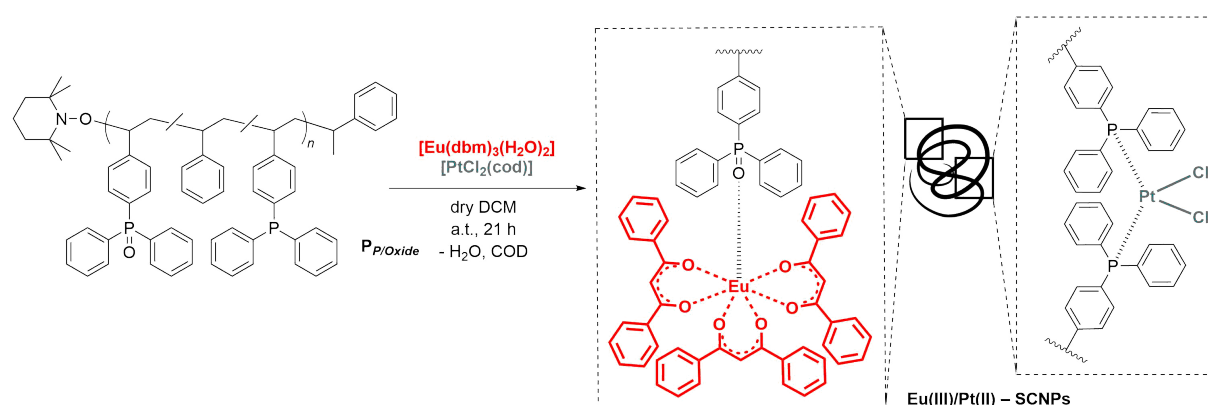
¹H NMR (400 MHz, CDCl₃): $\delta/\text{ppm} = 7.48$ (s, aromatic protons of 4-(diphenylphosphino)-styrene, H-a), 7.34–6.14 (m, aromatic protons of styrene and 4-vinylbenzoic acid, H-b/H-c), 2.41–0.66 (m, aliphatic protons, H-d).

¹⁹NMR (377 MHz, CDCl₃): $\delta/\text{ppm} = -115.80$ (br), -157.98 (br), -162.08 (br).

³¹P{¹H} NMR (162 MHz, CDCl₃): $\delta/\text{ppm} = 41.2$ (s, PPh₂Ar-AuC₆F₅).

IR (ATR): $\tilde{\nu}$ [cm⁻¹] = 3083 (w), 3060 (w), 3026 (m), 3002 (vw), 2924 (s), 2850 (w), 1617 (w), 1602 (m), 1585 (vw), 1546 (vw), 1493 (s), 1453 (s), 1439 (m), 1407 (m), 1376 (vw), 1356 (vw), 1183 (vw), 1155 (vw), 1103 (vw), 1072 (vw), 1061 (w), 1028 (w), 1002 (vw), 955 (m), 907 (vw), 843 (vw), 827 (vw), 790 (vw), 756 (m), 698 (vs), 539 (m).

9.7.6 Synthesis of Heterometallic Eu(III)/Pt(II)-SCNPs



Scheme 9.43: Orthogonal reaction between the phosphine oxide units in $\text{P}_{\text{P/Oxide}}$ with Eu(III) ions and between the phosphine units with Pt(II) ions. While the formation of the Eu(III)-complex proceeds most likely in a 1:1 metal-to-ligand ratio, the coordination to platinum(II) ions in a 2:1 ligand–metal ratio results, provided a sufficiently high dilution during synthesis, in a single-chain collapse. In this one-pot reaction two types of metal ions coordinate orthogonally to two functional moieties in one polymer system, yielding fluorescent Eu(III)/Pt(II)-SCNPs.

Poly(styrene-*co*-4-(diphenylphosphino)styrene-*co*-4-(diphenylphosphine oxide) (50.0 mg, 7.90 μmol phosphine oxide functional groups, 15.8 μmol phosphine functional groups, 1.00 equiv.) was dissolved in 20.0 mL dry DCM and purged with argon for 5 min. In a separate 250 mL flask, the precursor complexes $[\text{Eu}(\text{dbm})_3(\text{H}_2\text{O})_2]$ (6.77 mg, 7.90 μmol , 1.00 equiv.) and $[\text{PtCl}_2(\text{cod})]$ (2.95 mg, 7.90 μmol , 0.50 equiv.) were dissolved in 150 mL dry DCM and purged with argon for 30 min. Applying a syringe pump, the polymer solution was added to the solution of metal ions over a time period of 20 hours (dropping rate 1 mL \cdot hour $^{-1}$). After complete addition, the solution was stirred for another hour, before concentrated to 1–2 mL under reduced pressure. The remaining solution was precipitated into cold MeOH and stirred for 1 hour. The filtration of the colorless solid resulted in the final Eu(III)/Pt(II)-SCNPs.

Table 9.31: Characterization of Eu(III)/Pt(II)-SCNPs.

White powder.

SEC characterization (THF, RI): $M_n = 20\,200 \text{ g} \cdot \text{mol}^{-1}$, $D = 1.49$.

The linkage between Eu(III) and the phosphine oxide units in the polymer chain were not strong enough to withstand the harsh conditions of in a SEC measurement. Therefore, the above state results describe the SCNP formation upon Pt(II) addition. The removal of the europium(III) complexes from the polymer chain is observed by signals at high retention times, belonging to molecular substances. Since those signals do not arise in the elugram of the pure copolymer $P_{P/Oxide}$, they belong most likely to free Eu(III)-complexes.

^1H NMR (400 MHz, CDCl_3): $\delta/\text{ppm} = 16.89$ (s, $\text{Eu}(\text{dbm})_3\text{-CH}$), 8.08–7.97 (m, $\text{Eu}(\text{dbm})_3\text{-Ph}$), 7.78–6.07 (m, aromatic protons of all incorporated monomers), 7.61–7.47 (m, $\text{Eu}(\text{dbm})_3\text{-Ph}$), 2.45–0.65 (m, aliphatic protons, backbone).

^{31}P NMR (162 MHz, CDCl_3): $\delta/\text{ppm} = 29.1$ (br, $\text{O=PPh}_2\text{Ar}$), 19.5 (*trans*- $\text{PPh}_2\text{Ar-PtCl}_2\text{-PPh}_2\text{Ar}$), 13.5 (d, $^1J_{\text{P,Pt}} = 3661 \text{ Hz}$, *cis*- $\text{PPh}_2\text{Ar-PtCl}_2\text{-PPh}_2\text{Ar}$).

Ratio *cis/trans* approx. = 30:1

Due to the low amount of *trans*-species in the SCNPs, no satellites for a *trans*-Pt–P were detectable.

^{195}Pt NMR (86 MHz, CDCl_3): $\delta/\text{ppm} = -4420$ (t, $^1J_{\text{Pt,P}} = 3715 \text{ Hz}$, *cis*).

Due to the low amount of *trans*-species, the corresponding resonance was not detected.

IR (ATR): $\tilde{\nu} [\text{cm}^{-1}] = 3082$ (vw), 3059 (w), 3025 (m), 3001 (vw), 2923 (s), 2849 (w), 1600 (m), 1549 (vw), 1519 (vw), 1493 (s), 1452 (s), 1438 (m), 1405 (vw), 1377 (vw), 1312 (vw), 1262 (vw), 1202 (vw), 1183 (vw), 1155 (vw), 1119 (vw), 1097 (w), 1069 (vw), 1028 (w), 1002 (vw), 907 (vw), 753 (m), 697 (vs), 542 (m), 522 (w).

Bibliography

- [1] A. M. Hanlon, C. K. Lyon, E. B. Berda, *Macromolecules* **2016**, *49*, 2–14.
- [2] E. B. Berda, E. J. Foster, E. W. Meijer, *Macromolecules* **2010**, *43*, 1430–1437.
- [3] E. Harth, B. V. Horn, V. Y. Lee, D. S. Germack, C. P. Gonzales, R. D. Miller, C. J. Hawker, *J. Am. Chem. Soc.* **2002**, *124*, 8653–8660.
- [4] H. Rothfuss, N. D. Knöfel, P. Tzvetkova, N. C. Michenfelder, S. Baraban, A.-N. Unterreiner, P. W. Roesky, C. Barner-Kowollik, *Chem. Eur. J.* **2018**, *24*, 17475.
- [5] M. A. J. Gillissen, I. K. Voets, E. W. Meijer, A. R. A. Palmans, *Polym. Chem.* **2012**, 3166–3174.
- [6] S. D. Steichen, M. Caldorera-Moore, N. A. Peppas, *Eur. J. Pharm. Sci.* **2013**, *48*, 416–427.
- [7] M. Burnworth, L. Tang, J. R. Kumpfer, A. J. Duncan, F. L. Beyer, G. L. Fiore, S. J. Rowan, C. Weder, *Nature* **2011**, 334–337.
- [8] H. Rothfuss, N. D. Knöfel, P. W. Roesky, C. Barner-Kowollik, *J. Am. Chem. Soc.* **2018**, *140*, 5875–5881.
- [9] J. Willenbacher, O. Altintas, V. Trouillet, N. Knöfel, M. J. Monteiro, P. W. Roesky, C. Barner-Kowollik, *Polym. Chem.* **2015**, 4358–4365.
- [10] Y. Tsuji, R. Takeuchi, H. Ogawa, Y. Watanabe, *Chem. Lett.* **1986**, *15*, 293–294.
- [11] G. Odian, *Principles of Polymerization*, Wiley, **2004**.
- [12] W. H. Carothers, *Chem. Rev.* **1931**, *8*, 353–426.
- [13] W. H. Carothers, *J. Am. Chem. Soc.* **1929**, *51*, 2548–2559.
- [14] M. Zhang, S. June, T. Long in *Polymer Science, Vol. 5*, Elsevier, **2012**, pp. 7–47.
- [15] W. H. Carothers, *Trans. Faraday Soc.* **1936**, *32*, 39–49.
- [16] E. Norrish, R. G. W.; F. R. S.; Brookmann, *Proc. Royal Soc. Lond. Ser. A: Mathematical Physical and Engineering Sciences* **1939**, *171*, 147–171.
- [17] P. J. Flory, *J. Am. Chem. Soc.* **1937**, *59*, 241–253.
- [18] F. R. Mayo, *J. Am. Chem. Soc.* **1943**, *65*, 2324–2329.
- [19] R. F. T. Stepto, *Pure Appl. Chem.* **2009**, *81*, 779.
- [20] M. Gilbert in *Brydson's Plastics Materials*, (Ed.: M. Gilbert), Butterworth-Heinemann, **2017**, pp. 59–73.
- [21] P. J. Flory, *Principles of polymer chemistry*, Cornell Univ. Pr., Ithaca, NY, **1953**.
- [22] P. Nesvadba in *Encyclopedia of Radicals in Chemistry, Biology and Materials*, American Cancer Society, **2012**.

- [23] H. Sawada, *J. Macromol. Sci. Part C* **1969**, 3, 313–338.
- [24] M. Szwarc, *Nature* **1956**, 178, 1168–1169.
- [25] D. Baskaran, A. H. Müller, *Prog. Polym. Sci.* **2007**, 32, 50 Years of Living Polymerization, 173–219.
- [26] T. Otsu, M. Yoshida, T. Tazaki, *Macromol. Rapid Commun.* **1982**, 3, 133–140.
- [27] D. Greszta, D. Mardare, K. Matyjaszewski, *Macromolecules* **1994**, 27, 638–644.
- [28] W. A. Braunecker, K. Matyjaszewski, *Prog. Polym. Sci.* **2007**, 32, 50 years of living polymerization, 93–146.
- [29] D. Gigmes, *Nitroxide Mediated Polymerization: From Fundamentals to Applications in Materials Science*, Royal Society of Chemistry, **2015**.
- [30] C. J. Hawker, A. W. Bosman, E. Harth, *Chem. Rev.* **2001**, 101, 3661–3688.
- [31] C. J. Hawker, E. Elce, J. Dao, W. Volksen, T. P. Russell, G. G. Barclay, *Macromolecules* **1996**, 29, 2686–2688.
- [32] R. B. Grubbs, *Polym. Rev.* **2011**, 51, 104–137.
- [33] E. Rizzardo, D. H. Solomon, *Polym. Bull.* **1979**, 1, 529–534.
- [34] H. Fischer, *Macromolecules* **1997**, 30, 5666–5672.
- [35] H. Fischer, *J. Polym. Sci. A* **1999**, 37, 1885–1901.
- [36] G. Moad, E. Rizzardo, *Macromolecules* **1995**, 28, 8722–8728.
- [37] C. J. Hawker, G. G. Barclay, A. Orellana, J. Dao, W. Devonport, *Macromolecules* **1996**, 29, 5245–5254.
- [38] C. J. Hawker, *Angew. Chem. Int. Ed.* **1995**, 34, 1456–1459.
- [39] P. B. Zetterlund, *Macromol. React. Eng.* **2010**, 4, 663–671.
- [40] L. Marx, P. Hemery, *Polymer* **2009**, 50, 2752–2761.
- [41] K. Bian, M. F. Cunningham, *J. Polym. Sci. A Polym. Chem.* **2006**, 44, 414–426.
- [42] T. P. T. Le, G. Moad, E. Rizzardo, S. H. Thang, **1998**.
- [43] P. Delduc, C. Tailhan, S. Z. Zard, *J. Chem. Soc., Chem. Commun.* **1988**, 308–310.
- [44] S. Perrier, P. Takolpuckdee, *J. Polym. Sci. A Polym. Chem.* **2005**, 43, 5347–5393.
- [45] A. Goto, T. Fukuda, *Prog. Polym. Sci.* **2004**, 29, 329–385.
- [46] L. Barner, T. P. Davis, M. H. Stenzel, C. Barner-Kowollik, *Macromol. Rapid Commun.* **2007**, 28, 539–559.
- [47] C. Barner-Kowollik, *Handbook of RAFT Polymerization*, Wiley, **2008**.
- [48] S. Perrier, *Macromolecules* **2017**, 50, 7433–7447.
- [49] G. Moad, J. Chiefari, Y. K. Chong, J. Krstina, R. T. A. Mayadunne, A. Postma, E. Rizzardo, S. H. Thang, *Polym. Int.* **2000**, 49, 993–1001.
- [50] G. Moad, E. Rizzardo, S. H. Thang, *Polym. Int.* **2011**, 60, 9–25.
- [51] D. J. Keddie, G. Moad, E. Rizzardo, S. H. Thang, *Macromolecules* **2012**, 45, 5321–5342.
- [52] H. Willcock, R. K. O'Reilly, *Polym. Chem.* **2010**, 1, 149–157.

- [53] J. Rubio-Cervilla, H. Frisch, C. Barner-Kowollik, J. A. Pomposo, *Macromol. Rapid Commun.* **2018**, 1800491.
- [54] M. R. Hill, R. N. Carmean, B. S. Sumerlin, *Macromolecules* **2015**, *48*, 5459–5469.
- [55] A. Jenkins, P. Kratochvil, R. F. T. Stepto, U. W. Suter, *Pure Appl. Chem.* **2009**, *68*, 2287–2311.
- [56] M. D. Lechner, K. Gherke, E. H. Nordmeier, *Makromolekulare Chemie*, 5th Edition, Springer-Spektrum, **2014**.
- [57] F. R. Mayo, F. M. Lewis, *J. Am. Chem. Soc.* **1944**, *66*, 1594–1601.
- [58] J. Schweer, *Macromol. Theory Simul.* **1993**, *2*, 485–502.
- [59] M. A. R. Meier, C. Barner-Kowollik, *Adv. Mater.* **2019**, *0*, 1806027.
- [60] J.-F. Lutz, *Macromol. Rapid Commun.* **2017**, *38*, 1700582.
- [61] W. Konrad, F. R. Bloesser, K. S. Wetzler, A. C. Boukis, M. A. R. Meier, C. Barner-Kowollik, *Chem. Eur. J.* **2018**, *24*, 3413.
- [62] J.-F. Lutz, M. Ouchi, D. R. Liu, M. Sawamoto, *Science* **2013**, *341*.
- [63] C. G. Hardy, J. Zhang, Y. Yan, L. Ren, C. Tang, *Prog. Polym. Sci.* **2014**, *39*, Special Issue on Polymer Chemistry, 1742–1796.
- [64] G. Whittell, I. Manners, *Adv. Mater.* **2007**, *19*, 3439–3468.
- [65] Y. Wang, D. Astruc, A. S. Abd-El-Aziz, *Chem. Soc. Rev.* **2019**, *48*, 558–636.
- [66] A. Winter, U. S. Schubert, *Chem. Soc. Rev.* **2016**, *45*, 5311–5357.
- [67] K. C. Bentz, S. M. Cohen, *Angew. Chem. Int. Ed.* **2018**, *57*, 14992–15001.
- [68] J.-C. Eloi, L. Chabanne, G. R. Whittell, I. Manners, *Mater. Today* **2008**, *11*, 28–36.
- [69] J. Elbert, M. Gallei, C. Rüttiger, A. Brunsen, H. Didzoleit, B. Stühn, M. Rehahn, *Organometallics* **2013**, *32*, 5873–5878.
- [70] D. E. Herbert, U. F. J. Mayer, I. Manners, *Angew. Chem. Int. Ed.* **2007**, *46*, 5060–5081.
- [71] R. A., A. Musgrave, D. Russell, D. W. Hayward, G. R. Whittell, P. G. Lawrence, P. J. Gates, J. C. Green, I. Manners, *Nat. Chem.* **2017**, 743–750.
- [72] H.-J. Kim, J.-H. Lee, M. Lee, *Angew. Chem. Int. Ed.* **2005**, *44*, 5810–5814.
- [73] U. Velten, M. Rehahn, *Chem. Commun.* **1996**, 2639–2640.
- [74] X. de Hatten, D. Asil, R. H. Friend, J. R. Nitschke, *J. Am. Chem. Soc.* **2012**, *134*, 19170–19178.
- [75] L. Dennany, C. F. Hogan, T. E. Keyes, R. J. Forster, *Anal. Chem.* **2006**, *78*, 1412–1417.
- [76] Y. Sun, Z. Chen, E. Puodziukynaite, D. M. Jenkins, J. R. Reynolds, K. S. Schanze, *Macromolecules* **2012**, *45*, 2632–2642.
- [77] G. Polymeropoulos, G. Zapsas, K. Ntetsikas, P. Bilalis, Y. Gnanou, N. Hadjichristidis, *Macromolecules* **2017**, *50*, 1253–1290.
- [78] D. Bleger, R. Klajn, *Macromol. Rapid Commun.* **2018**, *39*, 1700827.
- [79] I. Cobo, M. Li, B. S. Sumerlin, S. Perrier, *Nat. Mater.* **2015**, *14*, 143–159.
- [80] A. P. P. Kröger, J. M. Paulusse, *J. Control. Release* **2018**, *286*, 326–347.

- [81] O. Altintas, C. Barner-Kowollik, *Macromol. Rapid Commun.* **2012**, 958–971.
- [82] J. A. Pomposo, *Polym. Int.* **2014**, 63, 589–592.
- [83] O. Altintas, C. Barner-Kowollik, *Macromol. Rapid Commun.* **2015**, 37, 29–46.
- [84] J. Pomposo, *Single-Chain Polymer Nanoparticles: Synthesis, Characterization, Simulations, and Applications*, Wiley, **2017**.
- [85] A. M. Hanlon, R. Chen, K. J. Rodriguez, C. Willis, J. G. Dickinson, M. Cashman, E. B. Berda, *Macromolecules* **2017**, 50, 2996–3003.
- [86] S. Basasoro, M. Gonzalez-Burgos, A. J. Moreno, F. L. Verso, A. Arbe, J. Colmenero, J. A. Pomposo, *Macromol. Rapid Commun.* **2016**, 37, 1060–1065.
- [87] H. Frisch, J. P. Menzel, F. R. Bloesser, D. E. Marschner, K. Mundsinger, C. Barner-Kowollik, *J. Am. Chem. Soc.* **2018**, 140, 9551–9557.
- [88] T. Chidanguro, D. R. Blank, A. Garrett, C. M. Reese, J. M. Schekman, X. Yu, D. L. Patton, N. Ayres, Y. C. Simon, *Dalton Trans.* **2018**, 47, 8663–8669.
- [89] E. H. H. Wong, S. J. Lam, E. Nam, G. G. Qiao, *ACS Macro Letters* **2014**, 3, 524–528.
- [90] P. G. Frank, B. T. Tuten, A. Prasher, D. Chao, E. B. Berda, *Macromol. Rapid Commun.* **2014**, 35, 249–253.
- [91] T. K. Claus, J. Zhang, L. Martin, M. Hartlieb, H. Mutlu, S. Perrier, G. Delaittre, C. Barner-Kowollik, *Macromol. Rapid Commun.* **2017**, 38, 1700264.
- [92] T. S. Fischer, S. Spann, Q. An, B. Luy, M. Tsotsalas, J. P. Blinco, H. Mutlu, C. Barner-Kowollik, *Chem. Sci.* **2018**, 9, 4696–4702.
- [93] C. Heiler, J. T. Offenloch, E. Blasco, C. Barner-Kowollik, *ACS Macro Letters* **2017**, 6, 56–61.
- [94] K. N. R. Wuest, H. Lu, D. S. Thomas, A. S. Goldmann, M. H. Stenzel, C. Barner-Kowollik, *ACS Macro Letters* **2017**, 6, 1168–1174.
- [95] O. Altintas, J. Willenbacher, K. N. R. Wuest, K. K. Oehlenschlaeger, P. Krolla-Sidenstein, H. Gliemann, C. Barner-Kowollik, *Macromolecules* **2013**, 46, 8092–8101.
- [96] J. Steinkoenig, H. Rothfuss, A. Lauer, B. T. Tuten, C. Barner-Kowollik, *J. Am. Chem. Soc.* **2017**, 139, 51–54.
- [97] S. Garmendia, A. P. Dove, D. Taton, R. K. O'Reilly, *Polym. Chem.* **2018**, 9, 5286–5294.
- [98] E. Huerta, P. J. Stals, E. W. Meijer, A. R. Palmans, *Angew. Chem. Int. Ed.* **2013**, 52, 2906–2910.
- [99] T. Terashima, T. Mes, T. F. A. De Greef, M. A. J. Gillissen, P. Besenius, A. R. A. Palmans, E. W. Meijer, *J. Am. Chem. Soc.* **2011**, 133, 4742–4745.
- [100] A. Sanchez-Sanchez, J. A. Pomposo, *Part. Part. Syst. Char.* **2013**, 31, 11–23.
- [101] B. Dai, Q. Wang, F. Yu, M. Zhu, *Sci. Rep.* **2015**, 5, 10553.
- [102] I. Perez-Baena, I. Loinaz, D. Padro, I. García, H. J. Grandea, I. Odriozola, *J. Mater. Chem.* **2010**, 6916–6922.
- [103] J. Jeong, Y.-J. Lee, B. Kim, K.-S. Jung, H.-j. Paik, *Polym. Chem.* **2015**, 3392–3397.
- [104] J. A. Day, S. M. Cohen, *J. Med. Chem.* **2013**, 56, 7997–8007.
- [105] S. Mavila, I. Rozenberg, N. G. Lemcoff, *Chem. Sci.* **2014**, 4196–4203.

- [106] A. Sanchez-Sanchez, A. Arbe, J. Colmenero, J. A. Pomposo, *ACS Macro Letters* **2014**, *3*, 439–443.
- [107] S. Thanneeru, J. K. Nganga, A. S. Amin, B. Liu, L. Jin, A. M. Angeles-Boza, J. He, *ChemCatChem* **2017**, *9*, 1157–1162.
- [108] Y. Bai, X. Feng, H. Xing, Y. Xu, B. K. Kim, N. Baig, T. Zhou, A. A. Gewirth, Y. Lu, E. Oldfield, S. C. Zimmerman, *J. Am. Chem. Soc.* **2016**, *138*, 11077–11080.
- [109] J. Chen, J. Wang, Y. Bai, K. Li, E. S. Garcia, A. L. Ferguson, S. C. Zimmerman, *J. Am. Chem. Soc.* **2018**, *140*, 13695–13702.
- [110] S. P. C. A. Tooley, E. B. Berda, *Polym. Chem.* **2015**, 7646–7651.
- [111] K. J. Rodriguez, A. M. Hanlon, C. K. Lyon, J. P. Cole, B. T. Tuten, C. A. Tooley, E. B. Berda, S. Pazicni, *Inorg. Chem.* **2016**, *55*, 9493–9496.
- [112] Y. Azuma, T. Terashima, M. Sawamoto, *ACS Macro Letters* **2017**, *6*, 830–835.
- [113] M. Artar, E. R. J. Souren, T. Terashima, E. W. Meijer, A. R. A. Palmans, *ACS Macro Letters* **2015**, *4*, 1099–1103.
- [114] E. Huerta, P. J. M. Stals, E. W. Meijer, A. R. A. Palmans, *Angew. Chem. Int. Ed.* **2013**, *52*, 2906–2910.
- [115] Z. Cui, H. Cao, Y. Ding, P. Gao, X. Lu, Y. Cai, *Polym. Chem.* **2017**, 3755–3763.
- [116] Z. Cui, L. Huang, Y. Ding, X. Zhu, X. Lu, Y. Cai, *ACS Macro Letters* **2018**, *7*, 572–575.
- [117] L. Greb, H. Mutlu, C. Barner-Kowollik, J.-M. Lehn, *J. Am. Chem. Soc.* **2016**, *138*, 1142–1145.
- [118] G. M. ter Huurne, I. K. Voets, A. R. A. Palmans, E. W. Meijer, *Macromolecules* **2018**, *51*, 8853–8861.
- [119] N. Hosono, A. M. Kushner, J. Chung, A. R. A. Palmans, Z. Guan, E. W. Meijer, *J. Am. Chem. Soc.* **2015**, *137*, 6880–6888.
- [120] S. Thanneeru, S. S. Duay, L. Jin, Y. Fu, A. M. Angeles-Boza, J. He, *ACS Macro Letters* **2017**, *6*, 652–656.
- [121] J. Steinkoenig, T. Nitsche, B. T. Tuten, C. Barner-Kowollik, *Macromolecules* **2018**, *51*, 3967–3974.
- [122] J. A. Pomposo, I. Perez-Baena, F. Lo Verso, A. J. Moreno, A. Arbe, J. Colmenero, *ACS Macro Letters* **2014**, *3*, 767–772.
- [123] F. L. Verso, J. A. Pomposo, J. Colmenero, A. J. Moreno, *Soft Matter* **2016**, 9039–9046.
- [124] F. L. Verso, J. A. Pomposo, J. Colmenero, A. J. Moreno, *Soft Matter* **2015**, 1369–1375.
- [125] A. J. Moreno, F. Lo Verso, A. Sanchez-Sanchez, A. Arbe, J. Colmenero, J. A. Pomposo, *Macromolecules* **2013**, *46*, 9748–9759.
- [126] M. González-Burgos, A. Arbe, A. J. Moreno, J. A. Pomposo, A. Radulescu, J. Colmenero, *Macromolecules* **2018**, *51*, 1573–1585.
- [127] A. B. Benito, M. K. Aiertza, M. Marradi, L. Gil-Iceta, T. Shekhter Zahavi, B. Szczupak, M. Jiménez-González, T. Reese, E. Scanziani, L. Passoni, M. Matteoli, M. De Maglie, A. Orenstein, M. Oron-Herman, G. Kostenich, L. Buzhansky, E. Gazit, H.-J. Grande, V. Gómez-Vallejo, J. Llop, I. Loinaz, *Biomacromolecules* **2016**, *17*, 3213–3221.
- [128] B. V. K. J. Schmidt, N. Fechner, J. Falkenhagen, J.-F. Lutz, *Nat. Chem.* **2011**, *3*, 234–238.

- [129] J. P. Cole, J. J. Lessard, K. J. Rodriguez, A. M. Hanlon, E. K. Reville, J. P. Mancinelli, E. B. Berda, *Polym. Chem.* **2017**, *7*, 5829–5835.
- [130] J. A. Pomposo, A. J. Moreno, A. Arbe, J. Colmenero, *ACS Omega* **2018**, *3*, 8648–8654.
- [131] D. Chen, Meena, S. K. Sharma, L. W. McLaughlin, *J. Am. Chem. Soc.* **2004**, *126*, 70–71.
- [132] D. Berek, *J. Sep. Science* **2010**, *33*, 315–335.
- [133] R. W. Nunes, J. R. Martin, J. F. Johnson, *Polym. Eng. Sci.* **1982**, *22*, 205–228.
- [134] A. M. Striegel, *Modern size-exclusion liquid chromatography : practice of gel permeation and gel filtration chromatography*, 2nd ed., Wiley, Hoboken, N.J, **2009**.
- [135] L. K. Kostanski, D. M. Keller, A. E. Hamielec, *J. Biochem. Bioph. Methods* **2004**, *58*, 159–186.
- [136] R. Garcia-Lopera, A. Codoner, C. Bano, C. Abad, A. Campos, *J. Chromatogr. Sci.* **2005**, *43*.
- [137] Z. Grubisic, P. Rempp, H. Benoit, *J. Polym. Sci. B Polym. Lett.* **1967**, *5*, 753–759.
- [138] A. Latorre-Sánchez, A. Alegría, F. Lo Verso, A. J. Moreno, A. Arbe, J. Colmenero, J. A. Pomposo, *Part. Part. Syst. Charact.* **2016**, *33*, 373–381.
- [139] J. A. Pomposo, J. Rubio-Cervilla, A. J. Moreno, F. Lo Verso, P. Bacova, A. Arbe, J. Colmenero, *Macromolecules* **2017**, *50*, 1732–1739.
- [140] L. J. Fetters, N. Hadjichristidis, J. S. Lindner, J. W. Mays, *J. Phys. Chem. Ref. Data* **1994**, *23*, 619–640.
- [141] H. J., K. G., G. D.N., *J Med Phys.* **2007**, *32*, 34–42.
- [142] E. O. Stejskal, J. E. Tanner, *J. Chem. Phys.* **1965**, *42*, 288–292.
- [143] A. Einstein, *Ann. Phys.* **1905**, *322*, 549–560.
- [144] C. Johnson, *Prog. Nucl. Magn. Reson. Spectrosc.* **1999**, *34*, 203–256.
- [145] E. Blasco, B. T. Tuten, H. Frisch, A. Lederer, C. Barner-Kowollik, *Polym. Chem.* **2017**, *8*, 5845–5851.
- [146] R. Pecora, *Dynamic Light Scattering: Applications of Photon Correlation Spectroscopy*, Springer US, **2013**.
- [147] W. Schaertl, *Light scattering from polymer solutions and nanoparticle dispersions*, Springer, Berlin, **2007**.
- [148] W. I. Goldberg, *Am. J. Phys.* **1999**, *67*, 1152–1160.
- [149] W. Brown, *Dynamic light scattering: the method and some applications*, Clarendon Press, **1993**.
- [150] C. Urban, P. Schurtenberger, *J. Colloid Interface Sci.* **1998**, *207*, 150–158.
- [151] A. J. Cox, A. J. DeWeerd, J. Linden, *Am. J. Phys.* **2002**, *70*, 620–625.
- [152] S. J., M. S. A., P. T.R, *Biophys Rev.* **2016**, *8*, 409–427.
- [153] M. Kaszuba, D. McKnight, M. T. Connah, F. K. McNeil-Watson, U. Nobbmann, *J. Nanopart. Res.* **2008**, *10*, 823–829.
- [154] K. Yamada in *Interrelations between Essential Metal Ions and Human Diseases*, (Eds.: A. Sigel, H. Sigel, R. K. Sigel), Springer Netherlands, Dordrecht, **2013**, pp. 295–320.
- [155] B. Pashaei, H. Shahroosvand, P. Abbasi, *RSC Adv.* **2015**, *5*, 94814–94848.

- [156] M. Scholl, S. Ding, C. W. Lee, R. H. Grubbs, *Org. Lett.* **1999**, *1*, 953–956.
- [157] R. Demuth, F. Kober, *Grundlagen der Komplexchemie*, O. Salle, **1992**.
- [158] H. Irving, R. J. P. Williams, *Nature* **1948**, 746–747.
- [159] N. Wiberg, E. Wiberg, A. Holleman, *Anorganische Chemie: Grundlagen und Hauptgruppenelemente, Band 2*, De Gruyter, **2016**.
- [160] R. G. Pearson, *J. Am. Chem. Soc.* **1963**, *85*, 3533–3539.
- [161] L. Gade, *Koordinationschemie*, Wiley, **1999**, Chapter 17.
- [162] M. Green, *J. Org. Chem.* **1995**, *500*, 127–148.
- [163] S. L. James, *Chem. Soc. Rev.* **2009**, *38*, 1744–1758.
- [164] C. A. Tolman, *Chem. Rev.* **1977**, *77*, 313–348.
- [165] M. C. Baird, J. T. Mague, J. A. Osborn, G. Wilkinson, *J. Chem. Soc. A* **1967**, 1347–1360.
- [166] A. Schnyder, A. Togni, U. Wiesli, *Organometallics* **1997**, *16*, 255–260.
- [167] G. Bringmann, A. J. P. Mortimer, P. A. Keller, M. J. Gresser, J. Garner, M. Breuning, *Angew. Chem. Int. Ed.* **2005**, *44*, 5384–5427.
- [168] W. S. Knowles, *Angew. Chem. Int. Ed.* **2002**, *41*, 1998–2007.
- [169] O. Kühn, *Phosphorus-31 NMR Spectroscopy: A Concise Introduction for the Synthetic Organic and Organometallic Chemist*, Springer Berlin Heidelberg, **2008**.
- [170] R. Appel, *Angew. Chem. Int. Ed.* **1975**, *14*, 801–811.
- [171] A. W. Platt, *Coord. Chem. Rev.* **2017**, *340*, Chemistry and Applications of the Lanthanides, 62–78.
- [172] G. Accorsi, A. Listorti, K. Yoosaf, N. Armaroli, *Chem. Soc. Rev.* **2009**, *38*, 1690–1700.
- [173] A. Bencini, V. Lippolis, *Coord. Chem. Rev.* **2010**, *254*, 2096–2180.
- [174] P. G. Sammes, G. Yahioğlu, *Chem. Soc. Rev.* **1994**, *23*, 327–334.
- [175] F. Teplý, *Collect. Czech. Chem. Commun.* **2011**, 859–917.
- [176] J. M. R. Narayanam, C. R. J. Stephenson, *Chem. Soc. Rev.* **2011**, *40*, 102–113.
- [177] K. Zeitler, *Angew. Chem. Int. Ed.* **2009**, 9785–9789.
- [178] J. Guerra, D. Cantillo, C. O. Kappe, *Catal. Sci. Technol.* **2016**, *6*, 4695–4699.
- [179] M. Iwamura, S. Takeuchi, T. Tahara, *J. Am. Chem. Soc.* **2007**, *129*, 5248–5256.
- [180] C. O. Dietrich-Buchecker, J. P. Sauvage, J. M. Kern, *J. Am. Chem. Soc.* **1984**, *106*, 3043–3045.
- [181] J. G. J. Weijnen, A. Koudijs, J. F. J. Engbersen, *J. Org. Chem.* **1992**, *57*, 7258–7265.
- [182] R. L. Rardin, W. B. Tolman, S. J. Lippard, *New J. Chem.* **1991**, *15*, 417–430.
- [183] O. C., *Progress in Inorganic Chemistry*, Wiley, **1968**.
- [184] G. Wilkinson, R. Gillard, J. McCleverty, *Comprehensive Coordination Chemistry: Ligands*, Franklin Book Company, Incorporated, **1987**.
- [185] D. Lawton, R. Mason, *J. Am. Chem. Soc.* **1965**, *87*, 921–922.
- [186] C. H. Hendon, A. Walsh, *Chem. Sci.* **2015**, *6*, 3674–3683.

- [187] N. E. Holden, T. Coplen, *Chemistry International – Newsmagazine for IUPAC* **2009**, *26*, 8–9.
- [188] W. J. Evans, *Polyhedron* **1987**, *6*, 803–835.
- [189] C. Evans, *Biochemistry of the Lanthanides*, Springer US, **2013**.
- [190] J. E. Geusic, H. M. Marcos, L. G. Van Uitert, *Appl. Phys. Lett.* **1964**, *4*, 182–184.
- [191] J.-C. G. Bünzli, C. Piguet, *Chem. Soc. Rev.* **2005**, *34*, 1048–1077.
- [192] X. H. Chen, T. Wu, G. Wu, R. H. Liu, H. Chen, F. Fang, *Nature* **2008**, 761–762.
- [193] M. Hatanaka, S. Yabushita, *J. Phys. Chem. A* **2009**, *113*, 12615–12625.
- [194] J. W. Verhoeven, *Pure Appl. Chem.* **2009**, *68*, 2223–2286.
- [195] M. A. Condrau, R. A. Schwendener, P. Niederer, M. Anliker, *Cytometry* **1994**, 187–194.
- [196] J. P. Leonard, C. B. Nolan, F. Stomeo, T. Gunnlaugsson in *Photochemistry and Photophysics of Coordination Compounds II*, (Eds.: V. Balzani, S. Campagna), Springer Berlin Heidelberg, Berlin, Heidelberg, **2007**, pp. 1–43.
- [197] R. W. Buckley, *Solid State Chemistry Research Trends*, Nova Science Publishers, **2007**.
- [198] G. Zucchi, A.-C. Ferrand, R. Scopelliti, J.-C. G. Bünzli, *Inorg. Chem.* **2002**, *41*, 2459–2465.
- [199] A. S. Kalyakina, V. V. Utochnikova, M. Zimmer, F. Dietrich, A. M. Kaczmarek, R. V. Deun, A. A. Vashchenko, A. S. Goloveshkin, M. Nieger, M. Gerhards, U. Schepers, S. Braese, *Chem. Commun.* **2018**, *54*, 5221–5224.
- [200] F. Degorce, A. Card, S. Soh, E. Trinquet, G. P. Knapik, B. Xie, *Curr. Chem. Genomics* **2009**, 22–32.
- [201] M. Harris, S. Carron, L. V. Elst, S. Laurent, R. N. Muller, T. N. Parac-Vogt, *Chem. Commun.* **2015**, *51*, 2984–2986.
- [202] J. C. Bailar, H. Itatani, *J. Am. Chem. Soc.* **1967**, *89*, 1592–1599.
- [203] H. C. Clark, C. Billard, C. S. Wong, *J. Organomet. Chem.* **1980**, *190*, C105–C107.
- [204] A. J. Chalk, J. F. Harrod, *J. Am. Chem. Soc.* **1965**, *87*, 16–21.
- [205] J. R. L. Priqueler, I. S. Butler, F. D. Rochon, *Appl. Spectrosc. Rev.* **2006**, *41*, 185–226.
- [206] A. Vekris, D. Meynard, M.-C. Haaz, M. Bayssas, J. Bonnet, J. Robert, *Cancer Res.* **2004**, *64*, 356–362.
- [207] N. D. Knöfel, H. Rothfuss, J. Willenbacher, C. Barner-Kowollik, P. W. Roesky, *Angew. Chem. Int. Ed.* **2017**, *56*, 4950–4954.
- [208] I. S. Mikhel, K. N. Gavrilov, A. I. Polosukhin, A. I. Rebrov, *Russ. Chem. Bull.* **1998**, *47*, 1585–1588.
- [209] G. A. Krestov, *Viniti Database RAS* **1968**, 1–17.
- [210] H. Lee, M. G. Campbell, R. Hernández Sánchez, J. Börgel, J. Raynaud, S. E. Parker, T. Ritter, *Organometallics* **2016**, *35*, 2923–2929.
- [211] S. Gama, I. Rodrigues, F. Mendes, I. C. Santos, E. Gabano, B. Klejevska, J. Gonzalez-Garcia, M. Ravera, R. Vilar, A. Paulo, *J. Inorg. Biochem.* **2016**, *160*, 275–286.
- [212] B. Wrackmeyer, *Chemie in unserer Zeit* **1994**, *28*, 309–320.
- [213] E. L. Hahn, D. E. Maxwell, *Phys. Rev.* **1952**, *88*, 1070–1084.

- [214] L. Beml, H. C. Clark, J. A. Davies, C. A. Fyfe, R. E. Wasylshen, *J. Am. Chem. Soc.* **1982**, *104*, 438–445.
- [215] S. Baehn, S. Imm, L. Neubert, M. Zhang, H. Neumann, M. Beller, *ChemCatChem* **2011**, *3*, 1853–1864.
- [216] F. Ragaini, S. Cenini, D. Brignoli, M. Gasperini, E. Gallo, *J. Org. Chem.* **2003**, *68*, 460–466.
- [217] M.-Y. Hu, Q. He, S.-J. Fan, Z.-C. Wang, L.-Y. Liu, Y.-J. Mu, Q. Peng, S.-F. Zhu, *Nat. Chem.* **2018**, *9*.
- [218] D. Maggioni, F. Fenili, L. D'Alfonso, D. Donghi, M. Panigati, I. Zanoni, R. Marzi, A. Manfredi, P. Ferruti, G. D'Alfonso, E. Ranucci, *Inorg. Chem.* **2012**, *51*, 12776–12788.
- [219] J. Zhao, W. Wu, J. Sun, S. Guo, *Chem. Soc. Rev.* **2013**, *42*, 5323–5351.
- [220] J. Feng, S.-Y. Song, R.-P. Deng, W.-Q. Fan, H.-J. Zhang, *Langmuir* **2010**, *26*, 3596–3600.
- [221] W. Huang, G. Masuda, S. Maeda, H. Tanaka, T. Hino, T. Ogawa, *Inorg. Chem.* **2008**, *47*, 468–480.
- [222] X. Liu, Y. Hu, B. Wang, Z. Su, *Synth. Met.* **2009**, *159*, 1557–1562.
- [223] Y. Liu, T. Paulöhr, S. I. Presolski, L. Albertazzi, A. R. A. Palmans, E. W. Meijer, *J. Am. Chem. Soc.* **2015**, *137*, 13096–13105.
- [224] Y. Liu, S. Pujals, P. J. M. Stals, T. Paulöhr, S. I. Presolski, E. W. Meijer, L. Albertazzi, A. R. A. Palmans, *J. Am. Chem. Soc.* **2018**, *140*, 3423–3433.
- [225] M. S. Donovan, A. B. Lowe, B. S. Sumerlin, C. L. McCormick, *Macromolecules* **2002**, *35*, 4123–4132.
- [226] B. Grassl, L. Billon, O. Borisov, J. Francois, *Polym. Int.* **2015**, *55*, 1169–1176.
- [227] K. Matyjaszewski, J. Xia, *Chem. Rev.* **2001**, *101*, 2921–2990.
- [228] K. Matyjaszewski, *Macromolecules* **2012**, *45*, 4015–4039.
- [229] D. B. Thomas, A. J. Convertine, L. J. Myrick, C. W. Scales, A. E. Smith, A. B. Lowe, Y. A. Vasilieva, N. Ayres, C. L. McCormick, *Macromolecules* **2004**, *37*, 8941–8950.
- [230] W. Steinhauer, R. Hoogenboom, H. Keul, M. Moeller, *Macromolecules* **2013**, *46*, 1447–1460.
- [231] K. Wang, Z. Song, C. Liu, W. Zhang, *Polym. Chem.* **2016**, *7*, 3423–3433.
- [232] X. Su, Z. Zhao, H. Li, X. Li, P. Wu, Z. Han, *Eur. Polym. J.* **2008**, *44*, 1849–1856.
- [233] J. T. Lai, D. Filla, R. Shea, *Macromolecules* **2002**, *35*, 6754–6756.
- [234] Z. Liu, J. Hu, J. Sun, G. He, Y. Li, G. Zhang, *J. Polym. Sci. A Polym. Chem.* **2010**, 3573–3586.
- [235] F. T. Wall, *J. Am. Chem. Soc.* **1941**, *63*, 1862–1866.
- [236] Q. Sun, Z. Lv, Q. Qu, L. Wang, L. Zhu, X. Meng, W. Chen, F. Xiao, *Chem. Asian J.* **2013**, 2822–2827.
- [237] K. Schierholz, M. Givehchi, P. Fabre, F. Nallet, E. Papon, O. Guerret, Y. Gnanou, *Macromolecules* **2003**, *36*, 5995–5999.
- [238] D. Li, W. J. Brittain, *Macromolecules* **1998**, *31*, 3852–3855.
- [239] O. Gibbons, W. M. Carroll, F. Aldabbagh, B. Yamada, *J. Polym. Sci. A Polym. Chem.* **2006**, *44*, 6410–6418.
- [240] D. Benoit, V. Chaplinski, R. Braslau, C. J. Hawker, *J. Am. Chem. Soc.* **1999**, *121*, 3904–3920.

- [241] K. Peter, M. Thelakkat, *Macromolecules* **2003**, *36*, 1779–1785.
- [242] L. Rasmussen, C. Jørgensen, *Inorg. Chim. Acta* **1969**, *3*, 547–551.
- [243] S. Kamel, H. A. Ali, A. A. Shamma, *J. Coord. Chem.* **2017**, *70*, 1910–1925.
- [244] L. Lei, S. Jing, R. I. Walton, X. Xin, D. O'Hare, *J. Chem. Soc. Dalton Trans.* **2002**, *0*, 3477–3481.
- [245] H. Irving, D. H. Mellor, *J. Chem. Soc.* **1962**, 5222–5237.
- [246] T. Tominaga, S. Matsumoto, T. Koshiya, Y. Yamamoto, *J. Chem. Soc. Faraday Trans. 1* **1988**, *85*, 4261–4266.
- [247] R. K. Adhikamsetty, N. R. Gollapalli, S. B. Jonnalagadda, *Int. J. Chem. Kinet.* **2008**, *40*, 515–523.
- [248] A. Afkhami, F. Mosaed, *Microchem. J.* **2001**, *68*, 35–40.
- [249] S. R. Maqsood, N. Islam, S. Bashir, B. Khan, A. H. Pandith, *J. Coord. Chem.* **2013**, *66*, 2308–2315.
- [250] E. Agustina, J. Goak, S. Lee, Y. Seo, J.-Y. Park, N. Lee, *ChemistryOpen* **2015**, *4*, 613–619.
- [251] P. S. Braterman, J. I. Song, R. D. Peacock, *Inorg. Chem.* **1992**, *31*, 555–559.
- [252] P. L. Ku, *Adv. Polym. Techn.* **1988**, *8*, 201–223.
- [253] L. Armelao, S. Quici, F. Barigelletti, G. Accorsi, G. Bottaro, M. Cavazzini, E. Tondello, *Coord. Chem. Rev.* **2010**, *254*, 487–505.
- [254] H. J. G. L. Z. Zhang, Y. F. J. Chen, T. Fan, L. Zhang, *J. Rare Earths* **2011**, *29*, 741–745.
- [255] N. B. D. Lima, S. M. C. Gonçalves, S. A. Júnior, A. M. Simas, *Sci. Rep.* **2013**, *3*, 2395.
- [256] P. D. Y. Hasegawa, S. Tateno, M. Yamamoto, D. T. Nakanishi, D. Y. Kitagawa, D. T. Seki, P. D. H. Ito, D. K. Fushimi, *Chem. Eur. J.* **2017**, *23*, 2666.
- [257] E. Moretti, L. Bellotto, M. Basile, C. Malba, F. Enrichi, A. Benedetti, S. Polizzi, *Mater. Chem. Phys.* **2013**, *142*, 445–452.
- [258] A. K. Singh, S. K. Singh, H. Mishra, R. Prakash, S. B. Rai, *J. Phys. Chem. B* **2010**, *114*, 13042–13051.
- [259] H. Friebolin, *Ein- und zweidimensionale NMR-Spektroskopie : Eine Einführung*, 5., vollst. überarb. und erw. Aufl., Wiley-VCH, Weinheim, **2013**.
- [260] L. Ruan, X. Gao, J. Zhao, C. Xu, D. Liang, *J. Mol. Struct.* **2017**, *1149*, 265–272.
- [261] E. Soini, T. Lövgren, C. B. Reimer, *Crit. Rev. Anal. Chem.* **1987**, *18*, 105–154.
- [262] M. A. Abubaker, K. Harrington, R. von Wandruszka, *Anal. Lett.* **1993**, *26*, 1681–1692.
- [263] Y. Yuetao, S. Qingde, Z. Guiwen, *Spectrochim. Acta Part A* **1999**, *55*, 1527–1533.
- [264] Y. Yang, S. Zhang, *Phys. Stat. Sol. (A)* **2003**, *198*, 176–182.
- [265] K. Binnemans, *Coord. Chem. Rev.* **2015**, *295*, 1–45.
- [266] A. M. Brouwer, *Pure Appl. Chem.* **2011**, *83*, 2213–2228.
- [267] P. G. Sammes, G. Yahioğlu, G. D. Yearwood, *J. Chem. Soc., Chem. Commun.* **1992**, 1282–1283.
- [268] Y. Yamaguchi, Y. Matsubara, T. Ochi, T. Wakamiya, Z.-i. Yoshida, *J. Am. Chem. Soc.* **2008**, *130*, 13867–13869.

- [269] D. T. Thielemann, M. Klinger, T. J. A. Wolf, Y. Lan, W. Wernsdorfer, M. Busse, P. W. Roesky, A.-N. Unterreiner, A. K. Powell, P. C. Junk, G. B. Deacon, *Inorg. Chem.* **2011**, *50*, 11990–12000.
- [270] A. Cannizzo, A. M. Blanco-Rodríguez, A. El Nahhas, J. Šebera, S. Záliš, A. Vlček, M. Chergui, *J. Am. Chem. Soc.* **2008**, *130*, 8967–8974.
- [271] N. Knöfel, H. Rothfuss, P. W. Barner-Kowollik, C. and Roesky, *Polym. Chem.* **2019**, *10*, 86–93.
- [272] P. Sharrock, M. Melník, *Can. J. Chem.* **1985**, *63*, 52–56.
- [273] Y. Chen, S. Sakakia, *Dalton Trans.* **2014**, *43*, 11478–11492.
- [274] P. K. Ross, M. D. Allendorf, E. I. Solomon, *J. Am. Chem. Soc.* **1989**, *111*, 4009–4021.
- [275] S. Mavila, D. C. E. S. Linde, L. Amir, R. Shikler, N. G. Lemcoff, *Angew. Chem. Int. Ed.* **2013**, *52*, 5767–5770.
- [276] K. Freytag, S. Säfken, K. Wolter, J. C. Namyslo, E. G. Hübner, *Polym. Chem.* **2017**, *8*, 7546.
- [277] E. A., *Turk. J. Phys.* **2000**, *24*, 667–672.
- [278] P. Cheng, D. Liao, S. Yan, Z. Jiang, G. Wang, *Transition Met. Chem.* **1996**, *21*, 515–518.
- [279] Y. Vidavsky, S. Bae, M. N. Silberstein, *J. Polym. Sci. Part A: Polym. Chem.* **2018**, *56*, 1117.
- [280] F. A. Cotton, C. A. Murillo, R. A. Walton, *Multiple Bonds between Metal Atoms*, Springer-Verlag New York, **2005**.
- [281] S. Rej, M. Majumdar, S. Kando, Y. Sugino, H. Tsurugi, K. Mashima, *Inorg. Chem.* **2017**, *56*, 634–644.
- [282] J. Hicks, S. P. Ring, N. J. Patmore, *Dalton Trans.* **2012**, *41*, 6641.
- [283] F. Cotton, L. Falvello, A. Reid, J. Tocher, *J. Organomet. Chem.* **1987**, *319*, 87–97.
- [284] N. D. Knöfel, C. Schweigert, T. J. Feuerstein, C. Schoo, N. Reinfandt, A.-N. Unterreiner, P. W. Roesky, *Inorg. Chem.* **2018**, *57*, 9364–9375.
- [285] F. A. Cotton, L. M. Daniels, E. A. Hillard, C. A. Murillo, *Inorg. Chem.* **2002**, *41*, 2466–2470.
- [286] J. Catterick, P. Thornton, *Advances in Inorganic Chemistry and Radiochemistry, Vol. 20*, (Eds.: ed. H. J. Emeleus, A. G. Sharpe), Academic Press, **1977**, p. 291.
- [287] T. A. Stephenson, E. Bannister, G. Wilkinson, *J. Chem. Soc.* **1964**, 2538–2541.
- [288] F. A. Cotton, D. G. Lay, *Inorg. Chem.* **1981**, *20*, 935–940.
- [289] A. J. Hempleman, R. J. H. Clark, C. D. Flint, *Inorg. Chem.* **1986**, *25*, 2915–2916.
- [290] M. Mikuriya, R. Indrawati, R. Hashido, S. Matsubara, C. Nakamura, D. Yoshioka, K. Yokota, M. Fukuzaki, M. Handa, *Magnetochemistry* **2018**, *4*.
- [291] M. H. Chisholm, T. L. Gustafson, C. Turro, *Acc. Chem. Res.* **2013**, *46*, 529–538.
- [292] M. H. Chisholm, S. E. Brown-Xu, T. F. Spilker, *Acc. Chem. Res.* **2015**, *48*, 877–885.
- [293] B. G. Alberding, M. H. Chisholm, C. B. Durr, J. C. Gallucci, Y. Ghosh, T. F. Spilker, *Dalton Trans.* **2014**, *43*, 11397.
- [294] D. Cousins, F. Hart, *J. Inorg. Nucl. Chem.* **1967**, *29*, 1745–1757.
- [295] X. C. Cambeiro, T. C. Boorman, P. Lu, I. Larrosa, *Angew. Chem. Int. Ed.* **2013**, *52*, 1781–1784.
- [296] A. Stephen, K. Hashmi, *Gold Bull.* **2004**, *37*, 51–65.

- [297] N. Marion, S. P. Nolan, *Chem. Soc. Rev.* **2008**, *37*, 1776–1782.
- [298] E. A. Andre'v, N. N. Kavtaradze, *Bull. Acad. Sci. USSR Div. Chem. Sci.* **1952**, *1*, 895–902.
- [299] F. Tisato, F. Vallotto, G. Pilloni, F. Refosco, C. Corvaja, B. Corain, *J. Chem. Soc. Chem. Commun.* **1994**, *0*, 2397–2398.
- [300] S. Bestgen, M. T. Gamer, S. Lebedkin, M. M. Kappes, P. W. Roesky, *Chem. Eur. J.* **2015**, *21*, 601–614.
- [301] A. Vogler, H. Kunkely, *Coord. Chem. Rev.* **2001**, *219-221*, 489–507.
- [302] M. Pérez-Iglesias, P. Espinet, J. A. Casares, *Inorg. Chem.* **2018**, *57*, 11193–11200.
- [303] R. Uson, A. Laguna, M. Laguna, D. A. Briggs, H. H. Murray, J. P. Fackler Jr. in *Inorganic Syntheses*, John Wiley & Sons, Ltd, **2007**, pp. 85–91.
- [304] D. S. Gill, J. Singh, R. Ludwig, M. D. Zeidler, *J. Chem. Soc. Faraday Trans.* **1993**, *89*, 3955–3958.
- [305] M. Kyuzou, W. Mori, J. Tanaka, *Inorg. Chim. Acta* **2010**, *363*, 930–934.
- [306] N. B. D. Lima, A. I. S. Silva, P. C. Gerson, Jr, S. M. C. Gonçalves, A. M. Simas, *PLOS ONE* **2016**, *10*, 1–14.
- [307] A. I. S. Silva, N. B. D. Lima, A. M. Simas, S. M. C. Gonçalves, *ACS Omega* **2017**, *2*, 6786–6794.
- [308] J. Wang, C. Han, G. Xie, Y. Wei, Q. Xue, P. Yan, H. Xu, *Chem. Eur. J.* **2014**, *20*, 11137–11148.
- [309] A. L. Grzesiak, A. J. Matzger, *Inorg. Chem.* **2007**, *46*, 453–457.
- [310] F.-H. Hu, L.-S. Wang, S.-F. Cai, *J. Chem. Eng. Data* **2009**, *54*, 1382–1384.
- [311] L. Daasch, D. Smith, *Anal. Chem.* **1951**, *23*, 853–868.
- [312] R. R. Shifrina, I. P. Romm, E. N. Gur'yanova, N. A. Rozanel'skaya, *J. Appl. Spectrosc.* **1981**, *34*, 84–88.
- [313] W. D. Horrocks, J. P. Sipe, *J. Am. Chem. Soc.* **1971**, *93*, 6800–6804.
- [314] W. Zhang, X. He, B. Ren, Y. Jiang, Z. Hu, *Tetrahedron Letters* **2015**, *56*, 2472–2475.
- [315] U. Helmstedt, S. Lebedkin, T. Höcher, S. Blaurock, E. Hey-Hawkins, *Inorg. Chem.* **2008**, *47*, 5815–5820.
- [316] A. Kusumaatmaja, T. Ando, K. Terada, S. Hirohara, T. Nakashima, T. Kawai, T. Terashima, M. Tanihara, *J. Polym. Sci. Part A: Polym. Chem.* **2013**, *51*, 2527–2535.
- [317] C. Strazielle, H. Benoit, O. Vogl, *Eur. Polym. J.* **1978**, *14*, 331–334.
- [318] K. Rurack, M. Spieles, *Anal. Chem.* **2011**, *83*, 1232–1242.
- [319] M. Grabolle, M. Spieles, V. Lesnyak, N. Gaponik, A. Eychmüller, U. Resch-Genger, *Anal. Chem.* **2009**, *81*, 6285–6294.
- [320] G. M. Sheldrick, *Acta Crystallogr. Sect. A* **2008**, *64*, 112–122.
- [321] G. M. Sheldrick, *Acta Crystallogr. Sect. A* **2015**, *71*, 3–8.
- [322] O. V. Dolomanov, L. J. Bourhis, R. J. Gildea, J. A. K. Howard, H. Puschmann, *J. Appl. Crystallogr.* **2009**, *42*, 339–341.

- [323] H. Woo, S. Cho, Y. Han, W.-S. Chae, D.-R. Ahn, Y. You, W. Nam, *J. Am. Chem. Soc.* **2013**, *135*, 4771–4787.
- [324] S. H. Bossmann, N. D. Ghatlia, M. F. Ottaviani, C. Turro, H. Dürr, N. J. Turro, *Synthesis* **1996**, 1313–1319.
- [325] C. Waterlot, D. Couturier, *J. Appl. Polym. Sci.* **2010**, 7–16.
- [326] A. Sunil, B. C. B. Bezuidenhout, J. M. J. van Rensburg, *Acta Crystallogr. Sect. E* **2008**, *64*, 939.

Appendix

The following sections provide NMR and IR data of the chemical structures, developed in the present dissertation, if not already displayed in the Chapters 3, 4, 5 and 6.

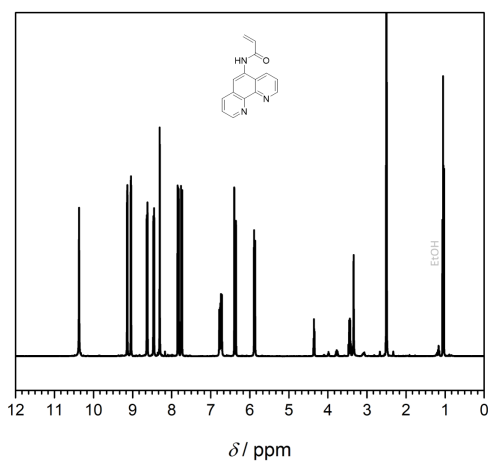


Figure 9.1: ¹H NMR spectrum of *N*-(1,10-phenanthroline-5-yl)acrylamide (4), DMSO-*d*₆.

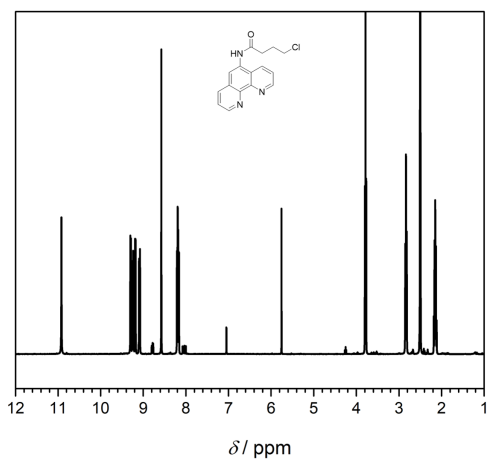


Figure 9.2: ¹H NMR spectrum of 4-chloro-*N*-(1,10-phenanthroline-5-yl)butane amide (5), DMSO-*d*₆.

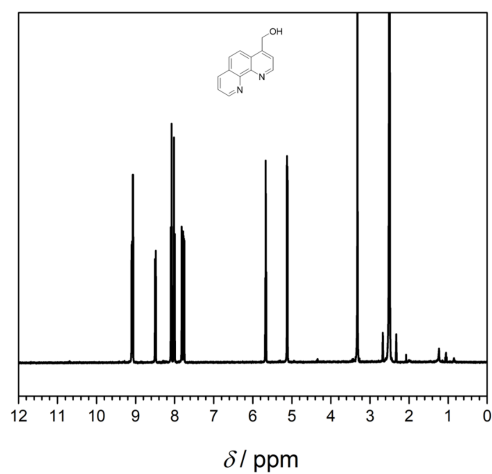


Figure 9.3: ¹H NMR spectrum of 1,10-phenanthroline-4-carbaldehyde (7), DMSO-d₆.

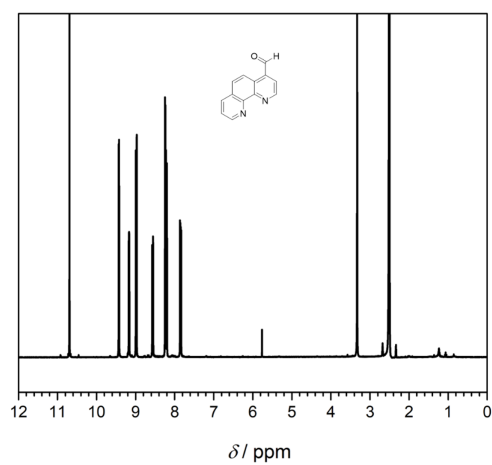


Figure 9.4: ¹H NMR spectrum of (1,10-phenanthroline-4-yl)methanol (8), DMSO-d₆.

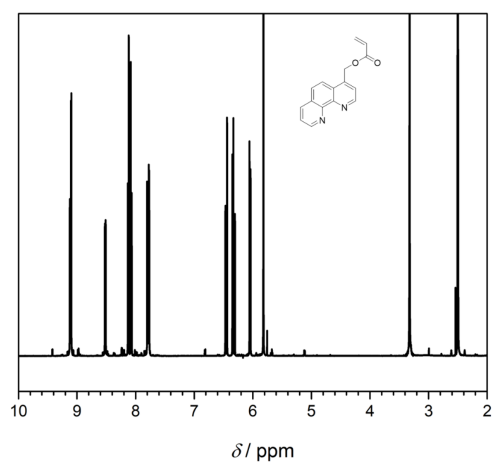


Figure 9.5: ¹H NMR spectrum of (1,10-phenanthroline-4-yl)methyl acrylate (9), DMSO-d₆.

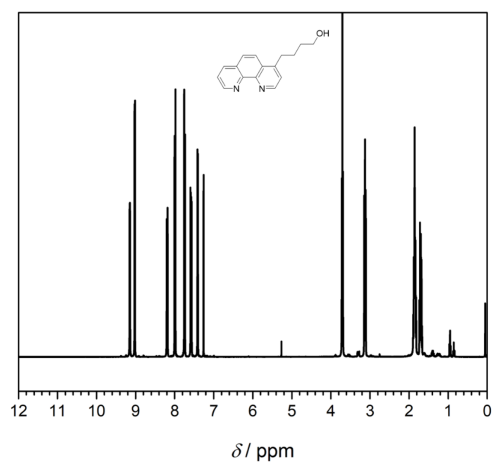


Figure 9.6: ¹H NMR spectrum of 4-(1,10-phenanthroline-4-yl)butane-1-ol (10), CDCl₃.

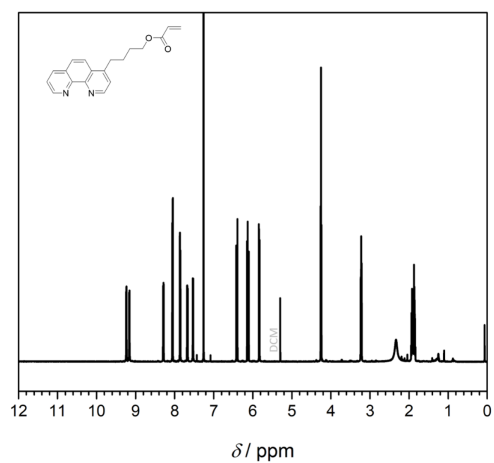


Figure 9.7: ¹H NMR spectrum of 4-(1,10-phenanthroline-4-yl)butyl acrylate (Phen-acrylate, 11), CDCl₃.

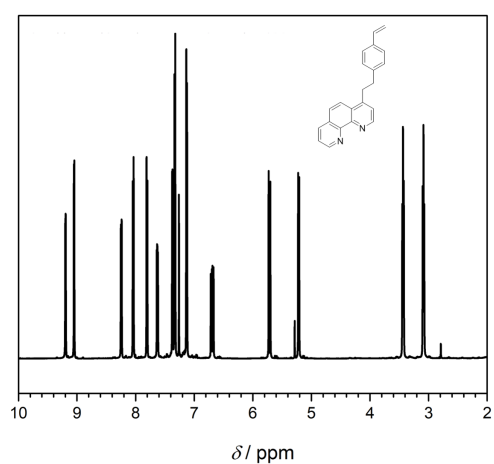


Figure 9.8: ¹H NMR spectrum of 4-(4-vinylphenethyl)-1,10-phenanthroline (Phen-styrene, 12), CDCl₃.

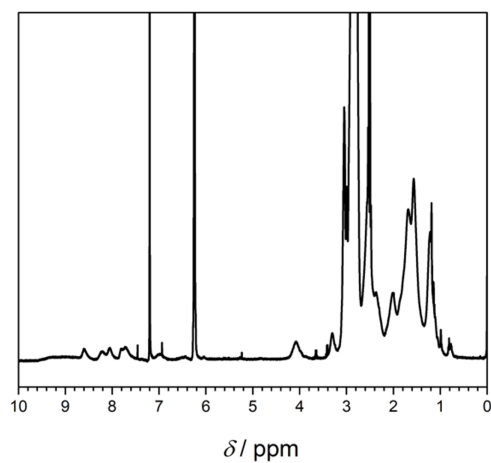


Figure 9.9: ^1H NMR spectrum of $\text{P}_{\text{polar}}\text{-Pd(II)}$, CDCl_3 .

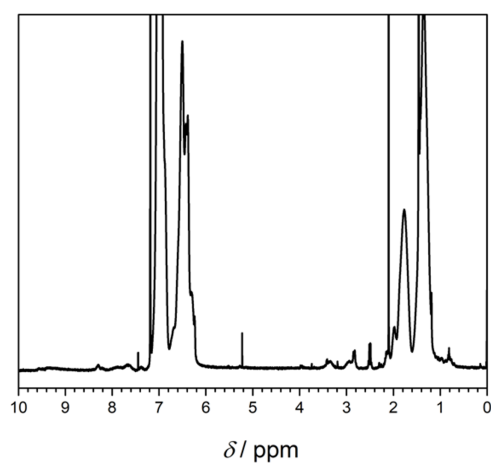


Figure 9.10: ^1H NMR spectrum of $\text{P}_{\text{np}}\text{-Pd(II)}$, CDCl_3 .

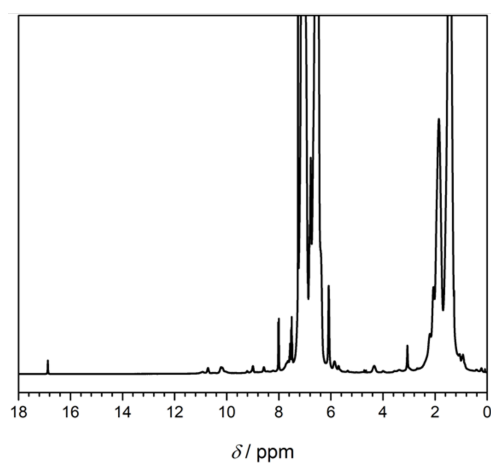


Figure 9.11: ^1H NMR spectrum of $\text{P}_{\text{np}}\text{-Eu(III)}$, CDCl_3 .

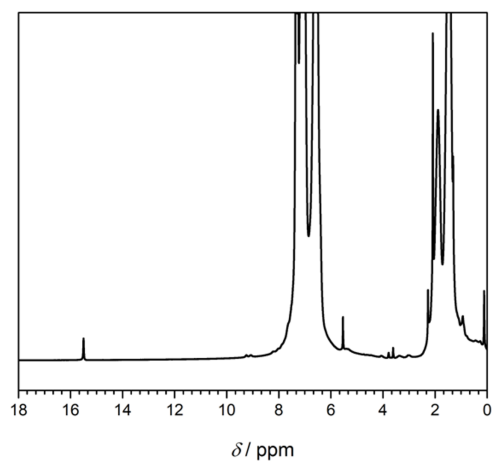


Figure 9.12: ^1H NMR spectrum of $\text{P}_{np}\text{-Tb(III)}$, CDCl_3 .

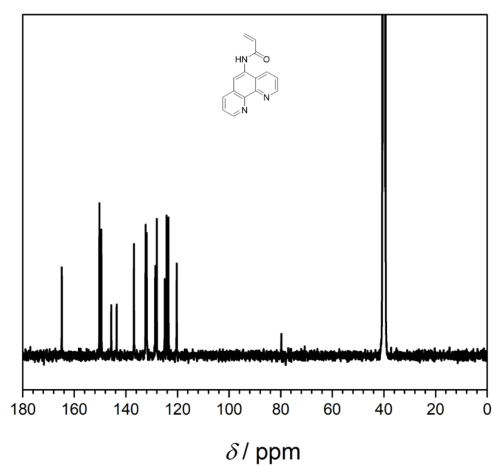


Figure 9.13: $^{13}\text{C}\{^1\text{H}\}$ NMR spectrum of N -(1,10-phenanthroline-5-yl)acrylamide (4), $\text{DMSO-}d_6$.

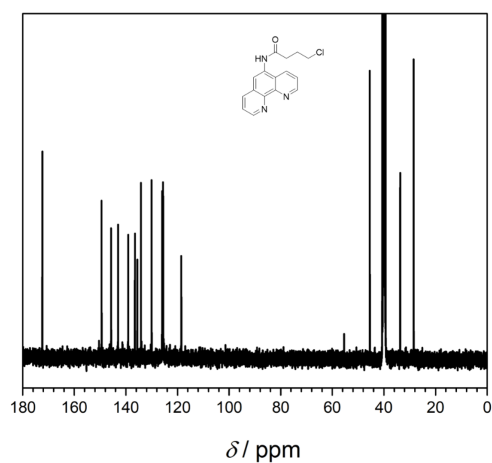


Figure 9.14: $^{13}\text{C}\{^1\text{H}\}$ NMR spectrum of 4-chloro- N -(1,10-phenanthroline-5-yl)butane amide (5), $\text{DMSO-}d_6$.

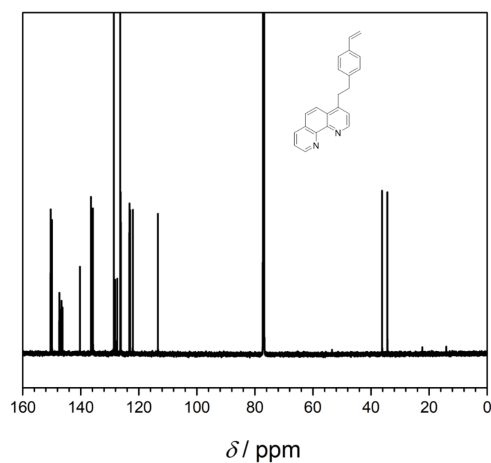


Figure 9.15: $^{13}\text{C}\{^1\text{H}\}$ NMR spectrum of 4-(4-vinylphenethyl)-1,10-phenanthroline (Phen-styrene, 12), CDCl_3 .

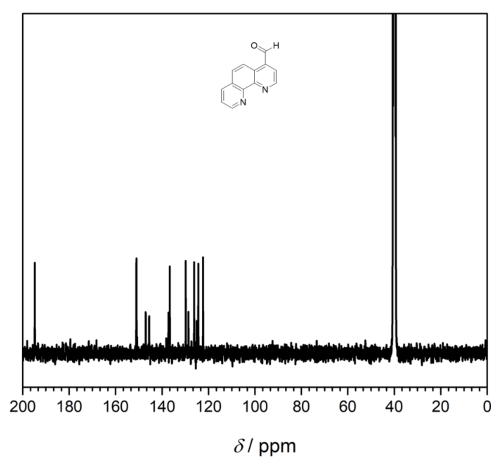


Figure 9.16: $^{13}\text{C}\{^1\text{H}\}$ NMR spectrum of 1,10-phenanthroline-4-carbaldehyde (7), $\text{DMSO}-d_6$.

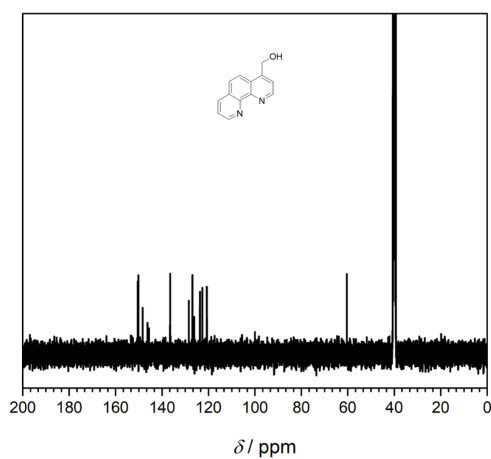


Figure 9.17: $^{13}\text{C}\{^1\text{H}\}$ NMR spectrum of (1,10-phenanthroline-4-yl)methanol (8), $\text{DMSO}-d_6$.

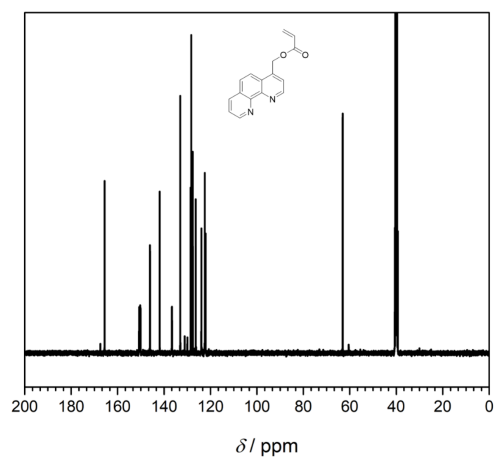


Figure 9.18: $^{13}\text{C}\{^1\text{H}\}$ NMR spectrum of (1,10-phenanthroline-4-yl)methyl acrylate (9), $\text{DMSO-}d_6$.

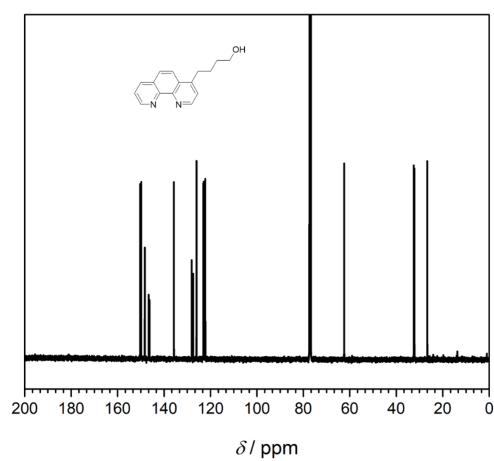


Figure 9.19: $^{13}\text{C}\{^1\text{H}\}$ NMR spectrum of 4-(1,10-phenanthroline-4-yl)butane-1-ol (10), CDCl_3 .

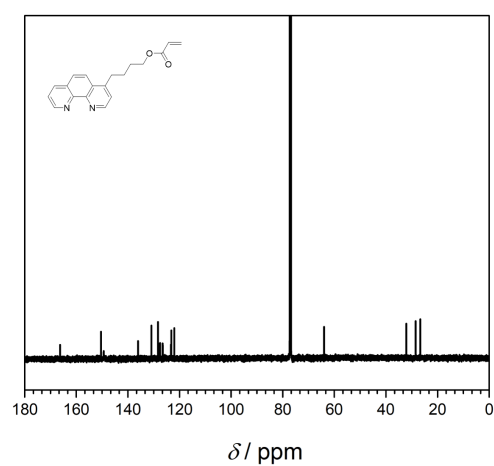


Figure 9.20: $^{13}\text{C}\{^1\text{H}\}$ NMR spectrum of 4-(1,10-phenanthroline-4-yl)butyl acrylate (Phen-acrylate, 11), CDCl_3 .

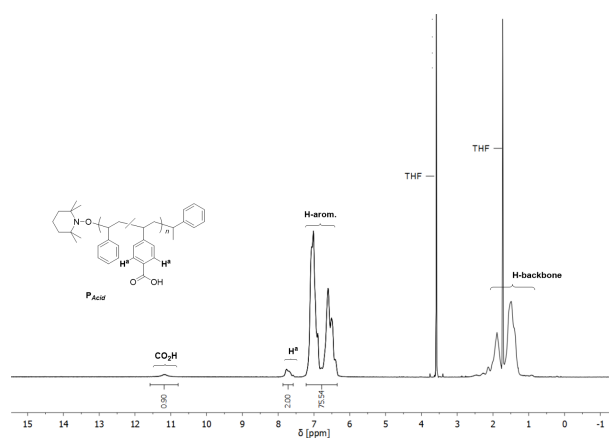


Figure 9.21: ^1H NMR spectrum of P_{Acid} , $\text{THF-}d_8$.

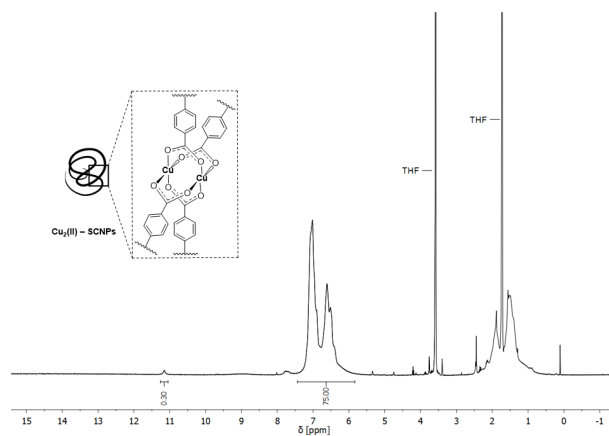


Figure 9.22: ^1H NMR spectrum of $\text{Cu}_2(\text{II})\text{-SCNPs}$, $\text{THF-}d_8$.

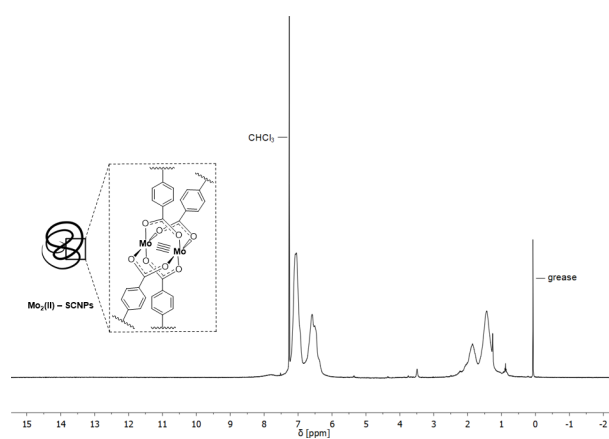


Figure 9.23: ^1H NMR spectrum of $\text{Mo}_2(\text{II})\text{-SCNPs}$, CDCl_3 .

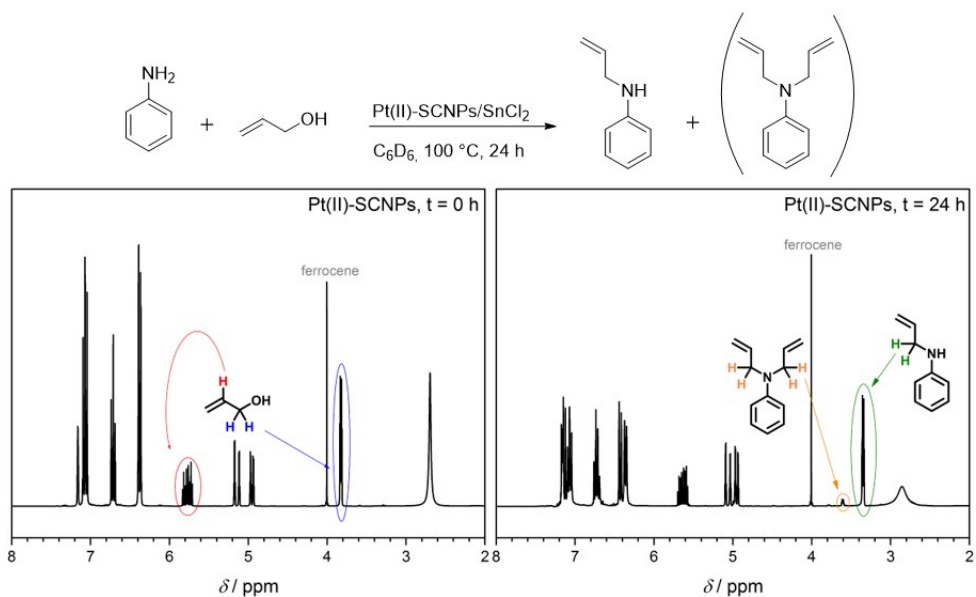


Figure 9.24: Reaction scheme for the reaction of 3-chloroaniline with allyl alcohol catalyzed by Pt(II)-SCNPs, depicting the corresponding ^1H NMR spectra (CDCl₃) at the beginning of the reaction (t = 0 hours) and after 24 hours.

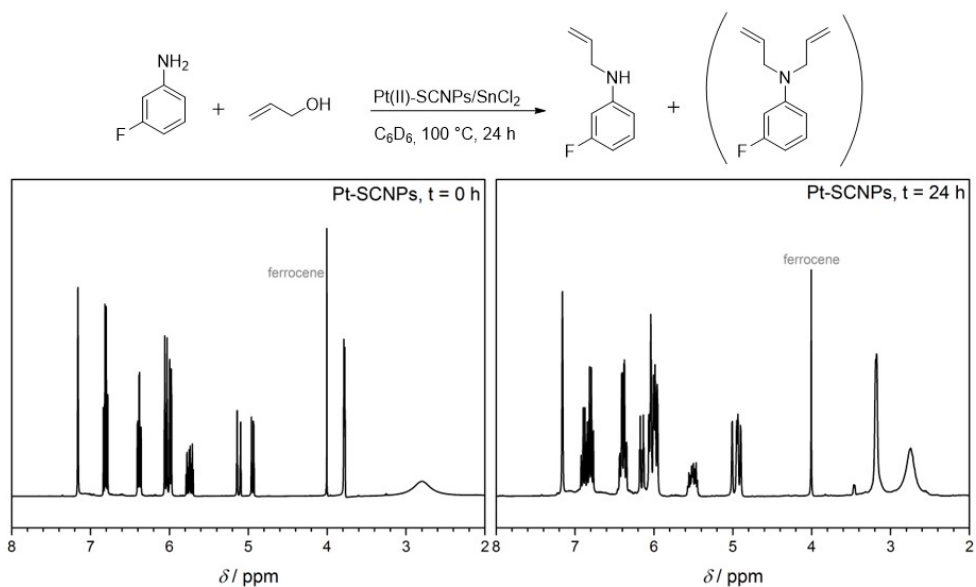


Figure 9.25: Reaction scheme for the reaction of 3-fluoroaniline with allyl alcohol catalyzed by Pt(II)-SCNPs, depicting the corresponding ^1H NMR spectra (CDCl₃) at the beginning of the reaction (t = 0 hours) and after 24 hours.

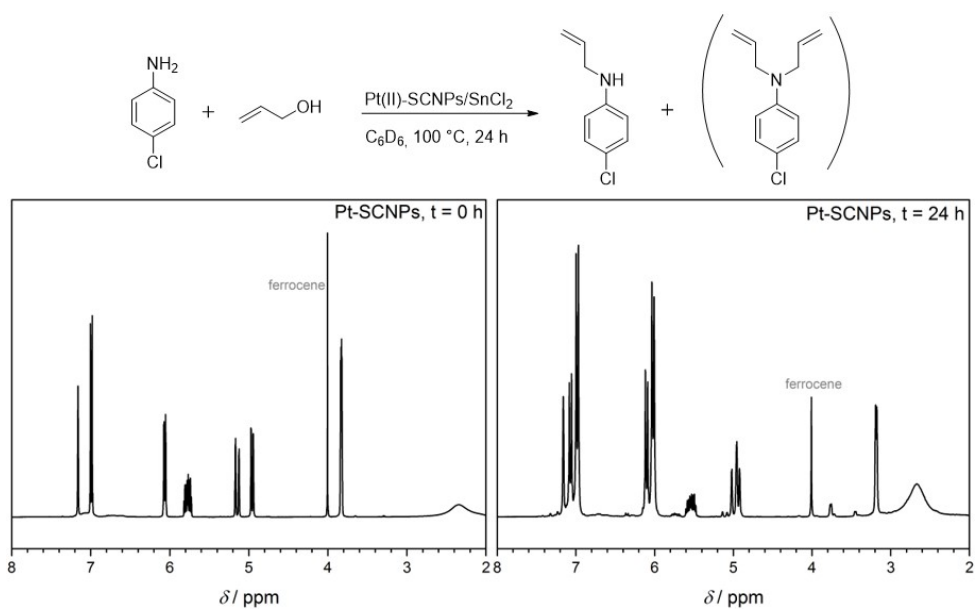


Figure 9.26: Reaction scheme for the reaction of 4-chloroaniline with allyl alcohol catalyzed by Pt(II)-SCNPs, depicting the corresponding ^1H NMR spectra (CDCl₃) at the beginning of the reaction ($t = 0$ hours) and after 24 hours.

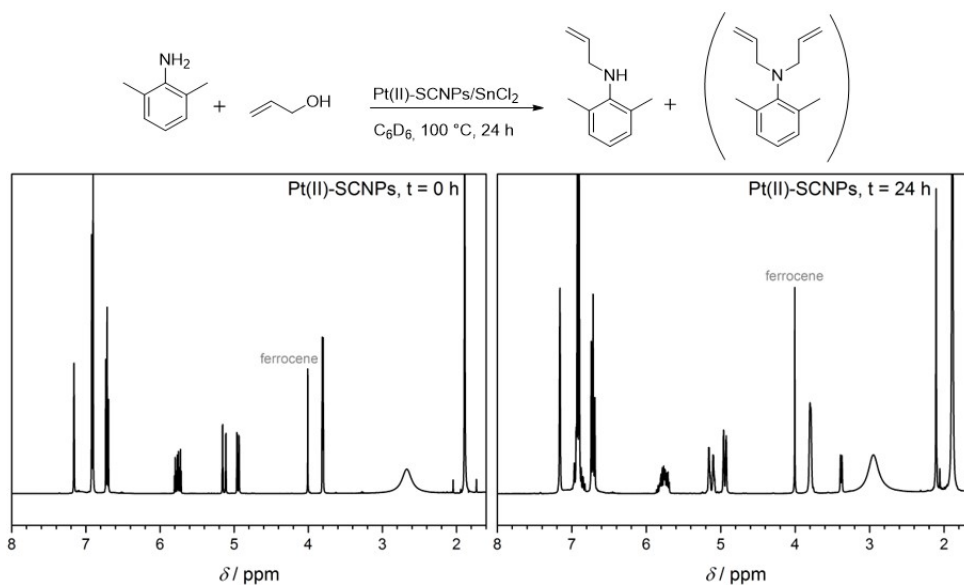


Figure 9.27: Reaction scheme for the reaction of 2,6-dimethylaniline with allyl alcohol catalyzed by Pt(II)-SCNPs, depicting the corresponding ^1H NMR spectra (CDCl₃) at the beginning of the reaction ($t = 0$ hours) and after 24 hours.

Abbreviations

acac	acetylacetonate
Aliquot 336	tricaprylylmethylammonium chloride
AO	atomic orbital
approx.	approximately
a.t.	ambient temperature
ATRP	atom transfer radical polymerization
bipy	2,2'-bipyridine
BTA	benzene-1,3,5-tricarboxamide
calcd.	calculated
CDCl ₃	deuterated chloroform
CEA	carboxyethyl acrylate
COD	cyclooctadiene
COE	cyclooctene
Đ	dispersity
DCC	<i>N,N'</i> -dicyclohexylcarbodiimide
DCM	dichloromethane
DBM	dibenzoylmethanide
DBTTC	<i>S,S</i> -dibenzyl trithiocarbonate
DDMAT	2-(dodecylthiocarbonothioylthio)-2-methylpropionic acid
DLS	dynamic light scattering
DMAA	<i>N,N</i> -dimethylacrylamide
DMAc	dimethylacetamide
DMAP	4-dimethylaminopyridine
DMF	dimethylformamide
DMSO	dimethylsulfoxide
DOSY	diffusion ordered spectroscopy
DSC	dynamic light scattering
EDC	1-ethyl-3-(3-dimethylaminopropyl)carbodiimide
Et ₂ O	diethylether
Et ₃ N	triethylamine
<i>et al.</i>	<i>et alii/aliae</i>
equiv.	equivalent

g	gerade (even)
I	nuclear spin
IR	infra red spectroscopy
ISC	intersystem crossing
IUPAC	International Union of Pure and Applied Chemistry
k_p	rate of propagation coefficient
L	ligand
LCST	lower critical solution temperature
LDA	lithium diisopropylamide
Ln	Lanthanides
MALLS	multiangle laser light scattering
MAMA-SG1	<i>N</i> -(2-methylpropyl)- <i>N</i> -(1-diethylphosphono-2,2-dimethylpropyl)- <i>O</i> -(2-carboxylprop-2-yl)hydroxylamine
Me	methyl
MeOH	methanol
M_n	number average molecular mass
M_w	mass average molecular mass
MLCT	metal ligand charge transfer
MO	molecular orbital
MRI	magnetic resonance imaging
NMP	nitroxide mediated polymerization
NMR	nuclear magnetic resonance
NOESY	nuclear overhauser effect spectroscopy
OD	optical density
PEGMA	poly(ethylene glycol) methacrylate
Phen	phenanthroline and its derivatives
Ph	phenyl
PMMA	poly(methyl methacrylate)
ppm	parts per million
q.	quaternary
QY	quantum yield
RAFT	reversible addition fragmentation chain transfer
r_H	hydrodynamic radius
RI	refractive index
RDRP	reversible deactivation radical polymerization
SCNP	single-chain nanoparticle
SEC	size exclusion chromatography
SG1	<i>N-tert</i> -butyl- <i>N</i> -[1-diethylphosphono-(2,2-dimethylpropyl) nitroxide]
TBAF	tetra- <i>n</i> -butylammonium fluorid
TEMPO	(2,2,6,6-tetramethylpiperidin-1-yl)oxidanyl
THT	tetrahydrothiophen

THF	tetrahydrofuran
TMS	tetramethylsilane
TOCSY	total correlation spectroscopy
TPPO	triphenylphosphine oxide
TRITT	2,2'-(thiocarbonylbis(sulfaneyl))bis(2-methylpropanoic acid)
u	ungerade (odd)
UV-Vis	ultraviolet-visible (spectroscopy)
XRD	x-ray diffraction

Publications

1. **M₂⁴⁺ Paddlewheel Clusters as Junction Points in Single-Chain Nanoparticles**

Knoefel, N.*; Rothfuss, H.*; Barner-Kowollik, C.; Roesky, P. R. *Polym. Chem.* **2019**, *10*, 86-93.

2. **Phenanthroline – A Versatile Ligand for Advanced Functional Polymeric Materials**

Rothfuss, H.*; Knöfel, N.*; Tzvetkova, P.; Michenfelder, N.; Baraban, S.; Unterreiner, A.-N.; Roesky, P. W.; Barner-Kowollik, C. *Chem. Eur. J.* **2018**, *24*, 17475-17486. (Highlighted as journal cover)

3. **Single-Chain Nanoparticles as Catalytic Nanoreactors;**

Rothfuss, H.*; Knöfel, N.*; Roesky, P. W.; Barner-Kowollik, C. *J. Am. Chem. Soc.* **2018**, *140*, 5875-5881. (Highlighted as journal cover)

4. **Platinum(II)-Crosslinked Single-Chain Nanoparticles: An Approach towards Recyclable Homogeneous Catalysts**

Knöfel, N.*; Rothfuss, H.*; Willenbacher, J.; Barner-Kowollik, C.; Roesky, P. W. *Angew. Chem. Int. Ed.* **2017**, *56*, 4950–4954. (Highlighted as journal cover)

5. **Imaging Single-Chain Nanoparticle Folding via High-Resolution Mass Spectrometry**

Steinkoenig, J.; Rothfuss, H.; Lauer, A.; Tuten, B. T.; Barner-Kowollik, C. *J. Am. Chem. Soc.* **2017**, *139*, 51-54.

* This authors contributed equally

Conference Contributions

- **Platinum(II) Complexed SCNPs: The First Reusable Homogeneous Catalysts in Chemical Reactions**
H. Rothfuss, N. Knöfel, P. W. Roesky, C. Barner-Kowollik; *UNESCO/IUPAC Conference on Macromolecules & Materials*, April **2017**, Stellenbosch, South Africa. Oral presentation.
- **1,10-Phenanthroline as a Versatile Ligand for Metalcomplexation in Single-Chain Nanoparticles**
H. Rothfuss, N. Knöfel, P. W. Roesky, C. Barner-Kowollik; *International Conference on Coordination Chemistry*, August **2018**, Sendai, Japan. Oral presentation.
- **Metal-complexed Single-Chain Nanoparticles as Catalytic Nanoreactors**
H. Rothfuss, N. Knöfel, P. W. Roesky, C. Barner-Kowollik; *Dimensional Control of Polymer Materials – From Synthesis to Function*, Oktober **2018**, Karlsruhe, Germany. Oral presentation.

Erklärung

Hiermit erkläre ich, die vorliegende Arbeit selbstständig angefertigt und keine anderen als die angegebenen Quellen und Hilfsmittel benutzt zu haben. Wörtlich oder inhaltlich übernommene Stellen habe ich als solche kenntlich gemacht. Die Regeln zur Sicherung der guten wissenschaftlichen Praxis des KIT in der jeweils gültigen Fassung wurden beachtet. Die elektronische Version dieser Arbeit stimmt mit der schriftlichen Version überein. Außerdem ist die Abgabe und Archivierung der Primärdaten gemäß Abs. A (6) der Regeln zur Sicherung guter wissenschaftlicher Praxis des KIT beim Institut gesichert.

Desweiteren erkläre ich, dass ich mich derzeit in keinem laufenden Promotionsverfahren befinde und auch keine vorausgegangenen Promotionsversuche unternommen habe.

Karlsruhe, den 26.03.2019

Hannah Rothfuß

Acknowledgements

An erster Stelle gilt meine große Dankbarkeit meinem Doktorvater Christopher Barner-Kowollik, der mir die Durchführung der vorliegenden Arbeit ermöglicht hat und mich jederzeit in meinen Projekten unterstützt und motiviert hat. Trotz deines Umzugs nach Australien standen wir immer in Kontakt und obwohl du uns 8 Stunden in der Zeit voraus bist, hast du mir oft schon nach 5 Minuten auf meine Emails geantwortet. Danke, dass ich mir immer deiner Unterstützung sicher sein konnte und du mich über diesen ganzen Zeitraum hinweg gefördert hast. Ich bin weiterhin sehr froh, dass ich innerhalb des Projektes eigene Ideen entwickeln und bearbeiten konnte, und positive Forschungsergebnisse sogar auf internationalen Konferenzen präsentieren durfte. Durch die Erweiterung der KIT Node um die australische QUT Node hatte ich zudem die Möglichkeit während eines halben Jahres Forschungsaufenthalts die andere Seite der Welt kennen zu lernen.

Großer Dank gilt meinem Kooperationspartner Nicolai Knöfel für die konstruktiven Diskussionen verschiedenster Themen, in denen wir am Ende doch immer Lösungen für Probleme gefunden und neue Ideen entwickelt haben. Ich bin sehr dankbar für die gemeinsame Zeit, in der wir nicht nur zusammenarbeitet haben, sondern auch Freunde geworden sind. Ein Dank geht hiermit auch an das KIT für die Telefonflatrate, die Nico und mir es ermöglicht jeden Tag mindestens einmal miteinander zu telefonieren.

Ich möchte mich weiterhin bei Prof. Dr. Peter Roesky bedanken, der mit uns immer in direkter Kooperation und Austausch stand, und auch mal für ein gemeinsamen Abendessen mit Nico und mir nach Australien kam. Mit ihrer Expertise haben Pavleta Tvetkova, Nadine Michenfelder und Dr. Andreas-Neil Unterreiner viel zum Gelingen verschiedener Projekte beigetragen, weshalb ich mich hiermit noch einmal bedanken möchte. Ein großer Dank geht auch an Eva Blasco. Nicht nur für die produktiven Gespräche und Tipps allgemein zum Thema Polymere, sondern auch für die angenehme Atmosphäre. Ich drücke dir die Daumen, dass es mit dem Junior-Group-Leader klappt.

Viel Unterstützung verschiedener Art kam auch aus dem eigenen Team. Zum Glück konnte ich während meiner Dissertation mit so vielen tollen Leute zusammen arbeiten und gemeinsam Zeit verbringen. Hiermit ein großes Dankeschön an alle momentanen Macroarc-Mitglieder am KIT wie am

QUT, sowie alle Ehemaligen. Anfangen bei Grillabenden vor dem Institut, Filmabenden zu Hause und speziell in Australien unsere gefühlt-tausenden Aktivitäten und Ausflüge. Hendrik, Fede, Lies, Jan, Tobi, Waldemar and Matthias, thanks to you all for such a great time. And special thanks to Fede, for sharing an apartment with me and some cockroaches ;) It still gives me the shivers. Ich möchte mich außerdem auch bei meiner Laborpartnerin Janin bedanken. Ich hätte mir niemand Besseren wünschen können, Labor und (Frei)Zeit zu teilen.

Für die Unterstützung bei synthetischen Arbeiten im Labor danke ich meinen Vertiefer-Studenten Bragavie Kulendran und Sergej Baraban, sowie Melissa Reith für die Durchführung ihrer Masterarbeit. Euch viel Erfolg weiterhin!

Ein großer Dank gilt auch Katharina, Evelyn, Frau Schneider und Vincent, die uns allezeit das Leben einfacher gemacht haben und uns so viel organisatorische Arbeit abgenommen haben.

Weiterhin möchte ich mich bei den Korrekturlesern meiner Arbeit bedanken, Alex Q., Alex S., Bryan, Caro, Fede, Hendrik, Jan, Matze, Rhiannon und meinem Vater :) Vielen, vielen Dank.

An dieser Stelle möchte ich mich auch bei Alex Q. bedanken, dafür, dass du mich als erster für die Polymerchemie begeistert hast und für viele schöne Zeiten.

Für die finanzielle Unterstützung bedanke ich mich der Stiftung Stipendien-Fonds des Verbandes der Chemischen Industrie für ein zweijähriges Stipendium und beim Sonderforschungsbereich SFB 1176. Dabei gilt großer Dank Dominik Voll und Conny Weber, die immer für einen reibungslosen Ablauf gesorgt haben.

Zuletzt möchte ich mich bei meiner Familie und Freunden für Zeit, Geduld und Unterstützung schon während des Studiums und auch in der anschließenden Promotion bedanken. Speziell bei meinen Eltern Ulrike und Helmut, die immer für mich da sind, selbst wenn ich kilometer weit entfernt bin. Denn dann kommen sie einfach in ihrem Urlaub bei mir vorbei und erkunden mit mir Fraser Island oder beobachten Wale. Weiterhin bin ich meiner Oma und Gerhard sehr dankbar, für erholsame gemeinsame Zeiten, Märzenbecher-Wanderungen, leckere Essen und aufmunternde Postkarten. Y muchisimas gracias a mi novio Carlos, que suerte estar contigo. Gracias por estar en mi vida, a mi lado.